The Clinical Translation of Platelet Derived Growth Factor and its Application in Models of Cardiac Dysfunction

Emily McKinna

Primary Supervisor

Prof. James Chong

Auxiliary Supervisors

A/Prof. Eddy Kizana, Dr. Robert Hume, Prof. Richard Harvey

THE UNIVERSITY OF SYDNEY

A thesis submitted in fulfilment of the requirements for admission to the degree of

Doctor of Philosophy

September 2023

Faculty of Medicine and Health
The University of Sydney

DECLARATION

I, Emily McKinna, hereby declare that this dissertation contains work which has not been presented for the award of any other degree at any university. The work presented in this dissertation is the result of my own investigation with the assistance from others acknowledged herein. Material written or published by other persons have been appropriately acknowledged and referenced in this dissertation.

Emily McKinna

September 2023

ABSTRACT

Despite significant research efforts cardiovascular diseases remain a leading cause of death world-wide. Significant among them is heart failure which has a 5-year mortality rate approaching 50% once reaching severe stages (such as New York Heart Association Class IV). Substantial efforts have been made to address the limited regeneration of the adult myocardium post myocardial infarction (MI), however there remains no treatment option to reverse the damage of large MIs. Recombinant human platelet derived growth factor-AB (rhPDGF-AB) has been reported to significantly improve cardiac function following MI in murine and porcine models. This has been shown to be due to effects on the cardiac extracellular matrix (ECM) and neovascularisation. Whilst these results pose rhPDGF-AB as a promising novel therapeutic post-MI, the manufacture of recombinant proteins has poor scalability, and the short biological half-life of this growth factor limits its prospects for clinical translation. To address this problem, we aimed to develop an alternative to rhPDGF-AB, resolving its shortcomings whilst maintaining its therapeutic effects. Utilising a key functional region of PDGF we hypothesised that peptide mimetics could replicate the effects of PDGF *in vitro* and *in vivo*.

This work commenced with identification of a key functional region within the PDGF chain that served as the foundation of our mimetic peptides. The effect of these peptides were then assessed *in vitro* based on known reparative functions of PDGF on the infarcted heart. In this thesis we establish lead candidate peptides JC5 and JC5a, due to their significant effects on cell migration, collagen contraction, angiogenesis, and activation of the PDGF receptor (PDGFR) by phosphorylation of Erk. We demonstrate that these peptides have similar effects compared to the full-length rhPDGF-AB protein.

Lead candidates JC5 and JC5a were designed to contain half-life extending conjugates providing the opportunity for enhanced pharmacokinetic properties. The efficacy of JC5 and JC5a was then assessed *in vivo* using a murine model of acute MI. This demonstrated the efficacy of JC5 and JC5a in significantly improving cardiac function 28 days post-MI. These effects seen *in vitro* and *in vivo* were comparable to the effects of rhPDGF-AB.

Finally, with the aim of identifying a model of chronic heart failure to further test *in vivo* efficacy of JC5 and JC5a, we validated a reported 'Two-Hit' approach mouse model of heart failure with preserved ejection fraction (HFpEF). Whilst successfully replicating some aspects of the HFpEF phenotype, our results did not show significant changes within the cardiac extra-cellular matrix (ECM). Given that hypothesised mechanisms of rhPDGF-AB post-MI repair rely on significant ECM change we concluded that this model of HFpEF was not appropriate for efficacy testing in the context of our work these novel peptide mimetics.

In conclusion, the work contained in this thesis shows that the effects of rhPDGF-AB can be mimicked *in vitro* using assays relevant to the functions of PDGF-AB and *in vivo* in a murine model of acute MI. We propose that our synthetic mimetic peptides, JC5 and JC5a, can be applied as alternatives to rhPDGF-AB as a novel therapy post-MI preventing the development of heart failure.

ACKNOWLEDGEMENTS

I would firstly like to thank my supervisors James, Rob, Eddy, and Richard. I have often joked with people that I wanted to be James when grew up but anyone close to me could tell you it wasn't really a joke. I have felt extremely lucky to have James as my primary supervisor but also as a mentor. James has supported me unwaveringly throughout my PhD and has always advocated for me and my projects. Watching James lead our group at CHR inspired me to pursue a career as a clinician scientist and has been invaluable in keep me motivated through times of adversity in my PhD. My co-supervisor Rob has taught me a tremendous amount about science but the most important of those lessons was how to keep loving science even when I really wanted to hate it. Throughout my PhD I have been inspired by Robs love of science and am hugely grateful to have such a genuinely good person and a wonderful scientist to look up to. I would also like to thank my co-supervisor Eddy for his guidance, support, and advice on my work throughout my PhD. Eddy has been a constant positive influence on my PhD and has been essential in shaping my ongoing early career research.

I would like to thank my co-supervisor Richard and the Harvey Lab for everything they taught me and for all their technical expertise throughout my PhD. I would specifically like to thank Vikram for his significant efforts towards my *in vivo* experiments for which I am extremely grateful for. Key aspects of my PhD couldn't have been completed without him. I am also very appreciative for all the support I received from Vaibhao and Bharti throughout my *in vivo* experiments, their assistance in a very challenging part of my PhD was a huge help in being able to finish this work. I learnt more in my time at the Harvey lab than I ever could have expected. It was character-building experience that has a significant impact on my experience in early

career research. This PhD has been a significant lesson in collaboration and a highlight of that was working with Daniel and Richard from the Payne Laboratory at the Sydney School of Chemistry. I am extremely grateful for how wonderful they were to work with and how their expertise in protein chemistry really brought this project to life. The project wouldn't be where it is now without them.

I have felt privileged to do my PhD at the Centre for Heart Research with a fantastic team in the cardiac regeneration group along with our colleagues in the gene therapy group. Firstly, I would like to thank my work mum and friend, Sindhu. She is the lynchpin that holds us all together and is constantly there to support, teach, and provide insight to everyone that comes through CHR. I am extremely grateful to have had her with me through every step of my PhD. I would like to thank and acknowledge the efforts of Sally and Alan in helping me analyse data for my PhD. Their help was hugely important to my project, and I greatly appreciate the significant efforts they put in. I would also like to thank all of the postdocs and RAs of CHR for their input and support and for all the time they gave to teach me during my time at CHR. I would especially like to thank Zoe, Cindy, and Leila for all of their guidance and support. My fellow PhD students in CHR have been wonderful friends and supports but also took the time to provide their expertise and teach me. I would specifically like to thank Tejas, Dinesh, and Samia for taking the time to teach me about the more clinical aspects of my projects particularly how to analyse my echo data, and Fairooj for her expertise in histology and immunohistochemistry.

I have an amazing support network that I couldn't have gotten through the last 4 years without, particularly the last 9 months. I would firstly like to thank my family, Andrew, Leanne, Tara, Oliver, Kayla, and Fiona. I'm sure I've been extremely difficult to live with at times throughout

my PhD, but my family continued to support me in every way they could no matter what. Also, a crucial part of my support network was my wonderful friends. My best friend's Grace and Talia have been invaluable supports throughout this time and have always been there to celebrate all of the wins and listen to me complain about the losses. My PhD also introduced me to some of my greatest friends, Alex, Erica, Ahmad, Jason, and Melad. They were always there to provide scientific and academic insight but also friendship and support that I am very grateful for. I would like to thank all the members of PBL E; Joy, Georgie, Marc, Nick, Olive, Rachel and Sam, and our wonderful tutors Julian, Nerida, and Milana for supporting me throughout this year and picking up the slack for me so much while I've been finishing my PhD. I have felt very privileged to be a part of this team and couldn't have gotten through the last 9 months without them.

This PhD has been a rollercoaster of an experience that was beyond what I could have ever imagined going into it. I am hugely grateful to everyone who contributed to my projects and took the time to teach me throughout this experience. You have all been essential to shaping my path in research and into my future endeavours.

AUTHOR ATTRIBUTION STATEMENT

The results presented in this thesis are the product of a significant collaborative effort across several groups that was essential to achieving the aims of this project. However, I, along with my primary supervisor James Chong and broader supervisory team, was responsible for conceiving and designing all experiments along with coordinating, negotiating, and following up with collaborators when specific expertise was required. All Chapters of this thesis are presented as traditional thesis chapters.

Chapter 2: This chapter was carried out in collaboration with the Harvey Laboratory at The Victor Chang Cardiac Research Institute, Darlinghurst. The experimental plans for this chapter were conceived by myself, my primary supervisor James Chong, and co-supervisor Richard Harvey. The *in vivo* component of this chapter was carried out in collaboration with Vikram Tallapragada of the Harvey Laboratory. Vikram collected the echocardiography data that I then analysed. Vikram and I in addition to Vaibhao Janbandhu also of the Harvey laboratory carried out tissue collection following the *in vivo* experiments. I carried out all histology and immunohistochemistry experiments. The proteomics carried out for this chapter was performed at the Sydney Mass Spectrometry facility at the Charles Perkins Centre. My co-supervisor Robert Hume provided invaluable expertise in the analysis of our proteomics data.

Chapters 3 and 4: These chapters were carried out in collaboration with the Payne Laboratory at the University of Sydney School of Chemistry, Sydney, and the Harvey Laboratory at The Victor Chang Cardiac Research Institute, Darlinghurst. The design of all peptides in these chapters were the result of a collaboration between myself, James Chong, Richard Payne, Daniel Ford, and

Richard Harvey. Richard Payne and Daniel Ford were essential to the development of the peptides used in this chapter and carried out all synthesis of peptides used in this work. The experimental plans were conceived by my primary supervisor, James Chong and I and we were responsible for coordinating the collaborative efforts of this project. My co-supervisor Richard Harvey also provided valuable expertise in the planning of experiments for this project. I carried out all the *in vitro* assays in chapter 2. Among these was the proliferation assay that also involved technical expertise from Osvaldo Contreras of the Harvey Laboratory. The *in vivo* work was carried out with Vikram Tallapragada who performed all surgeries and collected all echocardiography data in this chapter. The echocardiography was then analysed by myself and Sul Ki Kim of the Chong Laboratory, who acted as a second observer for inter-observer variability analysis. All histology experimental work for the toxicity studies was carried out by myself and then analysed by Alan Marcus of the Chong Laboratory. Blood profiling was completed by Idexx Laboratories.

Collaborating Institutes

1. School of Chemistry, The University of Sydney, Sydney NSW 2006
2. Victor Chang Cardiac Research Institute, Darlinghurst, NSW 2010, Australia
3. Sydney Mass Spectrometry, Charles Perkins Centre, The University of Sydney, Sydney NSW 2006

In addition to the statements above, in cases where I am not the corresponding author of a published item, permission to include the published material has been granted by the corresponding author.

Emily McKinna

September 2023

As supervisor for the candidature upon which this thesis is based, I can confirm that the authorship attribution statements above, and the chapter specific statements, are correct. Sincerely,

A/Prof James Chong

Primary supervisor

September 2023

PUBLICATIONS, PRESENTATIONS AND SCHOLARSHIPS

Publications

James Chong, **Emily McKinna**, Richard James Payne, Daniel Ford, Richard Harvey. Novel platelet derived growth factor peptide mimetic. PCT/AU2023/050866. *(Patent).*

Presentations

Emily McKinna, Vikram Tallapragada, Vaibhao Janbandhu, Robert Hume, Richard Harvey, James Chong. Rodent Model of Heart Failure with Preserved Ejection Fraction. *Westmead Hospital Week Research Symposium 2021 (Poster Presentation*).

Emily McKinna, Daniel Ford, Vikram Tallapragada, Robert Hume, Richard Payne, Richard Harvey, James Chong. Development of Novel Mimetic Peptides for the Treatment of Heart Failure. *Paul Korner Seminar 2022 – The Victor Chang Cardiac Research Institute (Oral Presentation).*

Scholarships

University of Sydney Research Training Program Scholarship (2019-23)

Total $116,837

Sydney Medical School, Postgraduate Research Support Scheme Scholarship (2020-22)

Total $1,756.59

TABLE OF CONTENTS

FIGURES

TABLES

ABBREVIATIONS

a.u.	Arbitrary Units
ACE	Angiotensin Converting Enzyme
ACOT2	Acyl-CoA Thioesterase 2
AkT	Protein Kinase B
BCA	Bicinchoninic Acid Assay
CAA	Chloroacetic acid
CCA	Collagen Contraction Assay
CVD	Cardiovascular Disease
DAVID	Database for Annotation, Visualisation, and Integrated Discovery
DMEM	Dulbecco's Modified Eagle's Medium
DOCA	Deoxycorticosterone acetate
DSS	Dahl Salt Sensitive
ECM	Extracellular Matrix
EdU	5-ethynyl-2'-deoxyuridine
EDV	End Diastolic Volume
EF	Ejection Fraction
Erk	Extracellular Signal Regulated Kinases
ESC	Embryonic Stem Cells
ESV	End Systolic Volume
FBS	Foetal Bovine Serum
Fc	Fragment Crystallisable
FcRN	Fc Neonatal Receptor
GLP	Good Laboratory Practice
GLS	Global Longitudinal Strain
GO	Gene Ontology
HCAEC	Human Coronary Artery Endothelial Cell
HE	Haematoxylin and Eosin
HFD	High Fat Diet
HFpEF	Heart Failure with Preserved Ejection Fraction
HFrEF	Heart Failure with Reduced Ejection Fraction
HILIC	Hydrophilic Interaction Liquid Chromatography
HLB	Hydrophilic-Hydrophobic-Balanced
HSA	Human Serum Albumin
IgG	Immunoglobulin G
iPSC	Induced Pluripotent Stem Cells
IB4	Isolectin B4
kDa	Kilodaltons
L1	Loop I
L2	Loop II
L3	Loop III
LA	Left Atria

LC-MS/MS	Liquid Chromatography-Tandem Mass Spectrometry
L-NAME	L-Arginine Methyl Ester
LV	Left Ventricle
LVEDV	Left Ventricular End Diastolic Volume
LVESV	Left Ventricular End Systolic Volume
MI	Myocardial Infarction
MP	Mid-Papillary
MS	Mass Spectrometry
NC	Normal Chow
NGS	Normal Goat Serum
NTC	No Treatment Control
pAkT	Phosphorylated Protein Kinase B
PBS	Phosphate Buffered Saline
PBST	Phosphate Buffered Saline- Tween
PD	Pharmacodynamics
PDGF	Platelet Derived Growth Factor
PDGFR	Platelet Derived Growth Factor Receptor
PDH	Pyruvate Dehydrogenase Complex
PSC-CM	Pluripotent Stem Cell Derived Cardiomyocytes
PDH	Pyruvate Dehydrogenase
Pdk4	Pyruvate Dehydrogenase Kinase 4
PEG	Polyethylene Glycol
pErk	Phosphorylated Extracellular Signal Regulated Kinases
PFA	Paraformaldehyde
PK	Pharmacokinetics
Plin5	Perilipin 5
PSRFG	Picrosirius Red and Fast Green
RA	Right Atria
rh	Recombinant Human
RIPA	Radioimmunoprecipitation Assay
RV	Right Ventricle
SD	Standard Deviation
SDC	Sodium Deoxycholate
SDS-PAGE	Sodium Dodecyl-Sulfate Polyacrylamide Gel Electrophoresis
SEM	Standard Error Mean
TAC	Transverse Aortic Constriction
TCEP	Tris(2-carboxyethyl) phosphine
TMT	Tandem Mass Tagged
UPLC	Liquid-chromatography Mass Spectrometry
VPR	Volume Pressure Ring
WGA	Wheat Germ Agglutinin

CHAPTER 1: LITERATURE REVIEW

1.1 INTRODUCTION

Cardiovascular Diseases (CVD) are the world's leading cause of morbidity and mortality. This is largely due to the hearts limited regenerative capacity making it especially susceptible to damage from both acute injury and chronic disease states. The hearts limited self-repair in the face of this damage frequently results in the development of heart failure that now has a 5-year mortality rate of approximately 50% (1). Significant efforts in minimising the prevalence of CVD and novel treatments combined with prevention strategies have resulted in a decrease in CVD mortality (2). However, to this date we have failed to successfully translate a method of reversing the damage of heart failure to the clinic and as a result CVD still accounts for over 17.8 million deaths annually (3).

1.2 HEART FAILURE

Myocardial infarction (MI) occurs when there is a complete or partial blockage in blood flow and oxygen to the heart. In many cases this blockage ruptures spontaneously, however in cases where clinical intervention is necessary, the prolonged blockage may result in death of cardiomyocytes and necrosis of the heart wall. Due to the limited self-renewal of mature cardiomyocytes this necrotic tissue is cleared by the immune system and replaced by a collagen rich scar tissue in the form of cardiac fibrosis (4). This damage to the heart during a myocardial infarct and subsequent scar formation is one of the primary causes of heart failure. Heart failure is a chronic condition that occurs when the heart is unable to pump blood effectively, either in diastole (filling) or systole (pumping) (5).

1.3 CARDIAC FIBROSIS

The collagen rich scar that occurs post-MI is made up of fibrous connective tissue that forms when there is an over production of extracellular matrix (ECM), composed of cells, fibrotic proteins, and proteoglycans (6). This development of fibrous tissue occurs in multiple organ systems and is an integral component of wound healing (7) Whilst its immediate effect is beneficial, chronic fibrosis can result in irreversible damage to organs impairing their function, leading to the development of a variety of disease states (8-10). In the context of the heart, chronic fibrosis results in ventricular remodelling, significantly impairing cardiac function (5). Cardiac fibrosis is a key component in the progression of several types of heart failure because of its stiff structure and limited contractility, resulting in significantly impaired heart function (11).

The three types of cardiac fibrosis are replacement fibrosis, interstitial fibrosis, and perivascular fibrosis. Replacement fibrosis occurs in the scar that forms after MI in the place of cardiomyocytes lost to ischemia. Interstitial fibrosis and perivascular fibrosis are frequently found together and can be the result of several factors including ageing, obesity, hypertension, and diabetes. Interstitial and perivascular fibrosis occur when there is increased deposition of the ECM within the interstitium and around blood vessels, respectively (12). This fibrotic ECM in the heart is primarily made up of fibrillar collagens with approximately 90% collagen I and 5% collagen III (13). These collagens are very stiff with high tensile strength providing structural support to the myocardium. However, in large quantities this also impairs its contractility (14, 15). Collagen III is typically more elastic than collagen I and can be found in different ratios in replacement and interstitial fibrosis. Collagen III is found more abundantly in interstitial fibrosis than it is in replacement fibrosis (15). A key difference between replacement and interstitial

fibrosis is that whilst replacement fibrosis is considered to be irreversible, interstitial fibrosis has been reported as reversible when the source of mechanical stress on the heart has been removed (16, 17). The ECM of the myocardium constantly remodels in response to changes in fibroblast activation, the activity of immune cells and presence of proteolytic enzymes. These changes are also present in fibrotic regions of increased ECM deposition. Removal of mechanical and metabolic stressors can result in positive remodelling of the myocardium in the instances of interstitial and perivascular fibrosis. This potential for positive remodelling and the role it plays in the development of heart failure makes fibrosis and the ECM an attractive target for novel therapies.

1.4 HEART FAILURE WITH PRESERVED EJECTION FRACTION

Heart failure with reduced ejection fraction (HFrEF) accounts for approximately 50% of reported heart failure cases (18), and often occurs as a result of a MI given the burden of ischemic heart disease. Traditionally, this was the most prevalent form of heart failure however, in more recent years another type of heart failure has become more widely recognised. Heart failure with preserved ejection fraction (HFpEF) is observed in the remaining 50% heart failure patients (19). However, it is widely believed that this is a notoriously underdiagnosed condition which would suggest its incidence is much greater than currently recorded (20) and is increasing at an estimated 1% per year (21). HFpEF is heart failure with ejection fraction above 50% whilst HFrEF patients have an ejection fraction below 50%. Ejection fraction is a measure of the percentage of blood pumped out of the left ventricle. The decrease in left ventricle filling pressure results in a smaller volume of blood entering the left ventricle and therefore, a decreased volume of blood that's pumped out through the aortic valve.

Impaired cardiac function in HFpEF is associated with cardiac fibrosis and hypertrophy inhibiting the heart's ability to pump blood (22). This is caused by remodelling of the myocardium in response to metabolic and mechanical stress often related to comorbidities, commonly obesity and hypertension (23). Concentric hypertrophy develops in HFpEF due to the increase in left ventricle wall thickness and a diminished capacity as a result of pressure overload on the left ventricle (24).

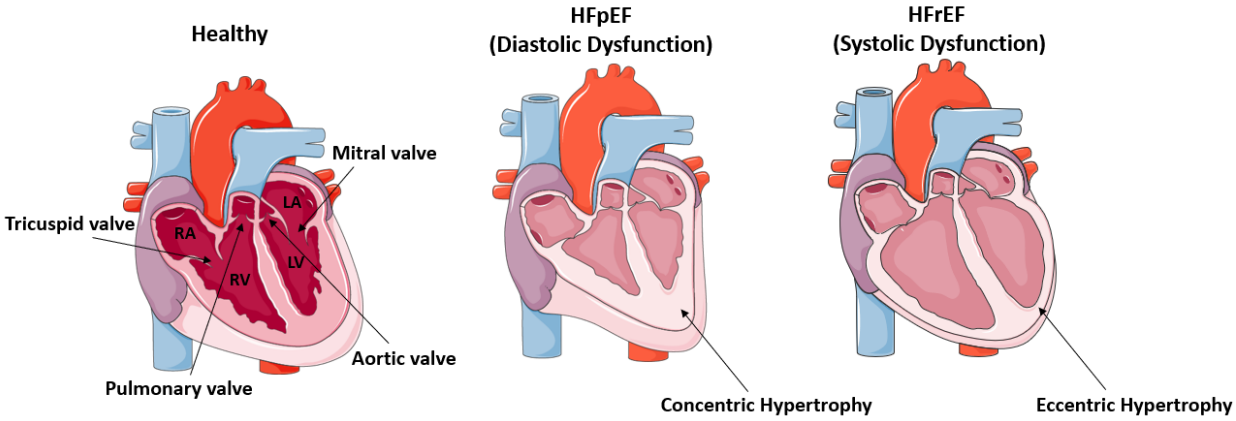

Figure 1.1: Heart failure pathophysiology.

Healthy heart anatomy – right atrium (RA), left atrium (LA), right ventricle (RV), and left ventricle (LV) and the four valves of the heart. HFpEF heart anatomy presenting with concentric hypertrophy. HFrEF heart anatomy presenting with eccentric hypertrophy.

Several parameters are measured via echocardiography to assess diastolic function. These include E/A ratio, E/e', left atrial volume and tricuspid regurgitation velocity (20). E/A ratio measures the flow velocity from the left atrium into the left ventricle, visualised using flow doppler imaging. The E wave (Figure 2A) measures passive filling in early diastole whilst the A wave measures peak flow velocity in late diastole. The E wave measurement is also used as a ratio with the e', measuring the tissue velocity of the mitral valve annular. The E wave will decrease as the filling pressure of the left ventricle decreases while there will be an increase in the A wave and left atrial volume. The left atrial volume increases due to pressure overload in the left ventricle requiring the left atria to compensate. The last of these parameters is tricuspid

regurgitation velocity which measures blood flow back up into the left atrium from the left ventricle. The combination of these parameters provides an accurate assessment of left ventricle filling pressure and diastolic function (20).

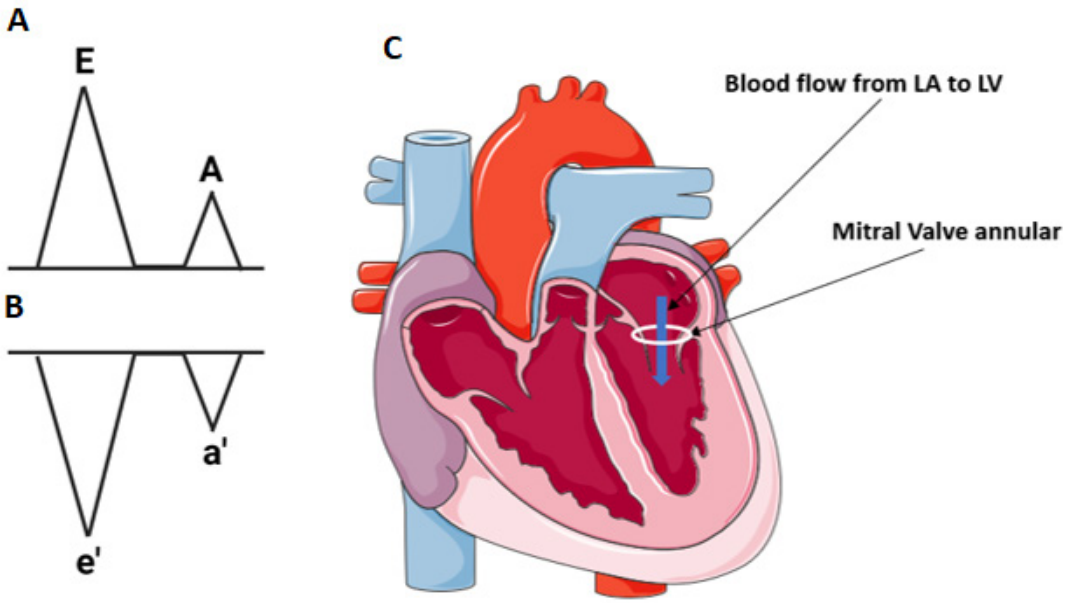

Figure 1.2: Echo parameters for diastolic dysfunction.

A) Schematic of normal E and A waves. Measuring flow through the mitral valve. B) Schematic of normal e' and a', indicating tissue velocity at the mitral valve annular. C) Heart anatomy identifying regions where diastology measurements are taken. Panels A and B adapted from (25).

Despite differing effects on left ventricular function, they both result in a reduction in blood flow to the body. The established key differences between HFrEF and HFpEF are ejection fraction, hypertrophy, comorbidities, risk factors and histology. Whilst clinical differences between HFpEF and HFrEF have been well defined, the molecular differences and similarities between the two phenotypes is not fully understood. This has contributed to an absence of treatment options available to HFpEF patients.

1.4.1 Heart Failure with Preserved Ejection Fraction Treatment

The lack of treatment options available to heart failure patients is a problem that researchers have attempted to address since the mid-20th century. The development of beta blockers and ACE inhibitors for heart failure treatment have significantly reduced mortality rates by 32% (26) and 22-26% (27), respectively. Despite the significant effect they have had on mortality rates and re-hospitalisation in HFrEF patients, neither have been able to reverse the damage of heart failure. Whilst successful in HFrEF patients, these treatments have been proven ineffective in HFpEF patients with all HFpEF clinical trials to date failing to meet primary endpoints. Additionally, patients in clinical trials tend to be younger with fewer comorbidities contributing to the concern that patients in the clinic would likely have poorer outcomes, further emphasising the need for novel therapies to treat HFpEF. This has contributed to a significant gap between mortality rates of HFrEF and HFpEF patients with 5-year mortality rates sitting at 25% (18) and 53%-74% (28) respectively.

Adding to the complexity of HFpEF is that approximately 50% of patients have 5 or more major comorbidities, resulting in a heterogenous patient population. Whilst this heterogeneity of the HFpEF patient population is a significant contributor to its lack of treatment options, another major factor is the absence of appropriate animal models. Animal models that more accurately reflect the HFpEF phenotype would provide a better understanding of the complex syndrome and how it differs from HFrEF, allowing for the development of viable novel therapies.

1.4.2 *In vivo* Models of Heart Failure with Preserved Ejection Fraction

HFpEF clinical trials have only recently begun to achieve their clinical endpoints and the number of successful trials remains low (29). This problem is partly attributed to our lack of accurate disease models. HFpEF affects multiple organ systems, often presenting with pulmonary oedema, renal dysfunction, and cardiac fibrosis. This makes it an especially difficult disease to replicate in animal models, limiting our ability to fully understand the pathophysiology of this disease and develop new treatments. Groups have attempted to replicate the disease in mice (30), rats (31) and hamsters (32), using a variety of methods to induce HFpEF. However, most of these have received significant criticism due to their inability to encapsulate the wide range of affected organ systems whilst successfully distinguishing HFpEF from HFrEF. Based on the current understanding of HFpEF an accurate animal model needs to have maintained left ventricle systolic function with diastolic dysfunction, hypertension, exercise intolerance, pulmonary oedema, and concentric cardiac hypertrophy. Furthermore, some groups also aim to establish renal dysfunction. Early models of HFpEF focused on a single aspect of the disease, typically one of its common comorbidities such as hypertension (33) or obesity (34). Whilst these models fall short of what is required in an accurate model, they have provided us with a strong foundation on which to develop clinically relevant models of HFpEF.

1.4.2.1 Surgically Induced Models of Heart Failure with Preserved Ejection Fraction

Hypertension is the most frequently identified comorbidity of HFpEF occurring in as many as 60% of patients (35). A common method of inducing hypertension as a model of HFpEF is through transverse aortic constriction (TAC), first developed as a pressure overload model for hypertension (33). TAC rodents are the most well-established model of HFpEF however, are also the most heavily criticised. Whilst hypertension is a key component of HFpEF and is necessary

in an accurate model of the disease, a model of hypertension does not fulfil the criteria for an accurate model of HFpEF. Therefore, TAC is more accurately a model of hypertension, not one of HFpEF.

1.4.2.2 Diet Induced Models of Heart Failure with Preserved Ejection Fraction

Dahl Salt Sensitive Rats

Another well established and common method of inducing HFpEF in rodents is a diet-based model, often using Dahl Salt Sensitive (DSS) rats. DSS rats were selectively bred from Sprague Dawley rats resulting in a population of rats that were prone to salt induced hypertension. DSS rats are fed a high-salt diet for a period of 16-20 weeks at which point they present with hypertension, pulmonary oedema, and cardiac hypertrophy (36). Whilst this is a reliable model in producing aspects of heart failure it does not develop all the physiological characteristics necessary when modelling HFpEF. Additionally, it has been reported to induce HFrEF in some cases, not successfully distinguishing between these two different forms of heart failure. This is especially significant given that progression from HFpEF to HFrEF is uncommon in humans, with there being very little clinical evidence that this process takes place (37).

Obesity Models of Heart Failure with Preserved Ejection Fraction

Obesity is a frequently observed comorbidity of HFpEF with over 80% of patients being overweight or obese (38). The increased mechanical load associated with obesity is known to contribute to the inflammation, exercise intolerance, arterial and skeletal muscle dysfunction along with a loss of ventricular function seen in patients diagnosed with HFpEF (39). This provides compelling evidence that an obesity model could be used to replicate HFpEF in small

animals. As a result, obesity models have been tested in this context (34, 40). Whilst many of these have been successful in replicating the weight gain, glucose intolerance and maintained ejection fraction seen in HFpEF, they often fall short of an accurate disease model. Hamdani et al. reported that following a 20-week high fat diet, obese ZSF1 rats had developed HFpEF based on renal dysfunction, diastolic dysfunction, pulmonary oedema, and the onset of hypertension. Whilst these are all sound markers of HFpEF development, further analysis indicated that diastolic dysfunction had occurred because of titin modification rather than the formation of interstitial fibrosis. Although this model may initially appear to be an accurate model of HFpEF, the absence of interstitial fibrosis is a significant flaw in its clinical relevance.

1.4.2.3 Pharmacologically Induced Models of Heart Failure with Preserved Ejection Fraction

Deoxycorticosterone Acetate (DOCA)

Deoxycorticosterone acetate (DOCA) is a steroid hormone that has been combined with high salt intake to induce HFpEF in a variety of murine models. Whilst unsuccessful when used alone, DOCA-high salt treatment, first developed a model of hypertension, has been successful in inducing hypertension, renal fibrosis, interstitial and perivascular fibrosis resulting in diastolic dysfunction (41, 42). Following a unilateral nephrectomy, DOCA pellets are implanted subcutaneously in the rodent prior to high salt intake by replacing their drinking water with a 0.9% saline solution. Eight weeks post commencement of DOCA-salt treatment the rodents present with hypertension, cardiac hypertrophy, fibrosis and reduced diastolic function. This model was later modified to more accurately replicate HFpEF (43) by incorporating aortic banding with the previously established protocol. Whilst combining the DOCA-salt model with aortic banding increased the hypertrophy and fibrosis of the left ventricle, the acute nature of

aortic banding to induce pressure overload on the left ventricle limits its clinical relevance. Despite this model successfully developing several key components of HFpEF, it is a high-risk model with the need for a unilateral nephrectomy (44) or aortic banding (45, 46) to develop a more accurate phenotype while still failing to reflect the complex nature of HFpEF.

Nitro-L-arginine-methyl-ester (L-NAME)

Nitro-L-arginine-methyl-ester (L-NAME) is a nitric oxide synthase inhibitor that is known to increase blood pressure (Kung et al 1995) and has been explored as a potential treatment for hypotension (47). As a result, it has been heavily utilised to induce hypertension in murine models. Pechanova et al. reported that absorption of L-NAME through drinking water over a period of four weeks, an increase in systolic blood pressure, significant myocardial fibrosis, and increased left ventricle size was observed. (48). Whilst this original publication did not feature cardiac functional outputs, later work expanded on this. Using L-NAME to achieve the same development of hypertension and cardiac fibrosis, the group also showed maintenance of left ventricle ejection fraction and a decrease in left ventricular diastolic volume (LVEDV) (49). Whilst L-NAME alone has not been successfully used to induce HFpEF, its effects on blood pressure and cardiac remodelling are well established.

1.4.2.4 "Two Hit" Approach

Whilst all these models have been able to induce some aspects of HFpEF, by focusing on a specific aspect of the disease they have been unable to recapitulate the full range of symptoms. Given the complexity of this condition, approaching it from one specific component can limit the accuracy and clinical relevance of the model. To improve on previous models, groups have incorporated multiple approaches in developing clinically relevant models of HFpEF. One key

example of a two-hit approach to induce HFpEF in a small animal model was reported by Schiattarella et al (50). The study induced HFpEF in C57BL/6N wild type mice via a 60% fat from calories diet and absorption of L-NAME fed to them through their drinking water at a concentration of $0.5gl^{-1}$. Mice were separated into three groups; one which received a high fat diet (HFD), another that received L-NAME, and the last group receiving a combination of both. An increase in weight and glucose intolerance was observed in the HFD group, while an increase in systolic and diastolic blood pressure was present in the L-NAME group. All three groups showed preserved ejection fraction as seen via echocardiography, whilst the combination group also presented with elevated left ventricular filling pressures and increased lung weight suggesting pulmonary oedema was induced. These results are consistent with the onset of HFpEF seen clinically. Whilst this a relatively new model in the field it has since been reproduced by others in the field, investigating HFpEF on a molecular level (51).

New *in vivo* models of HFpEF that accurately reflect the complex syndrome are required to fully understand the pathophysiology of the HFpEF phenotype at a molecular level. Whilst early models of HFpEF failed to accurately reflect the HFpEF phenotype, the newly published "Two Hit" approach to HFpEF has presented the field with a promising animal model for further investigation. Following validation, this model could provide us with novel insights into the molecular mechanisms driving HFpEF and highlight potential therapeutic targets.

1.4.3 Novel Therapies for Heart Failure with reduced Ejection Fraction

The development of pharmacologic interventions in cardiology has demonstrably reduced mortality of HFrEF (52). However, mortality rates remain high due to limited treatments that are able to reverse damage and restore cardiac function following large myocardial infarcts that

result in severe cardiac dysfunction. Although heart transplantation and ventricular assist devices are an option, limitations on organ supply and risks associated with these treatments mean that this is not a viable treatment option for most patients. Promising results have been seen in the pre-clinical space following extensive research. However, none of these have been successfully translated to the clinic. These include gene therapy (53) cytokine therapies (54) and cell-based therapies (55). Whilst gene therapies have had very promising pre-clinical results, they have up to this point failed to translate to the clinic. Contrary to this, stem cell therapies showed substantial promise in pre-clinical studies. Adult Stem Cell Therapies have been trialled in numerous Phase 3 clinical trials but with largely negative findings (56). Separately, a new generation of stem cell therapies using Pluripotent Stem Cells is just beginning with significant commercial interest, allowing them to progress to phase I clinical trials (56). Interestingly, there has been some suggestion that paracrine effects secreted from transplanted Adult Stem Cells may be having favourable effects on cardiac function. This raises protein therapy as an alternative to stem cell therapies. Platelet derived growth factor (PDGF) is a recombinant human protein that has been explored in small and large animal models of cardiac dysfunction (57, 58) Furthermore, it has been successfully translated to the clinic as an FDA approved treatment for chronic non healing wounds, in addition to musculoskeletal and maxillofacial disorders (59-61).

1.4.4 Cell Based Therapies

Cell based therapies for cardiac regeneration have predominantly focused on the use of pluripotent stem cells and mesenchymal stromal cells. Whilst early developments in the field were in cells of mesenchymal origin (62), the most notable recent reports utilised pluripotent embryonic stem cells (ESCs) (55, 63, 64) with those results then translated into induced pluripotent stem cells (iPSCs) (65). Early differentiation protocols (66-68) demonstrated the

ability to differentiate functional cardiomyocytes from ESCs. This work led into small animal murine models applying pluripotent stem cell derived cardiomyocytes (PSC-CMs) as a treatment post infarct (63, 69). This was followed by the first studies successfully engrafting human PSC-CMs into the hearts of non-human primates (55) that later demonstrated improved cardiac function (70). Despite these promising results, PSC-CMs as a therapeutic had limitations preventing its translation to the clinic. In addressing these, significant efforts have been made to prolong the survival of PSC-CMs (71), enhance engraftment into the native myocardium, and address the downstream arrythmia burden of grafted cells (72, 73). The culmination of these efforts have resulted in approval of the first PSC-CM clinical trials in humans, as well as the successful garnering of commercial support (74).

1.4.5 Protein Therapies

Protein therapeutics have become increasingly popular across multiple fields in medical research (75-77) since its first introduction to the clinic, outside of antibodies, with the use of recombinant human insulin (78). Whilst they have been less popular in cardiac regeneration than cell-based approaches, the shift towards the approval and application of protein therapies in pharmaceutical development presents the opportunity to advance lead candidates in cardiovascular protein therapies towards the clinic (79). Amongst these lead candidates are various endogenous growth factors that are aimed at modulation of the ECM and immune response, increasing angiogenesis, and protection of the remaining cardiomyocytes post-infarct. Whilst early clinical trials in this space were unsuccessful (80-82), others delivered promising results (83, 84) in addition to emerging lead candidates in more recent pre-clinical studies (57, 85). Developments in protein engineering have expanded the opportunities to progress these promising experimental therapies towards the clinic.

1.5 PLATELET DERIVED GROWTH FACTOR

Platelet derived growth factors (PDGFs), first reported in 1978, are a group of proteins that act as ubiquitous mitogens regulating cell proliferation and growth (86-88). PDGFs are dimeric glycoproteins made up of two peptide chains connected via a disulphide bond creating either a heterodimer or homodimer, depending on its isoform. Potential isoforms are AA, BB, AB, CC, and DD; the A and B chains were identified first (89), followed by C (90) and D (91) in later reports. PDGF signalling plays a significant role in embryonic development, while in adults it is predominantly implicated in disease states including inflammation, atherosclerosis (92), fibrosis (93), wound healing (94), and cancer (95). Early work on PDGF focused on its effects on cell growth, where it was reported to increase proliferation of endothelial cells (88), smooth muscle cells (87) and fibroblasts (86) *in vitro*. The role of PDGF in angiogenesis was also identified early with increased PDGF signalling linked to vascularisation of connective tissue in tumours (96). Continuing from this, PDGF was reported to facilitate tube formation of endothelial cells in *in vitro* 3D assays (88, 97). PDGF is also a well-established mediator of chemotaxis demonstrated both *in vivo* in smooth muscle cells (98) and *in vitro* in neutrophils, monocytes (99), fibroblasts (100, 101), and endothelial cells (102). PDGF has been heavily investigated and its structure and biological functions are well understood, providing a strong foundation for continuing work utilising these functions for various applications of PDGF.

1.5.1 Platelet Derived Growth Factor Receptors

PDGF functions by binding with PDGF receptors (PDGFR) (89) on the cell surface. PDGFs bind with the PDGFR ligand binding pocket, located in the second and third immunoglobulin domain. The receptors dimerise and are then activated by autophosphorylation of tyrosine and threonine residues at key sites within the cytosolic domain (103). This results in the downstream activation

of several key cellular pathways mediating cell growth. These include extracellular signal-regulated kinases/mitogen-activated protein kinases (Erk/MAPK) (Figure 1.3) which initiates proliferation, cell survival, angiogenesis, and chemotactic activity of cells (104). The receptor subunits are α and β which dimerise in the combinations: αα, ββ, and αβ. PDGF-BB, -AA, and -AB can all bind with PDGFRα (89) whilst only PDGF-BB and -AB can bind with high affinity to PDGFRβ (89, 105).

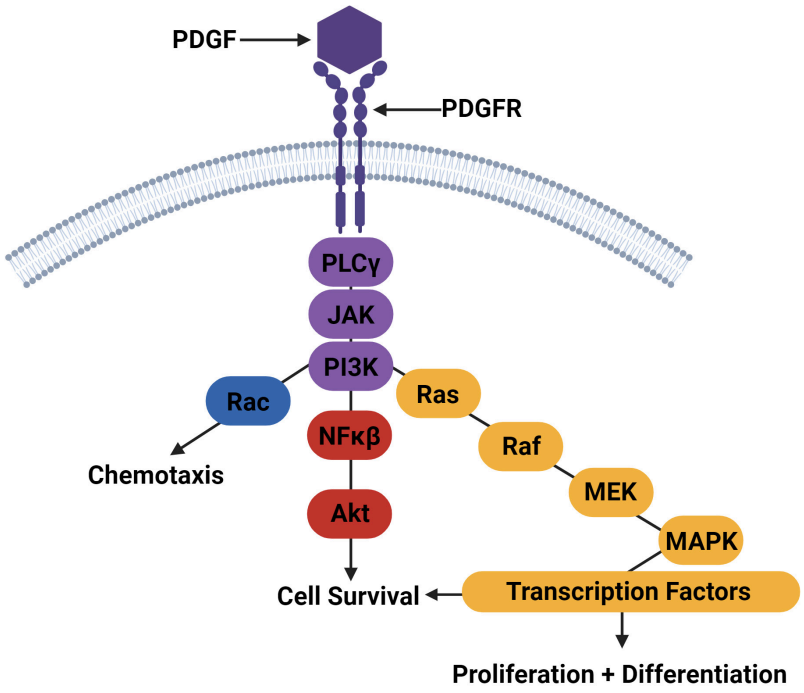

Figure 1.3: PDGF receptor signalling pathway.

Adapted from Evrova et al (106).

A key difference between the α and β receptors is that the PDGFRα is conformationally smaller and containing fewer specific residues at the ligand receptor interface. PDGFRβ contains increased numbers of aromatic residues at the ligand binding surface whilst their counterparts within PDGFRα are less aromatic (107). This results in increased versatility in the PDGFRα receptor allowing more isoforms to be bound. The only isoforms able to bind to the β receptor is the B chain whilst the A and B chains can bind to the α receptor (Figure 1.4). PDGF-BB is

reported as the most potent of the three heavily studied isoforms, AA, BB and AB (108). The PDGF-AB chain is reported to have an intermediate effect whilst PDGF-AA has the least potency *in vitro* (109). The versatile receptor binding ability of the B chain is believed to be the likely cause of this.

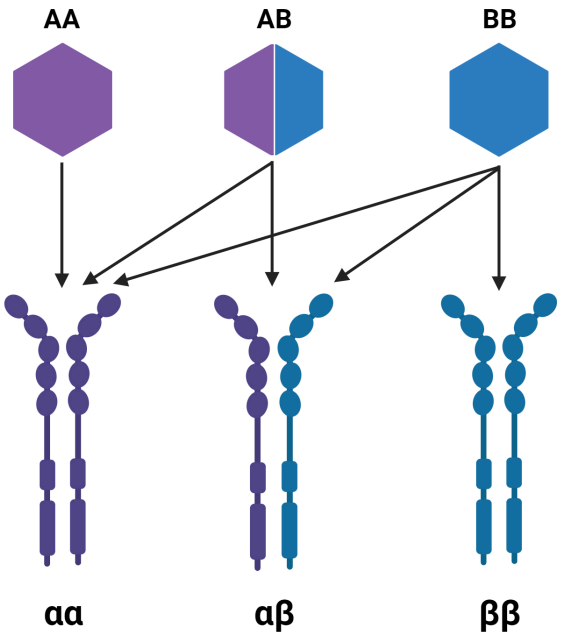

Figure 1.4: PDGF receptor binding combinations.

The PDGF-A chain contains only a binding site for the α receptor limiting its binding to the αα receptor only, the B chain contains binding sites for both the α and β receptors, allowing it to bind to all three receptor dimers. Adapted from Donovan et al (110).

PDGFRα plays a major role in gastrulation and the development of several key organs including the lungs (111), kidneys (90), testes (112), skin (113), and bones (114). PDGFRβ also plays a key role throughout foetal development as a regulator of early haematopoiesis and angiogenesis (115). Despite their significant role in development, PDGFs are tightly controlled in adults outside of wound healing with abnormal upregulation of PDGF being associated with several disease states including cancer (116), fibrosis (93), and inflammation (92). Of the two receptors,

the β receptor has been more frequently implicated in metastasis of tumours which has made it a common target in PDGF positive tumours, largely through the development of tyrosine kinase inhibitors. PDGF and its receptors have been linked with tumorigenesis due to roles in mitogenesis and angiogenesis. Importantly, whilst there is a correlation between increased PDGF signalling and metastasis of some tumours, PDGF alone is not sufficient to induce a tumour phenotype (117). Despite concerns about its role in tumorigenesis the primary functions of PDGFR signalling are in normal and vital physiological processes including as an essential mediator of wound healing.

1.5.2 Protein Structure

The PDGF family is characterised by a cysteine knot structural motif and rotaxane substructure which make up part of the 8 cysteines present in all single chains Oefner, D'Arcy (118), (119). The most abundant of these is the PDGF A and B chains that are 125 and 109 amino acids in length, respectively. Both single chains are made up of four beta sheets linked by three loops that each contribute to an aspect of PDGFs functions (120), seen below in Figure 1.5. In all PDGF chains, loops I and III contribute to receptor binding and activation, whilst loop II is crucial to dimer formation (120-122). The most highly conserved region within these is the VRKKP sequence located in both the A and B chain. Given that the VRKKP sequence is the only identical sequence between the two chains and both chains have binding affinity with the α receptor, it was initially identified as responsible for binding the α receptor. Significant binding affinity to the α (123) and β (124) receptors for both the A and B chains were then later attributed to the RKK sequence found within this region (123, 125).

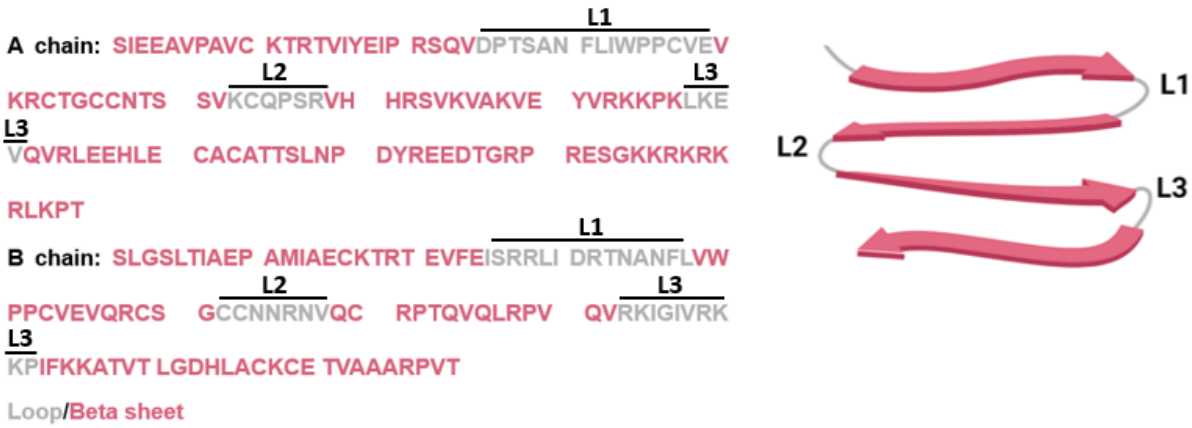

Figure 1.5: PDGF amino acid sequence and structure.

The four beta sheets of the A and B chains are linked by 3 loops. When folded in its normal structure loops I and III are conserved at one end. (L1 = loop I, L2 = loop II, and L3 = loop III).

The highly conserved RKK region has been associated with most key functions of the chain. The structure of loop III is seen above in Figure 1.5. PDGF-B loop III contains 10 amino acids, of which half have been directly linked to receptor activation, receptor binding or mitogenic activity *in vitro*. Several reports of modifying amino acids within loop III of the B chain have resulted in a reduction in receptor binding affinity or a change in binding specificity (120, 124, 126). Examples of this include switching of the first isoleucine to a tyrosine residue altering specificity of binding to the receptors (124). Similar examples exist in loop III of the A chain where replacement of the alanine to an arginine residue at the start of sequence switched receptor binding from the α receptor to the β receptor (126). Whilst loop III of the PDGF B chain has been attributed to mitogenic activity in addition to receptor binding and activation of both the α and β receptors, loop I is reported to maintain similar functions, to a lesser extent (120).

1.5.3 Clinical Applications of Platelet Derived Growth Factor

PDGF's role in mitogenesis and chemotaxis has been utilised in experimental treatments for diseases including chronic ulcers (127), bone remodelling (128) and cardiovascular diseases (57). Despite PDGF's position as a target for treating metastatic cancers, PDGF-BB is considered safe for therapeutic use. As a result, it has been approved by the FDA for clinical use in the treatment of musculoskeletal and maxillofacial disorders (129) along with chronic non-healing diabetic ulcers in topical form (REGRANEX/Becaplermin) (130). In the instance of Becaplermin, the associated companies published a warning that an increased incidence of tumours of a variety of types distal to the site of application were found associated with patients receiving 3 or more tubes of REGRANEX gel (0.01%) (131). This supports potential tumorgenicity of chronic administration of PDGF but does not suggest that low, short-term doses of PDGF would induce tumour growth. Downstream cohort studies on users of Becaplermin investigated the relationship between its use and incidences of metastatic cancers, finding that there was no significant link between the two (132). Further supporting this, it has been reported that whilst an upregulation of PDGF receptor signalling has been associated with an increased risk of metastases, PDGF alone is not capable of inducing a tumour phenotype (117). These therapeutics present the opportunity to pursue transient increases in PDGFR signalling as a method of stimulating wound healing processes and reducing inflammation in a variety of disease states.

1.5.4 Platelet Derived Growth Factor Analogues

Several PDGF based peptides have been developed, intended for application in atherosclerosis or other undisclosed clinical uses however, none of these peptides have ever been successfully translated (133-135). The previously discussed loop III region of the PDGF-B chain was a key

landmark in these developments providing evidence that this region is capable of functioning outside of the full-length protein structure *in vitro*.

An example of this was the development of 19 analogues based on the loop I and III regions of the PDGF-B chain (135) that were established as anti-proliferative agents. Here, analogues were reported to have receptor binding ability that was comparable to full length PDGF. In addition, another PDGF based peptide was later published in 2007 by Zamora et al. It also utilised the loop III region of the PDGF-B chain dimerised and was bound to a novel heparin binding domain (133) (134). The peptide, PBA2-1c, had comparable function to recombinant PDGF-BB in *in vitro* assays analysing proliferation, migration, and collagen contraction. PBA2-1c also was successful in activating the PDGFR via phosphorylation of Akt and Erk and binding to both the α and β receptors, confirmed by surface plasmon resonance. Whilst these both provide promising evidence of loop III's ability to function alone *in vitro*, neither group reported *in vivo* data, nor did they progress to the clinic. This highlights the potential to manipulate the PDGF chains for their biological function without maintaining the full ligand chains, however, also presents the need for further work to develop these analogues into clinically translation therapeutics.

1.5.5 Platelet Derived Growth Factor in the Heart

Fibroblasts play major roles in the ECM and paracrine signalling, and account for 12.7% of the total cells in the heart (136). As a major cell type within the ECM, they are essential for cardiac remodelling often in response to physiological changes, including exercise, and pathological changes in the form of injury such as a MI. A population of PDGFRα positive cardiac fibroblasts were first identified by Chong et al (137). The population of cells were colony forming fibroblasts of a proepicardial origin that maintained some stem cell like characteristics and were identified

in several cell types of mesodermal lineages. Co-cultures of PDGFRα+ cardiac fibroblasts with endothelial cells, smooth muscle cells, and cardiomyocytes showed significant effects of increased PDGFR signalling. Endothelial cells formed tubular networks in 3D Matrigel cultures, cardiomyocytes formed alpha actinin+ striated sarcomeres, and smooth muscle cells differentiated into myofibroblast like cells that were smooth muscle α-actin. The implications of this as a therapeutic remained unclear and further work was required to investigate the role these cells could play in enhancing cardiac regeneration post-MI.

Continuing from this, Asli et al. applied recombinant human PDGF-AB in a rodent model of acute MI (58). Immediately following a surgically induced MI via permanent ligation of the left anterior descending artery, mice were treated with PDGF-AB infused over a period of 5 days. Treatment with PDGF-AB increased proliferation, activation and self-renewal of cardiac fibroblasts resulting in improved cardiac function in addition to structural repair of the heart wall and scar seen in pro-regenerative effects on endothelial cells, cardiomyocytes, and fibroblasts. The promising effects of increased PDGFRα signalling is further supported by the effect of PDGF-AB on uninjured hearts. As an extension of this study, sham control mice underwent the same protocol excluding the surgically induced MI, which resulted in activation of quiescent fibroblasts without inducing proliferation. This study provided good evidence of recombinant PDGF-AB as novel therapy for cardiac injury and demonstrated the significant role of PDGFR signalling in cardiac repair and regeneration.

Whilst the early results of PDGF-AB in a murine model were promising, differences between rodent and human hearts, particularly on a cellular and molecular level necessitated validation of these effects in a clinically relevant large animal model. Achieving this, Thavapalachandran et

al. (2020) reported the use of PDGF as a treatment for heart failure in a pre-clinical porcine model of acute MI (57). PDGF-AB was administered at 65μg/kg immediately after reperfusion via an osmotic mini-pump, diffused over 7 days. Pigs treated with PDGF-AB showed a 40% improvement in survival, an 11.5% improvement in ejection fraction, along with improved myocardial contractility and enhanced angiogenesis. This study provided strong evidence using a large animal model to support PDGF-AB as a novel therapy for heart failure when administered post-acute MI. Interestingly, whilst there was an improvement in survival and cardiac function, the scar that formed post-infarct was not significantly different in size, regardless of treatment. Histological analysis identified increased collagen alignment within the scar indicating cardiac scar modulation as a possible mechanism for PDGF-ABs therapeutic effect post-MI. This was later supported by further investigation into the mechanisms driving this effect that highlighted the pleiotropic effects of PDGF-AB in this context (138). Notably PDGF-AB maintained therapeutic effects on post-MI scar despite a lack of increase in fibroblast proliferation. PDGFs role as a potent mitogen is well established (86-88) however, in this context reduced it myofibroblast differentiation and did not induce proliferation of fibroblasts resulting in no increase in fibrosis.

Despite very promising results in the rodent and pre-clinical porcine models, recombinant human PDGF-AB requires optimisation as a therapeutic to improve its prospects in clinical translation. These promising results at relatively low doses indicates high potency however, poor pharmacokinetic properties due to low plasma stability and small size. The very short half-life of PDGF, approximately 2 minutes (139), limits its delivery methods, requiring constant infusion over several days, and therefore requires improvement ahead of clinical translation. In addition to this, the high cost and long manufacturing time of producing recombinant proteins makes full

length PDGF-AB protein a less commercially desirable therapeutic. Optimisation of half-life in therapeutics allows for management of time that the therapeutic is in the body prior to excretion. This can provide ample time for the therapeutic to have a full effect whilst ensuring that it has been cleared fast enough to minimise potentially adverse off target effects (140). Increasing stability of therapeutics can also improve methods of delivery, shortening patients' hospital stays and the overall cost of therapy. By streamlining production and increasing the half-life, PDGF based peptide therapies could become more clinically desirable and commercially attractive novel therapies for heart failure. Evidence of successful manipulation of the PDGF chain in prior analogues (133-135) provides a promising avenue for enhancing its pharmacokinetic properties and downstream clinical applications.

1.6 LEAD OPTIMISATION

Successful clinical translation of novel therapies requires a clinically desirable and commercially attractive treatment that is selective, potent, and stable, maximising its safety and efficacy for therapeutic use. A method of achieving this is lead optimisation, the process of taking promising preclinical candidates and enhancing their pharmacological properties using medicinal chemistry to create viable novel treatments (141). Enhancement of selectivity reduces off target effects, whilst increasing potency minimises dosage and frequency of delivery. Optimising the half-life of a therapeutic can result in improved dosing and a potentially safer treatment (142). Lead optimisation allows for the enhancement of already promising biologics for improved therapeutic use through manipulating their stability, selectivity, and potency of lead candidates.

1.6.1 Pharmacokinetics/Pharmacodynamics

Pharmacokinetics and pharmacodynamics, commonly referred to as PK/PD, are modelling techniques in the field of pharmacology that are frequently utilised in drug development. Pharmacokinetics refers to the effects of the body on the drug whilst pharmacodynamics refers to the drugs effect on the body. Together they help us understand the dose and response relationship of therapeutics and provide information to determine benefits, dosage, and adverse effects of therapeutics. Pharmacokinetics studies focus on four stages of the bodies response to therapeutics: (1) Absorption, how the drug arrives at the point of action from the site of delivery, (2) Distribution, how the drug moves through the bloodstream to multiple organ systems, (3) Metabolism, how the drug is broken down by the body, followed by (4) Excretion, how the body then clears the drug (141). Half-life measurement is a significant experimental end point in pharmacokinetic studies as it can have substantial effects on the clinical application of potential novel therapies. Whilst extending half-life can have beneficial clinical implications in minimising dosage in addition to frequency and method of delivery, excessively extending half-life could potentially result in adverse off target effects. Refining half-life throughout lead optimisation allows for identification of the point where a therapeutic is given ample time to perform its therapeutic function whilst ensuring it's metabolised and cleared prior to the onset of adverse effects. This can result in improved efficacy and safety of the novel therapeutic.

Pharmacodynamics is the study of the physiological, biochemical, and molecular effects of drugs on the body and is key to establishing the clinical effects of novel therapeutics. These studies focus on four key areas: receptor interactions, efficacy, immune response, and toxicity. They are vital in clinical translation to determine the safety and efficacy of treatments prior to clinical trials (143). Enhancing the PK/PD properties of novel therapeutics allows for better clinical

applications and improves its prospects of clinical translation. In the context of PDGF, improving the pharmacokinetic qualities would allow for greater options for delivery method, improved dosing, and minimisation of off targets adverse effects.

1.6.2 Biologics

Biologics are therapeutics that have been derived from components of living organisms, with more common examples including proteins, cells, viruses, and antibodies. In recent years the pharmaceutical industry has shifted its focus towards biologics, largely due to an increase in profits and lower attrition rates when compared to traditional drug-based therapies (144). This shift has highlighted that whilst biologics have shown considerable promise in the treatment of disease, their use as therapeutics is often confounded in their naturally occurring state. These limitations lie within their pharmacological properties, the most prevalent being a lack of stability resulting in low half-lives and therefore poor clinical application (145). This is especially relevant in the field of protein therapies; regardless of their well-established efficacy they often have poor stability and bioavailability. Due to their small size, often below the size of kidney filtration at 70kDa, proteins and peptides are rapidly cleared from circulation (146). Additionally, many proteins and peptides are highly susceptible to protease cleavage resulting in poor plasma stability. Whilst these problems could be addressed by increasing dose and frequency of treatment, the risk of adverse or off target effects poses the need for a more appropriate solution. To address this problem several techniques have been developed to improve the therapeutic application of these proteins (147-149). Notable developments in this field include fusion proteins and protein mimetics, produced via chemical synthetic peptide or recombinant protein synthesis.

1.6.3 Fusion Proteins

Fusion proteins are a commonly used technique to improve the pharmacokinetic properties of peptides. Whilst most notable for their capacity to increase bioavailability of biologics (150) they have also been utilised to increase selectivity to specific markers on target cells (151). The primary mechanisms of increasing half-life through fusion proteins require increasing the size of a peptide via fusion with a larger, more stable protein, minimising clearance by kidney filtration and protecting the peptide from protease cleavage in the bloodstream. The most utilised protein in this technique is human serum albumin. An alternative to fusion with larger, stable carrier proteins is binding to the polysaccharide heparin or fragment crystallisable (Fc) fusions. Fc fusions are constructed by binding the therapeutic peptide to the Fc domain of an IgG antibody (147). Several examples of albumin, heparin and Fc fusion proteins have been very successful in translation into the clinic and are commercially available today (152-155).

1.6.4 Fc Fusion Proteins

Fc fusion proteins utilise the Fc neonatal receptor (FcRn) pathway to increase the half-life of biologics by recycling the peptide through the FcRn pathway. (147). Fc fusion proteins are covalently linked to the Fc region of an immunoglobulin G (IgG) antibody. The primary mechanism of Fc recycling is binding to the FcRn receptor following non-specific uptake by the endothelial cell (156). Once taken up by the endothelial cell the Fc and peptide or protein bound to it are protected from proteases (157). Proteins not protected by the IgG, specifically its Fc region, are degraded in the bloodstream whilst the protected Fc fusion protein is then able to be recycled back out into the blood stream where it can continue to the site of action. Fc fusion proteins have also been proven to be very efficacious and efficient to produce supported by several examples of successful clinical translation (153, 158). Fc fusion proteins that are clinically

available and commonly used include Eloctate, a novel therapeutic for haemophilia that is constructed using recombinant factor VIII covalently linked to an IgG Fc region (159). Combining the recombinant factor VIII with the Fc region double its plasma half-life in dogs (160), and extended its average half-life from 12 hours (161) to 16.4 hours (158) in humans, enhancing its clinical applications. Eloctate has also been commercially very successful, turning over €563 million in 2021 (162), providing strong evidence for the clinical and commercial viability of Fc fusion proteins as therapeutics.

1.6.5 Human Serum Albumin Fusion Proteins

Human serum albumin (HSA) is the most abundant protein in blood that acts as a carrier protein for fatty acids, hormones, and steroids. With a half-life of 19 days, it is also the most stable (163), which is due to its large size, with a molecular weight of 69kDa, and its structure containing 585 amino acids, 35 of which are cysteine residues (164) which play a major role in the stability of this protein. HSA fusion proteins are proteins bound to a synthetic or recombinant HSA to increase half-life. In addition to the stability of native HSA, these HSA fusion proteins can utilise native HSAs ability to bind to the neonatal Fc receptor, allowing them to utilise this recycling pathway in endothelial cells and protecting these proteins from protease cleavage (147). The combination of this protection from protease cleavage and the increased size from the HSA preventing clearing via glomerular filtration, results in a significant increase in half-life. Examples of this include Albiglutide, which is a commercially available and clinically approved treatment for type 2 diabetes synthesised from a glucagon-like peptide 1 bound to a HSA (165). This fusion significantly extended the half-life of this biologic from 1.5 minutes to 5-7 days (149), contributing to the successful clinical translation (166, 167) and commercialisation of this novel therapeutic. Whilst very effective in half-life extension, HSA fusion proteins have several

limitations in that they are extremely costly to produce, have very low solubility and present potential risks from their prolonged half-life. The development of a conjugate that utilises some of HSA's pharmacokinetic enhancing properties whilst addressing its limitations would be of significant value in lead optimisation.

1.6.6 Human Serum Albumin Conjugate

Whilst the efficacy of albumin fusion proteins is well established, their clinical use is somewhat limited, largely due to their significant size and low solubility. Low solubility limits clinical applications, whilst their large size results in time consuming and costly production limiting their commercialisation. To address this, Zorzi et al. developed three acylated heptapeptides, synthesised by binding 6 or 7 amino acids to a fatty acid (148). Each peptide demonstrated high binding affinity to albumins in the blood stream, with the highest affinity observed in the 7 amino acid palmitoyl based conjugate. All three peptides were successfully bound to albumin in the bloodstream of rats, mice, and human plasma, extending the half-life of their therapeutic peptide. These conjugates utilise a piggyback approach, binding to albumins to prolong the time to excretion 25-fold in the most effective conjugate. Zorzi et al. demonstrated this in the factor XIII anti-thrombotic therapy extending its half-life from 13 minutes to over 5 hours. This HSA conjugate provides many of the pharmacokinetic benefits of serum albumin fusion proteins whilst addressing some of its clinical and commercial limitations.

1.6.7 Protein Mimetics

Protein mimetics are molecules that mimic part, or all the biological function of a protein, often designed to be significantly smaller than the original protein containing additional therapeutic

properties. An example of this is reported in PDGF, mimicking the receptor binding portion of PDGF-BB binding to both the α and β receptor. Maintaining strong receptor binding activity of the PDGF-B chain allowed the mimetic peptide to conserve PDGFs biological function, shown in proliferation, collagen contraction and migration (133). Synthetically produced protein mimetics have been successfully translated into the clinic including the immune thrombocytopenia treatment Romiplostim (Nplate) (168, 169), a mimetic peptide of the thyroid peroxidase which is recombinantly produced and linked with a Fc region of an IgG as in the previously noted Fc fusion proteins (170). Protein mimetics have the potential to perform the desired therapeutic functions of native biologics whilst minimising some of the off-target effects. Mimetics are often also smaller than native biologics and synthetically produced, making them easier and more efficient to manufacture. By then binding these mimetics with half-life extending conjugates, their pharmacokinetic properties are further enhanced increasing their viability as novel therapeutics.

1.7 CONCLUSION

Despite significant efforts to mitigate the effects of cardiovascular disease, it remains a leading cause of morbidity and mortality worldwide. Amongst this is the continuing lack of treatment options available for heart failure that despite promising developments, remains an unmet need with no therapies yet clinically available to reverse its effects. Recombinant human PDGF-AB protein is a promising novel therapy to improve post-MI cardiac function with promising results in rodent and porcine models. Noted effects were driven by an increase in angiogenesis and in modulation of the cardiac scar, however, further refinement is required for this strategy to be developed further as a clinically viable therapy for heart failure. To address this, we set out to apply medicinal chemistry to enhance the pharmacokinetic properties of PDGF and assess its

function using a combination of known biological functions of PDGF *in vitro* and *in vivo* efficacy in murine models. Additionally, validation and further investigation into the mechanisms driving HFpEF in a murine model will allow us to determine the suitability of our novel therapy as a treatment for HFpEF, potentially widening the scope of its applications. By identifying a suitable murine model for HFpEF and investigating the molecular mechanisms driving it, we may be able to further the development of our pharmacokinetically enhanced PDGF mimetic peptide.

AIMS AND HYPOTHESES

Hypotheses

1. A validated murine model of HFpEF will provide a reliable and improved platform to test potential therapeutics specifically for candidates that impact cardiac extracellular matrix changes.
2. A peptide mimetic of the PDGF-B chain loop III region will maintain the biological function of PDGF receptor signalling and provide a foundation for incorporating mechanisms for pharmacokinetic enhancement.
3. Lead candidate PDGF-mimetic peptides established and tested through *in vitro* assays will provide a safe and efficacious method of improving cardiac function post myocardial infarction.

Aims

1. Validate a murine model of Heart Failure with Preserved Ejection Fraction (HFpEF).
2. Identify characteristics within a murine model of HFpEF that could be targeted by novel therapies.
3. Identify a region of the PDGF protein chains that can maintain biological function when tested as a discrete peptide.
4. Incorporate half-life extending elements into the design of novel PDGF-mimetic peptides whilst maintaining PDGF receptor signalling capacity.
5. Synthesise novel PDGF-mimetic peptides and test their efficacy for key known functions of PDGFs *in vitro*.
6. Assess the toxicology and safety of synthetic PDGF-mimetic peptides in an uninjured *in vivo* murine model at varying doses.
7. Determine the efficacy of PDGF-mimetic peptides in improving cardiac function in a post myocardial infarction murine model.

CHAPTER 2: MURINE MODEL OF HEART FAILURE WITH PRESERVED EJECTION FRACTION

2.1 INTRODUCTION

Heart failure with preserved ejection fraction (HFpEF) accounts for approximately 50% of heart failure patients (19) and has a 5-year mortality rate of 53-74% (28). HFpEF is characterised by diastolic dysfunction which occurs when there is a decrease in the hearts ability to fill the left ventricle in diastole resulting in a compensatory increase in left ventricular filling pressure. Additionally, approximately 50% of HFpEF patients have 5 or more major comorbidities (171). The most common of these include obesity, hypertension, diabetes mellitus, chronic kidney disease and coronary artery disease, all of which are also considered drivers in the development of HFpEF (171).

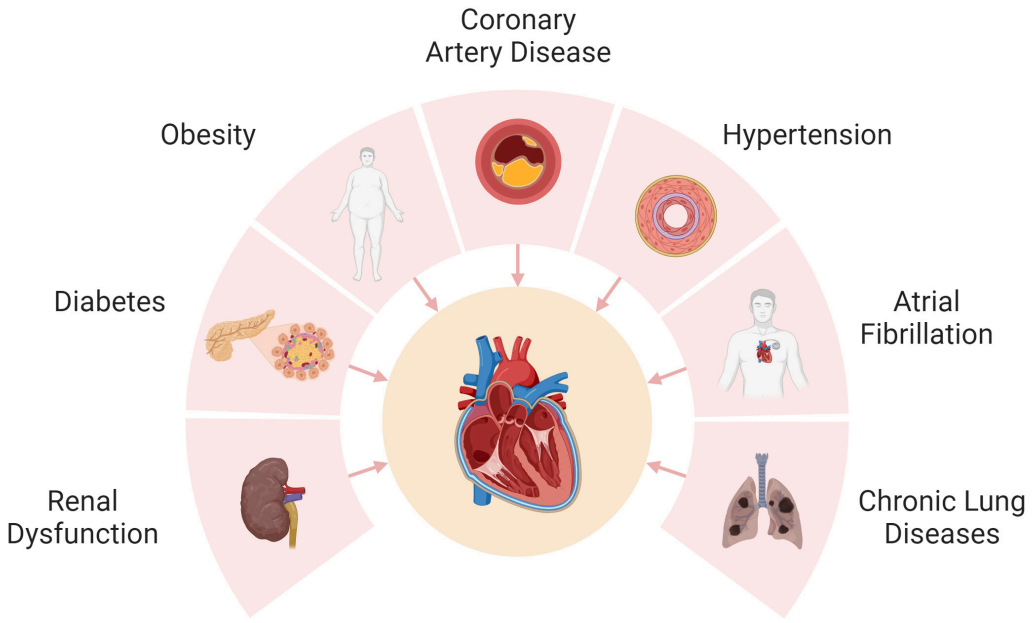

Figure 2.1.1: Common comorbidities driving HFpEF.

The most frequently reported comorbidities that contribute to HFpEF are chronic diseases, metabolic and mechanical stressors.

Despite significant developments in our understanding and therefore treatment of HFrEF, we have a limited understanding of the mechanisms driving HFpEF and limited treatment options. Two key factors that have contributed to this in HFpEF are the complexity and heterogeneity of the HFpEF patient population and the lack of animal models that accurately reflect this. Inaccurate animal models

have resulted in a limited understanding of the molecular mechanisms of HFpEF and poor *in vivo* testing conditions, limiting the translational value of experimental therapies. A downstream implication of this is that until recently, all clinical trials on interventions for HFpEF patients had failed to reach primary endpoints (29).

Models of HFpEF have focused heavily on a single aspect of the phenotype, resulting in a model that fails to accurately represent the complex nature of this syndrome. A key example of this is the surgically induced transverse aortic constriction (TAC) model (33) that has previously been widely used in the field. This model involves constricting the aorta using a suture or band to increase the pressure of the aorta, therefore increasing pressure of the left ventricle. Whilst TAC models have been a popular approach, several other methods of inducing HFpEF have been developed that also focus on singular components of the phenotype. These include diet and obesity-based models (34, 40), pharmacologically induced (43) and hypertension models (48), all of which have had limited clinical relevance and translational value.

Previous work in the field assessed the effects of HFD and L-NAME independently as methods of inducing heart failure in murine models. Early work on the effects of L-NAME on the heart reported that when consumed through drinking water for 4 weeks, L-NAME induced hypertension, myocardial fibrosis and an increase left ventricle mass (48). Later work built upon this with the addition of cardiac functional data, including a preserved ejection fraction and a decrease in end diastolic volume of the left ventricle (49). HDFs have been heavily explored in models of heart failure due to obesities significant role in cardiovascular diseases. Over 80% of HFpEF patients are overweight or obese making this a focal comorbidity in modelling the phenotype. A landmark model amongst these was the application of a HFD in obese ZSF1 rats for 20 weeks, resulting in hypertension, diastolic dysfunction,

renal dysfunction, and pulmonary oedema (172). Whilst all of these successfully modelled aspects of the HFpEF phenotype none of them have resulted in a holistic, clinically relevant model.

To address this gap in the field, Schiatterella et al. established the 'Two Hit Approach' to HFpEF (50) combining mechanical stress through hypertension induced by L-Arginine Methyl Ester (L-NAME) and cardiometabolic stress through 60% calories from fat HFD (50). This approach to developing a HFpEF phenotype was reported to induce hypertension, pulmonary oedema, cardiac hypertrophy, and interstitial fibrosis whilst decreasing exercise tolerance and achieving diastolic dysfunction whilst maintaining ejection fraction. The mechanical and metabolic stress of this model achieved the key clinical characteristics of HFpEF by inducing nitrosative stress over the course of 15 weeks. The combination of metabolic and mechanical stress in the 'Two Hit Approach' allowed for the successful production of the HFpEF phenotype in mice.

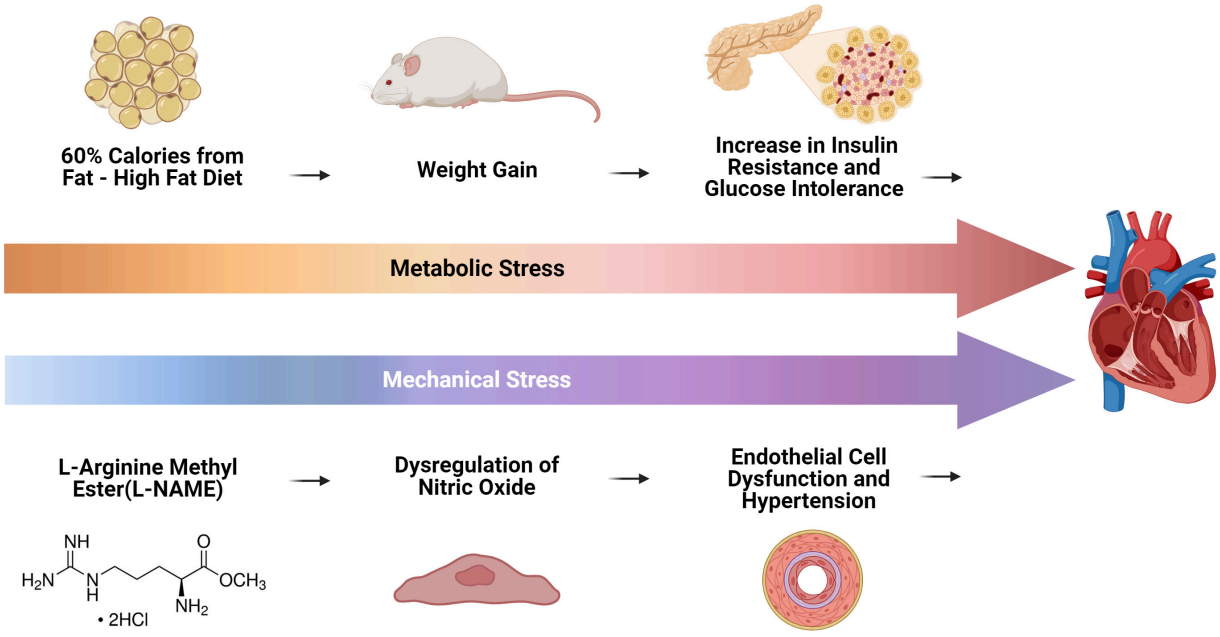

Figure 2.1.2: 'Two Hit' approach to HFpEF in a murine model.

Combining the metabolic and mechanical stress of HFD+L-NAME in mice produces the HFpEF phenotype characterised by diastolic dysfunction, in addition to several frequently reported comorbidities.

Hypothesis

A validated murine model of HFpEF will provide a reliable and improved platform to test potential therapeutics specifically for candidates that impact cardiac extracellular matrix changes.

Aims

1. Validate a murine model of Heart Failure with Preserved Ejection Fraction (HFpEF).
2. Identify characteristics within a murine model of HFpEF that could be targeted by novel therapies.

In this chapter, we aimed to validate the two-hit approach to HFpEF in a murine model by applying the 60% calories from fat diet with 0.5g/L L-NAME in drinking water over the course of 15 weeks in C57BL6/J mice. The development of HFpEF in these mice was monitored using weight, blood pressure measurements via tail cuff, echocardiography for systolic and diastolic parameters and exercise tolerance using a swim test. At the conclusion of the *in vivo* studies, we carried out histology, immunohistochemistry and tandem mass tagged (TMT) discovery proteomics to identify proteins driving this phenotype to potentially identify novel therapeutic targets for HFpEF and assess its value as means of testing our own novel therapeutics *in vivo*.

2.2 MATERIALS AND METHODS

2.2.1 Animal ethics

All animal experiments were approved by the Garvan/St Vincent's Animal Ethics Committee (AEC protocol #19/14) and were conducted in accordance with the NHMRC guidelines for animal research and the Australian code for the care and use of animals for scientific purposes. *In vivo* experiments were conducted on male C57BL/6J mice bred at the Victor Chang Cardiac Research Institute (Sydney, Australia) (Jackson Laboratory, 000664).

2.2.2 'Two Hit' Diet to Induce Heart Failure with Preserved Ejection Fraction

Male C567BL/6J mice were split into two cohorts: a HFpEF group (n=16) and Normal Chow control group (n=14). The HFpEF group were fed a high fat diet (HFD, 60% calories from fat) (Specialty Feeds, SF13-092) and water supplemented with 0.5g/L of L-arginine methyl esther (L-NAME) (Sigma Aldrich, N5751) for a period of 15 weeks to induce a HFpEF phenotype. The Normal Chow control group were fed a normal chow diet and water. Both groups water was pH corrected to physiological pH of 7.4, changed daily for 15 weeks. The development of HFpEF was monitored using blood pressure measurements via tail cuff, echocardiography, exercise tolerance swim test (methods below) and weight. Mice were weighed routinely at the conclusion of each week in the protocol.

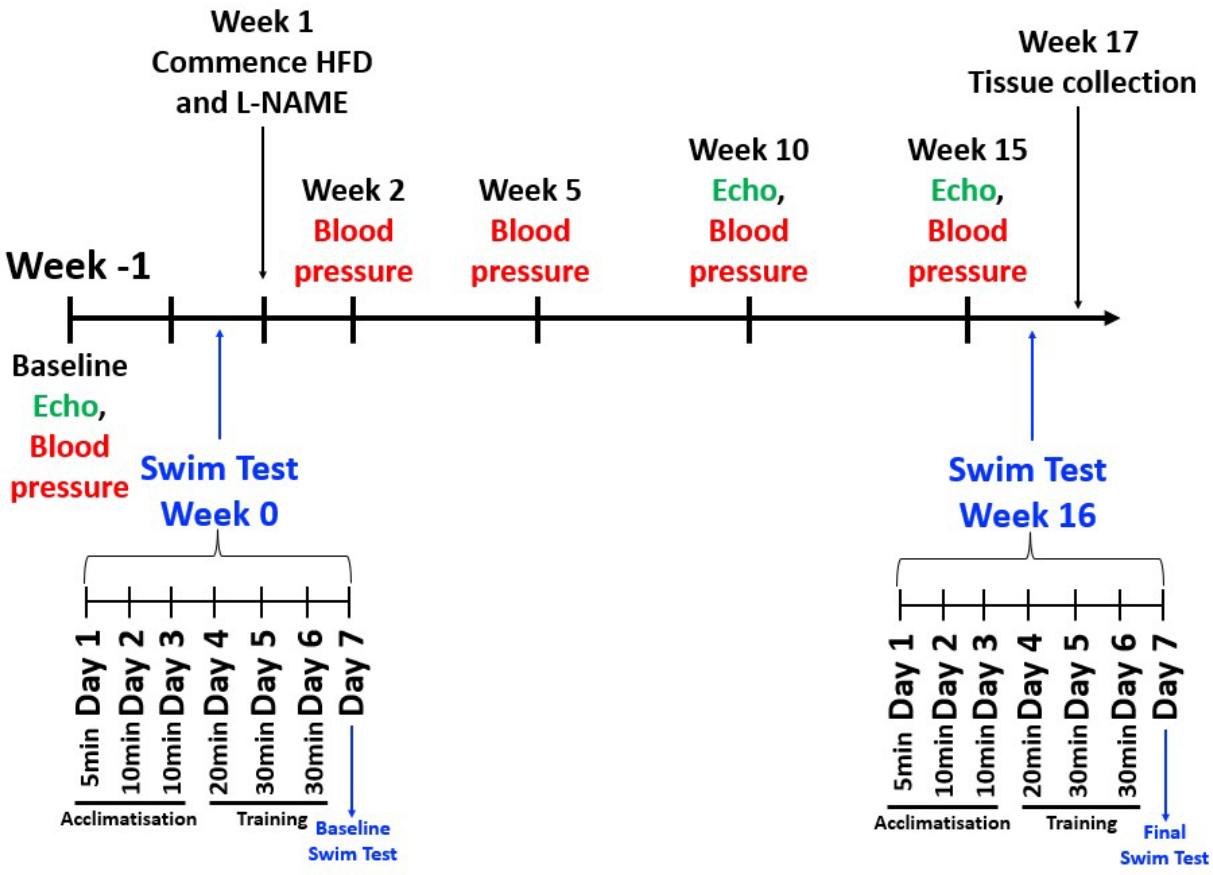

Figure 2.2.1: Experimental timeline for development of the HFpEF phenotype.

2.2.3 Blood Pressure via Tail Cuff

Mice blood pressure was recorded via tail cuff using the CODA non-invasive blood pressure system (Kent Scientific, Connecticut, USA). This involves placing mice inside a holder within which an O cuff and volume pressure recorder are placed on their tails. The shape of the holder allows for secure holding of the mouse whilst maintaining free movement of their tails, minimising any additional induced anxiety for the mouse throughout the protocol. The holder is placed on heat pad warmed to 35°C in addition to warming blanket to assist in managing mouse body temperature. An acclimatisation protocol was undertaken prior to baseline data collection for 3 days in addition to a short acclimatisation period prior to data collection at each time point. The initial 3-day acclimatisation began with mice being placed inside the holder for 1 minute, followed by 5 minutes on day 2, including placing the O cuff and volume pressure recorder (VPR) on their tails. On the final acclimatisation day

mice were placed in their holders with the O cuff and volume pressure recorder for 5 minutes followed by an acclimatisation run when blood pressure data was recorded but not used for further analysis.

Blood pressure data collection was carried out at baseline, week 2, week 5, week 10, and week 15. This was completed by placing the mice in the holders, with the tail O cuff and volume pressure ring (VPR) as described above. Re-acclimatisation prior to each data collection was achieved by allowing mice 5 minutes to adjust to the holder followed by 5 acclimatisation cycles before commencing data collection cycles. Data collection cycles were run 15 times with a minimum of 10 necessary for data analysis. Additional cycles were run to allow for external stimuli that could interfere with data collection avoiding re-commencing the protocol. This minimised distress of the mice, resulting in more reliable data and improved animal welfare. The average of these cycles was then calculated for systolic, diastolic, and mean blood pressure, then plotted in Prism (GraphPad, version 9.0.1).

2.2.4 Echocardiography

Echocardiography was performed throughout this protocol to assess cardiac function, including diastolic function. Measurements were performed by Dr Vikram Tallapragada of the Victor Chang Cardiac Research Institute at baseline, week 10 and week 15. Mice were lightly anesthetised using 0.5-1.5% isoflurane and echocardiography was performed using the Visual Sonics Vevo 2100 Preclinical Imaging System with a MS400 transducer (FUJIFILM Visual Sonics, Ontario, Canada). During the echo the mouses paws were taped down to the echo platform that was warmed and monitored the respiratory rate and electrocardiogram. Light anaesthetic allowed for a more accurate representation of diastolic function. Echocardiography data analysis was carried out using the bullet method (method below) and was completed by myself on the Vevo 3100 Analysis Software (FUJIFILM Visual Sonics, Ontario, Canada).

2.2.4.1 Bullet Method Analysis of Ventricular Function

Long and short axis echocardiography imaging was analysed for systolic parameters using the bullet method. The bullet method uses a 5/6 area by length formula to calculate left ventricle volume to determine left ventricular end systolic volume (LVESV), left ventricular end diastolic volume (LVDEV) and ejection fraction (EF). Area of the left ventricle was calculated using the short axis at 3 points through the ventricle from the 1mm below the mid-papillary (MP) level to 3mm below the MP level, measuring the endocardium and epicardium in systole and diastole. Length of the ventricle was measured using the long axis view in systole and diastole from the aortic valve to the apex. Analysis measurements were carried out using the Vevo 3100 Analysis Software (FUJIFILM Visual Sonics, Ontario, Canada) and calculated on Microsoft Excel (2016).

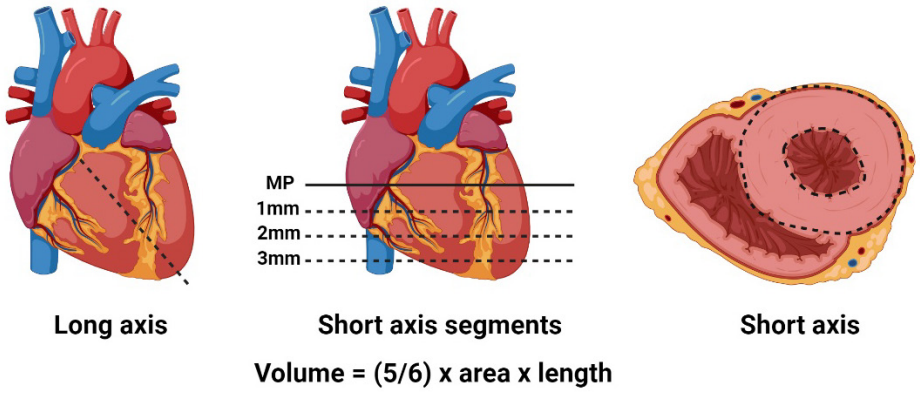

Figure 2.2.2: Bullet method measurements for echocardiography analysis.

2.2.5 Exercise Tolerance Swim Test

Exercise tolerance was tested at baseline and week 15 via a swim test. Prior to both swim tests acclimatisation was done to ensure mice were able to safely complete the test. Mice swam in buckets with water at an optimised height to ensure mice were not jumping off the bottom or able to climb out. Water temperature was maintained at 35°C using heat pads and warming the water prior to

testing for mouse comfort. Additionally, mice swimming groups were limited to 7 mice, ensuring optimal conditions for swimming. The swim protocol was a total of 7 days; 6 days of acclimatisation with the swim test on day 7. Acclimatisation included 3 acclimatisation days, increasing from 5 minutes on day 1, to 10 minutes on days 2 and 3, followed by 3 training days increasing from 20 minutes on day 4, to 30 minutes on days 5 and 6. Mice were given breaks throughout acclimatisation and training if it appeared necessary based on swimming ability and visible stress signs including climbing, dunking, or diving. The swim test completed on day 7 was conducted by placing mice in the buckets and allowing them to swim until exhaustion with 2 1-minute breaks in the testing time. Mouse weights and behaviours were carefully monitored throughout the duration of each swim week to ensure mice were not showing signs of significant stress as a result of daily swimming.

2.2.6 Tissue Collection

At the conclusion of their week 15 echocardiogram, mice were given potassium chloride to induce cardiac arrest prior to tissue collection. The atria were separated from the ventricles and the ventricles were then dissected longitudinally ensuring each half contained a left and right ventricle from base to apex. Half of each ventricle was fixed for histology and immunohistochemistry whilst the other half was frozen for further downstream experiments. All other organs collected were fixed using 4% paraformaldehyde (PFA) (Thermo Fisher, 28906) for 24 hours for histology and immunohistochemistry.

2.2.7 Histology

The heart sections assigned to histology were fixed overnight and stored in 70% ethanol prior (POCD, ETHABSWV70) to paraffin embedding for 12 hours. Hearts were sectioned at 4μm and baked for 2 hours prior to dewaxing. Sections were dewaxed by dipping in xylene (POCD, XYL1L) for 3 minutes, 3

times in fresh xylene each time. This was then repeated with 100% ethanol (POCD, ETHABS100) prior to 3 minutes in 70% ethanol and washed in running Milli Q water. Following dewaxing, histology sections were then stained with in 0.1% Sirius red in picric acid with 0.1% Fast Green (POCD, SIRIUSFAST500) or Haematoxylin (POCD, MODMAY) and Eosin (POCD, EOSVJ). Post staining, cover slipping was completed by dipping in xylene 3x20 times in different batches each time. The coverslip was then mounted to the slide using mounting medium (POCD, ULT5). All images were acquired on the Olympus VS120 Slide Scanner (Olympus Life Science, Massachusetts, USA).

2.2.7.1 Picrosirius Red and Fast Green

Once dewaxed as described above, sections were washed in running water and incubated in picrosirius red and fast green for 4 hours on a see-saw shaker, protected from the light. The slides were then washed in running water and dipped in absolute ethanol twice prior to cover slipping as described above.

2.2.7.2 Haematoxylin and Eosin

Once dewaxed as described above, sections were washed in running water and incubated in Mayer's Haematoxylin for 8 minutes at room temperature, following which the stain was differentiated by blueing via washing in running water for 3 minutes. Sections were then stained with Alcoholic Eosin for 5 seconds prior to dehydration in 100% ethanol twice and cover slipping as described above.

2.2.8 Immunohistochemistry

To detect changes in cardiomyocyte size and blood vessel density across our two groups, immunohistochemistry was carried out using wheat germ agglutinin (WGA) - Alexa Fluor 647 (Thermo Fisher, W32466) to stain cell borders and isolectin b4 (IB4)- Alexa Fluor 488 (Thermo Fisher, I21411)

to stain blood vessels. Following dewaxing, antigen retrieval was performed using sodium citrate buffer, adjusted to pH 6, for 20 minutes at 95°C in a decloaking chamber. The slides were then washed 3 times for 5 minutes in Phosphate Buffered Solution (PBS) (Gibco, 18912-014) prior to permeabilisation in 0.1% Triton X-100 (Sigma Aldrich, T9284) for 10 minutes. Non-specific antibody binding was then blocked using 5% normal goat serum (Sigma Aldrich, G9023) in PBS for 1 hour at room temperature. WGA and IB4 were diluted 1:100 in 5% normal goat serum in PBS and applied to the sections to be incubated overnight at 4°C. Following incubation in primary antibodies, the slides were washed 3 times for 5 minutes in PBS and incubated in 300nM DAPI (Sigma Aldrich, MBD0015) in PBS for 10 minutes. The slides were then washed in for 5 minutes in PBS and cover slipped using 1:2 glycerol in PBS. All slides were imaged using the Olympus VS120 Slide Scanner at 40x magnification.

2.2.9 Image Analysis

2.2.9.1 Fibrosis Quantification

Fibrosis was quantified using the sections stained with picrosirius red and fast green by calculating the percentage of picrosirius red from the green parts of the section. This was done via a macro in Image J. The macro used red, green, blue thresholding to separate the collagen (stained red) from the myocardium (stained green). Following this, the amount of collagen within the section was calculated to determine the percentage of collagen within the myocardium. Sections were analysed using the whole section, for only interstitial fibrosis by removing connective tissue of the valves and blood vessels, and for perivascular fibrosis by selecting regions of interest around blood vessels. To account for the possibility of localised fibrosis, 5 sections were taken from 5 evenly distributed depths through the tissue, ensuring the analysis represented accurate measurements of fibrosis.

2.2.9.2 Cardiomyocyte and Blood Vessel Analysis

Cardiomyocyte size and blood vessel analysis was carried out as previously described (173). Pre-processing of the images were carried out using the Image J Macros included in the protocol. This pre-processing involved splitting channels, improving the contrast, smoothing the images, and inverting the borders of the cardiomyocytes in preparation for measurements on CellProfiler (v4.2.4). Capillary counting and cardiomyocyte size measurements were performed on CellProfiler by segmenting the nuclei, cardiomyocytes, and capillaries, and then processing each of these objects and calculating results. Cardiomyocytes were counted using the cell boundaries and nuclei in addition to counting of capillaries and applying these results to calculate the number of capillaries per cardiomyocyte.

2.2.10 Tandem Mass Tagged Discovery Proteomics

2.2.10.1 Tandem Mass Tagged (TMT) Discovery Proteomics Sample Preparation

Tandem mass tagged (TMT) discovery proteomics was carried out by specialist staff at Sydney Mass Spectrometry, The Charles Perkins Centre. Heart tissue was powdered under liquid nitrogen, before 20mg was mixed with 400µl of sodium deoxycholate (SDC) buffer and heated to 95°C for 10 minutes at 1,000rpm, in a thermomixer. The samples were then processed in a bead beater for 3 minutes at 50Hz. 10mM Tris(2-carboxyethyl) phosphine (TCEP) and 40mM Chloroacetic acid (CAA) were added to each tube, and then returned to the thermomixer to reduce and alkylate proteins at 95°C for 10 minutes at 1,000rpm. Sample clean-up was carried out using chloroform/methanol precipitation and re-solubilised in 6M Urea/2MThiourea. Following Qubit quantitation, 100µg was taken from each sample and made up to 50µL with Urea/Thiourea. The proteins were then digested by the addition of 2µg of porcine trypsin and incubated at 37°C in a thermomixer for 16 hours at 1,000 rpm.

2.2.10.2 TMT labelling, Mid-pH fractionation and Data collection

The peptides were purified using Oasis hydrophilic-hydrophobic-balanced (HLB) with short cartridges (Waters Corp., Milford, MA, USA) and resuspended in a total volume of 30µL with 100mM HEPES buffer, pH 8.5. For each sample 7µg total peptides were labelled TMT pro 16plex Isobaric labelling reagent (Thermo Fisher Scientific, Waltham, MA, USA), following the manufacturer's instructions. The TMT-labelled peptides were purified using an HLB column and fractionated by offline basic pH reverse phase chromatography. Approximately 15µg peptides were loaded on to an in-house packed 320µm × 25cm column (3.5µm particle size, Xbridge BEH C18; Waters). Liquid chromatography mobile phase buffers were comprised of 10mM ammonium formate pH 7.9 and 90% (v/v) acetonitrile/10% (v/v) water. Peptides were eluted using a linear gradient of 5% to 50% over 45 mins at a flow rate of 6µL/min. 12 concatenated fractions were then dried down prior to analysis. The TMT-labelled hydrophilic interaction liquid chromatography (HILIC) fractions were resuspended in mass spectrometry (MS) loading buffer (3% (v/v) acetonitrile/0.1% (v/v) formic acid) and analysed online by nano-capillary liquid chromatography-tandem mass spectrometry (LC-MS/MS) using a Dionex Ultimate 3000 HPLC system (Thermo Fisher Scientific, Waltham, MA, USA) coupled to an in-house built fritless nano 75µm × 30cm column packed with ReproSil Pur 120 C18 stationary phase (1.9µm, Dr, Maisch GmbH, Germany). Separated compounds were analysed with a Orbitrap Eclipse Tribrid™ Mass Spectrometer (Thermo Fisher Scientific, Waltham, MA, USA). A synchronous precursor selection MS3 method was used for data collection. Proteome Discoverer 2.5 (Thermo Fisher Scientific, Waltham, MA, USA) was used to analyse the MS data, the settings included: the SEQUEST HT database search engine node, percolator validation for protein identification. The calculated abundance ratios for each sample against a pooled internal standard and normalised, relative to total protein signal, protein quantification values were exported for further analysis to Microsoft Excel (2016) and log fold-change values calculated.

Gene ontology (GO) term analysis was carried out using database for annotation, visualisation, and integrated discovery (DAVID, david.ncifcrf.gov) pathway analysis using proteins highlighted in TMT proteomics. TMT proteomics and GO term analysis results were plotted using RStudio. TMT proteomics was analysed using differential expression analysis of proteins with cutoffs set at Log2 fold change threshold of 0.5 and -Log10 P threshold of 0.05. The volcano plot was executed using the RStudio package EnhancedVolcano whilst GO term analysis was plotted using the RStudio package ggplot2. RStudio scripts for the volcano plot and GO term analysis were provided by Dr Robert Hume.

2.2.11 Immunohistochemistry and Confocal Microscopy

Immunofluorescent staining was carried out on ventricle sections collected from HFD+L-NAME and Normal Chow mice prior to confocal imaging to validate the most significant markers identified in TMT discovery proteomics. The sections were prepared for staining as described above in section 2.2.8 Immunohistochemistry. Following this, WGA diluted 1:100 in 5% normal goat serum in PBS-Tween (PBS/T) in addition to either anti-OXPAT (Thermo Fisher Scientific, PA1-46215) or anti-pyruvate dehydrogenase lipoamide kinase isozyme 4 (PDK4) (Thermo Fisher Scientific, PA5-13776) primary antibody both diluted 1:100, and applied to the sections for incubation overnight at 4°C. Following incubation in primary antibodies, the slides were washed 3 times for 5 minutes in PBS/T and incubated in Alexa-Fluor 488 anti-rabbit secondary antibody (Invitrogen, A-31566) diluted 1:1000 in 5% normal goat serum in PBS/T. The slides were then incubated in 1μL/ml DAPI in PBS for 10 minutes, washed for 5 minutes in PBS and cover slipped using 1:2 glycerol in PBS. All slides were imaged using the Leica TCS SP8 STED confocal microscope at 100x magnification. These images confirmed the quantitative results obtained through TMT proteomics and were therefore not further quantified.

2.2.12 Statistical Analysis

All statistics were carried out using GraphPad Prism (version 9.0.1). Comparison of the Normal Chow and HFD+L-NAME groups was completed using an unpaired T test with data presented as the mean ± standard deviation.

2.3 RESULTS

A total of 30 male mice were included in this study and assigned Normal Chow (n=14) or 60% calories from HFD and 0.5g/L L-NAME in drinking water (n=16). Over the course of 15 weeks mice weight, blood pressure, exercise tolerance and cardiac function were monitored to observe the development of HFpEF. At the conclusion of the *in vivo* study mice were euthanised for blood and tissue collection followed by histology, proteomics, and immunohistochemistry to investigate the underlying molecular mechanisms driving HFpEF.

Obesity is a frequently documented co-morbidity of HFpEF and was expected to develop in our mice as a result of 15 weeks HFD. Over the course of the experimental timeline, mice were weighed weekly to monitor the onset of obesity. At 15 weeks, the HFD+L-NAME cohort had become significantly heavier than their Normal Chow counterparts. Specifically, HFD+L-NAME mice weighed an average of 46.33g (±6.036), which was 13.40g (±1.671) (mean diff.) heavier than the average weight of the Normal Chow cohort at 32.94g (±1.595) (p value = <0.0001).

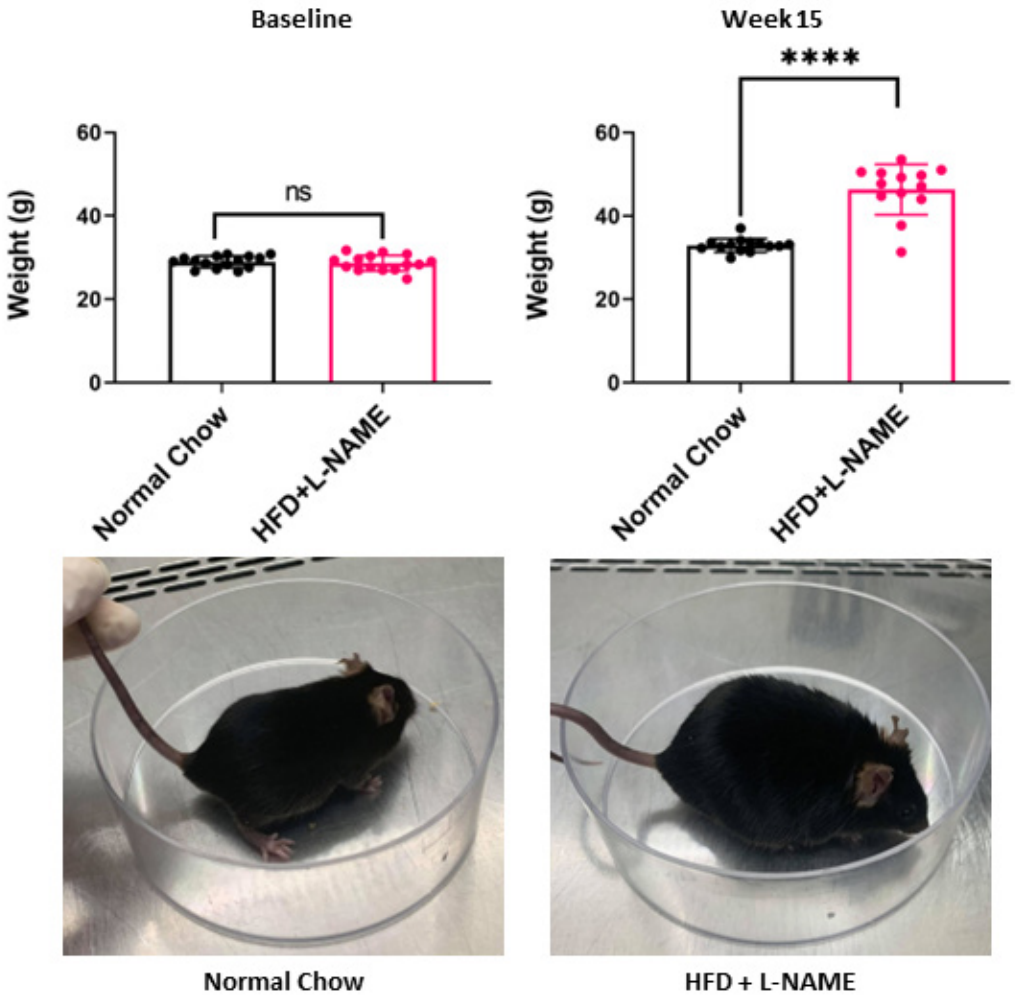

Figure 2.3.1: Increased weight of HFD+L-NAME versus Normal Chow mice.

HFD+L-NAME mice gained 13.40g (±1.671) (mean diff.) compared the Normal Chow mice at week 15 (p value = <0.0001). No significant difference was identified between the groups at the baseline. Error bars represent ± SD (Unpaired t-test) (n=13 HFD+LNAME/n=14 Normal Chow).

An increase in blood pressure was expected with the introduction of L-NAME to the rodents drinking water and was assessed in this model by measuring blood pressure via tail cuff over the course of the experimental timeline. At the baseline and week 5 there was no significant changes detected between Normal Chow and HFD+L-NAME mice (Figure 2.3.2). The first significant change was detected at week 10, HFD+L-NAME mice had a mean systolic of 115.1mmHg, diastolic of 24.4mmHg and a mean blood pressure of 134.3mmHg. The mean blood pressure of the Normal Chow mice was 42.45mmHg lower than that at 91.84mmHg (p value <0.001). It can be seen from Figure 2.3.2 that from the baseline to week 10 the blood pressure of Normal Chow mice decreased whilst the HFD+L-NAME mice maintained

their increased blood pressure leading to its significant result. We suggest the decreased blood pressure in the Normal Chow cohort was due to the mice becoming more comfortable with blood pressure monitoring via tail cuff over the course of the experimental timeline (174).

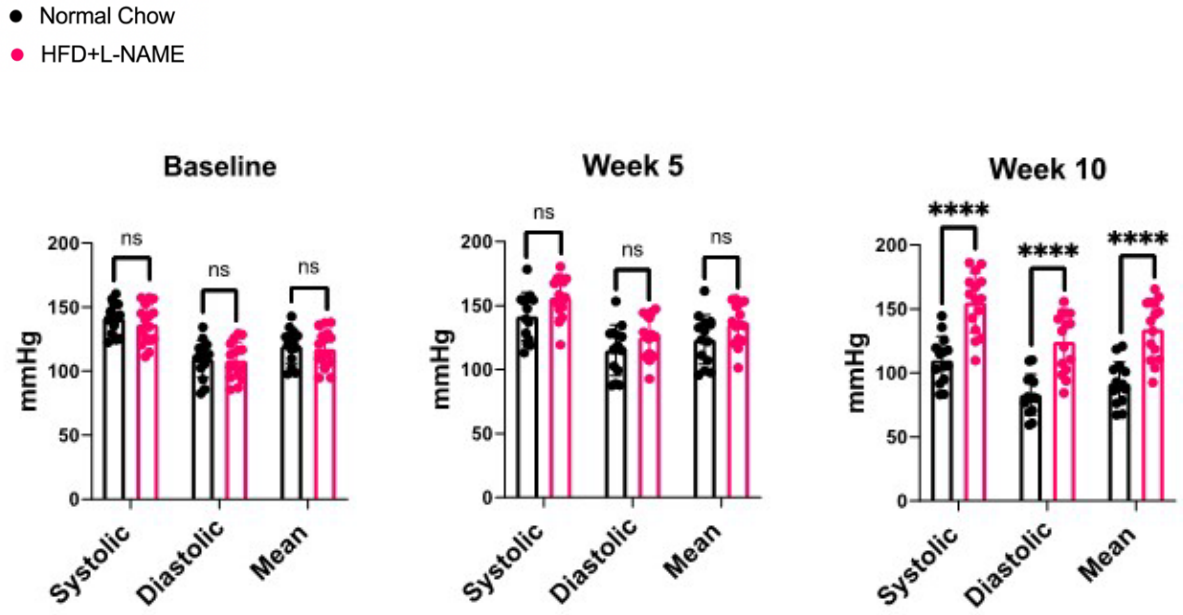

Figure 2.3.2: Onset of hypertension in HFD+L-NAME versus Normal Chow mice.

At the conclusion of week 10 the blood pressure of HFD+L-NAME mice was 42.45mmHg (±7.504) (mean diff.) higher than the Normal Chow mice. Error bars represent ± SD (Unpaired t-test) (n=15 HFD+LNAME/n=14 Normal Chow).

Reduced exercise tolerance is an established marker of HFpEF and is commonly assessed in the rodents using a treadmill running test. Due to ethical constraints, we adopted a swim test to analyse exercise tolerance in mice at the baseline and post 15 weeks of their assigned diet. Discrepancies in swimming ability were noted from the baseline between the two groups and became more significant at the conclusion of this study. At the baseline the Normal Chow group produced an average swim time of 24.01 minutes (±4.333) whilst the HFD+L-NAME group swam an average of 27.67 minutes (±4.353) (Figure 2.3.3). At week 15 the HFD+L-NAME mice swam an average of 19.37 minutes (±3.268) longer than their Normal Chow counterparts (p value <0.0001). HFD+L-NAME mice had an average

swim time of 43.86 minutes (±10.57) whilst the Normal Chow mice had an average swim time of 24.49 minutes (±5.217). The increased swim time for HFD+L-NAME mice is possibly due to the increased size of the mice allowing them to remain afloat combined with swimming slower allowing for less energy expenditure than their Normal Chow counterparts resulting in a significantly longer swim time. Despite being an established protocol for exercise training in rodents (175, 176), we identified limitations in using a swim test as an assessment of exercise tolerance in this model.

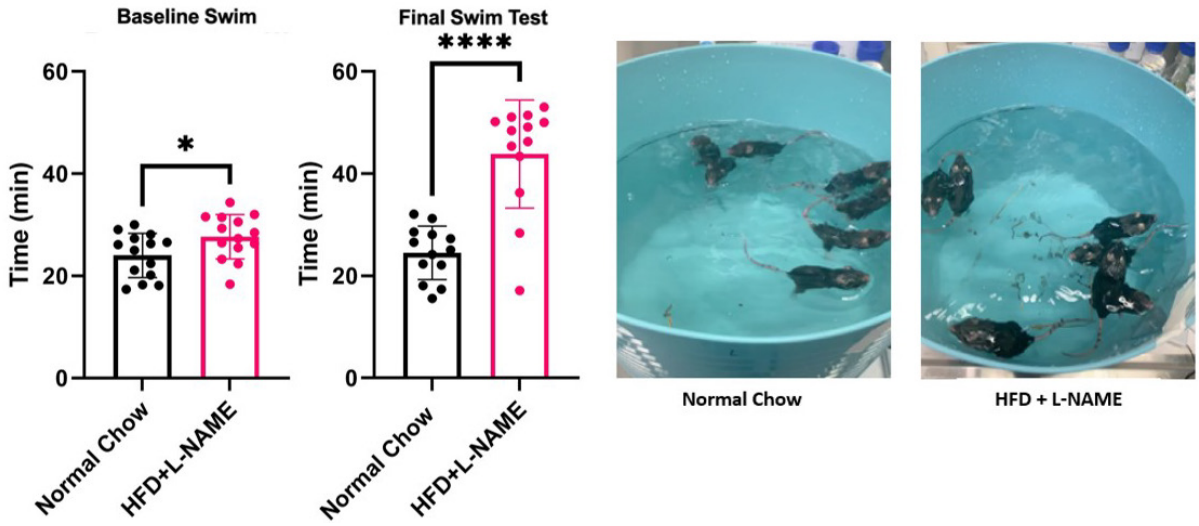

Figure 2.3.3: Increased exercise tolerance in HFD+L-NAME versus Normal Chow.

Following 15 weeks HFD+L-NAME mice swam an average of 19.37 minutes (±3.268) than the Normal Chow cohort (p value <0.0001). (n=13 HFD+LNAME/n=14 Normal Chow). Error bars represent ± SD (Unpaired t-test) (n=14/15).

HFpEF is characterised by diastolic dysfunction driven by a decrease in left ventricular filling pressure. This can be identified *in vivo* using echocardiography and analysing key diastolic parameters, these include left atrial volume, E/e', E/A wave, isovolumic relaxation time and strain. The capacity to assess these parameters can be limited in a murine model due to their small size and very high heart rate, hence our use of only E/e' and global longitudinal strain (Figure 2.3.8 and 2.3.6, respectively). E/e' indicates the tissue velocity at the mitral valve anulus whilst global longitudinal strain measures longitudinal shortening of the left ventricle. These markers were analysed at the baseline, week 10

and week 15 to assess the development of HFpEF in our mice over the duration of our experimental timeline.

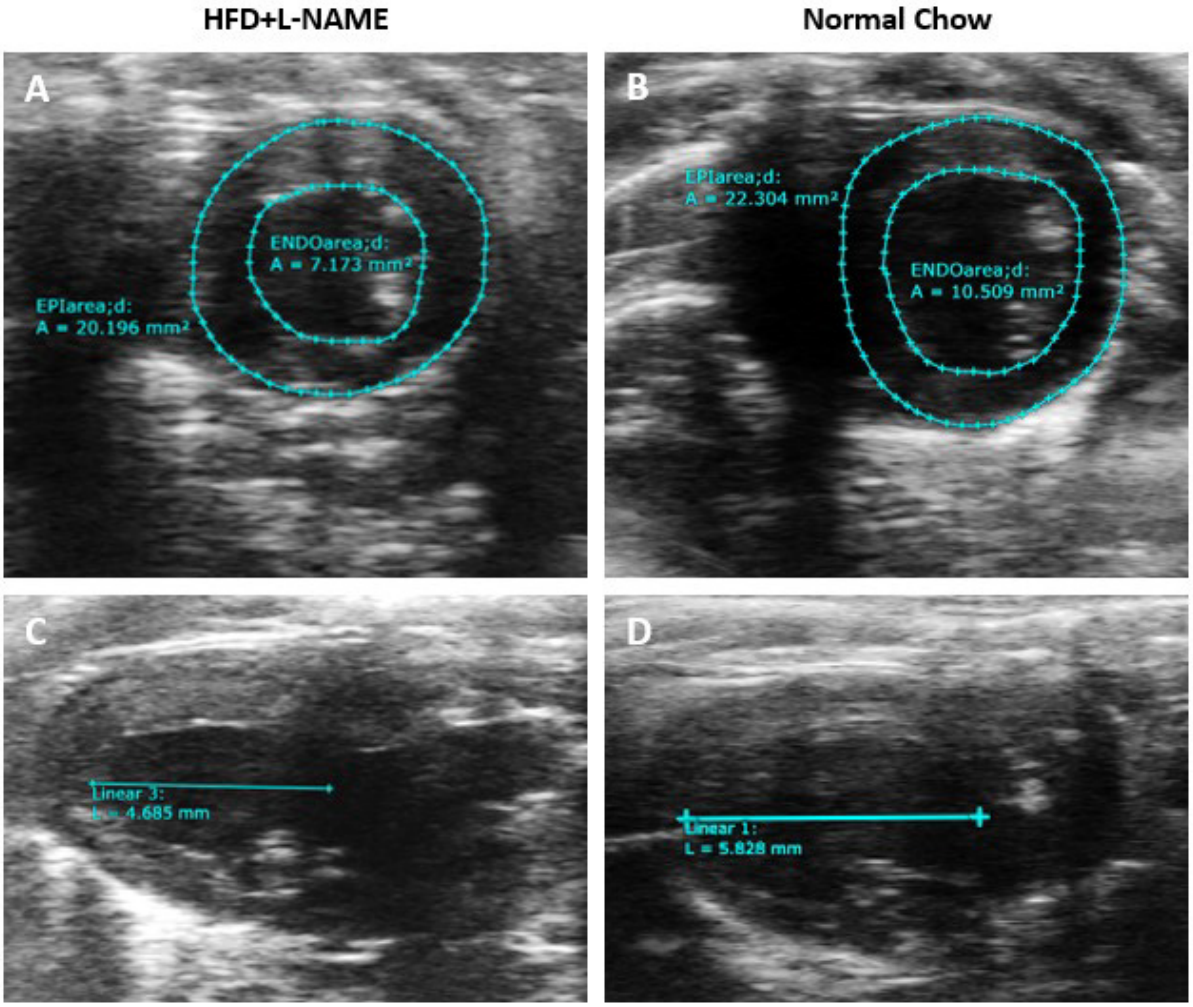

Figure 2.3.4: Echocardiography of Normal Chow and HFD+L-NAME C57BL6/J mice.

Echocardiography images displaying traces used to assess systolic parameters of cardiac function. A) Short axis view of a HFD+L-NAME mouse. B) Short axis view of a Normal Chow mouse. C) Long axis view of an HFD+L-NAME mouse. D) Long axis view of a Normal Chow mouse.

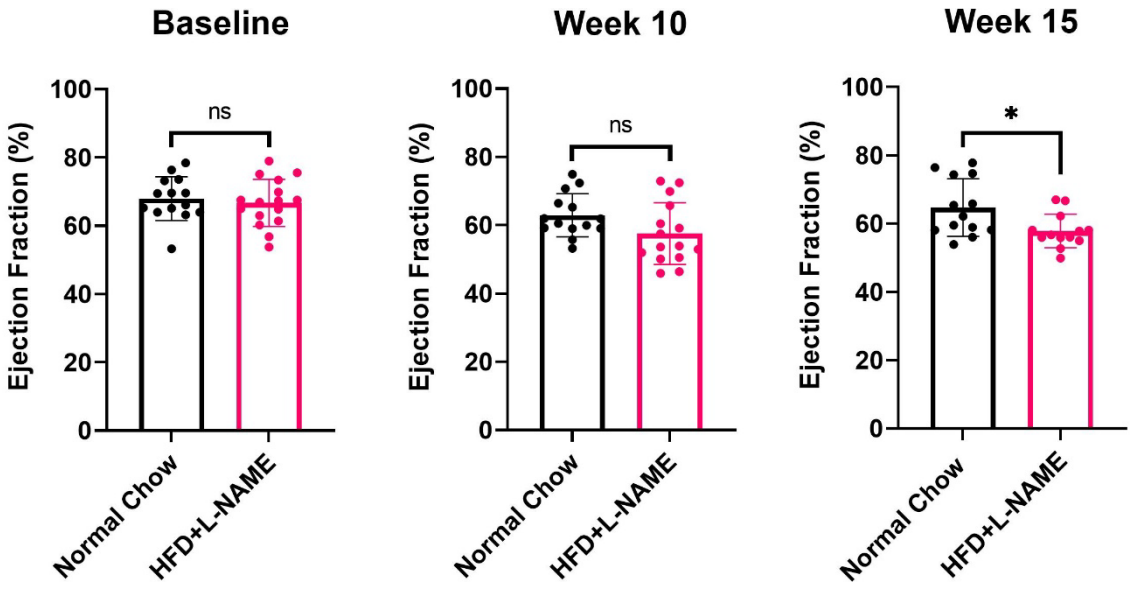

Figure 2.3.5: Maintenance of Left ventricular ejection fraction above 50% in HFD+L-NAME mice at week 10, and week 15.

Ejection fraction recorded at the baseline and week 10 identified no significant difference in ejection fraction between the HFD+L-NAME and Normal Chow mice. A significant decrease in ejection fraction was identified in HFD+L-NAME mice versus Normal Chow ($p = 0.0183$) however, the average ejection fraction of this group remained above 50%. Error bars represent ±SD (Unpaired t-test) (n=14/15).

A key parameter of cardiac function in modelling HFpEF is maintaining an ejection fraction above 50%. At the baseline mice had an average ejection fraction of 67.92% (±6.409) and 66.69% (±6.891) for Normal Chow and HFD+L-NAME respectively. The difference between the groups remained non-significant at week 10 with an average ejection fraction of 62.86% (±6.310) and 57.54% (±8.995) for Normal Chow and HFD+L-NAME respectively. Following 15 weeks of HFD+L-NAME in C57BL6/J mice there was a significant decrease in ejection fraction when compared to the Normal Chow control group (Figure 2.3.5). Normal Chow mice had an average ejection fraction of 64.69% (±8.410) versus an average ejection fraction of 57.85% (±4.931) in the HFD+L-NAME mice. Despite the significant decrease of 6.847% (mean diff.) ($p = 0.0183$), the HFD+L-NAME group still maintained an average ejection fraction above 50% with only 1 mouse dropping below the 50% threshold at 15 weeks.

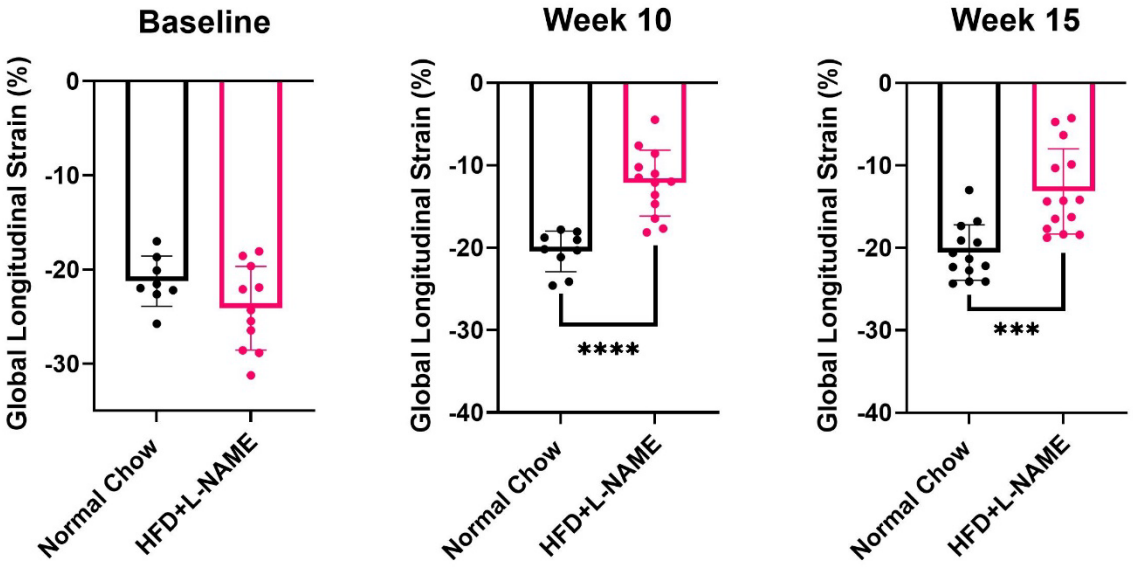

Figure 2.3.6: Increased global longitudinal strain of HFD+L-NAME mice at week 10, and week 15.

Global longitudinal strain was significantly increased in HFD+L-NAME mice at 10 ($p < 0.0001$) and 15 weeks ($p = 0.0002$) when compared to the Normal Chow group. Error bars represent ±SD (Unpaired t-test).

Global longitudinal strain (GLS) measures the sub-endocardial longitudinal muscle fibres of the heart that are typically effected when the heart is under stress or following damage to the myocardium. This is a good indicator of contractile function of the heart and are used as a parameter when assessing diastolic function. GLS is expected to increase as contractility of the heart is impaired. GLS was recorded at the baseline, week 10, and week 15 following treatment with HFD+L-NAME and compared to the Normal Chow control group. GLS was significantly increased in the HFD+L-NAME at both week 10 and 15 with an increase of 8.294% (mean diff.) ($p < 0.0001$) and 7.402% (mean diff.) ($p = 0.0002$), respectively (Figure 2.3.6). Following 10 weeks treatment with HFD+L-NAME C57BL6/J mice had an average GLS of -12.16% (±3.992) versus -20.45% (±2.466) in Normal Chow mice (Figure 2.3.6). At the later week 15 timepoint GLS had increased less in the HFD+L-NAME group than it had previously at week 10. At week 15 HFD+L-NAME mice had an average GLS of -13.16% (±1.382) versus -20.57% (±0.9320) in the Normal Chow group. This decrease was possibly due to limitations in accurately measuring GLS resulting in fewer mice being recorded at week 10 than week 15.

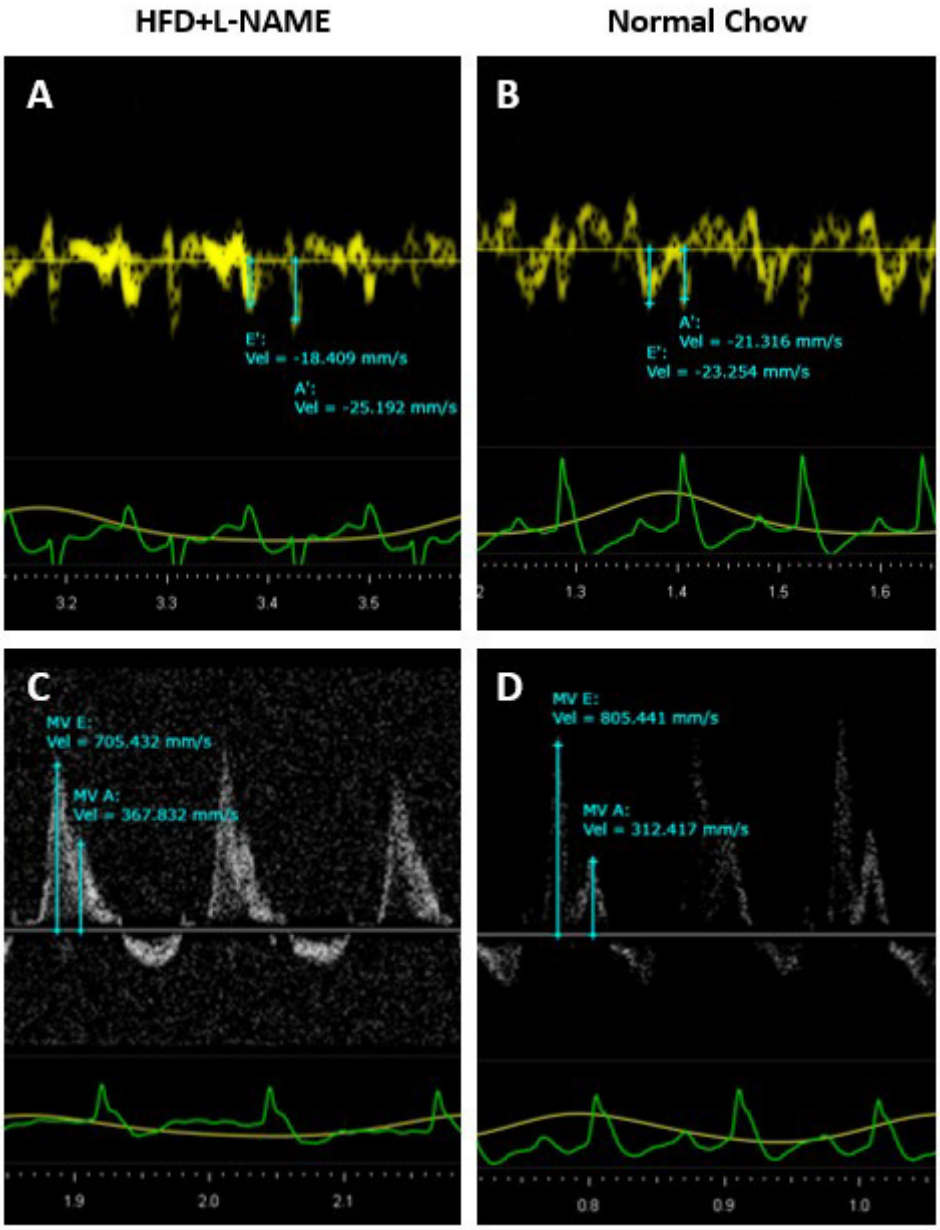

Figure 2.3.7: Tissue doppler and pulsed wave doppler of the mitral valve in diastole.

Tissue doppler velocity at he mitral valve annulus was assessed using tissue doppler by measuring e' and a' (labelled) in HFD+L-NAME (A) and Normal Chow (B) mice. Flow through the mitral valve measured using the E and A wave (labelled) in HFD+L-NAME (C) and Normal Chow (D) mice.

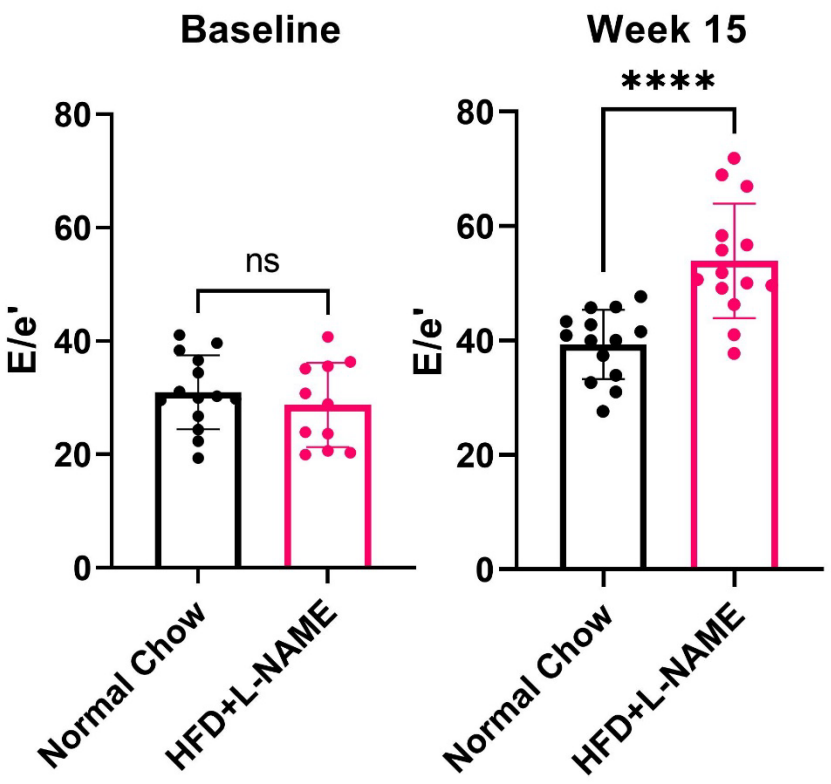

Figure 2.3.8: Increased E/e' in HFD+L-NAME mice at week 15 versus Normal Chow.

E/e' was significantly increased following 15 weeks of HFD+L-NAME in C57BL6/J mice when compared to the Normal Chow control group ($p < 0.0001$). Error bars represent ±SD (Unpaired t-test) (n=14/15).

E/e' is a frequently applied echocardiography parameter used in assessing diastolic function. E refers to the pulsed wave doppler flow measuring passive filling of the left ventricle in early diastole which is expected to decrease as ventricular relaxation becomes impaired in diastolic dysfunction (Figure 2.3.7 C-D). In conjunction with the E wave, e' is recorded by tissue doppler and measures the tissue velocity of the mitral vale annulus (Figure 2.3.7 A-B) which is expected to decrease with the development of diastolic dysfunction. A increase in the ratio of E/e' indicates a reduction in ventricular relaxation and filling capacity of the left ventricle supporting a diagnosis of diastolic dysfunction. Following 15 weeks of HFD+L-NAME mice displayed an increase in E/e' when compared to the Normal Chow control group (Figre 2.3.8). HFD+L-NAME mice had an average E/e' of 53.92 (±2.677) which was 14.61 (mean diff.) greater than the Normal Chow control group at 39.31 (±1.165) ($p < 0.0001$) (Figure

2.3.8). Ideally in assessing diastolic dysfunction we would include pulsed wave doppler E/A ratio measuring the change in flow in passive filling in early diastole versus peak flow velocity in late diastole. However, the resting heart rate of most mice was too high, >500bpm, to accurately distinguish between the E and A waves (Figure 2.3.7C-D) precluding the use of this parameter.

Following tissue collection, histology was carried out on all hearts collected at the conclusion of the study to identify any development of interstitial and perivascular fibrosis. Picrosirus red and fast green was used to visualise and later quantify fibrosis. An increase in collagen deposition throughout the interstitium is expected to occur as a result of HFpEF in the form of perivascular and insterstitial fibrosis. Sections were taken and stained from 5 points evenly distributed throughout the ventricles, each of these points are indicated along the x axis of Figure 2.3.9. Whilst some points throughout the hearts contained signficantly different levels of fibrosis between our two groups, this was not a consistent result which is reflected in the combined data (Figure 2.3.9). In the combined data the HFD+L-NAME mice contained 5% fibrosis ($\pm$2.742) whilst the Normal Chow cohort contained 3.612% fibrosis ($\pm$1.019) with a mean difference of only 1.388% (p value=0.2332). Following the ventricles, the atria were sectioned, stained and analysed using the same methods at 3 evenly distrubuted points throughout the tissue. Unlike the ventricles, the atria did not result in any changes in collagen deposition between the Normal Chow and HFD+L-NAME groups as seen in Figure 2.3.10. This data demonstrates that this model does not induce detectable increased interstitial fibrosis (Figure 2.3.9-2.3.10).

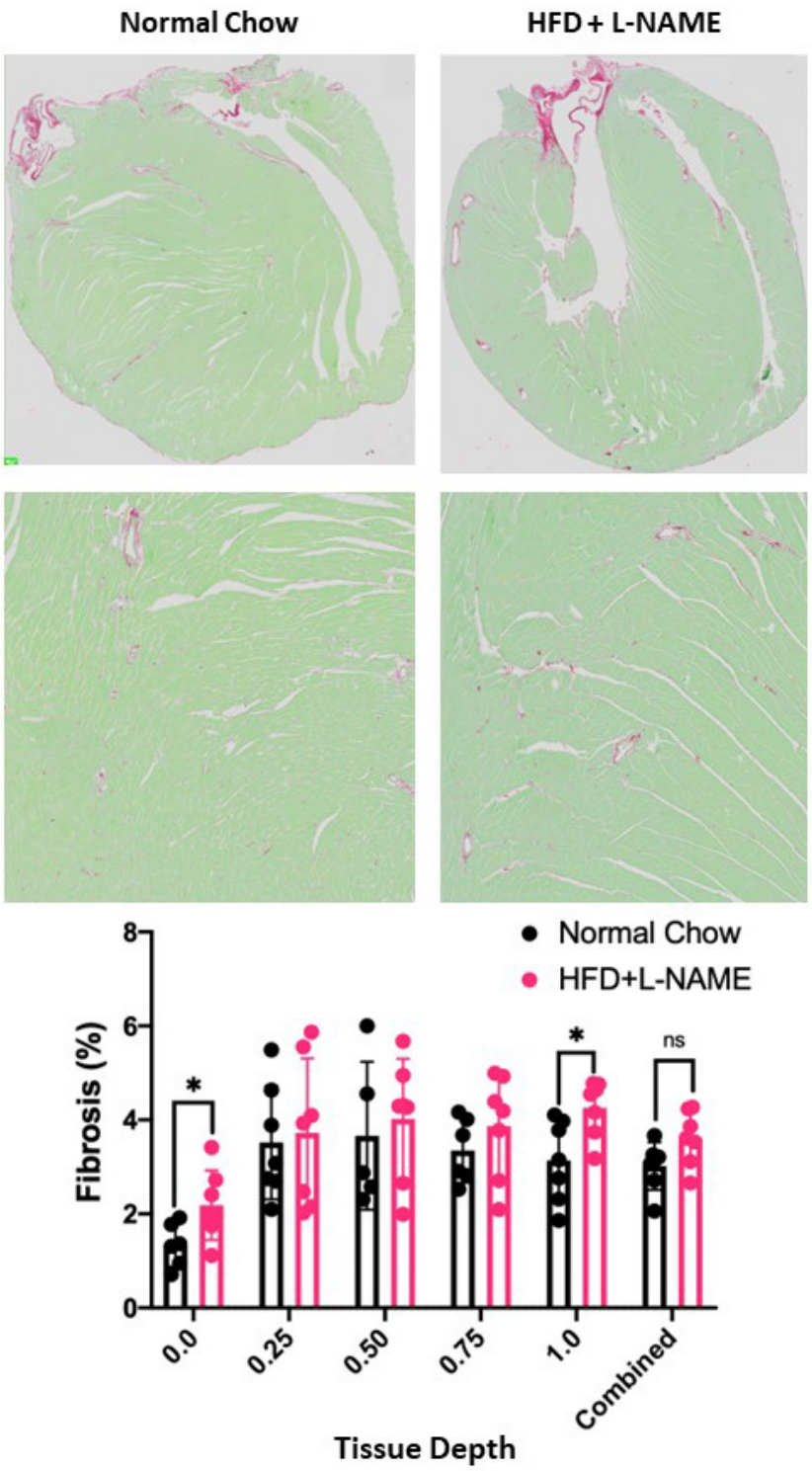

Figure 2.3.9: Limited changes in interstitial and perivascular fibrosis in ventricles post 15 weeks.

Limited changes in interstitial and perivascular fibrosis in the ventricles of HFD+L-NAME versus Normal Chow mice following 15 weeks of their assigned diet. X axis titles indicate depth through the tissue. Brightfield images 2x and 20x magnification. Error bars represent ± SD (Unpaired t-test) (n=6/7).

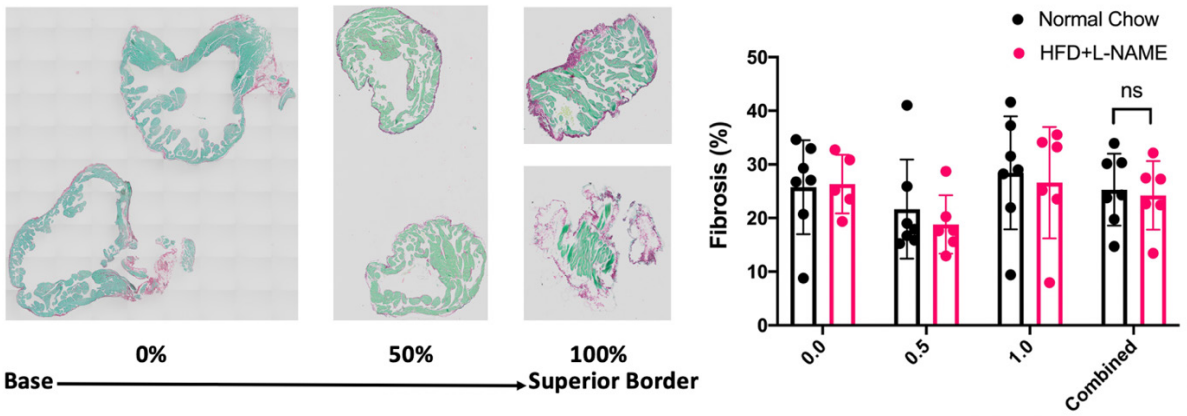

Figure 2.3.10: No changes in interstitial and perivascular fibrosis within the atria of HFD+L-NAME mice post 15 weeks.

No changes in interstitial and perivascular fibrosis in the atria of HFD+L-NAME versus Normal Chow mice following 15 weeks of their assigned diet. X axis titles indicate depth through the tissue and align with the corresponding percentage. Brightfield images 2x magnification. Error bars represent ± SD (Unpaired t-test) (n=6/7).

To identify changes in cardiomyocyte size and blood vessel density ventricle and atria sections were stained using Wheat Germ Agglutinin (WGA) for cell borders and Isolectin B4 (IB4) for blood vessels. This was carried out on 4 ventricle sections (Figure 2.3.11) and 3 atria sections (Figure 2.3.12) evenly distributed from each heart to thoroughly assess any detected changes. Following analysis, a significant increase in cardiomyocyte size was detected in the HFD+L-NAME ventricles with a normalised cardiomyocyte size of 124.5 (±15.73) versus the Normal Chow ventricles with 100 (±13.12) (p value=0.0082) (Figure 2.3.11). Despite a trend towards increased blood vessel density in the HFD+L-NAME ventricles, no significant change was identified. No changes were identified in atrial sections at week 15, following the same protocol. However, differences in the orientation of atrial tissue versus the ventricle tissue limited the accuracy of this analysis pipeline resulting in fewer replicates than the ventricles.

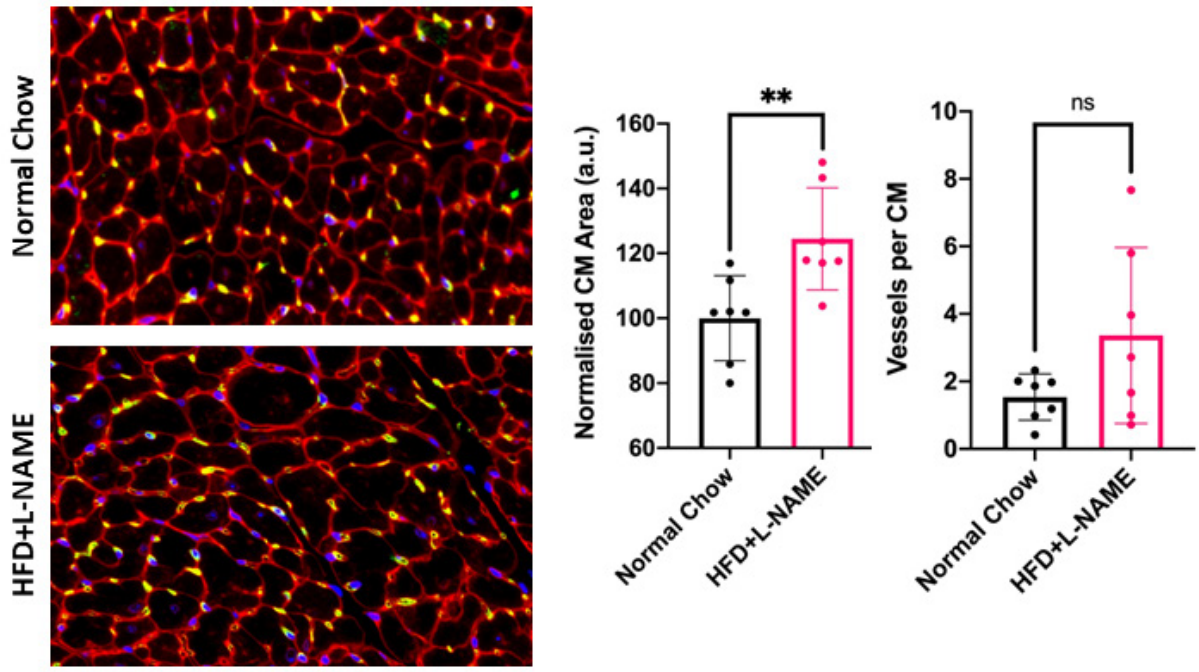

Figure 2.3.11: Increase in cardiomyocyte hypertrophy in the ventricles of HFD+L-NAME mice at 15 weeks.

WGA (Thermo Fisher Scientific, W32466) and IB4 staining (Thermo Fisher Scientific, 121411) (40x magnification) on the ventricles at week 15 identified a significant increase in cardiomyocyte hypertrophy, 24.5 greater in HFD+L-NAME mice than the Normal Chow controls. No significant change was identified in blood vessel density. Cardiomyocyte area data is normalised to the control group and presented in arbitrary units (a.u.) ± SD (Unpaired t-test) (n=7).

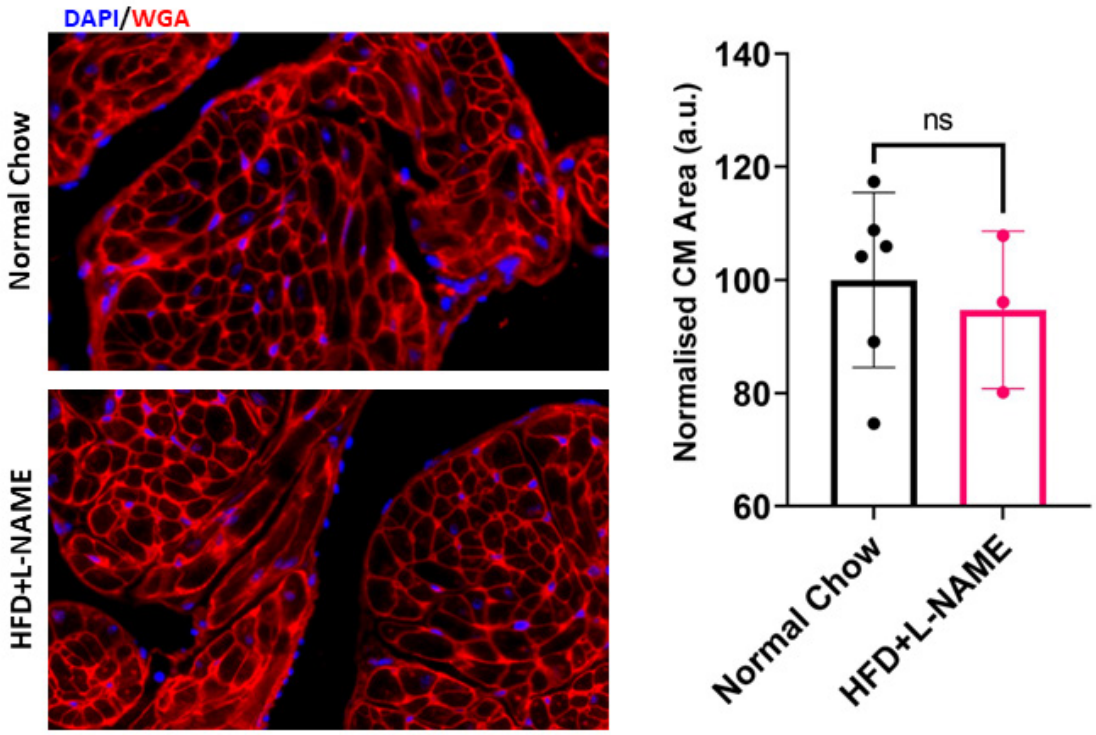

Figure 2.3.12: No change in cardiomyocyte hypertrophy in the atria of HFD+L-NAME mice at 15 weeks.

WGA (Thermo Fisher Scientific, W32466) and IB4 (Thermo Fisher Scientific, 121411) staining (40x magnification) on the atria of Normal Chow and HFD+L-NAME mice at 15 weeks identified no changes in cardiomyocyte area. Cardiomyocyte area data is normalised to the control group and presented in arbitrary units (a.u.) ± SD (n=3/6) (Paired t-test).

To further investigate the mechanisms driving HFpEF in this model we undertook TMT Discovery Proteomics (Figure 2.3.13) on half of the whole ventricles collected from each mouse (n=7 per group). The most significant change between HFD+L-NAME and Normal Chow hearts in this experiment was PDK4 which is commonly upregulated in hearts under metabolic stress. When comparing differential expression of proteins in HFD+L-NAME to Normal Chow, PDK4 was detected with a Log2 fold change of 2.371 (p=0.0010). In addition to PDK4, Perilipin 5 (Plin5) and Acyl-CoA thioesterase 2 (Acot2) were significantly upregulated in HFD+L-NAME versus Normal Chow with Log2 fold changes of 1.146 (p=0.0115) and 1.088 (p=0.0019) respectively.

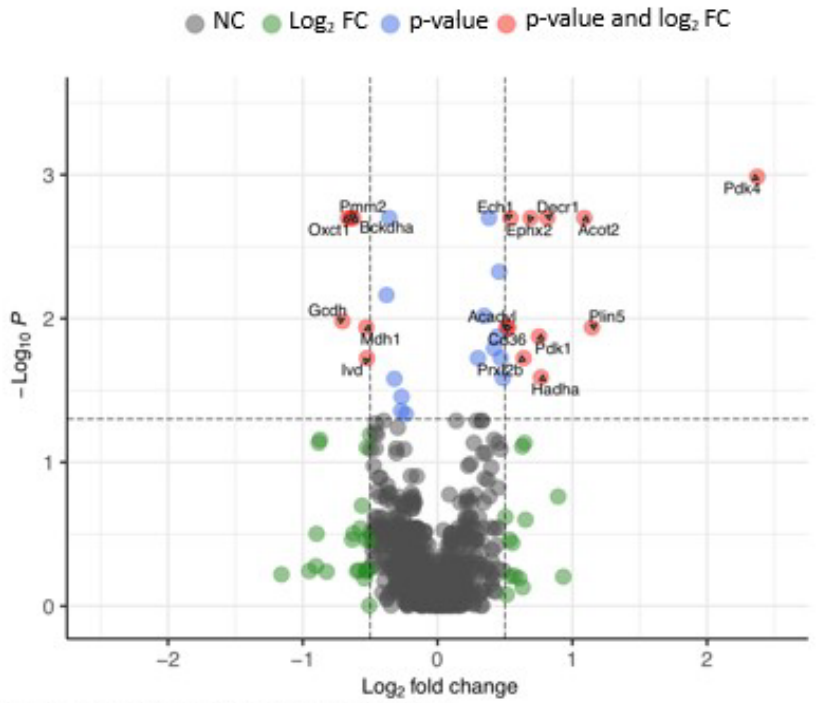

Upregulated Proteins in HFpEF Heart Tissue.

Protein	Process
Pdk4	Inhibitor of pyruvate dehydrogenase and glucose oxidation
Plin5	Lipid associated protein and regulator of lipolysis and lipogenesis
Acot2	Increases Fatty Acid β oxidation
Decr1	Beta oxidation and metabolism of polyunsaturated fats
Hadha	Beta oxidation of medium and long chain fatty acids
Pdk1	Isoenzyme of Pdk4
Ephx2	Hydrolysis of lipid epoxides; signalling; regulation of hypertension
Prxl2b	Antioxidant; lipid biosynthesis
Ech1	Fatty acid beta oxidation
CD36	Membrane fatty acid transporter; fatty acid metabolism
Acadvl	Fatty acid beta oxidation

Downregulated Proteins in HFpEF Heart Tissue.

Protein	Process
Lvd	Leucine metabolism; oxidation of short chain saturated fatty acids
Mdh1	Oxidative phosphorylation
Bckdha	Branched chain amino acid catabolism
Pmm2	Protein glycosylation
Oxct1	Ketone body energy utilisation
Gcdh	Amino acid oxidation

Figure 2.3.13: TMT discovery proteomics identified changes in metabolic markers.

TMT discovery proteomics carried out on ventricles collected from HFD+L-NAME and Normal Chow mice. Log_2 Fold Change threshold was set at 0.5 and $-Log_{10}$ P threshold was set at 0.05 (n=7). Following this proteomics run, GO term analysis (Figure 2.3.14) was carried out on all detected proteins with a Log2 fold change above 0.5 and a p - value $\leq$0.05, to identify pathways that are significantly impacted by the onset of HFpEF in this model. As seen in Figure 2.3.14, most of these pathways are involved in metabolism including the most significantly affected pathway, fatty acid metabolism. These results indicate metabolic changes as the key factor driving HFpEF development in this model. No changes have been identified in processes influencing the extracellular matrix throughout these analyses (Figure 2.3.13 and 2.3.14) further supporting the limited effect on fibrosis seen in Figure 2.3.9 and 2.3.10. Upregulation of Plin5 and Pdk4 were validated via immunohistochemistry and imaged using the Leica SP8 confocal microscope (Figure 2.3.15)

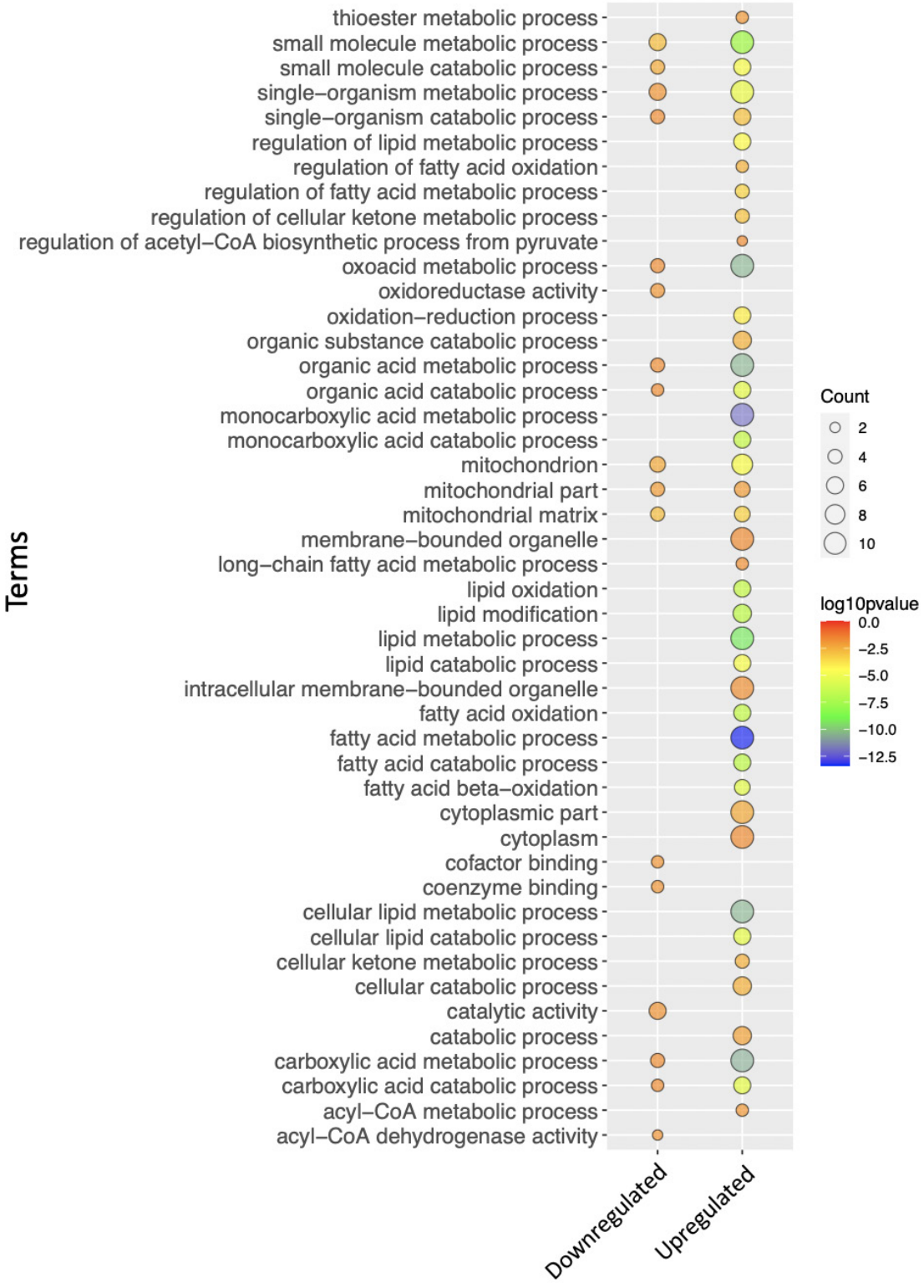

Figure 2.3.14: Significant changes in metabolic processes identified in up and downregulated proteins.

Significantly altered pathways were identified in HFD+L-NAME versus Normal Chow mice using GO term analysis. Gene count and Log_{10} P value are displayed (n=7). GO term analysis was carried out with the guidance and expert input of Dr Robert Hume.

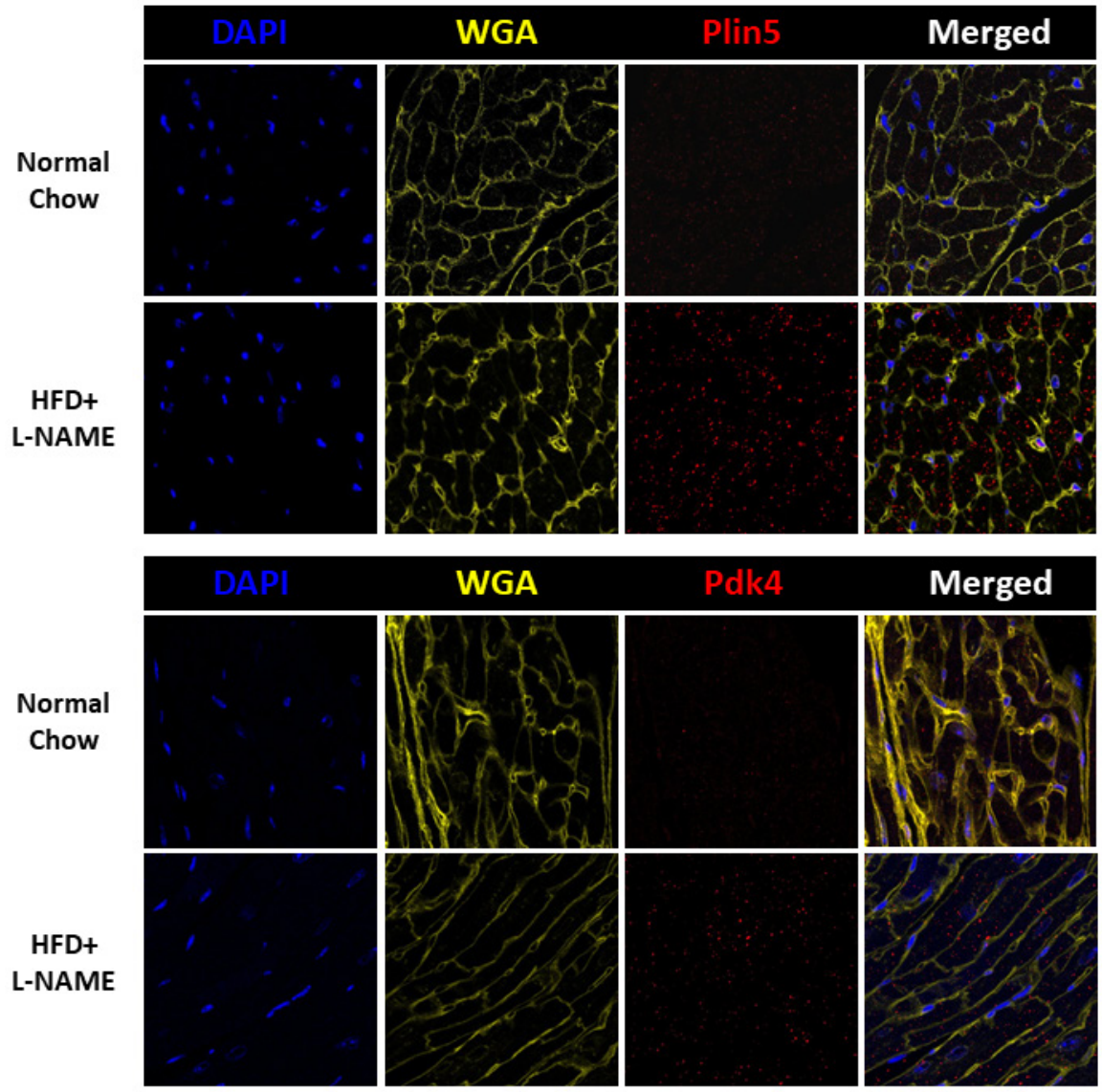

Figure 2.3.15: Validation of TMT discovery proteomics result using immunofluorescent staining.

Immunofluorescent staining for Plin5 (Thermo Fisher Scientific, PA1-46215) and Pdk4 (Thermo Fisher Scientific, PA5-46215) (100x magnification) confirmed the upregulation of these proteins in HFD+L-NAME mice when compared to the Normal Chow control (n=7).

2.4 DISCUSSION

Within the HFpEF patient population there remains a lack of unifying diagnosis that further complicates the challenge of therapeutic development in this field. Despite significant improvements in the creation of clinically relevant animal models, the heterogeneity within the human patient population, combined with combinations of comorbidities results in subsets of patients with unique therapeutic needs. A consequence is that very few clinical trials for therapeutic interventions in HFpEF have successfully met primary endpoints (29). Efforts have been made to address the unmet need of appropriate animal models that accurately reflect this complex syndrome, however, many continue to fall short. Based on the current understanding of HFpEF, an accurate animal model needs to have maintained left ventricular systolic function with diastolic dysfunction, hypertension, exercise intolerance, pulmonary oedema, and concentric cardiac hypertrophy.

A variety of rodent models have been developed to reflect HFpEF phenotype. Many focus on single aspects of the syndrome to produce the characteristic diastolic dysfunction. Commonly these focus on obesity and hypertension, which have been achieved using pharmacological, diet and/or surgical approaches. Hypertension has been achieved in murine models using several approaches. Most notably, L-NAME is used to induce hypertension through endothelial cell dysfunction as a result of nitric oxide synthase inhibition. Previous reports have noted the decrease in cardiac function and onset of myocardial fibrosis following left ventricular pressure overload as a result of L-NAME treatment (48, 49). Whilst hypertension is a common comorbidity of HFpEF, occurring in approximately 75% of patients (177), it only reflects part of the phenotype and therefore fails to reflect the additional metabolic factors that contribute to the development of HFpEF. Obesity based models have focused more heavily on the metabolic components of HFpEF and is clinically relevant to many HFpEF patients, as over 80% are overweight or obese (38). HDFs over the course of 20 weeks are reported to result in diastolic dysfunction, pulmonary oedema, and renal dysfunction, all

comorbidities associated with HFpEF (172). These approaches focus on single key aspects of the HFpEF phenotype. A recently published model exploiting a combination of these methods has proven to be more effective (50).

The two-hit approach to HFpEF, established by Schiattarella et al. in 2019, has become a frequently used model throughout the literature to investigate HFpEF (50, 51, 178, 179). In establishing this model, they reported a significant decline in diastolic function, secondary to the onset of hypertension induced by 0.5g/L of L-NAME in drinking water, combined with the metabolic stress of 60% calories from fat diet. Additionally, a decrease in exercise tolerance, pulmonary oedema, cardiac hypertrophy, and interstitial fibrosis were reported. Development of these clinical features of HFpEF in a murine model provided an accurate reflection of the HFpEF phenotype to utilise in future studies. The work presenting in this chapter aimed to validate this model in the C57BL6/J mouse. In doing so, the established model could be used by our group to explore potential benefits of candidate novel peptides described in Chapter 3: Development of Novel Platelet Derived Growth Factor-AB Mimetic Peptides.

We replicated several results reported in the Schiattarella et al publication. Specifically, we replicated the significant decrease in diastolic function (Figure 2.3.6-2.3.8), induced hypertension (Figure 2.3.4, observed significant weight gain (Figure 2.3.1) and induced cardiomyocyte hypertrophy (Figure 2.3.11). However, we identified key points of difference in our data when compared to others in the literature. These included our inconclusive results in exercise tolerance and insignificant changes in the ECM with no development of interstitial or perivascular fibrosis (Figure 2.3.9-2.3.10).

Schiattarella et al. quantified diastolic function using E/e' and GLS identifying a significant increase in both parameters. We replicated this in our own study using the same parameters (Figure 2.3.6 and 2.3.8) at 15 weeks indicating a decline in left ventricle relaxation and increased left ventricle filling pressure resulting in diastolic dysfunction. Ideally confirmation of diastolic dysfunction would include additional parameters such as E/A wave and left atrial volume (25) however, these parameters have limited accuracy in the mouse heart due to their high heart rate (180) requiring us to make these conclusions based on E/e' and GLS alone. A key component of cardiac function in HFpEF is the onset of diastolic dysfunction in conjunction with maintained systolic function (20). This was achieved in the 'Two Hit Approach' by Schiattarella et al. at 15 weeks indicated by maintained ejection fraction above 50% and no significant difference between Normal Chow and HFD+L-NAME mice. In our own study, we were successful in maintaining LVEF above 50% across both groups (Figure 2.3.5). However, the LVEF was significantly decreased in HFD+L-NAME mice versus Normal Chow control mice (Figure 2.3.5). Despite this decrease, preserved LVEF above 50% indicates maintained systolic function at 15 weeks. A key factor in developing this cardiac phenotype was mechanical stress in the form of pressure overload of the left ventricle as a result of hypertension. Hypertension was induced in this model using 0.5g/L L-NAME that inhibited nitric oxide synthase resulting in endothelial cell dysfunction and hypertension. Whilst this effect was present in both our own data (Figure 2.3.2) and Schiattarella's, this mechanism of action for L-NAME induced hypertension is well established (48). To drive the HFpEF phenotype in this model the mechanical stress was combined with metabolic stress with the application of the HFD. This resulted in significant weight gain in HFD+L-NAME mice over the course of 15 weeks (Figure 2.3.1) aligning with what was observed in the literature (50). The combined effect of these factors on the heart identified in our study was an increase in cardiomyocyte hypertrophy in the ventricles of HFD+L-NAME mice (Figure 2.3.11) quantified via immunohistochemistry. This result was also identified by Schiattarella et al., observed in increased heart weight by tibia length and immunohistochemistry.

Schiattarella et al. assessed changes in exercise tolerance using a treadmill running test that successfully identified a significant decrease in cardiac function in HFD+L-NAME mice at 15 weeks. Replicating this assay was not possible in our study due to our Animal Ethics Committee's concerns about ethical use of rodent treadmills and the distress induced to maintain exercise. To address this problem, we replaced this experiment with a swim test. Swimming is established as a training protocol in mice (175, 176) but has not been reported as a method of assessing exercise tolerance. Unfortunately, this method of assessing swimming ability in our mice was confounded by the significant increase in size of HFD+L-NAME mice resulting in increased buoyancy (Figure 2.3.3). Therefore, accurate measurement of exercise tolerance was not possible since HFD+L-NAME mice appeared to expend less energy to remain afloat leading to longer swim times. This assay was inconclusive in our study resulting in no definitive decline in exercise tolerance.

Perivascular and interstitial fibrosis and known features of HFpEF in humans and are considered key parameters when modelling the phenotype *in vitro*. In establishing the two-hit approach to HFpEF, Schiattarella et al. reported a significant increase in fibrosis using this method in C57BL6/N mice. This increase was quantified by Schiattarella et al. via histological analysis using Masson's trichrome staining for collagen. In our study, we also used histological staining with picrosirius red and fast green (counterstain) to visualise collagen changes throughout the myocardium (Figure 2.3.9-2.3.10). Sections were collected the whole way through the ventricles and atria of all mice and fibrosis quantification using Image J applied to stained sections. Despite significant efforts to identify changes in the ECM and any onset of perivascular and interstitial fibrosis, we were unable to replicate this result (Figure 2.3.9-2.3.10). One explanation may be our use of the C57BL6/J mouse strain that differed from the C57BL6/N strain utilised by Schiattarella et al. which we chose to do due to very limited local supply of the C57BL6/N strain. Supporting our results, other groups have also replicated aspects of the HFpEF phenotype from this model in C57BL6/J (51) mice, however none have reported ECM

changes or significant fibrosis. Causative differences between mouse strains is a possible hypothesis for these inconsistent findings however, further experimentation is required to confirm.

Further to these notable differences in our results compared to those of Schiattarella et al, were inconsistences in blood pressure monitoring. Whilst significant onset of hypertension is noted in the HFD+L-NAME treated mice at week 10, we did not identify a significant difference between Normal Chow and HFD+L-NAME mice at week 5 (Figure 2.3.2), as is seen in Schiattarella's 'Two Hit Approach'. Additionally, an unexpected decrease in blood pressure from week 5 to week 10 is noted in the Normal Chow cohort. Whilst the later onset of hypertension could be due to the aforementioned differences in strain, we believe that combined with the change in blood pressure noted in the Normal Chow cohort that it is more likely the result of limitations of the method used. Blood pressure was measured via tail cuff that has a number of well-established limitations particularly, stress induced by the handling and restraints necessary to carry out monitoring (181) in addition to providing only intermittent recording (182). Telemetry is considered the gold standard for blood pressure monitoring in rodents (181) and would have addressed many of the limitations of tail cuff monitoring, however this is an invasive and expensive method and was therefore not used in this study.

Late onset of hypertension observed in our HFD+L-NAME cohort could be a contributing factor in the insignificant development of interstitial and perivascular fibrosis in these mice. As previously discussed, significant fibrosis was reported in Schiattarella et al which differed to our own results. Given the earlier onset of hypertension also noted in their study, we hypothesise that the reduced time of hypertension in our HFD+L-NAME mice could be a contributing factor to this difference in disease phenotype. Further studies over a longer time course using the onset of hypertension as a marker for commencement of phenotype development would allow us to determine if our strain of mouse, C57BL6/J, also develops significant interstitial and perivascular fibrosis.

We performed TMT discovery proteomics to identify underlying changes in the myocardium that may not be visible histologically. Proteomic analysis of HFD+L-NAME mice highlighted significant changes in metabolic processes, including upregulated Pdk4, Plin5, and Acot2, indicating the hearts were under metabolic stress. PdK4 is a mitochondrial protein that is part of the pyruvate dehydrogenase complex (PDH). Its primary function is as a regulator of general metabolism. This regulatory role is carried out by inhibiting the oxidation of glucose and amino acids from pyruvate (183). In the heart, upregulation of Pdk4 has been associated with metabolic stress (184) most commonly induced by high fat diets and increased glycolysis (185), and following induced ischemia (186). Plin5 is a protein that coats lipid droplets increasing their stability by preventing hydrolysis (187). It is known to increase in conditions of lipid overload often associated with obesity (188). Additionally, it has been established as a regulator of myocardial lipid metabolism acting in a cardioprotective capacity during myocardial injury (189, 190). It has been suggested that increased Plin5 in these conditions is a compensatory mechanism to protect against lipid induced stress (188). Lastly, Acot2 facilitates mitochondrial fatty acid oxidation in the heart, among other organs (191), and is reported to increase following HFDs in rodent models (192). The significance of cardiometabolic processes in driving the HFpEF phenotype have recently been supported by reduced hospitalisation of patients following treatment with SGLT2i empagliflozin, an established treatment for type 2 diabetes patients, in HFpEF clinical trials (29). Importantly, these findings correlate with other proteomic analyses using this model (193). However, despite significant changes in metabolic processes, no changes have been identified in proteins of the ECM, correlating with our absence of detectable fibrosis.

The relatively low abundance of ECM proteins compared to proteins of the myocardium makes them difficult to detect. This imposes a significant limitation in detecting changes within the ECM. To address this problem, enrichment of the ECM during sample preparation ahead of proteomics could be used

to increase their abundance and detectability within the sample (194). However, we chose not to do this due to the insignificant changes in the ECM observed in our model throughout extensive histological analysis of the ventricles and atria. Whilst the significant changes in metabolic processes of the HFD+L-NAME cohort is consistent with the current understanding of metabolic stress on the heart during development of HFpEF (195), the lack of changes in the ECM is an important limitation in the context of our intended application of this model. Despite the insignificant changes identified in histological and proteomic analysis, single cell RNAseq carried out by our collaborators at the Harvey Lab, Victor Chang Cardiac Research Institute identified changes indicative of a potentially emerging fibrotic phenotype. In analysis completed by Dr Ralph Patrick, upregulation of several fibrosis genes was identified in addition to down regulation of *Igf1* (unpublished data) that is reported to have an anti-fibrotic effect in the heart (196). In future experiments, enrichment of the ECM for proteomics could be considered to identify subtle changes that may have gone undetected whilst longer term treatment of HFD+L-NAME may have elicited a fibrotic phenotype of HFpEF.

Previous work by our laboratories established the efficacy of recombinant human PDGF-AB in significantly improving cardiac function in murine (58) and porcine (57) models of acute myocardial infarction (MI). The mechanism of action for PDGF-AB, identified in the porcine model of acute MI, is through modulation of the cardiac scar with most of the effects of PDGF seen in the ECM and composition of replacement fibrosis (138). To investigate how these effects are translated in chronic heart failure, the Two Hit Approach to HFpEF was pursued. Based on early reports of this model we had hypothesised that changes in the ECM would provide us with a target for novel therapeutics, such as PDGF-AB (57, 58). However, given the very limited ECM change in the development of HFpEF in this model, the previously identified mechanism of action for PDGF-AB was deemed unlikely to have a significant downstream effect on cardiac function. We therefore concluded that whilst the model in this chapter accurately reflected some components of HFpEF (significant diastolic dysfunction), its

limited perivascular and interstitial fibrosis made this an inappropriate model for assessing the effects PDGF-AB on cardiac function.

The aims of this chapter were to 1) validate the two-hit approach to HFpEF and 2) investigate the mechanisms driving the HFpEF phenotype in this model. This could identify possible targets for novel therapeutics. Whilst our proteomics experiments were unable to identify changes in the ECM following the onset of HFpEF, it did highlight the significance of metabolic processes in this model. However, single cell RNAseq carried out by our collaborators pose the potential for an emerging fibrotic phenotype, the limited signs of physiological change as a result of these genomic differences still does not support the use of this model for investigation of PDGF mimetic peptides. Whilst validation of this model was successful in replicating many key components of the HFpEF phenotype, particularly diastolic dysfunction with preserved systolic function, hypertension, and obesity, we were unable to replicate all aspects of this phenotype utilising the two-hit approach in C57BL6/J mice.

2.5 CONCLUSION

Here we show that a recently reported 'Two Hit Approach' to HFpEF can successfully replicate some clinical aspects of the human HFpEF disease in male C57BL6/J mice. In doing this, we highlight the significance of metabolic processes driving the HFpEF phenotype. However, we also show that the model falls short with respect to inducing cardiac ECM change (lack of perivascular and interstitial fibrosis). Due to the established mechanism of action in our novel PDGF-AB therapeutic (138), the mouse model of HFpEF here is not be suitable for testing the cardiac reparative ability of PDGF-AB.

CHAPTER 3: DEVELOPMENT OF NOVEL MIMETIC PEPTIDES FOR PLATELET DERIVED GROWTH FACTOR

3.1 INTRODUCTION

Platelet derived growth factors (PDGF) are potent mitogens (86-88) and chemotactic agents (98), that play a significant role in wound healing (94) and angiogenesis (96) in adults but also play a part in foetal development (111, 113-115). PDGFs act by binding to the PDGF receptors (PDGFR), PDGFRα and PDGFRβ (89) via autophosphorylation, triggering a signalling cascade that effects proliferation, differentiation, cell survival and chemotaxis (104). In order to be biologically active, PDGF isoforms, made up of the either A, B, C or D chains, must dimerise as either heterodimers or homodimers e.g., AA, AB, BB, CC, and DD (89-91). Similarly, PDGF receptors must dimerise to be biologically active, as αα, αβ or ββ (103). PDGF-AB and PDGF-BB are used as controls throughout this chapter. PDGF-AB has been the basis of prior work completed by our laboratory whilst PDGF-BB contains a central component of our peptide design (57, 58). Additionally, Hume et al. showed that the effects of PDGF-AB and -BB on human cardiac fibroblasts cluster more closely than the effects of PDGF-AA in genomic analysis using bulk RNAseq (138). These results suggest that the effects of PDGF-AB and -BB are more similar in the context of the heart. Our groups have identified improved cardiac function following treatment with recombinant human PDGF-AB post myocardial infarction (MI) in murine and porcine models (57, 58). In the murine model improved cardiac function was noted alongside a reduction in size of the cardiac scar and pro-regenerative effects seen in endothelial cells, fibroblasts, and cardiomyocytes (58). The promising effects of PDGF-AB post-MI were replicated in the porcine model resulting in improved cardiac function however no change in size of the cardiac scar. Despite no reduction in cardiac scar, significant changes in alignment and composition of the scar post-MI provided evidence towards modulation of the scar as a likely mechanism for improved cardiac function following treatment with PDGF-AB (57).

In the PDGF-A and -B chains receptor binding is facilitated by the loop I and III regions of their chains (121, 122). Especially significant of these is the loop III region in the PDGF-B chain that has been implicated in binding to and activation of both PDGFRα (123) and PDGFRβ (124). Loop III's role in PDGFR signalling has been associated with an effect on proliferation and chemotaxis highlighting the significance of this region's role in PDGFs biological function (121). The significance of loop III in the PDGF-B chain was confirmed by applying it in the synthesis of PDGF analogues (133-135). The analogues produced by Jehanli et al. used loop III in multiple settings, either as a homodimer of the region or as a heterodimer with either loop I or II. These analogues confirmed the receptor binding and activation capacity of this region and its ability to maintain biological function when isolated from the remainder of the PDGF-B chain.

PDGF has been approved for therapeutic use in musculoskeletal and maxillofacial disorders (129) in addition to the treatment of chronic non-healing diabetic wounds in topical preparations (130). By utilising a topical preparation in this context, the PDGF-BB is able to perform its therapeutic function without encountering the limiting effects of enzymatic degradation on the ligand. All full chain PDGF ligands are highly potent and therefore only require small concentrations to illicit a functional effect, however, like many biologic therapeutics they have poor pharmacokinetic properties, limiting clinical applications. Molecules smaller than 45kDa are known to be rapidly cleared through glomerular filtration due to their small size as opposed to large plasma proteins such as albumin that has a molecular weight of 66.5kDa (197). PDGF-AB has a molecular weight of only 26.4kDa; additionally PDGF has a known susceptibility to enzymatic degradation in the blood stream (139). Together these factors result in a very short half-life of approximately 2 minutes (139). To increase the half-life of biologic therapies, a range of methods have been developed to alter their chemical structures. Unfortunately, a prolonged increase in PDGFR signalling can increase the risks of metastases occurring in diagnosed or undiagnosed cancer patients (116), emphasising the need for short term use. This

demonstrates the need for a half-life extending mechanism that prolongs the half-life of PDGF long enough to achieve its therapeutic function, but short enough to not increase risks of adverse off target effects. Importantly, despite this relationship between long term upregulation PDGFR signalling and increased risk of tumorigenesis, it has been established that PDGF alone is not capable of inducing tumour growth (117). In patients with prior metastases, prolonged use of PDGF-BB based therapeutics have been associated with increased recurrent metastases, highlighting the importance of short-term exposure (132).

Whilst biologic based therapies are very potent often resulting in good efficacy, poor pharmacokinetic properties can limit their clinical applications, particularly in the context of protein therapies. This problem is evident in the short half-life of PDGF (139) limiting its delivery in our previous animal models to infusion via an osmotic mini-pump which provides a gradual PDGF infusion of 0.5ul/hr, rather than treatment via bolus injection (57, 58). Enhancing the pharmacokinetic properties of PDGF through half-life extension could improve its translational prospects by broadening its delivery methods. To address this, we applied established mechanisms of half-life extension to our selected functional region with the aim of decreasing its susceptibility to enzymatic degradation and reducing its rapid clearing via glomerular filtration.

Methods of extending half-life in biologics typically focus on either increasing their size to avoid glomerular filtration or decreasing their susceptibility to protease cleavage. In our study, we focused on creating PDGF mimetics with increased peptide size by conjugating to human serum albumin (HSA) and adding a novel heparin binding domain. Furthermore, we aimed to increase the peptides stability by minimising effects of protease cleavage by cyclising and stapling. Cyclisation of a peptide involves binding of the C and N terminus of a peptide taking them from a linear to a cyclic structure whilst stapling in this context involves binding the 2 chains of the dimer using an irreversible hydrocarbon

bridge. Both of these methods protect against enzymatic degradation applying structural changes to the linear form of the loop III dimer. HSA conjugates have previously been reported as a successful alternative to albumin fusion proteins as a means of enhancing pharmacokinetic properties of biologic based therapies (148). In this study, Zorzi et al. showed a biologic HSA conjugate bound to Factor XIII increased the half-life from 13 minutes to over 5 hours by utilising a 'piggyback' approach to bind to free floating albumins in the blood stream. By binding to albumins, the peptide is able to avoid clearing by kidney filtration extending its half-life and allowing it more time to reach its site of action and perform its therapeutic function.

Albumin is the most abundant carrier protein in blood, with high stability owing to its size of 585 amino acids, 35 of which are cysteine residues (164), thus giving albumin a long plasma half-life of approximately 19 days (163). The long half-life of albumin is also partly due to its ability to utilise the Fc neonatal receptor (FcRn) pathway, cycling through endothelial cells protecting them from enzymatic degradation (147). The rate limiting function of albumin in the clearing of substances from the bloodstream has been investigated since the 1980s (198) which has become a focal mechanism of half-life extension throughout the 21st century (149, 165-167). Further benefits of using a synthetic peptide are the increased efficiency in production of synthetic peptides versus the labour intensive and complex production of recombinant full-length proteins and decreased quality control measures required for synthetic production (199).

Hypothesis

A peptide mimetic of the PDGF-B chain loop III region will maintain the biological function of PDGF receptor signalling and provide a foundation for incorporating mechanisms for pharmacokinetic enhancement.

Aims

1. Identify a region of the PDGF protein chains that can maintain biological function when tested as a discrete peptide.
2. Incorporate half-life extending elements into the design of novel PDGF-mimetic peptides whilst maintaining PDGF receptor signalling capacity.
3. Synthesise novel PDGF-mimetic peptides and test their efficacy for key known functions of PDGFs *in vitro*.

In this chapter we aimed to design, synthesise and test synthetic peptides that act as mimetics of PDGF-AB by maintaining its biological function whilst incorporating half-life extending mechanisms to potentially improve its pharmacokinetic properties. The level of biological function of all peptides in this chapter were determined using *in vitro* assays testing the key established function of PDGFs *in vitro*. These were chemotaxis, collagen contraction, angiogenesis, proliferation, and activation of the PDGFR through phosphorylation of Erk. PDGFs are known to increased cellular chemotaxis (98, 101, 102). *In vitro* assays of chemotaxis are limited however in this chapter we aimed to assess the effects of our mimetic peptides on chemotaxis using a scratch test. Following this we assessed the effects of our mimetic peptides on collagen contraction. Collagen contraction is a key component of wound healing and is expected to increase with increased exposure to PDGF (200). PDGFs play a significant role in angiogenesis both in wound healing and foetal development (96, 97). A tube forming assay was then carried out to model angiogenesis *in vitro* and investigate the effects of our mimetic peptides on endothelial cells in the context of tube formation. PDGF is well established as a potent mitogen with

an expected increase in cellular proliferation following treatment with PDGF (86-88). The effect of our mimetic peptides on proliferation was assessed in this chapter using an 5-ethynyl-2'-deoxyuridine (EdU) assay for newly synthesised DNA, quantified via flow cytometry. Finally, activation of the PDGFR was assessed by western blotting for phosphorylation of Erk in cells treated with our mimetic peptides, a key component of the PDGFR signalling pathway that has downstream effects on proliferation, chemotaxis, and cell survival (104, 126).

Despite the promising effects of PDGF as a therapeutic, its poor pharmacokinetic properties have limited its translational prospects. These promising effects can be seen within our own laboratories extensive prior work on the role of PDGF-AB (57, 58, 138) and PDGFR (137) signalling in the heart post-MI. Developments in protein engineering have broadened the possibilities within lead optimisation allowing for the enhancement of biologic based therapies largely through enhancing stability and pharmacokinetic properties. Through the process of lead optimisation, medicinal chemistry methods of enhancing pharmacokinetics combined with more efficient production may allow us to maintain the therapeutic benefits of PDGF-AB whilst enhancing its clinical applications.

3.2 MATERIALS AND METHODS

3.2.1 Peptide Design

Peptide design was carried out in collaboration with the Payne Laboratory at The University of Sydney, School of Chemistry. A region of PDGF was selected as the functional region based on reported findings in the literature (120, 124, 126, 133) that was then used across all peptides synthesised.

3.2.2 Peptide Synthesis

Peptide Synthesis was carried out by Dr Daniel Ford from the Payne Laboratory at The University of Sydney, School of Chemistry. Automated peptide synthesis was completed on the Biotage SYRO 1 Peptide Synthesizer (Biotage, Uppsala, Sweden) using rink amide resins and Fmoc protected amino acids (Mimotope). Following synthesis, the peptide chains were cleaved from the resin and underwent disulphide formation prior to high performance liquid chromatography purification. Liquid Chromatography-Mass Spectrometry (UPLC) was performed on a Shimadzu 2020 UPLC instrument with a Nexera X2 LC-30AD pump, Nexera X2 SPD-M30A UV/Vis diode array detector and a Shimadzu 2020 (ESI) mass spectrometer operating in either positive or negative mode (Shimadzu, Kyoto, Japan). For all *in vitro* applications, peptides were reconstituted in sterile water at 100µg/ml.

3.2.3 Cell Culture

3.2.3.1 C2C12 Mouse Myoblasts

C2C12 mouse myoblasts were cultured using Dulbecco's Modified Eagle Medium (DMEM) (Lonza, 12-604F) supplemented with 10% foetal bovine serum (FBS) (Gibco, 10099141) and 1x penicillin streptomycin (Gibco, 15140122). Cells were routinely passaged at approximately 60% confluence by washing with sterile phosphate buffered saline (PBS) (Lonza, 17-516F) and dissociating using 1x TrypLE

Express (Gibco, 12604021) for 3 minutes at 37°C. Cells were seeded at required density and cultured at 37°C with 5% CO2.

3.2.3.2 C3H10T1/2 Cells

C3H10T1/2 mouse embryo fibroblasts were cultured using DMEM supplemented with 10% fetal FBS and 1x penicillin streptomycin. Cells were routinely passaged at approximately 70% confluence by washing with PBS and dissociating using 1x TrypLE Express for 3 minutes at 37°C. Cells were seeded at required density and cultured at 37°C with 5% CO2.

3.2.3.3 Human Coronary Artery Endothelial Cells

Human coronary artery endothelial cells (HCAECs) were cultured using MesoEndo Basal cell growth medium (Cell Applications Inc, 212-500) with 10% FBS. Cells were routinely passaged by washing with PBS and dissociating using 1x TrypLE Express for 5 minutes at 37°C. Cells were seeded at required density and cultured at 37°C with 5% CO2.

3.2.4 *In vitro* Functional Assays

3.2.4.1 Wound Healing Assay

C2C12 cells were dissociated as described in section 3.2.3.1 and seeded at $2.5x10^5$ cells per well in a six well plate followed by serum starving for 24 hours in DMEM with 1% FBS. Each well was scratched horizontally using a P200 pipette tip and treated with 3ml of treatment group specific media: 10ng/ml PDGF-AB/-BB (positive controls) (Peprotech, 100-00AB, 100-14B), 10ng/ml of PDGF-AB with 10µM AG1296 (negative control) (Abcam, ab141170) or 1µg/ml mimetic peptides in DMEM supplemented with 1% FBS. Additionally, a no treatment control (NTC) group was treated with DMEM supplemented

with 1% FBS. Cells were then incubated at 37°C for 24 hours. At 24 hours the cells were washed in PBS and fixed using 4% PFA (ThermoFisher, 28906) for 10 minutes at room temperature and washed again twice with PBS. Cells were then stained with 0.05% crystal violet (Sigma Aldrich, C0775) for 15 minutes at room temperature and washed twice in PBS prior to brightfield imaging using an Olympus CKX41 microscope. Cell migration was analysed using Image J by calculating optical density in the scratch area at 24 hours. The scratch area was measured at the time of treatment and applied in our analysis at 24 hours. Each treatment group was carried out in duplicate and the average of each treatment group was plotted for statistical analysis.

3.2.4.2 Collagen Contraction Assay

C2C12 cells were dissociated as outlined in section 3.2.3.1 and suspended at $2x10^5$ cells in 167µL collagen solution from bovine skin (ThermoFisher, C4243) with 333µL of serum free DMEM per well in a 24 well plate. Collagen gels were crosslinked using 0.5M NaOH at a batch dependent concentration, mixed thoroughly to ensure even setting of the gel. Titration for NaOH concentration outlined in section 3.2.3.4. Following mixing of the NaOH with the collagen and media with cells, gels were left to set for 30 minutes at room temperature. Once all gels had set, gels were separated from the edge of the well using a P20 pipette tip and 500µl of treatment group specific media was added. PDGF-AB and BB were used at 10ng/ml in serum starved DMEM. Synthetic PDGF mimetic peptides were used at a concentration of 1µg/ml in serum starved DMEM. The AG1296 negative control media is made up of 10ng/ml of PDGF-AB and 10µM AG1296 in serum starved DMEM. The NTC group is treated with serum starved DMEM. Gels were then incubated for 24 hours at 37°C and imaged using the ChemiDoc Imaging System (Bio-Rad Laboratories, California, USA). Gel contraction was measured using Image J by measuring the circumference of each gel at time of treatment and at 24 hours. The percentage of contraction was then calculated. Each treatment group was carried out in triplicate and the average of each treatment group was plotted for statistical analysis.

3.2.4.3 NaOH Crosslinker Titration

NaOH crosslinker titration is done by combining 200µL of collagen solution from bovine skin with 400µL of the media used in the collagen contraction assay in eight Eppendorf tubes. 0.5M NaOH is added to each tube increasing by 1µL for each tube starting at 1µL in tube one and ending with 8µL in tube eight. The tubes are then left to set for 30 minutes at room temperature. NaOH concentration was determined based on colour and consistency of the gel following incubation. An ideal concentration of NaOH should result in a deep pink colour of the media, indicating a Neutral pH and a solid gel. This titration needs to be repeated with every new batch of collagen and for each different media used.

3.2.4.4 Endothelial Tube Forming Assay

Endothelial tube forming assay was completed on primary HCAECs dissociated as outlined in section 3.2.3.3 and resuspended at a concentration of $3.5x10^4$ in 100µL of serum free MesoEndo Basal Medium with or without growth factors dependent on treatment group. Prior to this, growth factor reduced Geltrex (Gibco, A1413201) was pipetted into a 96 well plate at 50µL per well and incubated for 30 minutes at 37°C. Following incubation cells were seeded on top of the Geltrex in treatment group dependent media and incubated for 24 hours at 37°C. PDGF-AB and BB were used at a concentration of 50ng/mL in serum free MesoEndo Basal Medium. PDGF mimetic peptides were used at a concentration of 5µg/mL in serum free MesoEndo Basal Medium. The AG1296 negative control was made up of 50ng/ml PDGF-AB and 10µM AG1296 in MesoEndo Basal Medium. The no treatment control group was treated with serum free MesoEndo Basal Medium. Following incubation gels, brightfield images were taken using the Olympus CKX41 and tube length and numbers were analysed using Image J.

3.2.4.5 Receptor Activation by Phosphorylation of Erk

3.2.4.5.1 Titration Assay

C2C12 cells were expanded and seeded into T75 flasks (Corning, 353135) for treatment with synthetic peptides and controls. Cells were serum starved for 24 hours at 37°C in serum free DMEM. Following serum starving cells were treated with treatment group specific media for 10 or 30 minutes, with mimetic peptide doses ranging from 500ng/ml to 5ug/ml. After incubation cells were washed with cold PBS and dissociated using TrypLE Express for 3 minutes. The cells were then centrifuged at 300xg for 5 minutes at 4°C and cell pellets were resuspended in 100µL of RIPA buffer for protein extraction.

3.2.4.5.2 Time Course Assay

C2C12 cells were expanded and seeded into T75 flasks for treatment with synthetic peptides and controls. Cells were serum starved for 24 hours at 37°C in serum free DMEM. Following serum starving cells were treated with treatment group specific media and incubated at 37°C for 5, 10, 20, 30 or 60 minutes. After incubation cells were washed with cold PBS and dissociated using TrypLE Express for 3 minutes. The cells were then centrifuged at 300xg for 5 minutes at 4°C and cell pellets were resuspended in 100µL of RIPA lysis buffer (Merck, 20-188) for protein extraction.

3.2.4.5.3 Protein Extraction and Quantification

Cells were incubated in RIPA lysis buffer with protease (Sigma Aldrich, 11873580001) and phosphatase (Sigma Aldrich, P5726) inhibitors on ice for 1 hour and centrifuged at 16,000xg for 20 minutes. The supernatant containing the protein was then collected and stored at -80°C. Protein quantification was carried out using the Pierce BCA Protein Assay Kit (ThermoFisher, 23225). After incubation for 30 minutes at 37°C results were obtained using the SpectraMax plate reader (Molecular Devices, California, USA) at 562nm.

3.2.4.5.4 Western Blot for Phosphorylation of Erk

Sodium Dodecyl-Sulfate Polyacrylamide Gel Electrophoresis (SDS-PAGE) was carried out using 4-20% polyacrylamide pre-cast gels (Bio-Rad, 4561094), loading 20μL per sample and 7μL of the protein ladder (Bio-Rad), and running for 1 hour at 90V. Following this the proteins were transferred onto a nitrocellulose membrane using the Bio-Rad Turbo Transfer system (Bio-Rad Laboratories, California, USA) carrying out a semi wet 7-minute transfer. To block non-specific antibody binding the membranes were incubated for 1 hour in 5% skim milk in PBST at room temperature. Following this they were incubated overnight at 4°C in primary antibody and then 1 hour at room temperature in secondary antibody after washing in PBST. To assess receptor activation via phosphorylation of Erk, the primary antibody Rabbit p44/42 MAPK (Erk1/2) (137F5) (Cell Signalling, 4695) and Rabbit Phospho-p44/42 MAPK (Erk1/2) (Thr202/Tyr204) (20G11) were both diluted 1 in 1000 in 5% skim milk in PBST. The secondary antibody used for both was anti-Rabbit secondary antibody diluted 1 in 10,000 in 5% skim milk in PBST. The blots were then imaged on the ChemiDoc Imaging System (Bio-Rad Laboratories, California, USA) using ThermoFisher SuperSignal™ West Femto Maximum Sensitivity Substrate (ThermoFisher, 34094).

3.2.4.5.5 Western Blots for PDGF Antibody Optimisation

Recombinant human PDGF-AA, -BB, and -AB (Peprotech, 100-13A, 100-14A, 100-00AB) were run on an SDS-PAGE using the same western blot protocol as outlined above (section 3.2.4.5.4) as positive controls for PDGF antibody validation and optimising. The described protocol for transferring to the nitrocellulose membrane and blocking for non-specific antibody binding was carried out prior to overnight incubation at 4°C. This was followed by washing in PBST and incubation in the appropriate antibody diluted 1 in 10,000 5% skim milk in PBST. The blots were then imaged on the ChemiDoc Imaging System (Bio-Rad Laboratories, California, USA) using ThermoFisher SuperSignal™ West Femto

Maximum Sensitivity Substrate (ThermoFisher, 34094). All primary antibodies were used in a range of concentrations based on manufacturers guides diluted in 5% skim milk in PBST. Primary antibodies tested are listed below in Table 3.2.1.

Table 3.2.1: PDGF antibody optimisation.

Antibody Name	Manufacturer	Catalogue Number
PDGF-A polyclonal antibody	ThermoFisher Scientific	PA5-99405
Anti-PDGFB antibody	Sigma Aldrich	SAB4502136
Recombinant anti-PDGF B antibody	Abcam	ab178409
Anti-PDGF B antibody	Abcam	ab181341
PDGF B antibody	Novus	NBP1-58279

3.2.4.6 Flow Cytometry for EdU

Flow cytometry was carried out to assess the proliferative effects of the mimetic peptides versus our various control groups. This was completed by staining for EdU using the Abcam EdU proliferation assay kit (Abcam, ab222421). CH310T1/2 cells were passaged as outlined in section 3.2.3.2 and seeded in T25 flasks prior to treatment. C3/H10T1/2 cells were treated with 20ng/ml PDGF-BB and PDGF-AB, and 2µg/ml of peptides JC5 and JC5a. In addition to these groups was a 1% FBS in DMEM NTC group, 10% FBS in DMEM as an additional positive control, and AG1296 negative control groups. The negative control groups were 10µM AG1296 in DMEM and 10µM AG1296 co-treated with each of our PDGF and peptide treatments. Following 22 hours of treatment, 10µM EdU was added to the cells and incubated for 2 hours. The cells were then dissociated as outlined in section 3.2.3.2, collected in FACS tubes, and washed in 500µL of cold PBS prior to centrifuging at 500xg for 5 minutes and fixation in 4% PFA at room temperature for 15 minutes. The assay was then carried out according to the manufacturer's instructions and analysed using the BD LSR Fortessa Laser Cell Analyser (BD Biosciences, Erembodegem, Belgium).

3.2.5 Introduction of Negative Control Peptides

The functional region of the negative control peptides was scrambled randomly to remove its biological function, followed by manual confirmation that key amino acids in the chain were no longer placed together. These were then bound to the same HSA conjugate present in JC5 and JC5a, either with 1 or 2 conjugates to correlate with their respective mimetic peptide. Synthesis was carried out using the same method outlined in section 3.2.2. To confirm the negative control peptides had not maintained biological activity, the *in vitro* assays carried out in Research Chapter 3: Development of Novel Platelet Derived Growth Factor-AB Mimetic Peptides, were repeated using the same controls in addition to JC5 and JC5a. The methods for these assays are outlined in section 3.2.4. All peptides were synthesised by Dr Daniel Ford from the Payne Laboratory at the University of Sydney, School of Chemistry.

3.2.6 Statistical Analysis

All statistics were carried out using GraphPad Prism (version 9.0.1). One way ANOVA statistical tests were carried out to determine statistical significance for all assays comparing the mean of each treatment group with the mean of all other treatment groups. Statistical significance was set to a P value of <0.05 in all experiments.

3.3 RESULTS

Our initial approach to address the pharmacokinetic limitations of PDGF-AB as a therapeutic was to maintain the full protein chain and identify key amino acids within the chain that were cleavage targets of proteolytic enzymes and replace these with synthetic amino acids unrecognisable to proteases. This approach, if successful, would allow for minimal interruption of the full-length protein providing the greatest opportunity to maintain its full biological function. This method first required identification of these specific sequences within the chain which would require highly specific antibodies to both the A and B chains. Despite significant optimisation, antibodies that could reliably distinguish between the two chains could not be identified (Figure 3.3.1). Whilst successful in validating an A chain specific antibody, the same could not be achieved for the B chain. All antibodies tested failed to distinguish each chain and demonstrated significant non-specific binding outside of the PDGFs (Figure 3.3.1). Additionally, further investigation into the likely protease cleavage sites on the A and B chains of PDGF identified 483 possible protease cleavage combinations involving 208 of the 234 amino acids in the full-length heterodimer (Table 3.3.1). Therefore, our initial approach did not appear possible, and we redirected efforts towards production of mimetic peptides utilising a key functional region within the specific PDGF chains in addition to pursuing other methods of improving its pharmacokinetic properties.

Table 3.3.1: Enzyme cleavage sites on human PDGF-AB heterodimer.

Potential cleavage sites in the human PDGF-AB heterodimer. Number of cleavages indicates the number of sites an enzyme could potentially cleave. The position of the cleavage site is the amino acid position along the chain that is susceptible to enzyme cleavage for the specific enzyme.

Enzyme	Number of cleavages	Position of cleavage sites
Arg-C Proteinase	24	13, 21, 42, 58, 62, 73, 84, 103, 109, 111, 117, 119, 121, 144, 152, 153, 157, 173, 181, 186, 193, 198, 204, 231.
Asp-N endopeptidase	5	24, 100, 105, 155, 217.
Asp-N endopeptidase + N-terminal Glu	25	2, 3, 17, 24, 38, 69, 79, 85, 86, 89, 100, 103, 104, 105, 111, 133, 139, 145, 148, 155, 169, 200, 216, 217, 224.
BNPS-Skatole	2	34, 165.
CNBr	1	137.
Chymotrypsin-high specificity (C-term to [FYW], not before P)	7	17, 31, 71, 102, 148, 162, 209.
Chymotrypsin-low specificity (C-term to [FYWML], not before P)	25	17, 31, 32, 60, 61, 71, 78, 85, 88, 89, 98, 102, 122, 127, 130, 137, 148, 154, 162, 163, 192, 209, 216, 219, 220.
Clostripain	24	13, 21, 42, 58, 62, 73, 84, 103, 109, 111, 117, 119, 121, 144, 152, 153, 157, 173, 181, 186, 193, 198, 204, 231.
Formic acid	5	25, 101, 106, 156, 218.
Glutamyl endopeptidase	20	3, 4, 18, 39, 70, 80, 86, 87, 90, 104, 105, 112, 134, 140, 146, 149, 170, 201, 217, 225.
Iodosobenzoic acid	2	34, 165.
LysC	21	11, 41, 53, 65, 68, 74, 75, 77, 79, 115, 116, 118, 120, 123, 142, 199, 205, 206, 210, 211, 223.
LysN	21	10, 40, 52, 64, 67, 73, 74, 76, 78, 114, 115, 117, 119, 122, 141, 198, 204, 205, 209, 210, 222.
NTCB (2-nitro-5-thiocyanobenzoic acid)	16	9, 36, 42, 45, 46, 53, 90, 92, 140, 167, 173, 176, 177, 184, 221, 223.
Pepsin (pH1.3)	23	30, 31, 32, 78, 85, 88, 89, 97, 126, 127, 129, 130, 147, 148, 161, 162, 163, 191, 209, 215, 216, 219, 220.
Pepsin (pH>2)	27	16, 17, 30, 31, 32, 71, 78, 85, 88, 89, 97, 102, 126, 127, 129, 130, 147, 148, 161, 162, 163, 191, 209, 215, 216, 219, 220.
Proline-endopeptidase [*]	7	76, 110, 124, 187, 194, 207, 232.

Proteinase K	112	2, 3, 4, 5, 6, 8, 9, 12, 14, 15, 16, 17, 18, 19, 24, 27, 29, 31, 32, 33, 34, 38, 39, 40, 44, 49, 52, 59, 64, 66, 67, 69, 70, 71, 72, 78, 80, 81, 83, 85, 86, 87, 89, 90, 92, 94, 95, 96, 98, 102, 104, 105, 107, 112, 122, 125, 127, 130, 131, 132, 133, 134, 136, 138, 139, 140, 143, 145, 146, 147, 148, 149, 150, 154, 155, 158, 160, 162, 163, 164, 165, 169, 170, 171, 183, 188, 190, 192, 195, 197, 200, 201, 202, 203, 208, 209, 212, 213, 214, 215, 216, 217, 220, 221, 225, 226, 227, 228, 229, 230, 233, 234.
Staphylococcal peptidase I	17	3, 18, 39, 70, 80, 86, 90, 104, 112, 134, 140, 146, 149, 170, 201, 217, 225.
Thermolysin	61	1, 7, 8, 14, 15, 23, 28, 30, 31, 32, 37, 51, 58, 63, 65, 66, 68, 71, 77, 82, 84, 88, 91, 93, 97, 121, 126, 129, 131, 132, 135, 136, 137, 138, 147, 153, 154, 159, 161, 162, 163, 168, 182, 189, 191, 194, 196, 199, 202, 207, 208, 211, 213, 215, 219, 220, 226, 227, 228, 229, 232.
Trypsin	38	11, 13, 21, 41, 42, 53, 58, 62, 65, 68, 73, 74, 77, 79, 84, 103, 111, 115, 116, 117, 118, 119, 120, 121, 142, 144, 152, 153, 157, 173, 181, 198, 199, 204, 205, 210, 211, 223.

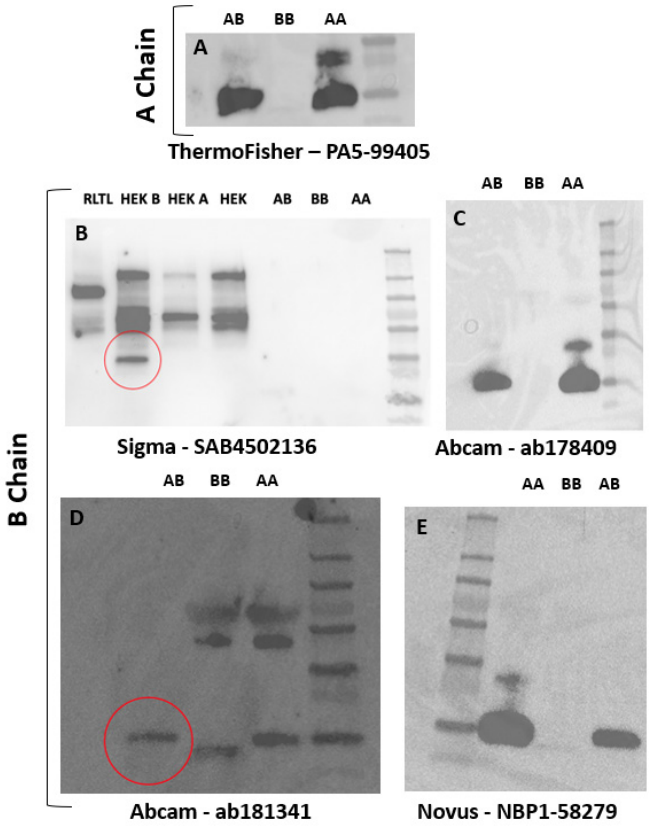

Figure 3.3.1: Platelet derived growth factor antibody optimising.

Western blots of recombinant human PDGF-AA, -BB, and -AB (A-E) with HEK cells transfected with PDGF-A (HEK A) and PDGF-B (HEK B), and rat liver tissue lysate (RLTL) (B). Binding to PDGF-B at the expected size is indicated by the red circles on blots with significant non-specific binding.

3.3.1 Peptide Design – Group 1

Throughout this chapter we designed and synthesised 9 synthetic peptides aimed at functioning as mimetics of PDGF-AB and tested them *in vitro* using assays based on the established key functions of PDGF. These assays were in migration, proliferation, collagen contraction, tube formation, and receptor activation using C2C12 cells, C3H10T1/2 cells, and HCAECs. Extensive revision of the literature highlighted key sequences within the full-length chain, most of which were within loop III of the PDGF-B chain. As a result, the design of all 9 peptides were based on the use of loop III from the B chain as its functional region. These peptides were separated into 3 groups: Group 1 that aimed to confirm the function of loop III in PDGF signaling and if this region was able to act alone; Group 2 aimed to enhance the pharmacokinetic properties of this functional region by incorporating several half-life extending mechanisms; Group 3 contained a refined peptide based on the results of Group 2 and compared it to the lead peptide at the conclusion of Group 2. Loop III was selected as the focal functional region of our mimetic peptides due to its established role in receptor binding and activation, mitogenesis and chemotaxis (120, 124, 126). These established roles have been confirmed in prior tested analogues of PDGF providing a further basis for this choice (133-135).

Group 1 contained 4 peptides named JC1, JC2, JC3 and JC4 (Figure 3.3.2). JC1 and JC2 both contained a homodimer of PDGF loop III region bound to a heparin binding domain, linked using either 4 or 3 Ahx linkers, respectively. These peptides were based on previous PDGF mimetic analogues developed by Zamora et al (133, 134). JC3 contained only a homodimer of the loop III region whilst JC4 contained this same homodimer bound to a homodimer on the heparin binding domain. These peptides were developed in collaboration with the Payne Laboratory at the School of Chemistry, University of Sydney. Dr Daniel Ford synthesised all peptides used.

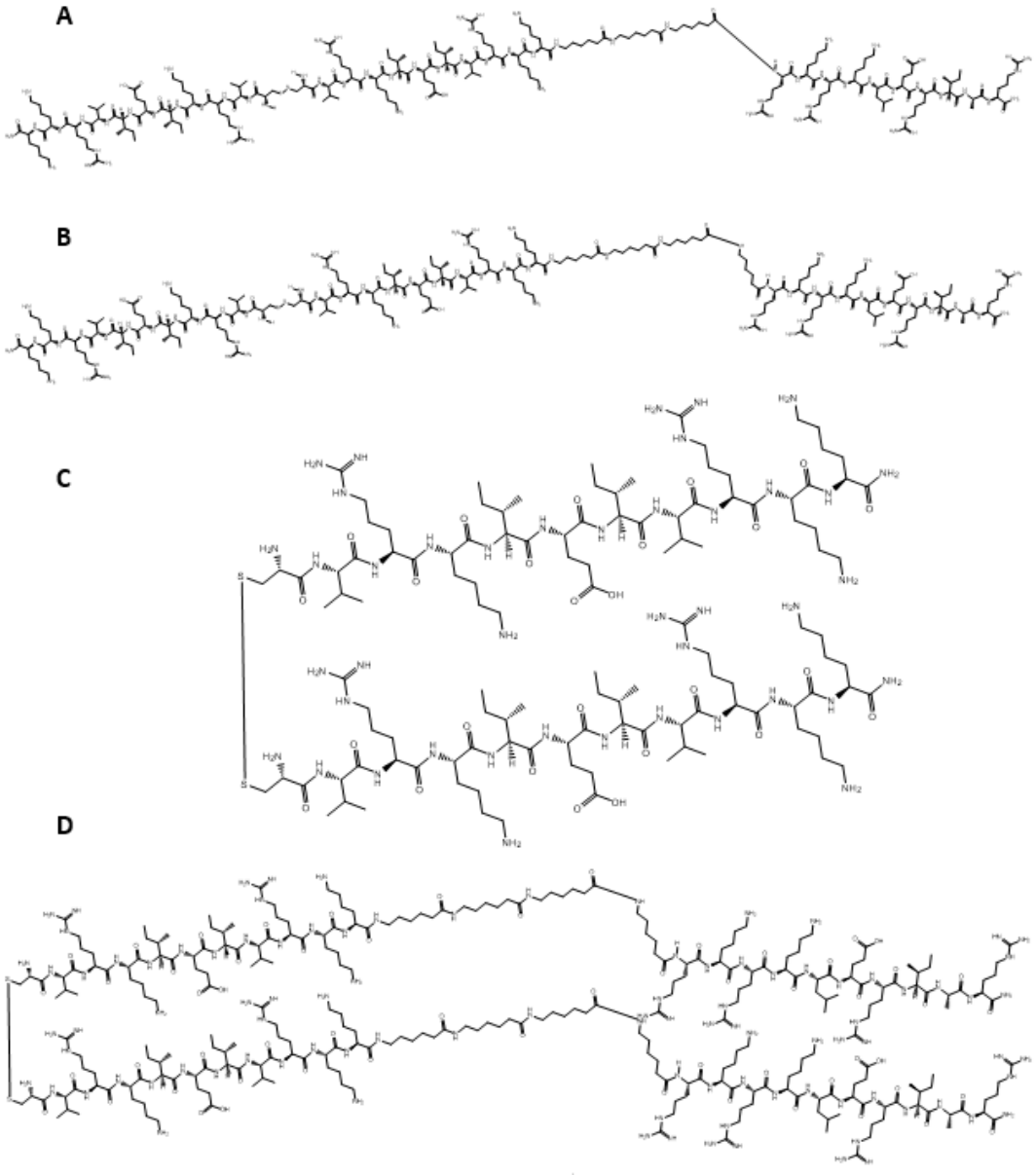

Figure 3.3.2: Chemical structures of Group 1 PDGF mimetic peptides.

A) JC1 – a dimer of the loop III region of the PDGF-B chain with a heparin binding domain linked by four Ahx linkers. B) JC2 – a dimer of the loop III region of the PDGF-B chain with a heparin binding domain linked by three Ahx linkers. C) JC3 – a dimer of the PDGF-B chain with no heparin binding domain. D) JC4 – a dimer of the loop III region of the PDGF-B chain with a dimer of the heparin binding domain. These peptides were developed in collaboration with the Payne Laboratory at the School of Chemistry, University of Sydney. Dr Daniel Ford synthesised all peptides used.

3.3.2 *In vitro* Assay Design

In vitro assessment of the biological functions of our mimetic peptides was carried out testing chemotaxis, collagen contraction, angiogenesis, receptor activation and proliferation. The controls applied across these assays were recombinant human PDGF-AB and PDGF-BB as positive controls, AG1296 as a negative control and a serum starved NTC. PDGF-AB and -BB were selected as positive controls due to our understanding of their closely linked effect on cardiac fibroblasts (138), the importance of the B chain in our peptide design, and our groups prior work in PDGF-AB as a novel therapeutic post-MI (57, 58). AG1296 is a PDGFR inhibitor that's mechanism of action is an ATP-competitive inhibitor specific to the α and β receptors of PDGF, suppressing endogenous PDGFR activity limiting this as a confounding variable. This mechanism of action makes it an effective negative control is confirming the effect of PDGF and our PDGF based mimetics. A serum starved NTC was selected due to the effects of FBS on cellular signaling pathways that overlap significantly with the PDGFR signaling pathways. The results of this overlap can be seen in migration, collagen contraction, proliferation, angiogenesis, and phosphorylation of Erk making a serum starved NTC more appropriate in these experiments. Preliminary *in vitro* experiments were carried out on Group 1 peptides with these results used to inform our peptide design of Group 2. The *in vitro* effects of our peptide mimetics were further explored with Group 2 to build upon the results of Group 1 and inform the design of our final lead candidate peptide.

3.3.3 Chemotaxis – Group 1

Chemotaxis was assessed using a scratch wound healing assay combined with treatment with positive controls PDGF-AB, PDGF-BB, negative control AG1296 co-treated with PDGF-AB, the serum starved NTC or JC1, JC2, JC3 or JC4 (Group 1 peptides) for 24 hours. Following treatment, increased migration was expectedly observed in PDGF-AB and PDGF-BB positive controls, as well as JC1, JC3, and JC4, when compared to the negative control AG1296 + PDGF-AB. However, only the PDGF-BB treated group had significantly greater levels of migration than the no treatment control group (Figure 3.3.3). Specifically, PDGF-BB-treated cells migrated across 49.33% (±9.866) of the scratch which was 19.67% (mean diff.) greater than the no treatment control group ($p=0.0133$) at 29.67% (±6.110) migration and 27.00% (mean diff.) greater than the AG1296 + PDGF-AB group ($p=0.0007$) at 22.33% (±4.163) migration. A lesser effect was seen in PDGF-AB, migrating 40.67% (±2.517) and the mimetic peptides JC1, JC3, and JC4 that migrated 42.33% (±3.055), 40.33% (±6.110), and 43% (±7.211), respectively. Despite the lesser effect than that of PDGF-BB, all 4 of these groups were significantly increased when compared to the negative control AG1296 + PDGF-AB (PDGF-AB $p=0.0230$, JC1 $p=0.0116$, JC3 $p=0.0263$, JC4 $p=0.0088$) (Figure 3.3.3). There were no significant changes in migration between the positive controls PDGF-AB and PDGF-BB and the mimetic peptides JC1, JC3 or JC4. These results indicate that loop III can maintain similar chemotactic function to recombinant human PDGF-AB in the context of these 3 mimetic peptides in this assay.

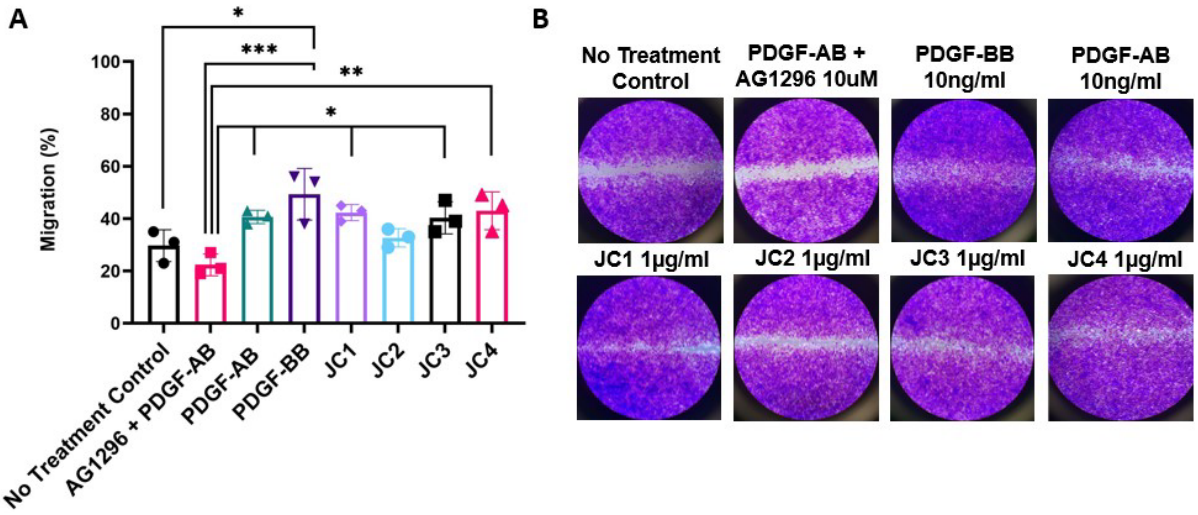

Figure 3.3.3: Increased migration of C2C12 mouse fibroblast cells treated with PDGF and PDGF mimetic peptides.

C2C12 mouse fibroblast cells were treated with 10ng/ml PDGF-AB, PDGF-BB, and 1µg/ml of PDGF mimetics JC1, JC2, JC3 and JC4 in a 2D scratch assay with 24 hours peptide treatment. A) Migration quantified using ImageJ analysis. B) Representative images of scratch assay following 24 hours with respective treatment groups. *p<0.05, **p<0.01, ***p<0.001. Error bars represent ±SD (n=3). One way ANOVA.

3.3.4 Collagen Contraction – Group 1

Collagen contraction is an important function during wound healing of many tissues including the heart (200). This can be simulated *in vitro* using a collagen gel contraction assay. This was assessed using C2C12 cells treated with the positive controls 10ng/ml recombinant PDGF-BB and PDGF-AB, negative control 10µM AG1296 co-treated with 10ng/ml recombinant PDGF-AB, a serum starved NTC and 1µg/ml of the Group 1 JC1/2/3/4 peptides. C2C12 mouse myoblasts were seeded in a 3D collagen gel crosslinked with NaOH and incubated at 37°C for 24 hours following treatment with either controls or mimetic peptides.

At the conclusion of 24 hours treatment, all mimetic peptides and both positive controls had significantly impacted collagen contraction when compared to the negative control AG1296 + PDGF-AB (Figure 3.3.4). The most significant of these was PDGF-BB that contracted to 17.22%

(±2.636) of its initial surface area, 32.27% (mean diff.) more than the negative control at 54.49% (±8.731) ($p<0.0001$). PDGF-AB contracted to 24.19% (±5.237) which was 30.30% (mean diff.) greater than the negative control ($p=0.0006$). Each of the mimetic peptides performed similarly to PDGF-AB with JC1 contracting to 23.38% (±1.519), 31.11 (mean diff.) greater than the negative control ($p=0.0004$). JC2 contracted to 26.04% (±3.018) which was 28.45 (mean diff.) greater than the negative control ($p=0.0014$). JC3 contracted to 27.12% (±4.349) which was 27.37 (mean diff.) greater than the negative control ($p=0.0022$). JC4 contracted to 27.39% (±1.719) which was 27.11 (mean diff.) greater than the negative control ($p=0.0025$). These results show the Group 1 peptides maintain collagen contracting ability to a similar level of recombinant human PDGF-AB *in vitro* in C2C12 cells, although to a lesser extent than is seen in recombinant human PDGF-BB. Furthermore, they indicate that the loop III region of the PDGF B chain can maintain some functions of PDGF *in vitro* when compared to the recombinant full-length protein.

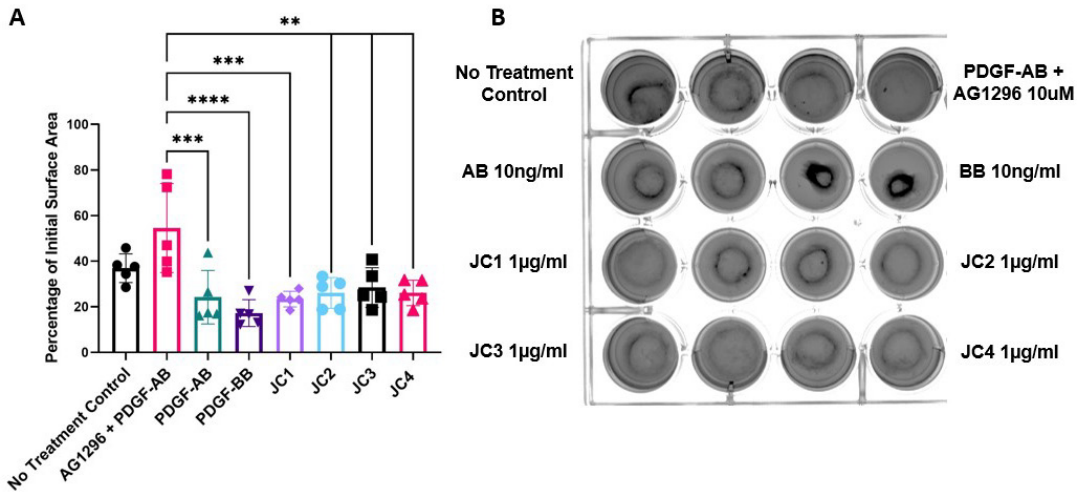

Figure 3.3.4: Increased collagen contraction of C2C12 mouse fibroblasts treated with PDGF and Group 1 PDGF mimetic peptides.

C2C12 mouse fibroblasts seeded in a 3D collagen matrix treated with 10ng/ml of PDGF-AB and PDGF-BB and 1µg/mL of JC1, JC2, JC3, and JC4 for 24 hours. A) Collagen contraction quantified using ImageJ analysis. B) Representative image of collagen gels at 24 hours following treatment. *p<0.05, **p<0.01, ***p<0.001, ****p<0.0001. Error bars represent ±SD (n=5). One way ANOVA.

3.3.5 Peptide Design – Group 2

Group 2 mimetic peptides contained (Figure 3.3.5); JC5, JC6, JC7, and JC8. All these peptides contained a homodimer of the loop III region of the PDGF B chain following the positive results observed during Group 1 testing. In addition to this functional region, each peptide contained a potential half-life extending mechanism. JC5 contained a HSA conjugate, designed to 'piggy-back' onto native albumins in the blood stream to avoid clearance via glomerular filtration. JC6 was a redox locked dimer, designed to reduce the susceptibility of the peptide to protease cleavage. JC7 contained a novel heparin binding domain, whilst JC8 was designed as a cyclic peptide to reduce its susceptibility to protease cleavage. Following synthesis, JC8 was insoluble and unable to be tested *in vitro,* eliminating it as a potential candidate for further testing. These peptides were developed in collaboration with the Payne Laboratory at the School of Chemistry, University of Sydney. Dr Daniel Ford synthesised all peptides used.

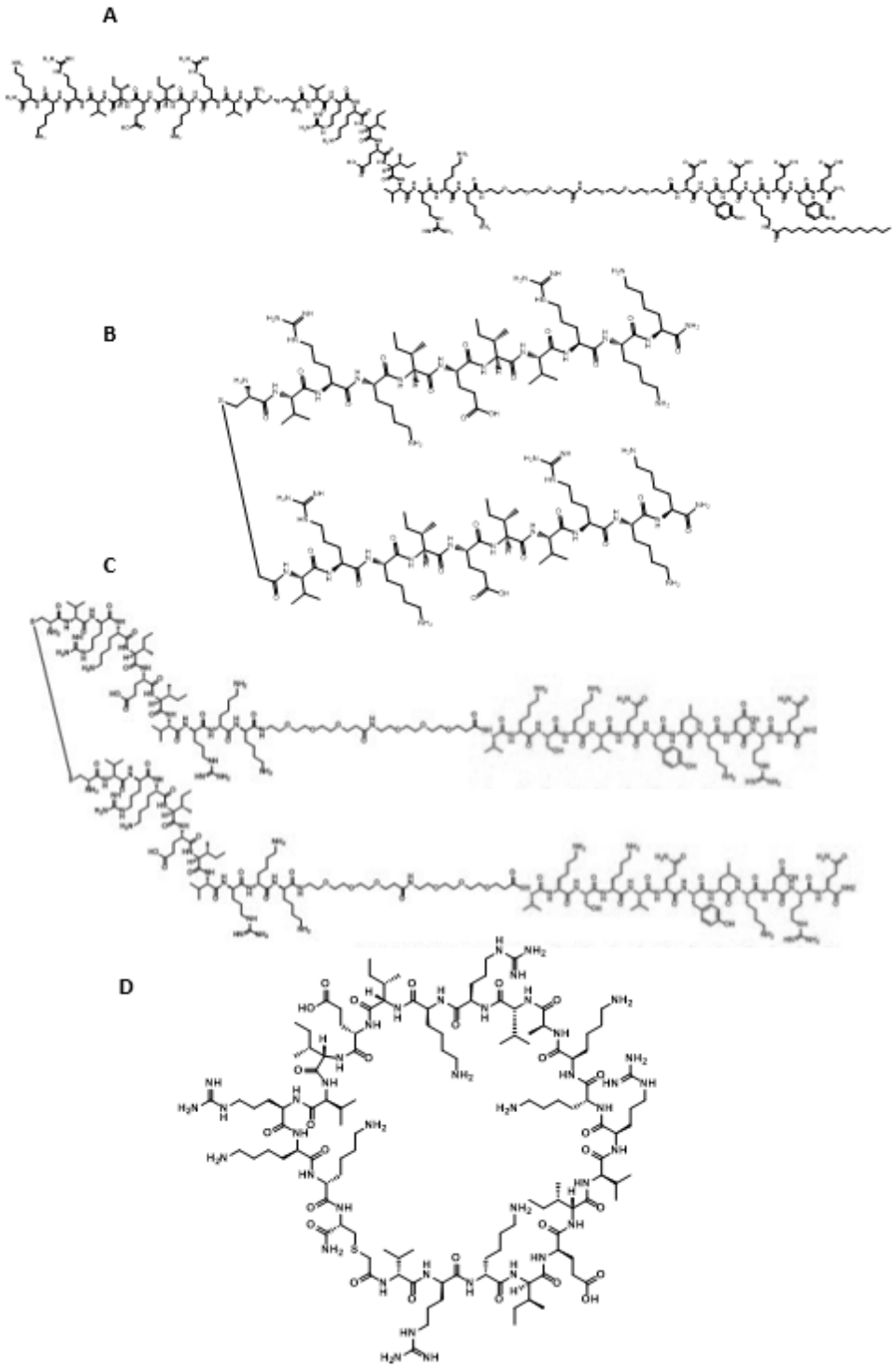

Figure 3.3.5: Chemical structures of Group 2 PDGF mimetic peptides.

A) JC5 – a dimer of the loop III region of the PDGF-B chain with a human serum albumin conjugate. B) JC6 – a redox locked dimer of the loop III region of the PDGF-B chain. C) JC7 – a dimer of the PDGF-B chain with a dimer of a novel heparin binding domain. D) JC8 – a cyclic peptide dimer of the loop III region of the PDGF-B chain. These peptides were developed in collaboration with the Payne Laboratory at the School of Chemistry, University of Sydney. Dr Daniel Ford synthesised all peptides used.

3.3.6 Chemotaxis – Group 2

As was outlined for the Group 1 peptides, chemotaxis was assessed using a scratch assay with C2C12 cells treated with our control groups and the remaining 3 Group 2 peptides at 1µg/ml. A significant increase in migration of C2C12 cells treated with recombinant PDGF-BB and peptide JC5 is shown in Figure 3.3.6. The migration of the positive control PDGF-BB treated cells was 64.63% (±21.60), not significantly higher than migration of JC5 treated cells at 56.85% (±16.14). The NTC group migrated 13.89% (±7.769) similarly to the negative control AG1296+PDGF-AB treated cells that migrated 15.72% (±12.02). PDGF-BB treated cells had a 50.74% (mean diff.) increase when compared to the NTC ($p=0.0033$) and a 48.91% (mean diff.) increase when compared to the negative control ($p=0.0046$). Cells treated with novel mimetic peptide JC5 had a 42.95% (mean diff.) increase when compared to the NTC group ($p=0.0130$) and a 41.13% (mean diff.) increase when compared to the negative control ($p=0.0179$). In summary, novel mimetic peptide JC5 demonstrated a chemotactic function similar to recombinant human PDGF-BB.

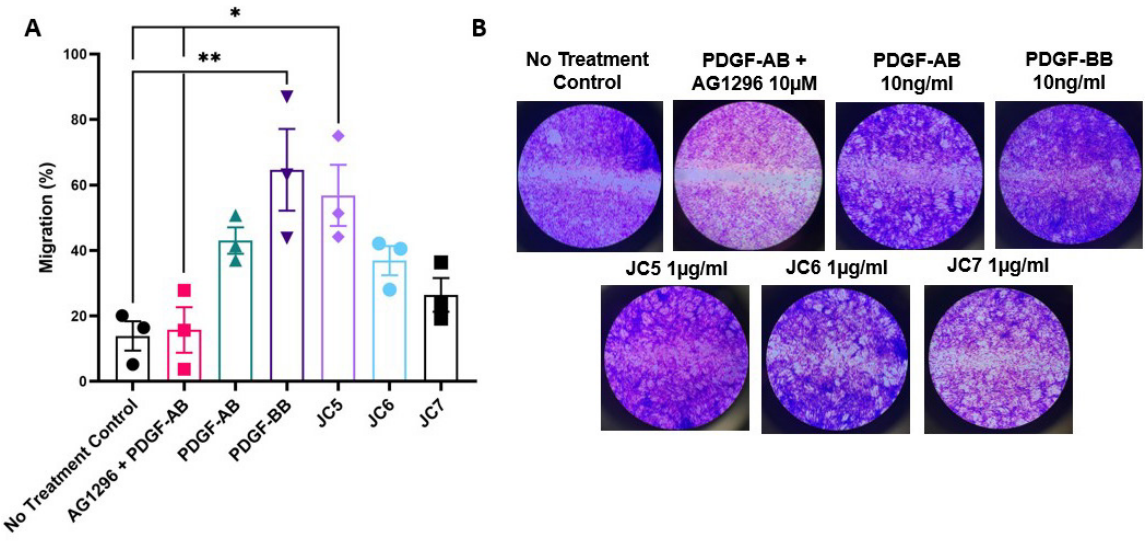

Figure 3.3.6: Increased migration of C2C12 mouse fibroblast cells treated with PDGF and novel PDGF mimetic peptides.

C2C12 mouse fibroblast cells were treated with 10ng/ml PDGF-AB, PDGF-BB, and 1µg/ml of PDGF mimetics JC5, JC6 and JC7 in a 2D scratch assay with 24 hours peptide treatment. A) Migration quantified using ImageJ analysis. B) Representative images of scratch assay following 24 hours with respective treatment groups. *p<0.05, **p<0.01. Error bars represent ±SD (n=3). One way ANOVA.

3.3.7 Collagen Contraction – Group 2

Increased collagen contraction is known to occur following treatment with PDGF and was observed in this assay following treatment with PDGF-BB, PDGF-AB, and peptides JC5 and JC7 (Figure 3.3.7). The increase in collagen contraction was statistically significant when compared to our negative control AG1296+PDGF-AB, however none of these were statistically significant when compared to the NTC. These results are consistent with other reported data on PDGF in collagen contraction assays (201). Following a 24-hour incubation C2C12 cells treated with PDGF-AB had contracted the collagen gel to 22.46% (±2.503) of its initial surface area, whilst PDGF-BB had contracted to 19.65% (±2.997), JC5 had contracted to 19.63% (±2.476) and JC7 had contracted to 21.83% (±3.713). The negative control AG1296 co-treated with PDGF-AB contracted to 57.41% (±10.53) which was 35.71% (mean diff.) less than PDGF-AB (p = 0.0027),

37.76% (mean diff.) less than PDGF-BB (p=0.0015), 37.78% (mean diff.) less than our novel mimetic peptide JC5 (p=0.0015), and 35.58% (mean diff.) less than our novel mimetic peptide JC7 (p=0.0059). The NTC contracted to 37.72% (±3.527) which was not significantly less than any treatment group, including the positive controls PDGF-AB and PDGF-BB. In summary, our novel mimetic peptides have similar collagen contracting ability to recombinant human PDGF-AB and PDGF-BB.

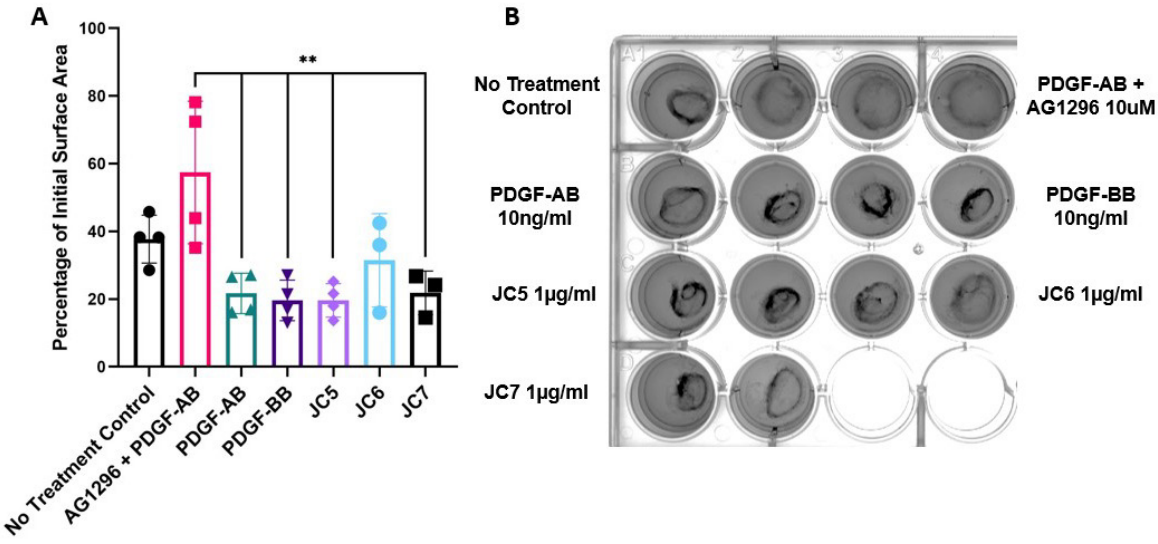

Figure 3.3.7: Increased collagen contraction of C2C12 mouse fibroblasts treated with PDGF and novel PDGF mimetic peptides.

C2C12 mouse fibroblasts seeded in a 3D collagen matrix treated with 10ng/ml of PDGF-AB and PDGF-BB and 1µg/mL of JC5, JC6, and JC7 for 24 hours. A) Collagen contraction quantified using ImageJ analysis. B) Representative image of collagen gels at 24 hours following treatment taken using the ChemiDoc gel imager. *p<0.05, **p<0.01, ***p<0.001, ****p<0.0001. Error bars represent ±SD (n=5). One way ANOVA.

3.3.8 Angiogenesis

PDGF has a well-established role in angiogenesis *in vivo*. To simulate this function *in vitro*, a vascular tube forming assay on primary HCAECs was carried out using the strongest performing peptides of Group 1 and Group 2. This assay involved seeding cells on a 3D growth factor reduced basement membrane extract and incubating for 24 hours with the PDGF-AB, PDGF-BB, NTC, AG1296+PDGF-AB negative control, JC5 or JC4. Following treatment, the ability of the cells to form tubes throughout the gel indicates their ability to induce angiogenesis. PDGF is angiogenic and reported to facilitate tube formation of endothelial cells in *in vitro* 3D assays (97).

Cells treated with PDGF-AB, PDGF-BB or JC5 produced longer more uniform tubes than both untreated cells and cells treated with the negative control AG1296+PDGF-AB (Figure 3.3.8). Positive controls PDGF-AB and PDGF-BB produced tubes that were 560.7µm (±53.93) and 616.3µm (±39.07), respectively. These were not significantly different to JC4 and JC5 that produced tubes that were 601.3µm (±35.64) and 591.3µm (±73.23), respectively. The no treatment control and AG1296+PDGF-AB negative control produced tubes that were 305µm (±104.1) and 307.7µ (±77.03), respectively. The PDGF-AB treatment group had an increased tube length of 255.7µm (mean diff.) compared to the NTC (p=0.0062) and 253µm (mean diff.) compared to the negative control (p=0.0068). The PDGF-BB treatment group had an increased tube length of 311.3µm (mean diff.) compared to the NTC (p=0.0013) and 308.7µm (mean diff.) compared to the negative control (p=0.0014). The JC4 treatment group had an increased tube length of 296.3µm (mean diff.) compared to the NTC (p=0.0019) and 293.7µm (mean diff.) compared to the negative control (p=0.0021). The JC5 treatment group had an increased tube length of 286.3µm (mean diff.) compared to the NTC (p=0.0025) and 283.7µm (mean diff.) compared to the negative control (p=0.0027). These results show that JC4 and JC5 protein

mimetics both had similar vascular tube forming ability to recombinant human PDGF-AB and PDGF-BB, suggesting an associated angiogenic potential.

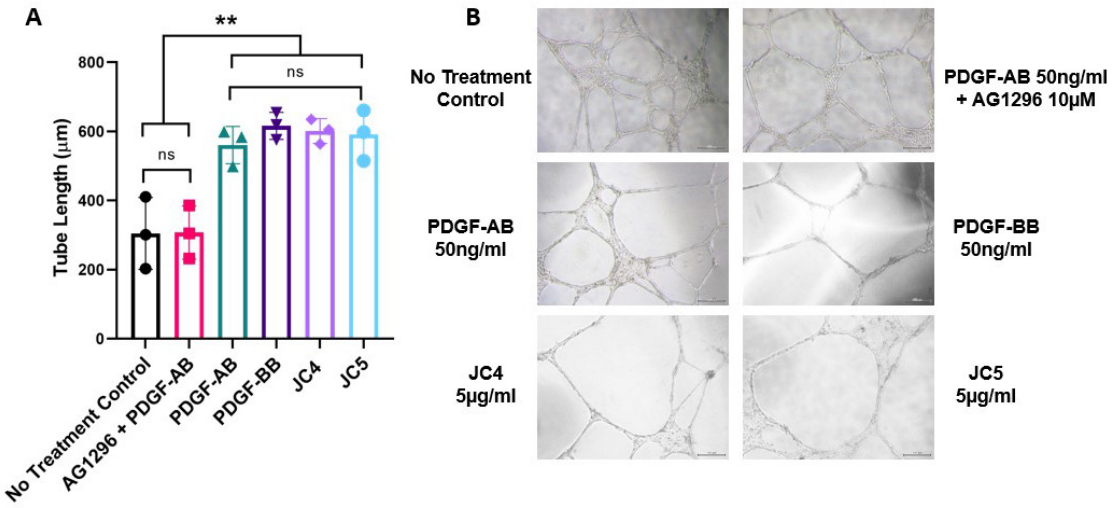

Figure 3.3.8: Increased tube length of human coronary artery endothelial cells treated with PDGF and PDGF mimetic peptides.

Human coronary artery endothelial cells treated with 50ng/ml of PDGF-AB, PDGF-BB, 5µg/ml of the PDGF mimetic JC4 and JC5. A) Tube length quantified using ImageJ analysis. B) Representative brightfield images of 3D gels at 24 hours following treatment. ns=not significant, *p<0.05, **p<0.01. Error bars represent ±SD (n=3). One way ANOVA.

3.3.9 Peptide Design – JC5a

Based on the increased migration, collagen contraction and uniformity in tube formation that was observed following treatment with the novel mimetic peptide JC5, this was determined to be our lead candidate. Following *in vitro* testing of the Group 2 peptides a refined version of JC5, JC5a, was introduced. JC5a contained the same loop III functional region but rather than a single HSA conjugate, it contained 2 of this half-life extending mechanism (Figure 3.3.9). The loop III dimer was formed via a disulfide bond whilst the HSA conjugates were bound to each functional region using 3 polyethylene glycol (PEG) subunits.

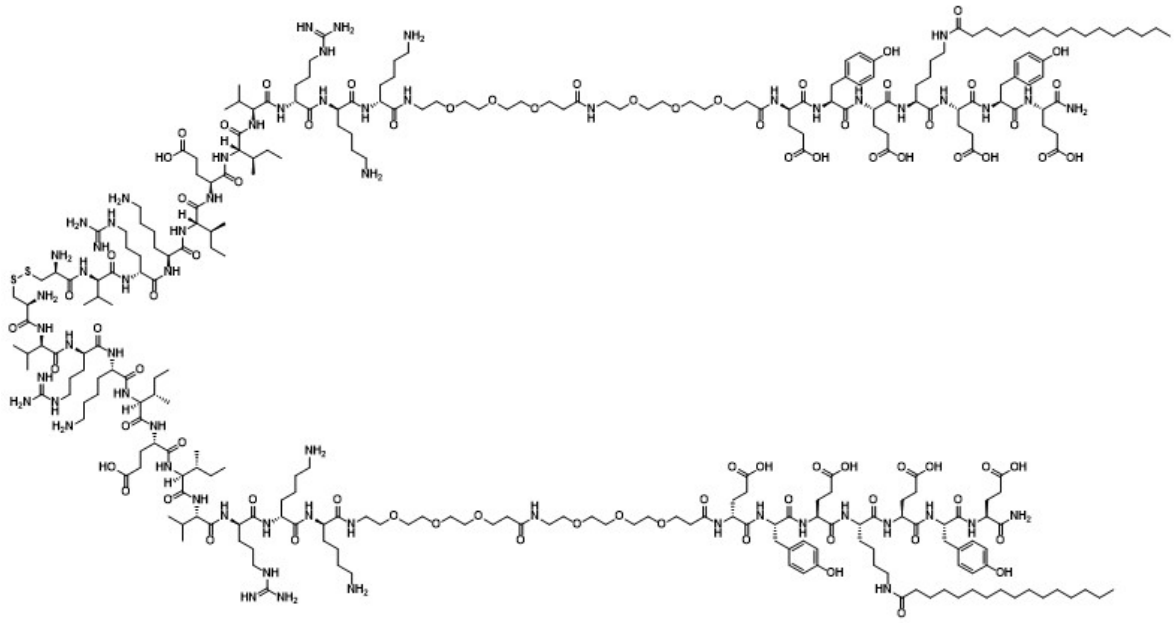

Figure 3.3.9: Novel mimetic peptide JC5a.

The chemical structure of JC5a is composed of a homodimer of the loop III region of the PDGF B chain linked to 2 human serum albumin conjugates by 3 polyethylene glycol subunits. These peptides were developed in collaboration with the Payne Laboratory at the School of Chemistry, University of Sydney. Dr Daniel Ford synthesised all peptides used.

3.3.10 Chemotaxis – JC5a

A significant increase in migration of C2C12 cells treated with recombinant PDGF-BB and peptides JC5 and JC5a is shown in Figure 3.3.10. The migration of the positive control PDGF-BB treated cells was 75.02% (±18.14), not significantly higher than migration of JC5 treated cells at 68.28% (±17.80) and was lower than JC5a at 79.88% (±9.096). The no treatment control group migrated 20.32% (±12.08) similarly to the negative control AG1296+PDGF-AB treated cells that migrated 16.57% (±9.602). PDGF-BB treated cells had a 54.70% (mean diff.) increase when compared to the NTC ($p<0.0001$) and a 58.45% (mean diff.) increase when compared to the negative control ($p<0.0001$). Cells treated with novel mimetic peptide JC5 had a 47.96% (mean diff.) increase when compared to the NTC group ($p<0.0001$) and a 51.71% (mean diff.) increase when compared to the negative control ($p<0.0001$). Cells treated with novel mimetic peptide

JC5a had a 59.56% (mean diff.) increase when compared to the NTC group ($p<0.0001$) and a 62.71% (mean diff.) increase when compared to the negative control ($p<0.0001$). In summary, our novel peptide demonstrated a chemotactic function similar to recombinant human PDGF-AB and PDGF-BB.

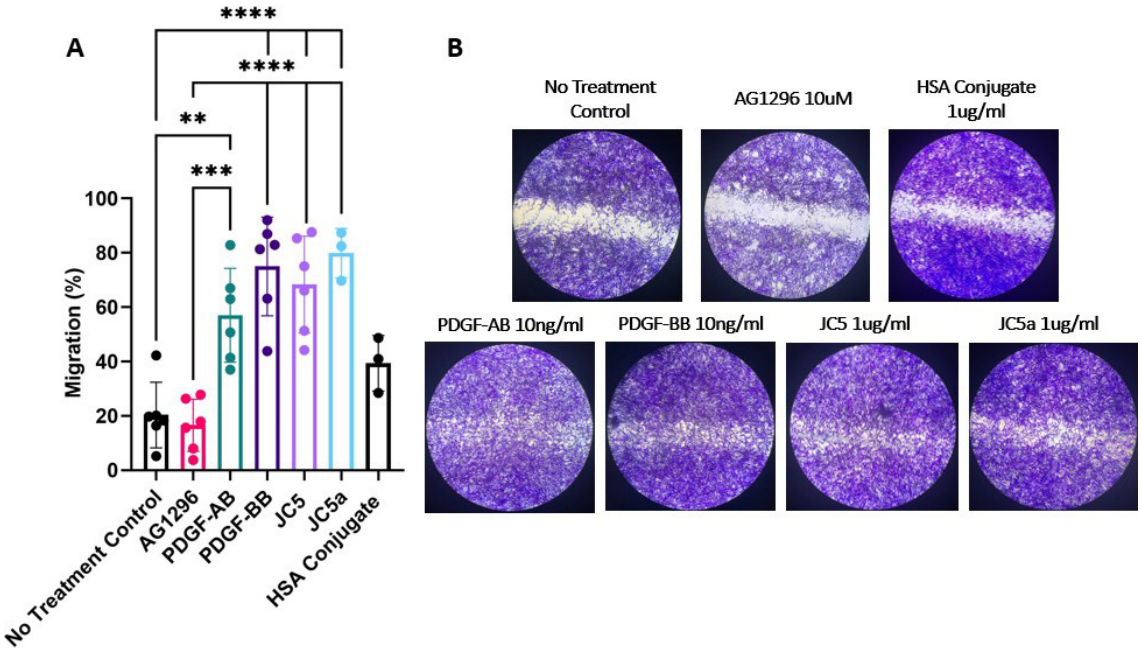

Figure 3.3.10: Increased migration of C2C12 mouse fibroblast cells treated with PDGF and novel PDGF mimetic peptides JC5 and JC5a.

C2C12 mouse fibroblast cells were treated with 10ng/ml PDGF-AB, PDGF-BB, and 1µg/ml of PDGF mimetics JC5 and JC5a in a 2D scratch assay with 24 hours peptide treatment. A) Migration quantified using ImageJ analysis. B) Representative images of scratch assay following 24 hours with respective treatment groups. *p<0.05, **p<0.01, ***p<0.001, ****p<0.0001. Error bars represent ±SD (n=6/3). One way ANOVA.

3.3.11 Collagen Contraction – JC5a

Increased collagen contraction is known to occur following treatment with PDGF and was observed in this assay following treatment with PDGF-BB, PDGF-AB, and peptides JC5 and JC5a (Figure 3.3.11). The increase in collagen contraction was statistically significant when compared to our negative control AG1296+PDGF-AB whilst, PDGF-AB, PDGF-BB and JC5 were statistically significant when compared to the NTC. These results are consistent with other reported data on PDGF in collagen contraction assays. Following a 24-hour incubation C2C12 cells treated with PDGF-AB had contracted the collagen gel to 22.46% (±7.081) of its initial surface area, whilst PDGF-BB had contracted to 23.42% (±7.522), JC5 had contracted to 23.01% (±6.040) and JC5a had contracted to 33.28% (±6.979). The negative control AG1296 co-treated with PDGF-AB contracted to 55.25% (±15.61) which was 32.79% (mean diff.) less than PDGF-AB ($p>0.0001$), 31.83% (mean diff.) less than PDGF-BB ($p>0.0001$), 32.23% (mean diff.) less than our novel mimetic peptide JC5 ($p>0.0001$), and 21.96% (mean diff.) less than our novel mimetic peptide JC5a ($p=0.0120$). The NTC contracted to 41.27% (±7.675) which was 18.82% (mean diff.) less than PDGF-AB ($p=0.0073$), 17.86% (mean diff.) less than PDGF-BB ($p=0.0126$), and 18.26% (mean diff.) less than our novel mimetic peptide JC5 ($p=0.0100$). In summary, our novel mimetic peptides have similar collagen contracting ability to recombinant human PDGF-AB and PDGF-BB.

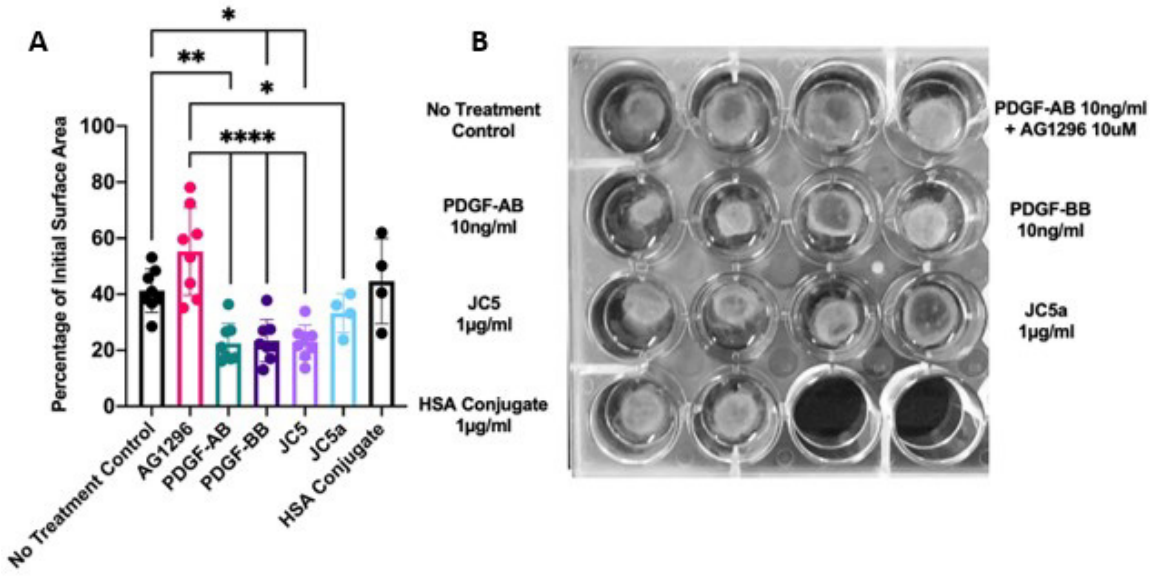

Figure 3.3.11: Increased collagen contraction of C2C12 mouse fibroblasts treated with PDGF and PDGF mimetic peptides JC5 and JC5a.

C2C12 mouse fibroblasts seeded in a 3D collagen matrix treated with 10ng/ml of PDGF-AB and PDGF-BB and 1µg/mL of JC5 and JC5a for 24 hours. A) Collagen contraction quantified using ImageJ analysis. B) Representative image of collagen gels at 24 hours following treatment taken using the ChemiDoc gel imager. *p<0.05, **p<0.01, ***p<0.001, ****p<0.0001. Error bars represent ±SD, n=8/4. One way ANOVA.

3.3.12 Receptor Activation

PDGF receptor activation takes place via autophosphorylation of tyrosine and threonine residues at key sites throughout the intracellular domain. Autophosphorylation engages different signalling pathways, including Erk (MAPK) which participates in proliferation, cell survival, angiogenesis, and chemotactic activity of cells. Phosphorylation of Erk indicates successful activation of the PDGF receptor. In Figure 3.3.12, phosphorylation of Erk (pErk) can be seen in the PDGF-BB treated group and the JC5 treated group when compared to the no treatment control, AG1296 + PDGF-AB negative control and PDGF-AB groups. Phosphorylation increases at 10 minutes and returns to baseline levels of phosphorylation by the 30-minute time point. In Figure 3.3.13, phosphorylation of Erk (pErk) can be seen in the PDGF-BB treated C2C12

cells and the JC5a treated cells when compared to the no treatment control, AG1296 + PDGF-AB negative control and PDGF-AB cells. We have also observed a preserved phosphorylation of Erk (pErk) following treatment with our PDGF mimetic peptide JC5a for 30 minutes. These results indicate successful activation of the PDGF receptor following treatment with JC5 and JC5a. Further it is noted that the AB ligand requires presence of PDGFRα, which is very lowly expressed in C2C12 cells, whereas PDGFRβ is expressed at high levels; thus, pErk is induced by PDGF-BB but not PDGF-AB.

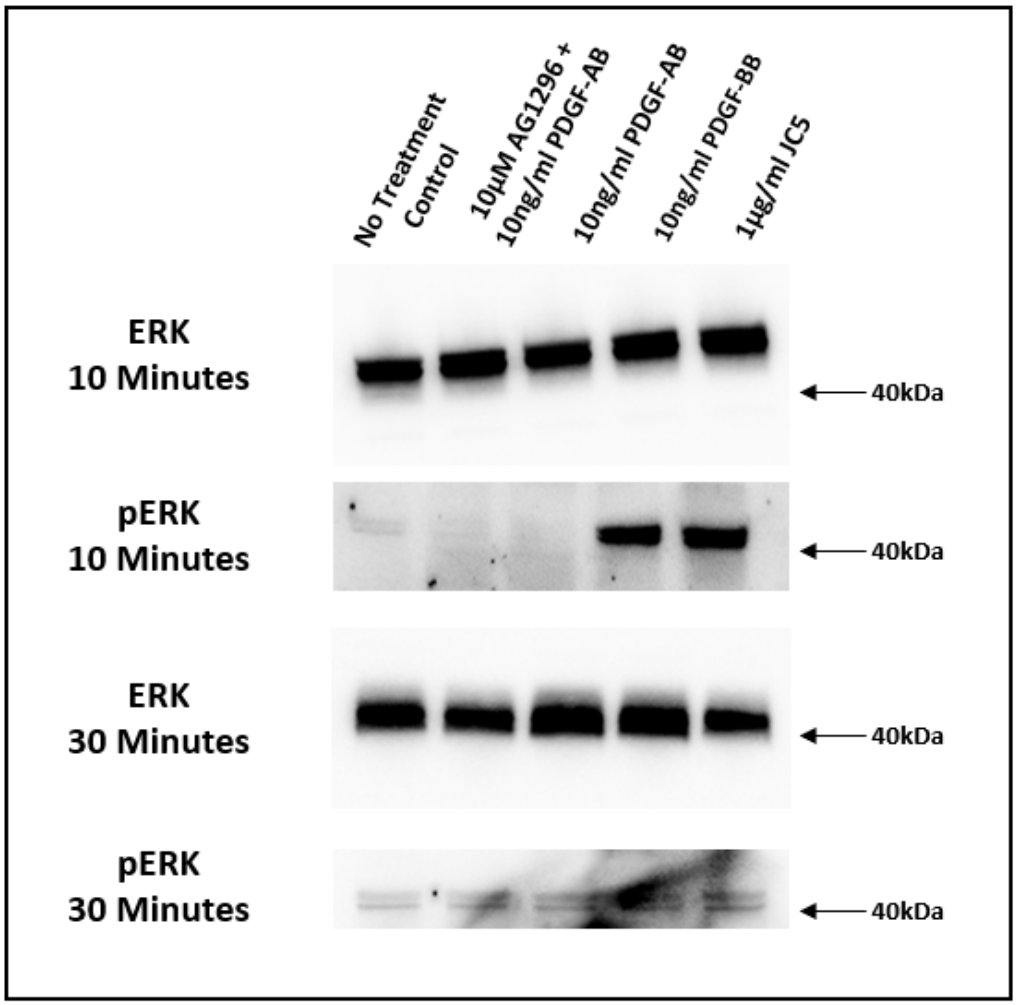

Figure 3.3.12: Phosphorylation of Erk following treatment of C2C12 cells with PDGF and PDGF mimetic peptide JC5.

Western blots for total (Erk) and phosphorylated Erk (pErk) at 42 and 44 kDa following treatment with 10ng/ml PDGF-BB and 1μg/ml of our novel mimetic peptide JC5 (n=3).

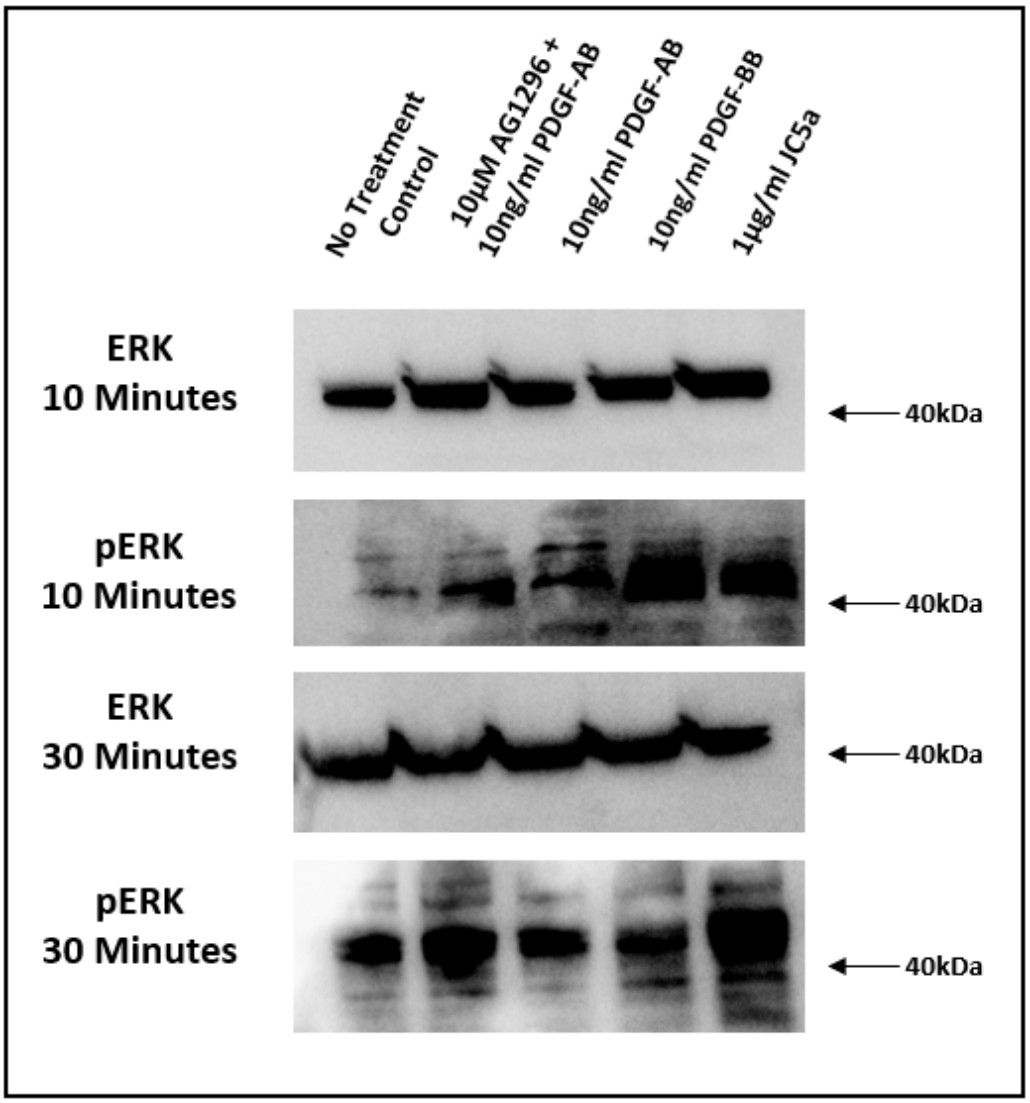

Figure 3.3.13: Phosphorylation of Erk following treatment of C2C12 cells with PDGF and PDGF mimetic peptide JC5a.

Western blots for total (Erk) and phosphorylated Erk (pErk) at 42 and 44 kDa following treatment with 10ng/ml PDGF-BB and 1μg/ml of our novel mimetic peptide JC5a (n=3).

3.3.13 Proliferation

The mitotic effects of PDGF mimetic peptides JC5 and JC5a were tested using cultured C3H10T1 /2 mouse embryonic fibroblasts (Figure 3.3.14). Proliferation was assayed after a pulse of nucleotide analogue 5-ethynyl-2'-deoxyuridine (EdU), which binds to DNA during S-phase and fluorescent detection of EdU using flow cytometry to identify proliferative cells. Cells were treated with 20ng/ml PDGF-BB or PDGF-AB, and 2μg/ml of peptides JC5 or JC5a, 10% FBS was used as a positive control, and co-treatments with specific PDGF receptor antagonist, AG1296, was used to ascertain whether proliferation occurred via the PDGF ligand/receptor pathway. Assays were performed in biological triplicate.

Both 10% FBS (positive control) and PDGF-BB stimulated EdU uptake >2 fold ($p<0.001$), with the latter significantly inhibited by AG1296, confirming stimulation via the PDGF ligand-receptor pathway. However, PDGF-AB, JC5 and JC5a did not significantly stimulate proliferation relative to 1% FBS. Thus, even though the PDGF peptide moiety of JC5 and JC5a were based on the loop III sequence of PDGF-BB, they did not show significant proliferative activity in this assay. The inhibition of EdU levels shown with PDGF-AB and JC5 after cotreatments with AG1296 ($p<0.001$ and $p<0.005$, respectively) suggests a weak stimulation of the PDGF ligand-receptor pathway with PDGF-AB and JC5, although at much lower levels than that seen with PDGF-BB. In summary, novel mimetic peptides JC5 and JC5a display an effect on proliferation in C3H10T1/2 that is significantly less than PDGF-BB (Figure 3.3.14). This contrasts the results seen in cell migration, collagen gel contraction and angiogenesis assays, where PDGFAB, PDGF-BB, JC5 and JC5a show comparable activities (Figures 3.3.10-3.3.13). These data suggest novel biological activities for JC5 and JC5a.

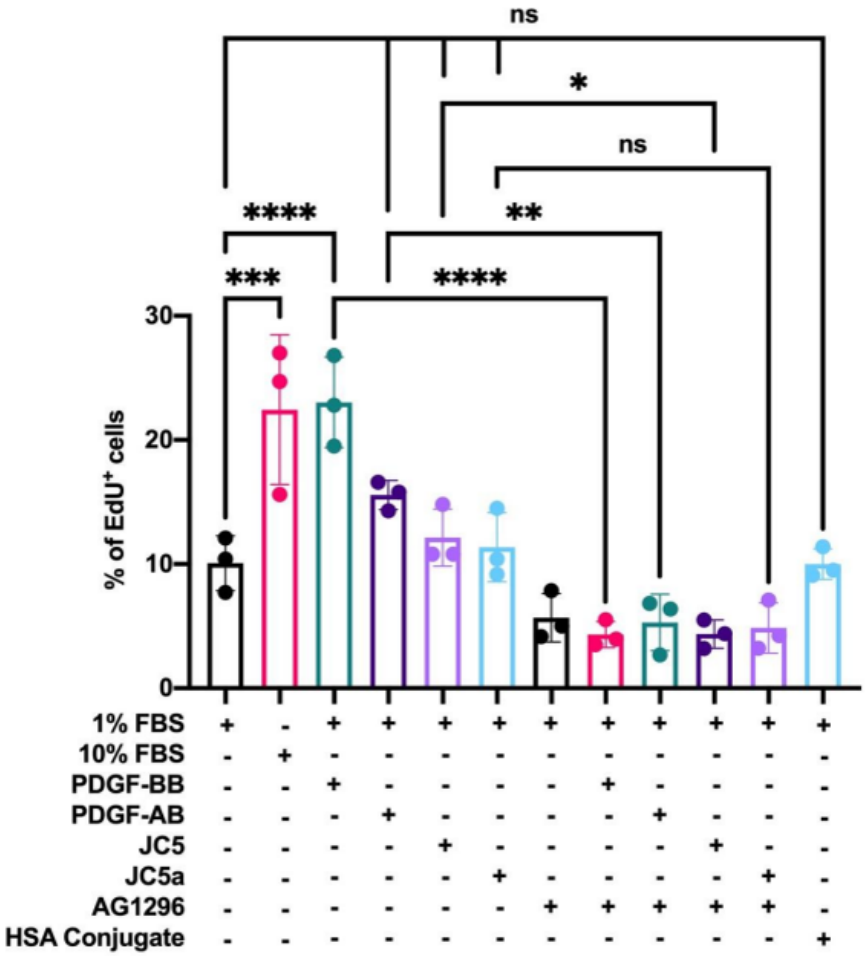

Figure 3.3.14: Proliferation of C3/H10T1/2 cells following treatment with PDGF and novel PDGF mimetic peptides.

C3/H10T1/2 mouse embryo cells were treated with 20ng/ml PDGF-AB, PDGF-BB, and 2µg/ml of novel PDGF mimetics JC5 and JC5a. Following 24 hours the cells were stained using EdU and quantified via flow cytometry. ns= not significant, *p<0.05, **p<0.01, ***p<0.001, ****p<0.0001. Error bars represent ±SD, n=3. One way ANOVA. Flow cytometry was completed in collaboration with Dr Osvaldo Contreras.

3.3.14 Negative Control Peptides

Peptides JC5 and JC5a were selected at the conclusion of the *in vitro* assays. Two additional biologically inactive negative control peptides were introduced at this point ($JC5_{NC}$ and $JC5a_{NC}$) (Figure 3.3.15). To establish the role of the loop III region of the PDGF-B chain in these peptides and as further controls for their function *in vivo* we designed and synthesised 2 biological

inactive negative control peptides that contained a scrambled sequence of the functional region, Loop III from the PDGF-B chain, linked to either 1 or 2 HSA conjugates as is on JC5 and JC5a, respectively (Figure 3.3.15). These peptides were developed in collaboration with the Payne Laboratory at the School of Chemistry, University of Sydney. Dr Daniel Ford synthesised all peptides used.

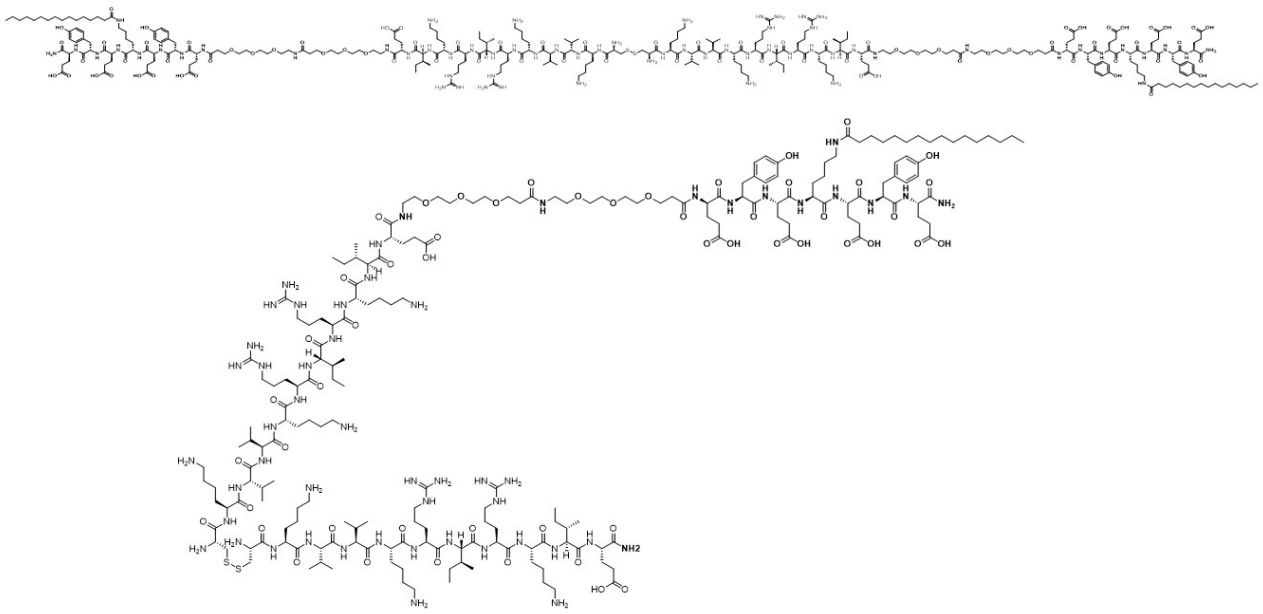

Figure 3.3.15: Biologically inactive negative control peptides.

The chemical structure of the biologically inactive negative control peptides is composed of a homodimer of the scrambled loop III region of the PDGF B chain linked to either 1 or 2 human serum albumin conjugates by 3 polyethylene glycol subunits. These peptides were developed in collaboration with the Payne Laboratory at the School of Chemistry, University of Sydney. Dr Daniel Ford synthesised all peptides used.

Confirmation that the negative control peptides maintained no biological function was completed by repeating the *in vitro* assays carried out previously using the same controls PDGF-AB, PDGF-BB, co-treatment with AG1296 and NTC in addition to comparison with our selected mimetic peptides JC5 and JC5a versus the 2 newly introduced negative control peptides.

The migration assay carried out to assess the *in vitro* efficacy of JC5 and JC5a was repeated using additional controls of JC5 and JC5a co-treated with PDGF inhibitor AG1296 and the new biological inactive negative control peptides. This assay was completed by treating C2C12 mouse myoblast cells with their respective treatment groups for 24 hours prior to fixing in 4% PFA and staining with crystal violet. Following 24 hours of treatment with the $JC5_{NC}$ and $JC5a_{NC,}$ neither peptide demonstrated significant migration compared to the NTC group and were significantly less effective than their active peptide counterpart. With respect to JC5, its negative control $JC5_{NC}$ resulted in 32.76% (±7.696) versus 69.75% (±15.98) in JC5 treated cells (p=0.0015). Similar results were seen regarding JC5a with $JC5a_{NC}$ treated cells migrating 33.35% (±8.262) whilst JC5a treated cells migrated 68.70% (±15.35) (p=0.0029).

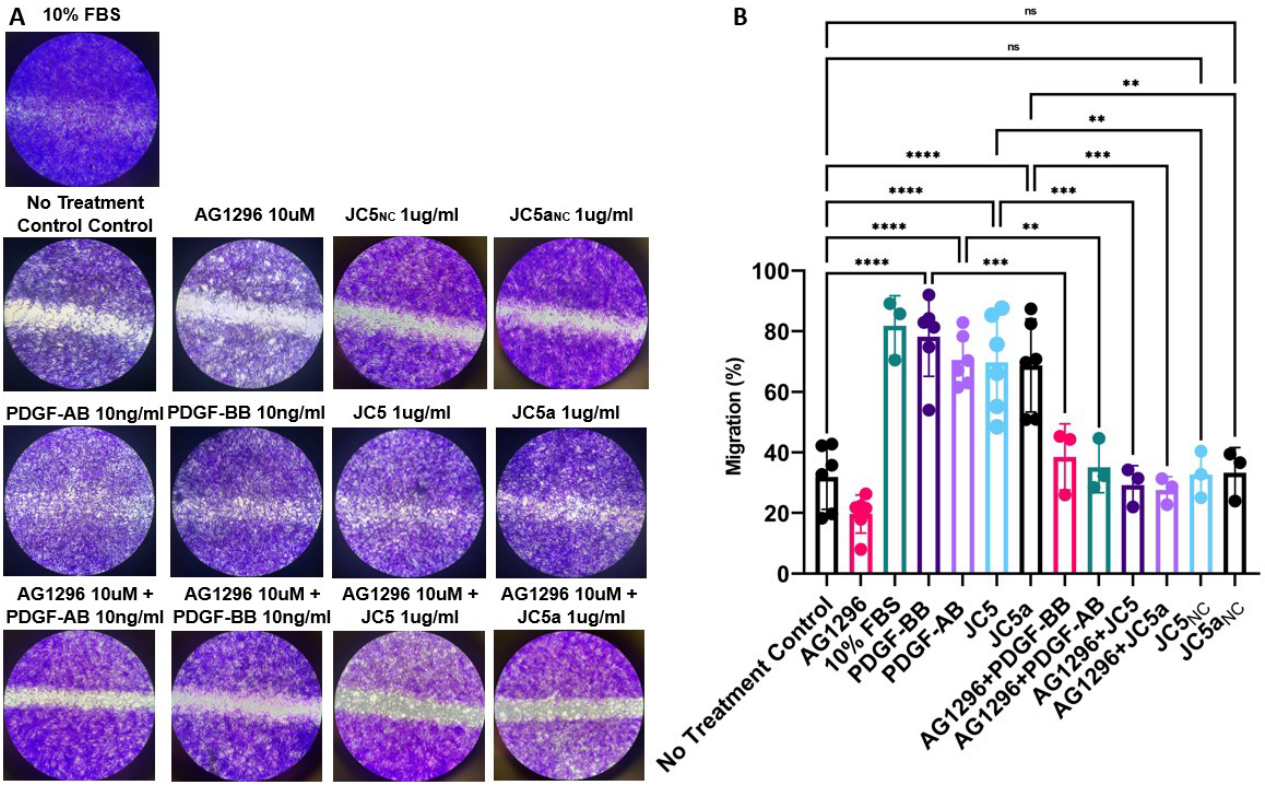

Figure 3.3.16: No migration of C2C12 mouse fibroblast cells treated with negative control peptides JC5NC and JC5aNC.

C2C12 mouse fibroblast cells were treated with 10ng/ml PDGF-AB, PDGF-BB, and 1µg/ml of PDGF mimetics JC5, JC5a, JC5NC and JC5aNC in a 2D scratch assay with 24 hours peptide treatment. A) Migration quantified using ImageJ analysis. B) Representative images of scratch assay following 24 hours with respective treatment groups. ns= not significant, **p<0.01, ***p<0.001, ****p<0.0001. Error bars represent ±SD. One way ANOVA.

Further assessment of the biological activity of our negative control peptides *in vitro* was carried out by repeating the collagen contraction assay with our additional controls. Following treatment for 24 hours, C2C12 mouse myoblast cells seeded in a 3D collagen matrix with $JC5_{NC}$ contracted the collagen to 59.83% (±19.60) of its initial surface area whilst cells treated with $JC5a_{NC}$ contracted to 50.20% (±10.29). These were 38.51 (mean diff.) (p=0.0003) and 24.67 (mean diff.) (p=0.0937) less than their active peptide counterpart for JC5 and JC5a, respectively. Importantly, the difference between JC5a and $JC5a_{NC}$ was not significant in this assay.

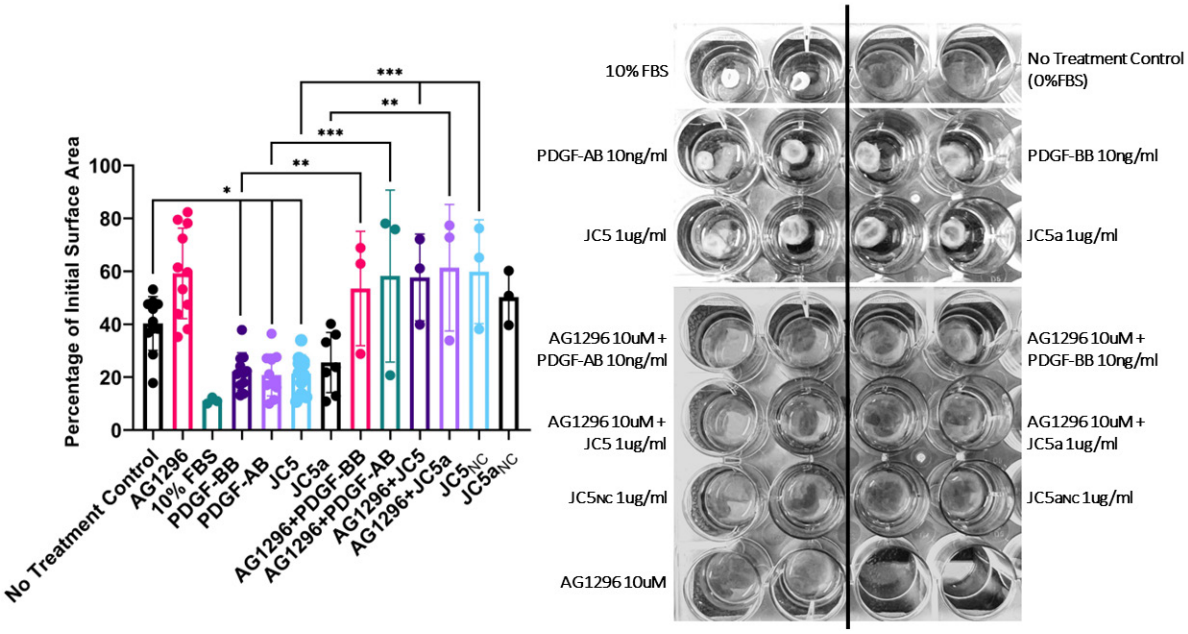

Figure 3.3.17: No collagen contraction of C2C12 cells treated with negative control peptides JC5NC and JC5aNC.

C2C12 mouse fibroblasts seeded in a 3D collagen matrix treated with 10ng/ml of PDGF-AB and PDGF-BB and 1µg/mL of JC5, JC5a, JC5NC and JC5aNC for 24 hours. A) Collagen contraction quantified using ImageJ analysis. B) Representative image of collagen gels in duplicate at 24 hours following treatment taken using the ChemiDoc gel imager. *p<0.05, **p<0.01, ***p<0.001. Error bars represent ±SD. One way ANOVA.

	Half-life Extending Mechanism	Migration	Collagen Contraction	Tube Formation	Receptor Activation
JC1	✗	✓	✓	—	—
JC2	✗	✗	✓	—	—
JC3	✗	✓	✓	—	—
JC4	✗	✓	✓	✓	—
JC5	✓	✓	✓	✓	✓
JC6	✓	✗	✗	—	—
JC7	✓	✗	✓	—	—
JC5a	✓	✓	✓	✓	✓

Figure 3.3.18: Mimetic peptide in vitro efficacy summary.

3.4 DISCUSSION

Despite significant research efforts, cardiovascular diseases continue to be the leading cause of morbidity and mortality worldwide. Whilst developments have been made in the treatment and prevention of many of these, there remains no treatment options available for heart failure outside of heart transplantation. In attempting to address this problem, previous work by our laboratories highlighted the important role of PDGFR signalling in the injured heart (137) and the potential of recombinant human PDGF-AB to improve cardiac function post-MI in murine (58) and porcine models (57, 138). Despite its promising therapeutic benefits, PDGF-AB is limited in clinical translation due difficulties in scalability and its poor pharmacokinetics. The aim of this chapter was to design and synthesise a mimetic peptide that could address these limitations by maintaining the biological function of PDGF-AB *in vitro* and utilised a half-life extending mechanism.

Enhancement of the pharmacokinetic properties of PDGF is essential in improving its clinical applications and translational prospects. Our initial plan to address this involved the identification of amino acids within the full-length protein that were highly susceptible to enzymatic degradation and replace these with synthetic amino acids that are unrecognisable to proteases. Early investigations into the full-length protein highlighted 483 possible protease cleavage combinations in the 234 amino acid full-length heterodimer (Table 3.3.1). In addition to this, we were unable to validate and optimise necessary antibodies with enough specificity to the A and B chain to execute this method (Figure 3.3.1). Whilst western blotting for PDGF A and B chains are commonly reported (202, 203), they rarely need to distinguish between the 2 chains. As a result, we redirected our approach to designing synthetic mimetic peptides, utilising alternative pharmacokinetic enhancing mechanisms.

Selection of Loop III from the PDGF-B chain was based on extensive literature investigating the role of this sequence in binding to both the α and β receptors and the downstream effects of this on cells *in vitro*. Alteration of key amino acids within the sequence have been reported to reduce binding affinity to the receptors or switch strength of binding affinity from the β to the α receptor (124). These reports have been supported by PDGF analogues (135) and mimetics (133, 134) that have utilised this region and successfully maintained receptor binding and activation in addition to downstream cellular effects. Whilst these reports provided evidence for the significance of Loop III as a functional region *in vitro*, none had provided evidence of Loop III's role *in vivo*.

A vital component of the PDGF structure is the dimer formation with PDGFs existing as homodimers and heterodimers of the A and B chains and homodimers of the C and D chain. PDGF is biologically inactive outside of the dimer formation, necessitating a dimer when designing PDGF based peptides in order to maintain biological function. The Loop II region of all PDGF chains is essential due to its role in dimer formation (120), containing several essential cysteines required for forming the inter- and intra- disulphide bonds that form the cysteine knot structure of PDGF. In our peptide design, we did not include Loop II region, however, in PDGF based peptides this region becomes non-essential as additional cysteines can be introduced to the chain forming a dimer. Whilst additional cysteine residues can ensure formation of a dimer in a sequence as short as Loop III, the cystine knot structure that is characteristic of PDGFs is unable to be formed. The cysteine knot structure is essential in the function of PDGF ligands and whilst this is largely due to its role in dimerisation (120) it remained a point of concern in designing a PDGF based peptide. The *in vitro* assay results of this chapter indicate that the cysteine knot structure is unnecessary in this context to maintain an effect *in vitro*. All peptides

designed in this chapter contain a homodimer of loop III bound by disulfide bonds as a result of cysteine residues inserted at the ends of each chain. *In vitro* assays in this chapter allowed us to confirm that the insertion of cysteine residues on each end of the chain was sufficient to form a dimer capable of ensuring biological activity necessary for receptor binding and activation. Further experiments are required to determine if this remains true in an *in vivo* system and will be carried out using a murine model of myocardial infarction.

Utilising a homodimer of the Loop III region, we designed and synthesised 9 synthetic peptides across 3 groups, with the aim of producing a mimetic of PDGF-AB. The efficacy of these peptides was assessed *in vitro* based on well-established key functions of PDGF: proliferation, migration, collagen contraction, tube formation and receptor activation. Throughout these assays 2 positive controls, PDGF-AB and -BB, in addition to a no treatment control and an AG1296 negative control were applied to ensure the validity of these results. AG1296 is a potent selective inhibitor of PDGFR signalling that suppresses endogenous PDGFR activity. This was evident across all *in vitro* assays with AG1296 suppressing PDGFR activity below the level identified in untreated groups (Figure 3.3.3-3.3.4, 3.3.6-3.3.8, 3.3.10-3.3.14, 3.3.16-3.3.17). Whilst AG1296 did have an effect on endogenous PDGFR activity, this effect was not statistically significant in any *in vitro* assays.

For our developed peptides *in vitro* testing, we formed two groups. Group 1 consisted of 4 peptides that aimed to confirm the function of Loop III and determine whether the region can maintain its biological function when isolated from the remainder of the chain (Figure 3.3.2). Within Group 1, all peptides displayed some level of PDGF like function whilst 2 of them successfully induced both migration (Figure 3.3.3) and collagen contraction (Figure 3.3.4)

similarly to PDGF-AB and -BB. These results indicated loop III was capable of functioning in isolation from the remainder of the chain aligning with the *in vitro* results of previously reported PDGF based analogues and mimetics (133-135).

Following the results of Group 1, we progressed with Group 2, combining the homodimer of the loop III with a mechanism of enhancing the pharmacokinetic properties of each peptide (Figure 3.3.5). Each of these mechanisms had been explored throughout the literature and were well established but had not been previously combined with a PDGF based therapy. Commencing Group 2, 4 peptides were synthesised, 1 of these was insoluble resulting in 3 Group 2 peptides being carried forward into *in vitro* assays. Early *in vitro* assays on Group 2 highlighted JC5 as a lead candidate due to its ability to mimic the function of PDGF *in vitro* (Figure 3.3.6-3.3.8, 3.3.12, and 3.3.14).

Our lead candidate peptide, JC5, significantly increased migration of cells similarly to the positive controls PDGF-AB and -BB (Figure 3.3.6). This was assessed *in vitro* for all peptides synthesised in this chapter, using a scratch assay. Chemotaxis is a significant function of PDGF that is a well-established downstream effect of increased PDGFR signalling. The effects of PDGF on cellular chemotaxis are well reported (99-101) and other PDGF based mimetics have demonstrated this effect utilising a dimer of the loop III region (133). The increased migration noted from several peptides in this chapter, including JC5, aligns with the reported effects of PDGF and PDGF mimetics in the literature. This indicates that in the context of this work, the loop III region of the PDGF-B chain is capable of mimicking the effect of PDGF on chemotaxis. With respect to JC5, this conclusion remains true in collagen contraction (Figure 3.3.7), tube formation (Figure 3.3.8), and receptor activation (Figure 3.3.12), further aligning with the reported effects of PDGF *in vitro*

(97, 103) and PDGF mimetics (133). The effects on collagen contraction were confirmed using a 3D collagen gel matrix, observing contraction following 24 hours treatment whilst a similar assay was carried out on endothelial cells assessing tube formation in Geltrex. Receptor activation was identified via phosphorylation of Erk, a key component of the PDGFR signalling pathway with downstream effects on chemotaxis, proliferation, angiogenesis, and cell survival (104). Mimetic peptide JC5a was designed as a more refined version of our lead candidate JC5, containing the same homodimer of loop III with both chains linked to their own HSA conjugate (Figure 3.3.9). JC5a maintained similar function to JC5 across all assays (Figure 3.3.10, 3.3.13-3.3.14) with the exception of collagen contract where a reduced effect from JC5a was noted (Figure 3.3.11).

PDGF has been reported as a potent mitogen (86-88). However, in the context of my experimental work the proliferative effects of PDGF-AB and JC5 were limited, and no effect was identified in JC5a. Although this does not align with many reports of PDGFs effect on mitogenesis and the reported effects of PDGF mimetics (133) it does align with the insignificant effect of proliferation identified following PDGF treatment in our group's previous studies (57, 58, 138, 204). *In vivo*, these studies demonstrated the beneficial effects of PDGF-AB on cardiac function whilst resulting in no significant increase in scar post MI. These were later supported by mechanistic studies highlighting the lack of proliferative effect in murine and porcine hearts treated with PDGF-AB in addition to human cardiac fibroblasts treated with PDGF-AB *in vitro*. Our group has also performed RNA sequencing experiments of infarcted pig hearts treated with PDGF and found no significant effect on cell cycle markers were identified in this model (138). Furthermore, we have performed RNA sequencing of human cardiac fibroblasts *in vitro* and in murine hearts post MI finding that genes associated with cell cycle pathways were reduced relative to controls. Together this work highlights the significant effects of PDGF on the ECM,

angiogenesis, chemotaxis, an immune response (138) as the mechanisms driving improved cardiac function following treatment with PDGF.

Remodelling of the left ventricle post-MI is a combined effect of degradation of the ECM and development of cardiac fibrosis in the infarct zone (205). The significance of the ECM in this declining cardiac function makes it an attractive target for novel therapeutics post-MI. The previous work by our groups provided evidence to support PDGF-AB as a novel therapeutic acting on the ECM (57, 58). This was seen through reduction in cardiac scar in the murine model and modulation of the cardiac scar in the porcine model. Modulation of the cardiac scar was supported as the mechanism of action in further work identifying significant genomic changes following PDGF-AB in mice and pigs *in vivo* and human cardiac fibroblasts *in vitro* (138). In addition to this, a significant decrease of cardiac fibroblast differentiation to myofibroblasts following treatment with PDGF-AB was observed across all species (138). Due to PDGFs role as a potent mitogen (87) and reports of PDGF increasing fibrogenesis (206) it would be expected that PDGF would likely increase fibrosis, doing so by acting on the cell cycle. However, these further studies into the mechanism of PDGF highlighted the lack of significant effect on proliferation in this context, with significant down regulation of the cell cycle in human cardiac fibroblasts following treatment with PDGF-AB (138). Interestingly, in this same experiment significant changes in genes of the ECM and significant upregulation of the immune response were identified following treatment with PDGF-AB. The conclusion of these factors combined is that treatment with PDGF-AB induces a phenotype of human cardiac fibroblasts distinct from myofibroblasts with significant effects on angiogenesis, migration, and the immune response (138). This data supports previous reports of cardiac scar modulation as a mechanism driving improved cardiac function in PDGF-AB *in vivo* studies. It also aligns with the significant effects of

PDGF-AB and our novel mimetic peptides on migration, and angiogenesis, and the minimal effect on proliferation *in vitro* seen throughout this chapter. These experiments carried out by Hume et al. also highlighted the very similar effects of PDGF-AB and -BB in genomic analysis of human cardiac fibroblasts. This further supports our use of the loop III region from the PDGF-B chain in developing a PDGF-AB mimetic.

Albumin fusion proteins are an established and effective method of improving the pharmacokinetic properties of biologic based therapies, that have previously enabled clinical translation and commercialisation of various therapies (149, 165). Despite its success in enhancing therapeutics, its large size and low solubility limits its commercial and clinical applications, and in the context of PDGF may extend its half-life longer than our desired window. The HSA conjugate utilised in JC5 and JC5a provided a mechanism of extending half-life without maintaining all mechanisms found in albumin fusion proteins. The result of this is that peptides bound to the conjugate are protected from protease cleavage with a decreased rate of glomerular filtration but are unable to cycle through the FcRN pathway. The cause of this is poorly understood, however the result is limiting the prolonged half-life of peptides bound to this conjugate. The HSA conjugate was constructed using a palmitoyl based fatty acid conjugate that has binding capacity for HSA and utilised a 'piggy-back' approach to extending half-life (148). Rather than binding the Loop III region to a full-size albumin, binding to a HSA conjugate that could bind to native albumins in the bloodstream allowed for the efficient production of a synthetic peptide that had good solubility, addressing the shortcomings of albumin fusion proteins while still taking on its balanced pharmacokinetic enhancement. Due to the effects of PDGF on the cell cycle and its role in angiogenesis, a prolonged increase in PDGFR signalling could have negative impacts on the safety of a PDGF based therapeutic. In previous PDGF based

therapies, prolonged exposure to PDGF-BB was associated with an increase incidence of metastases (132). Selecting a half-life extending mechanism that balanced improved pharmacokinetics without prolonged exposure of a PDGF based peptide was a significant aspect of our peptide design. Further work is required to assess the pharmacokinetic properties of our novel mimetic peptides JC5 and JC5a. This may be carried out *in vitro* using plasma stability assays (207) and *in vivo* in a murine model (208). These experiments combined would be a significant contribution towards our understanding of the dose response relationship in JC5 and JC5a.

All peptide mimetics within this chapter were based on a functional region of the Loop III region of the PDGF-B chain, dimerised using cysteines inserted at each end of both chains. In the context of our lead candidate peptides, JC5 (Figure 3.3.5A) and JC5a (Figure 3.3.9), this was combined with the HSA conjugate to potentially enhance the pharmacokinetic properties of PDGF. In *in vitro* testing of these peptides, we showed that the biological activity of PDGF-AB could be maintained in a novel mimetic peptide based on its ability to induce migration (JC5 Figure 3.3.6, JC5a Figure 3.3.10), collagen contraction (JC5 Figure 3.3.7, JC5a Figure 3.3.11), receptor activation (JC5 Figure 3.3.12 JC5a Figure 3.3.13) and tube formation (Figure 3.3.8). Whilst the Loop III region had been utilised in prior PDGF based analogues, providing evidence for its functional role, maintenance of this function was essential following binding to the HSA conjugate. The *in vitro* assay results of novel mimetic peptides JC5 and JC5a provided evidence to support the use of a dimer of an isolated region of PDGF to produce a synthetic mimetic peptide, with potentially enhanced pharmacokinetic properties using the fatty acid-based HSA conjugate. The results presented in this work successfully addressed the aims of this chapter

whilst providing us with 2 lead candidate peptides (Figure 3.3.18) to transition into *in vivo* safety and efficacy testing.

3.5 CONCLUSION

Recombinant human PDGF-AB has been established as an effective novel therapy to improve cardiac function post-MI in murine and porcine models (57, 58). However, its labour-intensive synthesis limits scalability whilst its poor pharmacokinetic properties limit its clinical applications. To address these problems, we aimed to design and synthesise a synthetic peptide mimetic to be a more clinically viable and commercially attractive alternative. The *in vitro* assay results of this chapter highlight the efficacy of our chosen functional region, loop III, of the PDGF B chain in mimicking the function of PDGF *in vitro*. From these cell migration, collagen contraction, tube formation and receptor activation studies JC5 and its subsequent peptide JC5a (Figure 3.3.18) stood out as promising lead candidates for *in vivo* safety and efficacy testing as possible replacements for PDGF-AB, improving the prospects of clinical translation for our PDGF based therapeutic post-MI.

CHAPTER 4: APPLICATION OF NOVEL MIMETIC PEPTIDES IN A MURINE MODEL OF ACUTE MYOCARDIAL INFARCTION

4.1 INTRODUCTION

Platelet derived growth factors (PDGFs) are cysteine knot growth factors with primary functions in mitogenesis (86-88), chemotaxis (98, 100, 101), angiogenesis (115) and wound healing (94). In addition, they have proven effective in utilising these functions to improve outcomes in some disease states. For example, PDGF based therapies have been FDA approved for the treatment of musculoskeletal and maxillofacial disorders (129) and diabetic non-healing ulcers (130). Furthermore, in preclinical models PDGFs have been successfully tested as potential therapies for cardiovascular diseases (57, 58), chronic non-healing wounds (127), and bone remodelling (128). Within our research group, the PDGF isoform PDGF-AB has been reported to significantly improve cardiac function in murine (58) and porcine models (57), with its effect attributed to modulation of the ECM, cardiac scar and increased angiogenesis.

In the aforementioned murine model, Asli et al. delivered recombinant human PDGF-AB via osmotic mini-pump for 5 days following a surgically induced myocardial infarction (MI), carried out by permanent occlusion of the left anterior descending (LAD) artery. Using echocardiographic and histological assessment, this study demonstrated infarcted PDGF-AB-treated mice show an increased ejection fraction and a reduced scar size, compared to controls. This improved cardiac function was likely driven by the pro-regenerative effects on endothelial cells, fibroblasts, and cardiomyocytes. Treatment with PDGF-AB also resulted in increased activation, proliferation, and self-renewal of fibroblasts alongside PDGFRα signalling highlighting the effect of increased PDGFR signalling on cardiac fibroblasts (58).

Building upon this work, our lab developed a porcine model to confirm the therapeutics benefits of post-MI PDGF-AB treatment in a large animal model. Thavapalachandran et al. delivered recombinant human PDGF-AB via osmotic mini-pump for 7 days post-MI and assessed cardiac function 28 days post-MI by cardiac magnetic resonance imaging and left ventricular pressure volume loop analysis. These results highlighted a significant increase in left ventricular ejection fraction (LVEF) at day 28 post-MI in animals treated with PDGF-AB. This increase in LVEF was as a result of a significant increase in end systolic volume suggesting that the improved cardiac function was a result of improved contractility of the left ventricle. Histological analysis was carried out to identify changes in the EMC and angiogenesis in the scar. This showed increased collagen alignment within the scar, altered ratios of collagen subtypes within the scar and increased angiogenesis following treatment with PDGF-AB. Despite these changes, scar size was not significantly different between treated and non-treated animals indicating the mechanism of action of PDGF-AB in this model is through modulation of the cardiac scar and increased angiogenesis post-MI. This work progressed translation of cardiac PDGF-AB therapy from a murine model into a more clinically relevant large animal model (57).

In Chapter 3: Development of Novel Platelet Derived Growth Factor-AB Mimetic Peptides, we designed, synthesised, and assessed the biological function of peptide mimetics of PDGF. Based on these results, 2 mimetic peptides were selected for *in vivo* testing. As our colleagues have previously shown that PDGF-AB improves function in a post-MI murine model (58), we aimed to assess the safety and efficacy of these peptides in the same model. Initially, safety and toxicology of the peptides were assessed using a combination of healthy male and female C57BL6/J mice, whilst efficacy was assessed in male C57BL6/J mice post surgically induced MI. The key functional region of these peptides is taken from loop III of the PDGF-B chain that is

essential to receptor binding and activation with downstream cellular effects on proliferation, migration, and collagen contraction (121, 122, 124). To confirm the role of the PDGF-B chain Loop III region in these peptides we introduced 2 biologically inactive negative control peptides for use in the *in vivo* assays. The negative control peptides contained a scrambled functional region and either 1 or 2 half-life extending conjugates. The other groups used to assess these peptides effect post-MI were PDGF-AB as a positive control, a vehicle only PBS control and sham-surgery control group. Sham control mice were included to control for the effects of the mini-pump insertion surgery, that received an osmotic mini-pump with no MI treated with either 32.50mg/kg JC5 or JC5a. The negative control peptides $JC5_{NC}$ and $JC5a_{NC}$ were tested *in vitro* in Chapter 3, to ensure they maintained no biological function. Concerns were raised at the conclusion of those experiments as JC5a was not significantly different in effect to its negative control peptide $JC5a_{NC}$. As a result of this and our limited understanding of the negative control peptides, we chose to exclude them from the *in vivo* efficacy study, however, they were still included for toxicity and safety testing. This study was designed to replicate the conditions of previous PDGF studies on murine models carried out by our groups (57, 58). This *in vivo* timeline included echocardiography at the baseline (before infarction), day 2, and day 28 to assess changes in cardiac function during PDGF peptide mimetic treatment as compared to PDGF-AB and the other control groups. Successful translation of the results presented in Chapter 3, into a clinically relevant murine model could provide us with an alternative to recombinant PDGF-AB as a novel therapy for heart failure, capable of maintaining its therapeutic effects whilst addressing its limitations to enhance its progression in clinical translation.

Hypothesis

Lead candidate PDGF-mimetic peptides established and tested through *in vitro* assays will provide a safe and efficacious method of improving cardiac function post myocardial infarction.

Aims

1. Assess the toxicology and safety of synthetic PDGF-mimetic peptides in an uninjured *in vivo* murine model at varying doses.
2. Determine the efficacy of PDGF-mimetic peptides in improving cardiac function in a post myocardial infarction murine model.

4.2 MATERIALS AND METHODS

4.2.1 Animal Experiments

All animal experiments were approved by the Garvan/St Vincent's Animal Ethics Committee (AEC Protocol #19/14 and #22/18) and were conducted in accordance with the NHMRC guidelines for animal research and the Australian code for the care and use of animals for scientific purposes. *In vivo* experiments were conducted on C57BL/6J mice bred and housed at the Victor Chang Cardiac Research Institute (Darlinghurst) BioCORE (Jackson Laboratory, 000664). All animal experiments were carried out with the technical expertise of Dr Vikram Tallapragada.

4.2.2 *In vivo* Safety Studies

The safety of our synthetic peptides was assessed *in vivo* using a two-part safety study made up of Phase A – maximum tolerated dose study and Phase B – toxicity study. Doses of synthetic peptides are detailed in Table 4.3.1. The standard dose was determined using the known dosage of recombinant human PDGF-AB used successfully in previous murine studies. An estimated drop in potency of our peptides versus full-length PDGF was also accounted for. Additional dose groups for toxicity testing were selected based on standard *in vivo* toxicity protocols in the field (209-211). Monitoring over the course of both phases included weighing of the mice, food and water intake, and close observation for signs of distress and acute toxicity. Specific signs of distress and acute toxicity were: weight loss ≥20%, hunched posture, abdominal distension, piloerection, diarrhoea, any signs of respiratory distress (e.g., changed respiratory rate, gasping, and dyspnoea), lethargy, health tilt, tremors, seizures, circling or paresis, and persistent self-induced trauma. At the conclusion of each experimental timeline the heart, lungs, liver, kidneys, spleen, and brain were weighed, visually inspected gross pathological changes then fixed in 10% neutral buffered formalin in preparation for histological examination as detailed below.

Table 4.2.1: Safety study dosage groups.

Group	Dosage
Low Dose	3.25mg/kg
Standard/Mid Dose	6.50mg/kg
Mid High Dose	13mg/kg
High Dose	32.50mg/kg

4.2.3 Maximum Tolerated Dose Study

Phase A, the maximum tolerated dose study, comprised 4 dose groups of 3 males and females for each peptide. The peptides were delivered via intraperitoneal injection on day 1 followed by monitoring 3 times daily up to day 7. Dose groups were increased stepwise weekly at the successful conclusion of the dose group study prior. At the conclusion of each study, tissue and blood collection was carried out as above.

4.2.4 Toxicity Study

Phase B, the toxicity study, was carried out over a period of 28 days using 6 male mice per peptide. The peptides were delivered via osmotic mini-pump at the highest dose tolerated in Phase A. Following mini-pump insertion on day 1, mice received daily pain management up to day 7 and then twice weekly monitoring up to day 28. Tissue and blood collection were carried out as outlined above and analysed downstream via histology and pathology. Osmotic mini-pump insertion was carried out by Dr Vikram Tallapragada.

4.2.5 Histology

To identify and analyse any off-target effects of the peptides on the major organs collected they were dissected in half and paraffin embedded prior to sectioning. The heart, kidneys, spleen, and liver were dissected longitudinally, the brain was dissected down the sagittal plane and the lungs were left intact.

All dissected organs were embedded with each half in an opposite orientation to allow for the most detailed sectioning of each organ. Each lung was oriented in opposite direction to achieve the same detailed sectioning. Following sectioning, 2 sections of each organ were stained with haematoxylin (POCD, MODMAY) and eosin (POCD, EOSVJ) and an additional 2 sections were stained for picrosirius red and fast green (POCD, SIRIUSFAST500) to identify any potential changes in collagen deposition. Histological staining was carried out as described in section 2.2.7.1 (Picrosirius red and fast green) and section 2.2.7.2 (Haematoxylin and eosin). All sections were then imaged using the Olympus VS120 slide scanner (Olympus Life Science, Massachusetts, USA) at 10x magnification. These images were analysed by veterinarian Dr Alan Marcus for structural abnormalities, fibrogenesis, and areas of increased cell proliferation.

4.2.6 Blood Profiling

Immediately following the Phase B tissue collection, 800µL of blood was collected from the jugular vein and sent for profiling at a specialist commercial veterinary laboratory (Idexx, NSW). Analysis of blood biochemistry and haematology were carried out, the results of which were combined with the histology data from these mice to identify any potential off target effects of these peptides.

4.2.7 Efficacy Study Surgery

To assess the efficacy of our mimetic peptides an efficacy study was carried out in a murine model of MI. A surgically induced MI was carried out via permanent occlusion of the LAD artery in addition to insertion of an osmotic mini-pump (Alzet, 1007D), loaded with 100µL a designated treatment. Recombinant human PDGF-AB was loaded at a concertation of 20µg/mL whilst JC5 and JC5a were loaded at a concentration of 3250µg/mL. Prior to commencing the MI surgery mice were anesthetised with an intraperitoneal injection of ketamine (100mg/kg) and xylazine (20mg/kg). This was maintained

throughout the surgery using 2% isoflurane and 100% oxygen via intubation using a 20-gauge cannula that is placed using a lamp to illuminate the pharyngeal region. Ventilation was set at a volume of 0.5ml and 120 breaths per minute. The surgery was then carried out by opening the thorax, firstly by opening the subcutaneous and muscle layers using scissors down to the level of the ribs. The fourth intercostal space was then opened, and a retractor was placed to expose the heart. Once the LAD was identified, it was ligated using a 7/0 prolene suture on a tapered needle. A 3mm section of 4-0silk was placed on top of the vessel to avoid the suture cutting through the myocardium. During the same procedure a 0.5cm incision was made on the dorsal surface of the mouse with a subcutaneous pocket formed to place the osmotic mini-pump. The catheter (Alzet, 0007701) from the mini-pump is then placed in the jugular vein for infusion of the designated treatment at 0.5µL/hour for 7 days. Each of the layers of the thorax and dorsal incision were then closed using prolene. Mice received 0.75mg/kg of buprenorphine following surgery and twice daily for 3 days post-MI. Occlusion of the LAD and osmotic mini-pump insertion was carried out by Dr Vikram Tallapragada. Echocardiography was used to analyse cardiac function over the study, firstly at the baseline prior to surgery and then at day 2 and day 28 to detect any significant differences between treatment groups. At the conclusion of the experimental timeline the hearts were collected, weighed, and fixed in 10% neutral buffered formalin for downstream analysis. Mice in the efficacy study were randomised using a random order generator and then manually modified to ensure no more than 2 of each treatment group were grouped in a single day. All operators were blinded throughout the surgeries, echocardiography, tissue collection and downstream analysis.

4.2.8 Echocardiography

Echocardiography was performed throughout this protocol to assess cardiac function. This was performed by Dr Vikram Tallapragada of the Victor Chang Cardiac Research Institute at Baseline, day 2, and day 28. Mice were lightly anesthetised using 0.5-1.5% isoflurane and echocardiography was

performed using the Visual Sonics Vevo 2100 Preclinical Imaging System with a MS400 transducer (FUJIFILM Visual Sonics, Ontario, Canada). Blinded echocardiography data analysis was carried out using the bullet method and was completed by Dr Sul Ki Kim of the Centre for Heart Research, The Westmead Institute for Medical research and myself allowing for inter-reader variability analysis (Methods included in section 4.2.9). Long and short axis echocardiography imaging was analysed for systolic parameters using the bullet method. The bullet method uses a 5/6 area by length formula to calculate left ventricle volume to determine left ventricular end systolic volume (LVESV), left ventricular end diastolic volume (LVDEV) and ejection fraction (EF). Area of the left ventricle was calculated using the short axis at 3 points through the ventricle from the 1mm below the mid-papillary (MP) level to 3mm below the MP level, measuring the endocardium and epicardium in systole and diastole. Length of the ventricle was measured using the long axis view in systole and diastole from the aortic valve to the apex. Analysis measurements were carried out using the Vevo 3100 Analysis Software (FUJIFILM Visual Sonics, Ontario, Canada) and calculated on Microsoft Excel (2016).

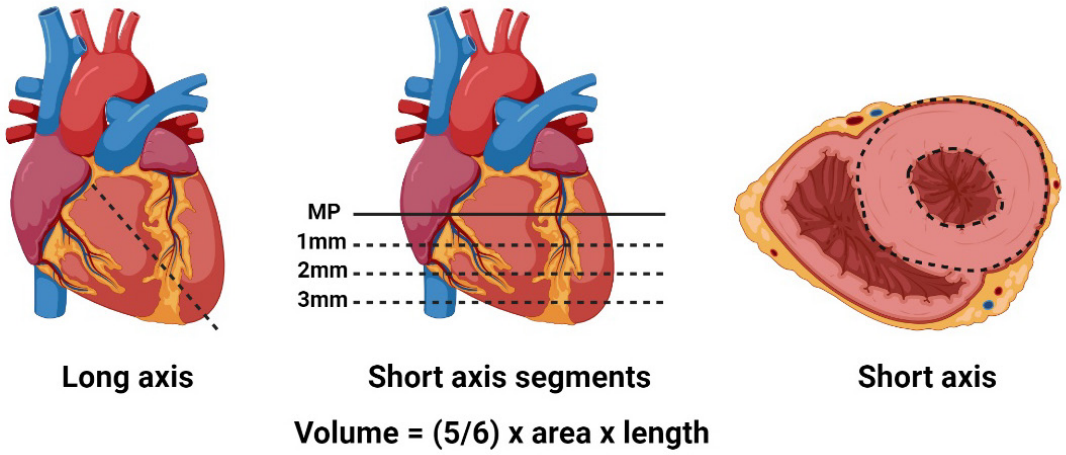

Figure 4.2.1: Bullet method measurements for echocardiography analysis.

4.2.9 Statistical Analysis

All statistics were carried out using GraphPad Prism (version 9.0.1). One way ANOVA statistical tests were carried out to determine statistical significance for all assays comparing all treatment groups to the PBS vehicle control group. Inter-reader variability on the echo analysis was carried out using a Bland-Altman method comparison test to identify significant differences in analysis between different observers.

4.3 RESULTS

To assess the safety and efficacy of our mimetic peptides we carried out a two-part toxicity study (see Figures 4.3.3-4.3.4 below) followed by an efficacy study (see Figure 4.3.7 below) in a murine model of acute MI. Phase A of our toxicity study was carried out as a maximum tolerated dose study on both male and female C57BL6/J mice. Mice were given 1 our 4 synthetic peptides via intraperitoneal injection and monitored 3 times daily until tissue and blood collection on day 7. We tested four dose groups increasing step wise each week at the safe completion of the prior dose group. Phase B was carried out using the highest tolerated dose of Phase A on only male C57BL6/J mice. The peptides were delivered via osmotic mini-pump that infused at a constant rate over days, with mice monitored daily for the first seven days and then twice weekly until tissue and blood collection on day 28. Delivery via osmotic mini-pump was chosen to replicate the delivery method of the efficacy study. At the completion of Phase B, blood biochemistry and hematology in addition to histology on the heart, lungs, liver, kidneys, spleen, and brain was carried out to identify signs of toxicity and adverse off target effects. Peptides were selected for transitioning into *in vivo* experiments based on the results of the *in vitro* assays carried out in Chapter 3: Development of Novel Platelet Derived Growth Factor-AB Mimetic Peptides (Figure 3.3.18). From the *in vitro* assays we concluded that JC5 (Figure 4.3.1) displayed comparable function to PDGF-AB across migration, collagen contraction, tube formation, receptor activation and proliferation (Figure 3.3.18). These lead to the more refined version of this peptide, JC5a (Figure 4.3.2), that displayed comparable function to JC5 (Figure 3.3.18).

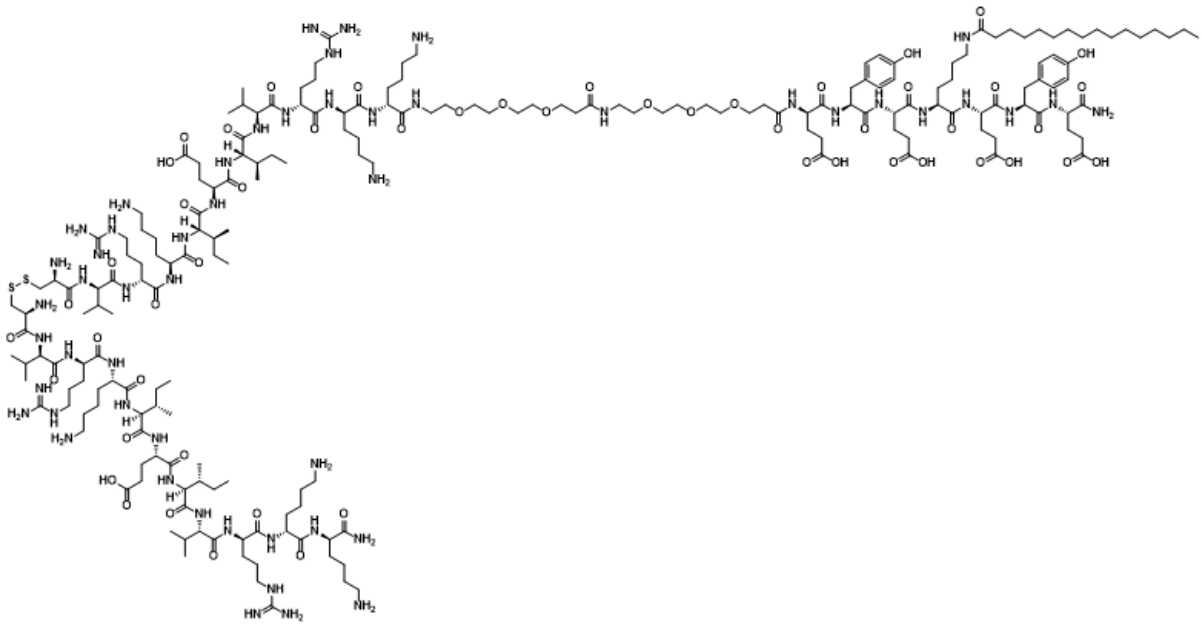

Figure 4.3.1: Novel mimetic peptide JC5 selected for in vivo testing.

The chemical structure of JC5 is composed of a homodimer of the loop III region of the PDGF B chain linked to a human serum albumin conjugate by 3 polyethylene glycol subunits. These peptides were developed in collaboration with the Payne Laboratory at the School of Chemistry, University of Sydney. Dr Daniel Ford synthesised all peptides used.

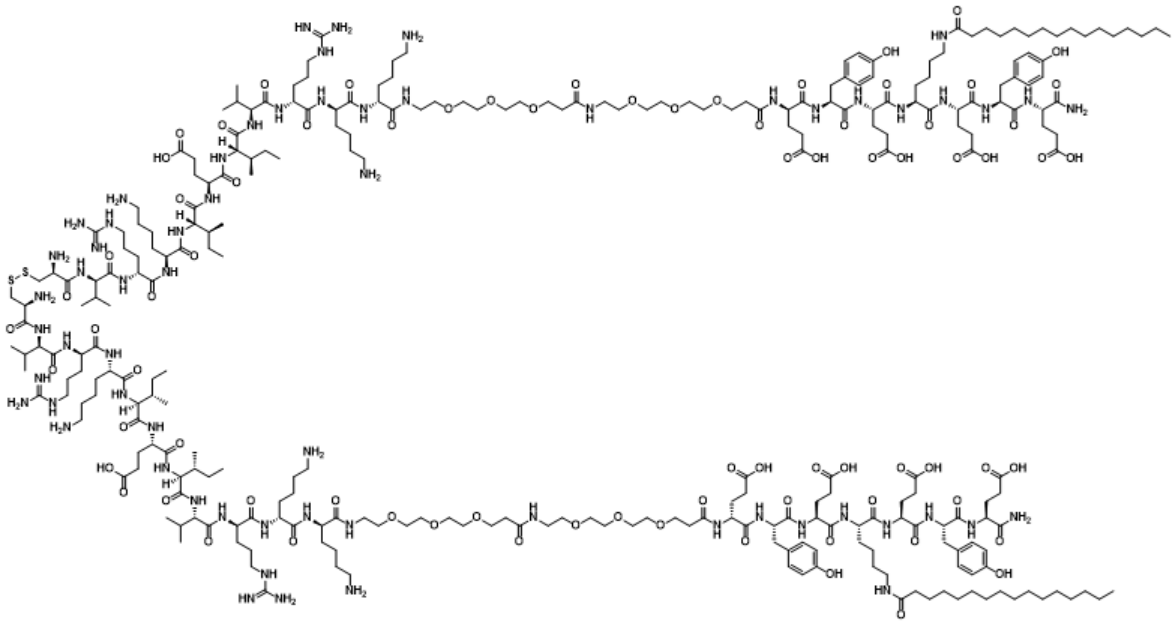

Figure 4.3.2: Novel mimetic peptide JC5a selected for in vivo testing.

The chemical structure of JC5a is composed of a homodimer of the loop III region of the PDGF B chain linked to 2 human serum albumin conjugates by 3 polyethylene glycol subunits. These peptides were developed in collaboration with the Payne Laboratory at the School of Chemistry, University of Sydney. Dr Daniel Ford synthesised all peptides used.

4.3.1 Toxicity and Safety Study

4.3.1.1 Phase A – Maximum Tolerated Dose Study

Preliminary toxicity studies were carried out to assess acute safety and toxicity. Mice received an IP injection of 1 of the 4 peptides on day 1 and were monitored 3 times daily for signs of distress or acute toxicity until day 7. To determine a maximum tolerated dose a new dose group was completed each week increasing step wise at the successful completion of the dose prior, starting with the lowest dose 3.25mg/kg and escalating to 32.50mg/kg. Throughout Phase A no signs of acute toxicity or signs of distress were noted in any mice across all doses for all peptides in both males and females and there were no mortalities (Figure 4.3.3).

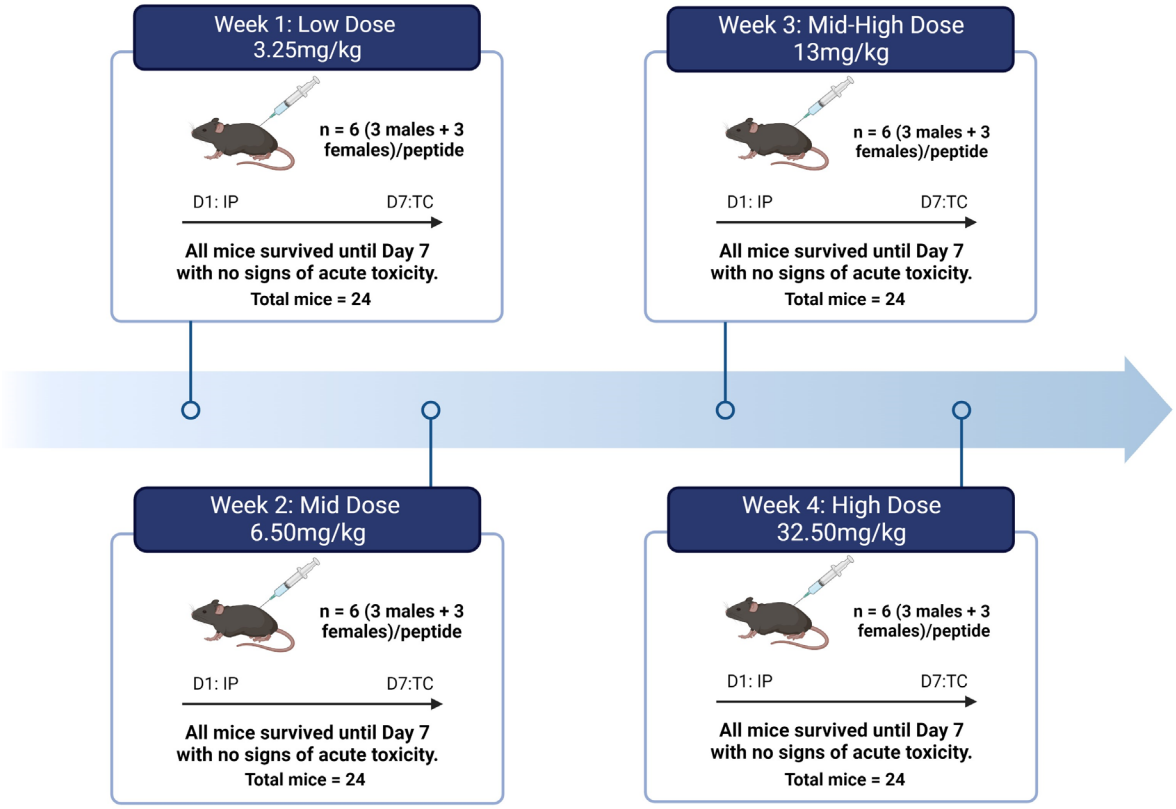

Figure 4.3.3: Mice showed no signs of acute toxicity over 7 days following intraperitoneal injection.

Following IP injection none of the mice treated with the 4 peptides across each dose groups presented with signs of distress or acute toxicity. (n=6 [3 males + 3 females]/peptide). This study was carried out with the technical expertise of Dr Vikram Tallapragada.

4.3.1.2 Phase B – Toxicity Study

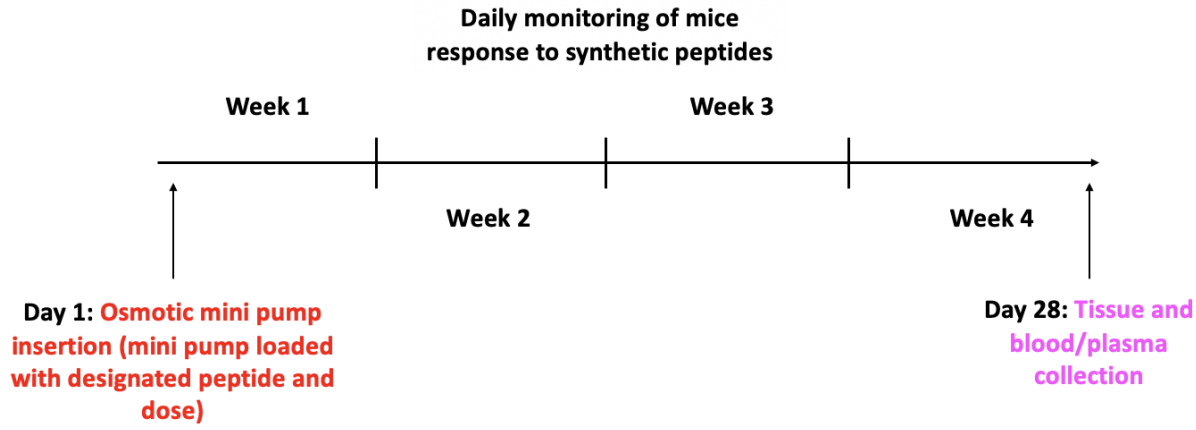

Figure 4.3.4: Phase B toxicity study – experimental timeline

Osmotic mini-pump insertion was performed by Dr Vikram Tallapragada.

Moving forward with the highest dose of 32.50mg/kg successfully completed in Phase A, Phase B was commenced with the aim of identifying potential off target effects longer term and to reflect the administration route in the planned efficacy study. To achieve this, male C57BL6/J mice received their designated peptide at 32.50mg/kg via osmotic mini-pump on day 1 and were monitored for 28 days for signs of distress or toxicity prior to blood and tissue collection on day 28 (Figure 4.3.4). At day 28 major organs were fixed for histology whilst blood and plasma were collected for blood profiling. Analysis of blood profiling (Table 4.3.2-4.3.3) and histology (Figure 4.3.5-4.3.6) results was completed by veterinarian Dr Alan Marcus. Blood profiling consisting of haematology and blood biochemistry parameters was then carried out by Idexx Laboratories. Haematology analysis identified no significant changes across the peptide groups with the exception of a mild increase in monocytes in 2 of 3 mice in the JC5 group (Table 4.3.2). Biochemistry identified decreased total protein, albumin, and creatinine, and increased urea, calcium, and sodium across all groups including scrambled peptide controls. This is likely due to species/strain differences in recorded reference ranges (Table 4.3.3). The reference ranges set by Idexx Laboratories were for mus musculus species but not specifically the

C57BL6/J strain. Further assessment of these results indicated they align with reported reference ranges specific to this strain (212, 213).

Table 4.3.1: Maximum tolerated dose study haematology parameters.

Blood profiling identified minor changes in haematology parameters of Phase B mice, 28 days post treatment with each of the 4 peptides. Blue indicates below the reference range. Red indicates above the reference range (n=3/peptide)

Test	JC5			JC5^{NC}			JC5a			JC5a^{NC}		
	n1	**n2**	**n3**	**n1**	**n2**	**n3**	**n1**	**n2**	**n3**	**n1**	**n2**	**n3**
Red Blood Cells (6.3-10.1) x10^{12}/L	9.2	9.1	8.5	7.4	8.4	8.0	8.0	7.8	8.3	8.6	7.2	8.9
Haematocrit (0.33-0.48) L/L	0.42	0.4	0.37	0.33	0.37	0.35	0.37	0.36	0.38	0.42	0.33	0.40
Haemoglobin (101-161) g/L	134	133	123	108	123	115	120	122	124	135	**85**	131
MCV (42-56) fL	46	44	44	45	44	44	46	46	46	49	46	45
MCH (14-18) pg	15	15	14	15	15	14	15	16	15	16	**12**	15
MCHC (295-351) g/L	319	333	332	327	332	329	324	339	326	321	**258**	328
% Reticulocytes (0.0-11.3) %	3.6	3.9	3.8	3.2	3.5	4.6	4.1	4.9	3.6	5.6	4	3.7
Reticulocytes x10^{9}/L	331	355	323	237	294	368	328	382	299	482	288	329
WBC (5.1-11.6) x10^{9}/L	6.9	5.8	**5**	5.2	5.1	**3.5**	**3.4**	4.7	8.3	9.3	**4.7**	**3.9**
% Neutrophils	12	12	10	28.4	26.1	35.3	11	9	8	14	12	14
% Lymphocytes	79	78	84	68.3	67.4	55.9	85	89	90	81	82	84
% Monocytes	7	8	5	3.3	6.5	8.8	3	2	2	3	4	2
% Eosinophils	2	1	1	0	0	0	1	0	0	2	2	0
% Basophils	0	1	0	0	0	0	0	0	0	0	0	0
Neutrophils (0.0-2.8) x10^{9}/L	0.8	0.7	0.5	1.5	1.3	1.2	0.4	0.4	0.7	1.3	0.6	0.5
Lymphocytes (0.0-12.0) x10^{9}/L	5.5	4.5	4.2	3.6	3.4	2	2.9	4.2	7.5	7.5	3.9	3.3
Monocytes (0.0-0.4) x10^{9}/L	**0.5**	**0.5**	0.3	0.2	0.3	0.3	0.1	0.1	0.2	0.3	0.2	0.1
Eosinophils (0.0-0.3) x10^{9}/L	0.1	0.1	0.1	0	0	0	0	0	0	0.2	0.1	0
Basophils (0.0-0.0) x10^{9}/L	0	**0.1**	0	0	0	0	0	0	0	0	0	0
Platelets (252-1612) x10^{9}/L	667	438	1167	341	-	610	-	-	-	-	1412	-

Table 4.3.2: Maximum tolerated dose study blood biochemistry parameters.

Blood profiling identified minor changes in biochemistry parameters of Phase B mice, 28 days post treatment with each of the 4 peptides. (n=3/peptide)

Test	JC5			JC5^{NC}			JC5a			JC5a^{NC}		
	n1	**n2**	**n3**	**n1**	**n2**	**n3**	**n1**	**n2**	**n3**	**n1**	**n2**	**n3**
Glucose (FO) mmol/L	13.7	12.3	10.9	10.9	10.6	12	11.9	11.6	11	10.9	12	11
Creatinine (0.04-0.12) mmol/L	**0.01**	**0.01**	**0.01**	-	-	-	**0.01**	-	**0.01**	**0.01**	**0.01**	0.01
Urea (1.8-5.2) mmol/L	**10**	**7**	**8.1**	**9.5**	**13.4**	**11.1**	**9.5**	-	**9.3**	**7.6**	**10.6**	**8.1**
Phosphorus (1.3-3.0) mmol/L	2.3	**1.2**	1.5	-	1.4	2.1	2	-	1.8	2	2.3	2.5
Calcium (1.2-1.9) mmol/L	**2.3**	-	**2.2**	-	**2.1**	**2.2**	**2.1**	-	**2.2**	**2.2**	**2.1**	**2.2**
Sodium (132-144) mmol/L	**148**	**147**	**145**	**147**	141	**145**	-	-	-	-	-	-
Potassium (5.1-5.7) mmol/L	**4.6**	**5**	5.6	**6.0**	5.4	5.1	-	-	-	-	-	-
Chloride (96-129) mmol/L	114	115	112	113	109	111	-	-	-	-	-	-
Bicarbonate mmol/L	8	-	7	-	12	9	-	-	-	-	-	-
Anion Gap mmol/L	30.6	-	31.6	-	25.4	30.1	-	-	-	-	-	-
Total Protein (58-66) g/L	**44**	**40**	**42**	**43**	**41**	**43**	**44**	**38**	**43**	**41**	**45**	**45**
Albumin (32-36) g/L	**26**	**28**	**28**	**27**	**26**	**26**	**26**	**22**	**26**	**23**	**26**	**26**
Globulin g/L	18	12	14	16	15	17	18	16	17	18	19	19
ALT IU/L	23	27	16	26	23	37	21	17	14	13	17	17
AST IU/L	61	70	52	47	50	69	44	81	38	53	46	37
ALP (28-104) IU/L	67	71	76	43	33	50	57	50	64	81	55	51
GGT IU/L	0	0	3	0	0	0	0	0	0	0	0	0
Bilirubin (0-24) umol/L	1	2	0	0	0	0	3	0	2	5	0	0
Cholesterol (0.7-2.9) umol/L	2.6	2.1	2.1	2.1	2.1	2	2	1.5	1.9	1.4	2.2	2.1
Creatinine Kinase IU/L	639	140	418	130	690	1017	1967	1511	343	1972	829	703

Histological analysis was completed on all the hearts, lungs, liver, kidneys, spleen, and brain of all mice from Phase B. Haematoxylin and eosin staining (Figure 4.3.5) was performed to identify changes in tissue composition and potential pathological changes, whilst picrosirius red and fast green (Figure 4.3.6) staining was used to identify any changes in collagen deposition within the ECM (n=6/peptide). All mice across all groups presented with some degree of consolidation and increased cellularity in the lungs. This was likely as a result of fixative protocols rather a pathological change. Poor fixation of lungs is known to cause consolidation of the alveolar and give the appearance of increased cellularity (214). Additionally, vacuolation and retraction were present in the brain but are also likely artefactual due to post mortem absorption of cerebrospinal fluid that occurs during fixation (215). Hyperpigmentation in regions of some spleen indicates splenic melanosis present in some mice which is not specific to any single group and is considered a normal condition for this specific strain (216) and fell within expected ranges. Interindividual variation in apparent hepatocyte glycogen storage was noted in the livers (Figure 4.3.5). Combining results from blood profiling, histological and clinical observations (including lack of weight changes), Dr Alan Marcus concluded there were likely no concerns regarding safety of the peptides based on these results.

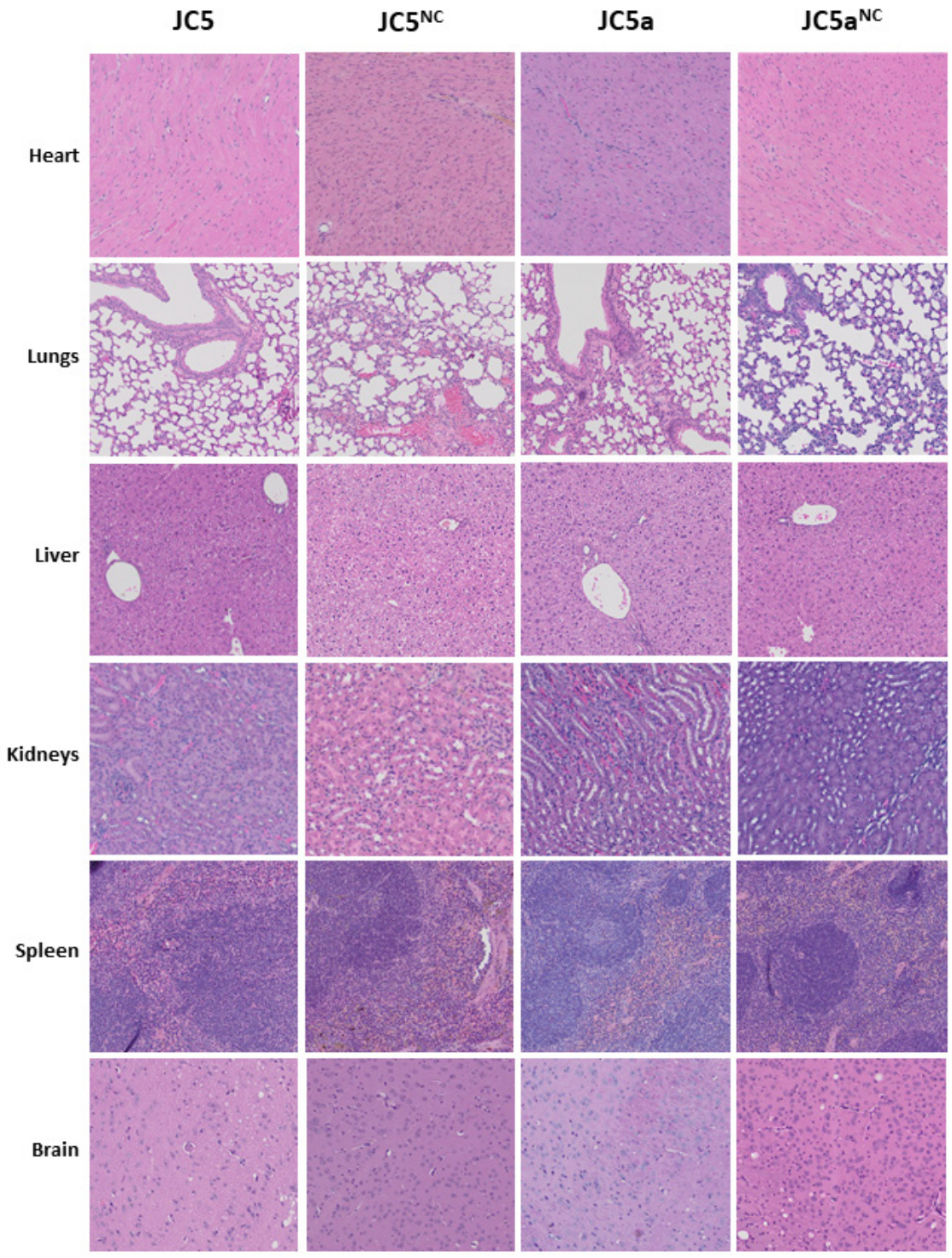

Figure 4.3.5: Treatment with novel mimetic peptides shows no signs of toxicity or aberrant cell growth.

Representative images of haematoxylin and eosin staining of all major organs (10x magnification) of Phase B mice. Analysis of histology was carried out by Dr Alan Marcus.

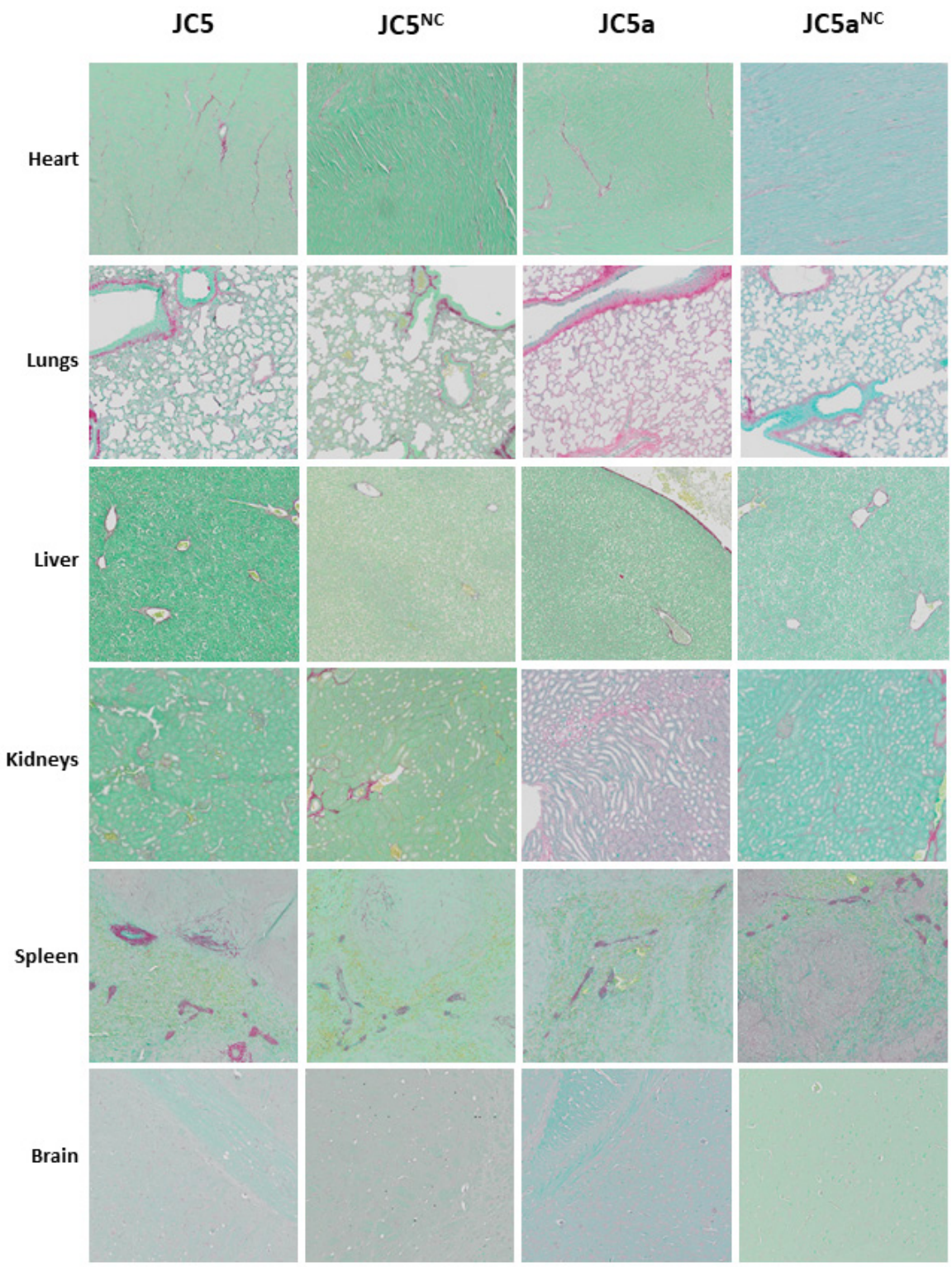

Figure 4.3.6: No signs of toxicity or aberrant cell growth following treatment with novel mimetic peptides.

Representative images of picrosirius red and fast green staining of all major organs (10x magnification) of Phase B mice**.** Analysis of histology was carried out by Dr Alan Marcus.

4.3.2 *In vivo* Efficacy Study

The *in vivo* efficacy of lead candidate peptides was assessed using a murine model of acute MI established using a surgically induced MI via permanent occlusion of the LAD artery (Figure 4.3.7). Cardiac function was measured using echocardiography with a pre-infarct baseline and post-MI measurements at day 2 and a day 28, followed by tissue collection and calculation of heart weight divided by tibia length. For echocardiographic analyses, the bullet method was employed, which shows improved accuracy over other analysis methods (217). Mice were randomised into treatment groups receiving either the positive control recombinant human PDGF-AB, novel mimetic peptide JC5, novel mimetic peptide JC5a, or PBS as a vehicle control, via implanted osmotic mini-pump at the time of infarction. In addition to this sham-surgery non-infarcted healthy mice controls were included, receiving either 32.50mg/kg of novel mimetic peptides JC5 or JC5a via osmotic mini-pump. Sham control mice underwent the same mini-pump insertion surgery on day 1 and all echocardiography imaging analysis as MI mice.

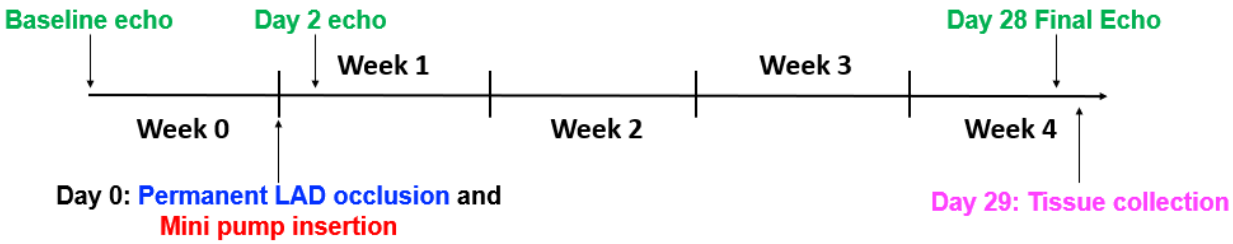

Figure 4.3.7: Efficacy study experimental timeline.

Occlusion of the LAD and osmotic mini-pump insertion was carried out by Dr Vikram Tallapragada.

At 28 days post-MI, mice treated with PDGF-AB (MI) and JC5 (MI) had a significantly increased LVEF when compared to mice that received the PBS (MI) vehicle control (Figure 4.3.8A). Mice treated with PDGF-AB (MI) had a day 28 LVEF of 43.44% (±11.90) similar to mice treated with JC5 (MI) that had LVEF of 42.06% (±13.41). This was significantly greater than control mice receiving PBS (MI) with LVEF 26.89% (±6.966) (PDGF-AB p=0.0073, JC5 p=0.0129, Figure 4.3.8A). Novel mimetic peptide JC5a (MI)

demonstrated a trend towards increased LVEF but this was not statistically significant (p=0.0655) when compared to PBS (MI) with LVEF at day 28 of 39.24% (±13.51) (Figure 4.3.8A). The validity of the day 28 LVEF results was confirmed using a Bland-Altman inter-observer variability analysis for the blinded operators analysing echocardiographic data (Figure 4.3.9). The bias was 14.06 (±7.346), consistent across all replicates when comparing observer 1 to observer 2. This falls within reported ranges for rodent echocardiography of injured hearts (218, 219). Together, these data demonstrate the PDGF peptide mimetic JC5 was as effective at improving post-MI function as PDGF-AB.

In mice treated with positive control PDGF-AB (MI) and novel mimetic peptide JC5 (MI), there was a significant decrease in both ESV and EDV at day 28 when compared to the vehicle control, PBS (MI), cohort (Figure 4.3.8B-C). JC5 and PDGF-AB had a day 28 ESV of 67.01µL (±42.94) and 55.04µL (±23.66) respectively. These were significantly reduced when compared to the PBS vehicle control, at 116.6µL (±45.00) (JC5 p=0.0032, PDGF-AB p=0.0003, Figure 4.3.8B). The same could be seen with respect to EDV in both PDGF-AB and JC5 when compared to the PBS control (JC5 p=0.0185, PDGF-AB p=0.0016, Figure 4.3.8C). The decreased EDV of PDGF-AB and JC5 treated mice is visible in the echocardiography images presented in Figure 4.3.10.

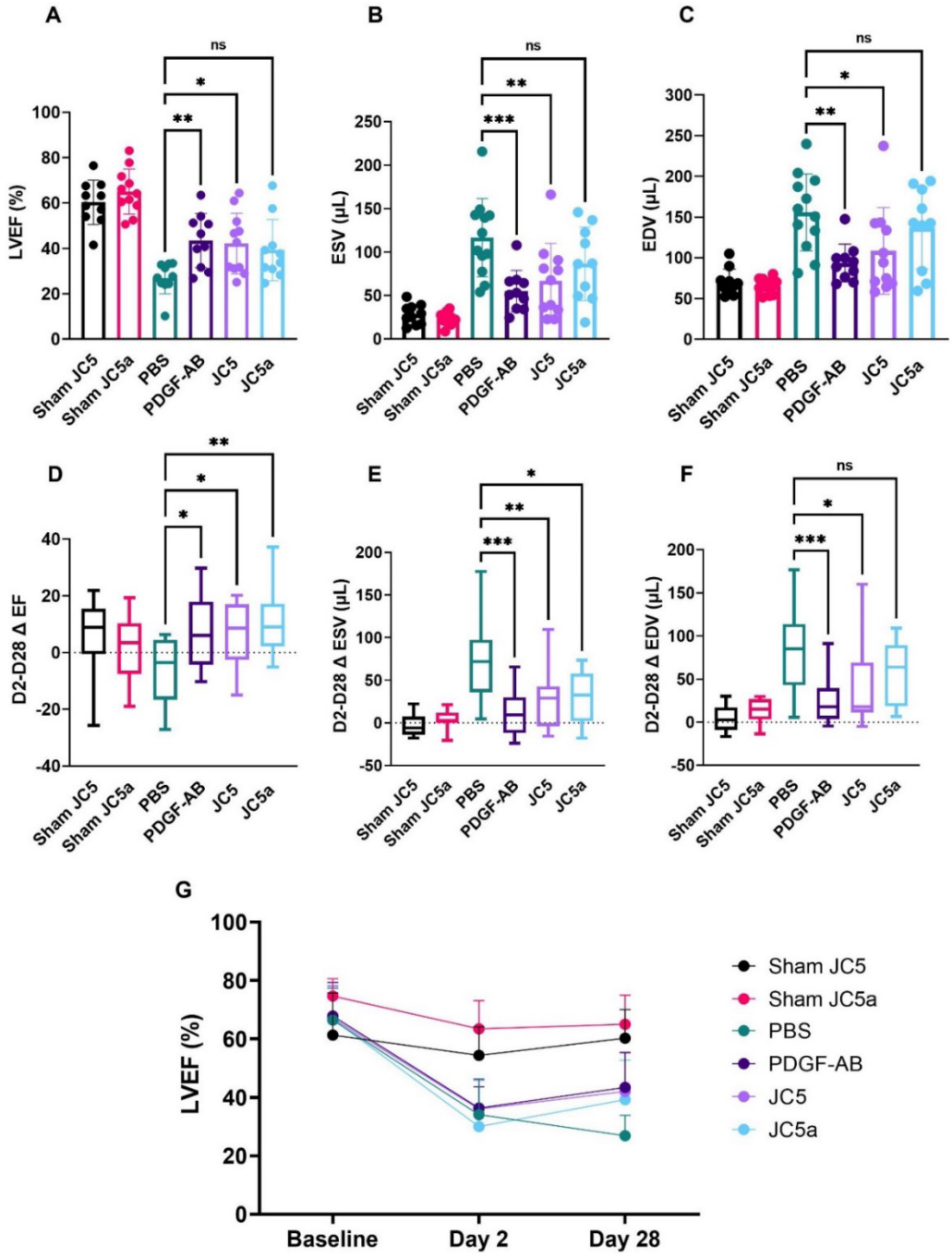

Figure 4.3.8: Improved cardiac function at day 28 post myocardial infarction.

A) Left ventricular ejection fraction (LVEF) of mice 28 days post-MI. B) End systolic volume (ESV) of C57BL6/J mice 28 days post-MI. C) End systolic volume (ESV) of C57BL6/J mice 28 days post-MI. D) Day 2 – day 28 delta (Δ) ejection fraction. E) Day 2 – day 28 delta (Δ) end systolic volume (ESV). F) Day 2 – day 28 delta (Δ) end diastolic volume (EDV). G) Timeline of mean LVEF per treatment group. A-C) Error bars represent ± SD. D-F) Data presented as median ± minimum and maximum values. G) Data presented as mean and error. One way ANOVA comparing all groups to the PBS vehicle control group (n=10/11). ns=not significant, *p<0.05, **p<0.01, ***p<0.001. Echocardiography data was collected by Dr Vikram Tallapragada.

Whilst JC5a (MI) treated mice did not have a significantly increased LVEF on day 28 when compared to PBS (MI), JC5a (MI) did result in the greatest increase in LVEF from day 2 to day 28 (Figure 4.3.8D). Following treatment with 32.50mg/kg of novel mimetic peptide JC5a (MI), mice had an average change in LVEF of 10.82% from day 2 to day 28 compared to PBS mice at -7.203% (±12.16) (p=0.0082) (Figure 4.3.8D). JC5a treated were also noted having a slightly reduced day 2 LVEF when compared to all other groups (Figure 4.3.8G). Mice treated with the positive control PDGF-AB (MI) and JC5 (MI) also had a significant increase in LVEF from day 2 to day 28 when compared to PBS (MI). Mice treated with PDGF-AB (MI) had an average day 2 to day 28 Δ of 7.104% (±13.19) (PDGF-AB p=0.0393) whilst mice treated with JC5 (MI) had an average day 2 to day 28 Δ of 6.686% (±12.22) (JC5 p=0.0409). Additionally, mice treated with PDGF-AB, JC5, and JC5a resulted in a significant decrease from day 2 to day 28 in ESV (Figure 4.3.8E) (PDGF-AB p=0.0001, JC5 p=0.0030, JC5a p=0.0114). However, only JC5 and PDGF-AB resulted in a significant day 2 to day 28 Δ for EDV (Figure 4.3.8F). These results show JC5a is also as effective at improving cardiac function in mice, as JC5 and PDGF-AB.

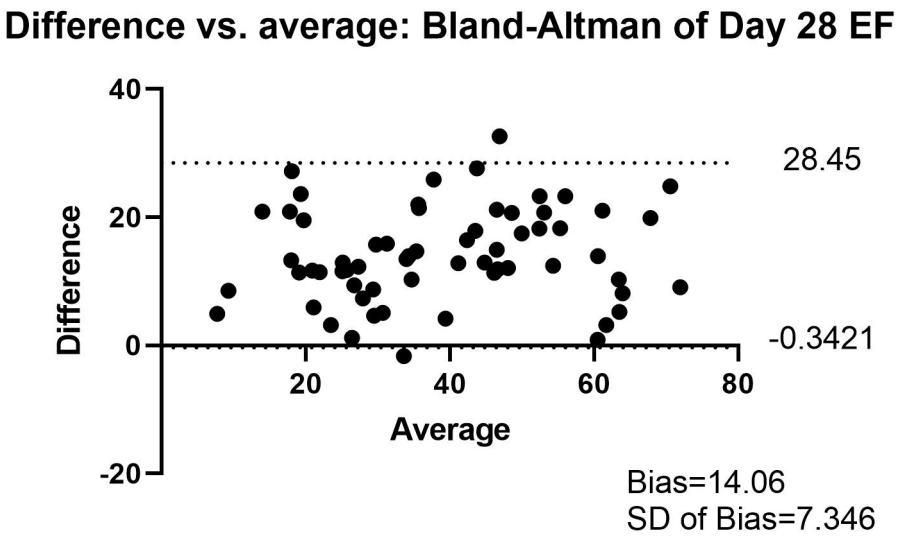

Figure 4.3.9: Inter-observer variability of day 28 left ventricular ejection fraction (LVEF).

Inter-observer variability at day 28 was within normal limits for rodent echocardiography with a bias of 14.06 (±7.346). Error bars represent 95% limits of agreement. Dr Sul Ki Kim acted as the second observer for this analysis.

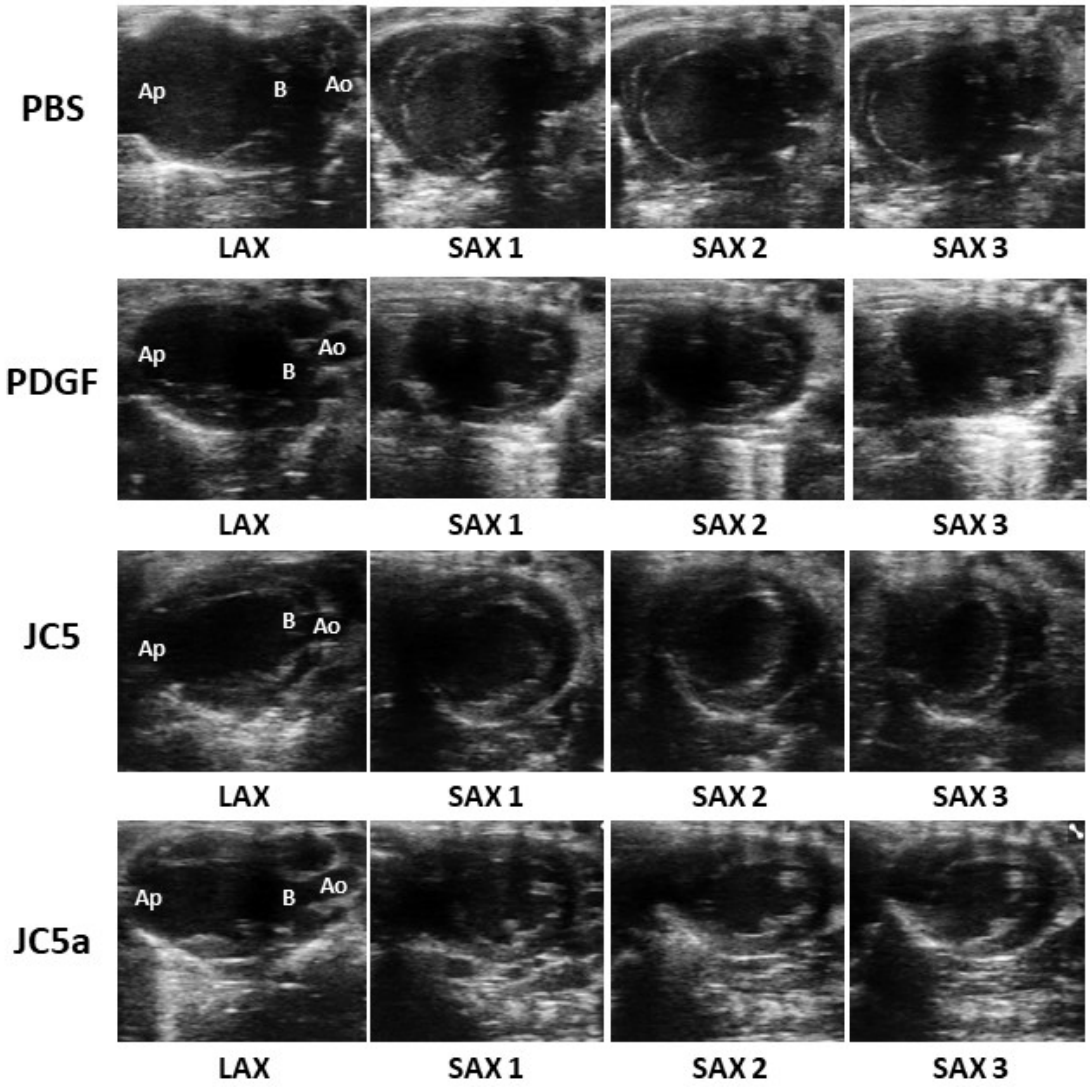

Figure 4.3.10: Day 28 Echocardiography Images.

Echocardiography at day 28 showing the long axis (LAX) and short axis (SAX) views at the 3 levels (basal to apical) used for our measurements. Sax levels are as indicated in Figure 4.2.1. All images presented are in diastole. Ap=apex, B=base, Ao=aorta. Echocardiography data was collected by Dr Vikram Tallapragada.

To assess the effects of novel mimetic peptides JC5 and JC5a on cardiac scar we carried out picrosirius red and fast green staining on paraffin embedded sections of the hearts collected at day 28. Scar size was quantified using percentage of collagen in each section. Despite significant improvements in cardiac function, no significant effect was identified in cardiac scar size at 28 days post MI (Figure 4.3.11). Given the effect of PDGF on fibrogenesis and proliferation of cells, this analysis allowed us to confirm that JC5 and JC5a do not result in increased scar size. Additionally, a decrease in cardiac scar

could have indicated a potential mechanism leading to improved cardiac function. No significant change in scar size identified through these experiments indicate that JC5 and JC5a did not result in increased fibrogenesis a day 28 however, also indicates that effects on scar size are unlikely the mechanism of action leading to improve cardiac function.

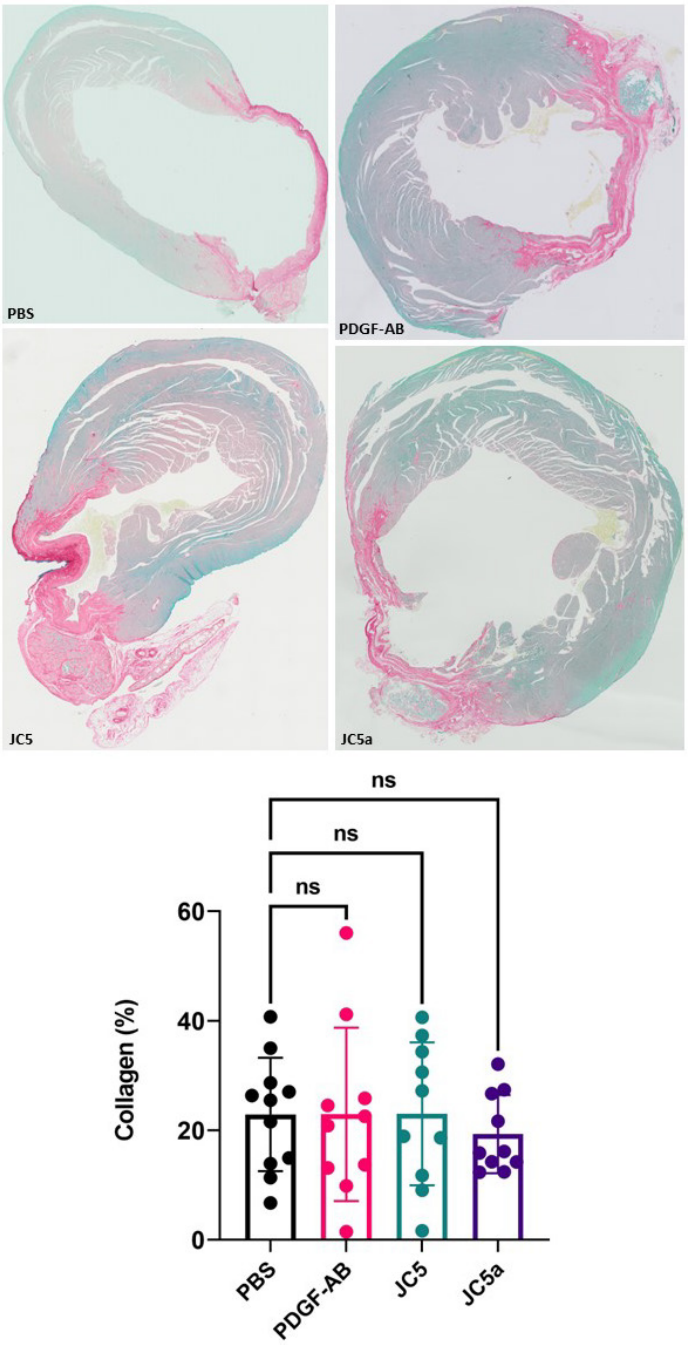

Figure 4.3.11: No significant effects on size of cardiac scar at day 28 post myocardial infarction.

Scar quantification of picrosirius red and fast green stained sections at day 28 identified no significant changes in scar size. One way ANOVA comparing all groups to the PBS vehicle control group (n=10/11). ns=not significant.

In summary, these results show the safety and efficacy of JC5 and JC5a in C57BL6/J mice. Following the maximum tolerated dose study and 28-day toxicity study, no significant markers of acute toxicity or off target adverse effects were present. This indicates that both peptides were safe for therapeutic use in the subsequent efficacy study. Our efficacy study assessing the effects of JC5 and JC5a 28 days post-MI showed increased cardiac function following treatment with both peptides and similar effects to that of our positive control PDGF-AB.

4.4 DISCUSSION

Preclinical studies have established PDGF-AB as a promising novel therapy for heart failure (57, 58). However, despite its promising therapeutic effects its poor pharmacokinetics and costly inefficient synthesis has limited clinical translation. Whilst analogues of PDGF have been produced previously with good *in vitro* results (133), none have ever been reported *in vivo*. Throughout lead optimisation of the peptides designed and synthesised in Chapter 3: Development of Novel Platelet Derived Growth Factor-AB Mimetics, JC5 and JC5a were identified as lead candidates for translation into *in vivo* studies. The aim of this chapter was to assess the safety and efficacy of these lead candidates in an established murine model of acute MI, comparing the effects of these on cardiac function against recombinant human PDGF-AB.

To assess the safety of our novel mimetic peptides we carried out a two-part toxicity study starting with a maximum tolerated dose study (Figure 4.3.3) and a 28-day toxicity study (Figure 4.3.4). The *in vivo* safety and toxicity studies were based on previous toxicity studies of other therapeutics in the literature (209-211). Maximum tolerated dose was assessed in C57BL6/J mice for several cytotoxic chemotherapies using weight and clinical score as endpoints for determining safety (211). The clinical score in their study was determined based on appearance, body condition, and activity. Similarly, a 2-

part toxicity study was carried out on the small molecule sirtuin inhibitor, Inhauzi. This applied a similar maximum tolerated dose study as previously outlined with the addition of blood profiling and histological analysis to further investigate the effects of their therapeutic (209). We replicated this approach in our own toxicology and safety studies for our novel mimetic peptides, JC5 and JC5a. At the conclusion of the *in vivo* study, histology and blood profiling were carried out to identify potential adverse effects of each of the peptides. Based on the known cellular effects of increased PDGFR signalling, our primary concern in carrying out the 28-day toxicity study was to identify signs of abnormal proliferation, tumorigenicity or changes in the ECM. It is understood that PDGFR signalling alone cannot induce metastatic growth (117), however, it is a well-established potent mitogen (86, 87) posing the need to ensure these effects do not result in adverse off target effects. Whilst minor changes were identified throughout these experiments (Table 4.3.2-4.3.3 and Figure 4.3.5-4.3.6), veterinarian Dr Alan Marcus concluded that these changes did not indicate any significant adverse or off target effects. The previously reported studies support the use of blood profiling and histological analysis to assess the safety of therapeutics in murine models (209). Despite concluding from these results that JC5 and JC5a were safe for further in vivo efficacy testing, these studies need to be repeated applying Good Laboratory Practice standards in future work. A notable limitation of the present study is the absence of a saline treated control group. Each cohort of the present studies were treated with 1 of our 4 mimetic peptides, either the biologically active JC5 or JC5a or their biologically inactive negative control counterparts. Due to the lack of saline treated control group, conclusions drawn from the blood profiling and histology were based on expected species-specific ranges from the literature (212, 213). The introduction of a saline treated control group would allow for more accurate assessment of the effects of our peptides, ensuring their safety for *in vivo* use.

Echocardiography measurements at day 28 identified a significant increase in cardiac function in mice treated with recombinant human PDGF-AB and novel mimetic peptide JC5 when compared to PBS

vehicle control mice (Figure 4.3.8). This was determined by changes in LVEF, ESV, and EDV. Greater significance was identified in decreased ESV than EDV indicating the effect of PDGF-AB, JC5, and JC5a was more a result of improved contractility rather than reduced dilation of the left ventricle. Importantly, these results correlate with previous results in PDGF-AB *in vivo* models by our groups (57, 58). For example, our previous murine MI model identified significantly reduced ESV and EDV following 28 days treatment with PDGF-AB. Furthermore, this previous study showed greater significance in ESV (58), which is in agreement with our results for PDGF-AB and also our PDGF based mimetic peptides JC5 and JC5a. In the porcine model assessing effects of PDGF-AB on cardiac function, a significant decrease was only noted in ESV, indicating that the increased LVEF was driven by improvements in contractile function. The mechanism of this in the porcine model supported these results, identifying no significant decrease in size of the scar post-MI but rather a significant change in the composition of the scar resulting in improved contractility (57). Interestingly, our analysis of cardiac scar size at day 28 (Figure 4.3.11) identified no significant changes in scar size in mice treated with PDGF-AB and both novel mimetic peptides JC5 and JC5a, aligning with this previous porcine model. This differed from the earlier murine model that reported a decrease in size of the scar but included no further analysis of scar composition (58). Further investigations into composition of the ECM are needed to determine if the same mechanism identified in previous models on PDGF-AB is the cause of the cardiac functional change following treatment with JC5 and JC5a described here.

The change in LVEF, ESV, and EDV from day 2 to day 28 was plotted to account for differences in day 2 cardiac function in the event that any group had larger infarcts than others. On average mice in the JC5a had worse day 2 LVEFs than all other groups indicating this group had larger induced MIs. Increased infarct size at day 2 is potentially a confounding variable to consider when comparing treatment groups at the day 28 timepoint. Whilst JC5a did not significantly improve cardiac function based on its day 28 LVEF, ESV, and EDV compared to other groups, plotting the day 2 to day 28 Δ

highlighted a significant increase in cardiac function when compared to the PBS vehicle control group. This was not maintained with respect to EDV for JC5a however, was for ESV indicating that JC5a had improved contractility at day 28. The improvement in LVEF and ESV is consistent with the effects of PDGF-AB in the murine and porcine models (57, 58).

The work in this chapter provides evidence of *in vivo* therapeutic benefits of our lead candidate peptides, JC5 and JC5a. Significant efforts have been made in previous work to establish the mechanism of action for PDGF-AB post-MI. This has included collagen alignment studies and investigations into the composition of the post-infarct cardiac scar. Additionally genomic analysis has highlighted roles of the ECM and immune response pathways following treatment with PDGF-AB (138). Future work on JC5 and JC5a will require similar investigation into their mechanism of action and how this aligns with what we know of PDGFs mechanism. These future studies will require analysis of the ECM specifically with collagen alignment and composition of the scar can be performed on mouse hearts collected from the *in vivo* efficacy study reported in this chapter. In addition to this, further work is required to assess the pharmacokinetics and pharmacodynamics of our lead candidate peptides. Both peptides utilised a HSA conjugate that has been reported to successfully extend the half-life of synthetic peptides (148). To assess the efficacy of this conjugate in the context of JC5 and JC5a, *in vitro* plasma stability assays and *in vivo* pharmacokinetics studies will be required. Pharmacokinetics and pharmacodynamics (Pk/Pd) experiments could have been carried out prior to the commencement of *in vivo* safety and efficacy studies however, we elected to prioritise testing the efficacy of our lead candidates. Pk/Pd *in vivo* studies require expertise outside the scope of our group with Good Laboratory Practice and ISO certification not held by our facilities. These would, therefore, require engagement from an external third party making these studies a costly endeavour. Commencing *in vivo* data collection with pilot safety and efficacy studies provided necessary data to support commencing necessary pharmacokinetics and pharmacodynamics studies. Other experiments

that could be considered to increase our understanding of JC5 and JC5a's relationship with PDGF receptors are *in vitro* assays studying their binding specificity and affinity. These could be done using surface plasmon resonance to measure the binding affinity of our mimetic peptides (220, 221) to each of the PDGF receptors alongside phosphoproteomics to identify off target receptor phosphorylation (222, 223) that may be present following treatment with our novel mimetic peptides. All of these assays would contribute to a better understanding of the potency, stability, and specificity of our lead candidates. Finally, successful translation of JC5 and JC5a as therapeutics for post-MI cardiac dysfunction will require confirmatory studies in a more clinically relevant large animal model of MI.

Our prior work in human recombinant PDGF-AB highlighted its therapeutic value post-MI in murine and porcine models however, its limitation in scalability and poor pharmacokinetics hinders its translation prospects. The loop III region of the PDGF-B chain had been previously utilised successfully in mimetics and analogues of PDGF *in vitro* (133-135), however these reports did not progress into *in vivo* studies. In the previous chapter entitled Chapter 3: Development of Novel Platelet Derived Growth Factor-AB Mimetics, we confirmed the effectiveness of loop III of the PDGF-B chain to recapitulate biological functions of PDGF using *in vitro* assays.

4.5 CONCLUSION

This chapter assesses the safety and efficacy of our lead candidate novel mimetic peptides, JC5 and JC5a. We have shown in a murine model of MI that these peptides improve cardiac function without adverse off-target effects or acute toxicity and therefore mimic the therapeutic effects of recombinant human PDGF-AB demonstrated previously by our groups (Asli et al, Thavapalachandran et al). Furthermore, greater efficiency in manufacturing and potentially enhanced pharmacokinetic properties confer advantageous commercialisation and clinical translation prospects providing exciting alternatives to the full-length recombinant protein.

CHAPTER 5: DISCUSSION, FUTURE DIRECTIONS AND CONCLUSIONS

5.1 GENERAL DISCUSSION

Cardiovascular disease remains the leading cause of morbidity and mortality world-wide, prevalent among them is heart failure with a 5-year mortality rate approaching 50% (1). Whilst significant developments have been made in the treatment of myocardial infarctions (MI) and heart failure there are still no viable treatment options to reverse the damage of heart failure after large infarcts outside of transplantation. The cardiac scar that forms post-MI as a result of adult cardiomyocytes very limited regenerative capacity is a significant contributor to the worsening cardiac function post-MI, making it an exciting therapeutic target following large infarcts (205).

Significant efforts have been made to address the poor regeneration of adult myocardium post-MI with notable approaches seen in stem cell therapies (55), gene therapy (53), and protein therapy (57). Despite promising pre-clinical results, none of these have been successfully translated into clinical use to date. A key limitation across all of these approaches is the highly skilled staff, complex manufacturing, and extensive quality control required to execute these therapeutics. Significant improvements in recombinant protein and peptide manufacturing have been made by the pharmaceutical industry moving into the 21st century resulting in very successful commercialisation and increased clinical translation of these therapeutics (168, 169). This has allowed for application of biologic based therapeutics with their efficacy beyond what was possible in traditional drug-based pharmaceuticals whilst ensuring feasibility for clinical use.

5.1.1 *In Vitro* Findings

Previous work by our groups highlighted the potential of recombinant human PDGF-AB (rhPDGF-AB) to modulate the cardiac scar as a mechanism of improving cardiac function post-MI in murine and porcine models (57, 58, 138). Whilst this posed rhPDGF-AB as a promising novel therapeutic, its poor

pharmacokinetic properties, and inefficient and costly synthesis limited its clinical translation. To address this, we developed novel mimetic peptides of PDGF-AB with half-life extending mechanisms, allowing for potentially improved pharmacokinetics whilst maintaining the biological function of PDGF-AB. Previous examples of PDGF mimetic peptides and analogues have demonstrated the ability to maintain the key functions of PDGF by utilising regions essential to receptor binding and activation (133-135). Among these a mimetic peptide with binding affinity to both the α and β receptors has been reported to induce migration, proliferation, collagen contraction and receptor activation (133, 134). Whilst analogues and peptide mimetics of PDGF have had very promising results *in vitro*, none have reported successfully translating these results into an *in vivo* model.

Lead optimisation allowed for the design and synthesis of novel mimetic peptides of PDGF-AB that replicated its therapeutic benefits whilst enhancing its pharmacokinetics making it a more clinically desirable and commercially attractive novel therapy for heart failure. This commenced with the identification of the loop III region of the PDGF-B chain that is known to be significant in the receptor signalling activity of PDGF (122, 124). Utilising this region, we designed and synthesised 9 mimetic peptides that were tested *in vitro* based on their efficacy compared to rhPDGF-AB and -BB. Our selected *in vitro* assays focused on migration (99-102), collagen contraction (201), tube formation (88, 97), proliferation (86-88), and receptor activation (103, 104). Whilst the effects of PDGF in these *in vitro* assays is well documented, our own work in the mechanism of action for PDGF in the context of our own work further highlighted the significance of these effects (138). In work carried out by Hume et al, the significant effect of PDGF on the extracellular matrix (ECM), angiogenesis, and chemotaxis is described. Additionally, the limited effect of PDGF on the cell cycle in this context is highlighted (138). This work further supported the use of our selected *in vitro* assays in assessing the effects of our lead candidates against rhPDGF-AB. In this work we showed that the loop III region is capable of executing receptor activation and downstream signalling cellular effects. It also highlighted JC5 and JC5a as lead

candidates based on their effects on migration, collagen contraction, tube formation and receptor activation. JC5 and JC5a were distinct to other peptides designed for these experiments as they contained a human serum albumin (HSA) conjugate with the potential to increase stability and half-life of the PDGF region. This HSA conjugate was previously reported bound to a Factor VIII therapeutic peptide enhancing its half-life by 25-fold (148).

5.1.2 *In Vivo* Findings

Whilst JC5 and JC5a were strong lead candidates based on our *in vitro* findings we needed to ensure they could mimic the effects of rhPDGF-AB *in vivo* in a model of acute MI, and that they could do so without eliciting adverse off target effects. To do this, the safety and efficacy of our novel mimetic peptides were tested *in vivo* in C57BL6/J mice. The design of our toxicity study was based on reported toxicity and safety studies on novel therapeutics in mice (209, 211). In addition to the general histology carried out in the literature we included picrosirius red and fast green staining to examine changes in collagen deposition. Given the known effects of increased PDGFR signalling on fibrosis in several organs (93, 224, 225), we determined this was necessary in assessing for adverse off target effects. The two-part toxicity study identified no significant adverse effects or signs of toxicity following treatment with JC5 and JC5a which aligns with the established safety of short-term exposure to rhPDGF (60). Whilst these experiments provided us with evidence to support the safety of JC5 and JC5a for *in vivo* efficacy testing, these experiments are not sufficient for clinical translation and will require more extensive, good laboratory practice (GLP) grade studies. Efficacy studies then established improved cardiac function following treatment with the mimetic peptides, JC5 and JC5a. Efficacy was assessed in a murine model of acute MI by permanently ligating the left anterior descending (LAD) artery. Whilst other more clinically relevant models, such as an ischemia reperfusion injury, may have been utilised in these studies (226), we chose a permanent occlusion model to reflect our previous work on rhPDGF-AB (58). In order to address the key aim of this work in producing a mimetic of

rhPDGF-AB, we felt it was essential to replicate our previous studies in the full-length protein to accurately assess the comparative effects of JC5 and JC5a. At 28 days post-MI mice treated with JC5 and JC5a had improved cardiac function compared to PBS vehicle control mice, similarly to mice treated with rhPDGF-AB. An increase in ejection fraction from day 2 to day 28 was identified in both peptide treated groups and the rhPDGF-AB treated group, aligning with the results of previous *in vivo* efficacy studies using rhPDGF-AB post-MI in murine and porcine models (57, 58). From these results we concluded that the comparable effect of our lead candidates JC5 and JC5a observed *in vitro*, were successfully translated to a comparable effect *in vivo*. In summary, novel mimetic peptides JC5 and JC5a, composed of the loop III homodimer and HSA conjugate, successfully mimicked the effects of rhPDGF-AB *in vitro* and *in vivo*, improving cardiac function in a murine model of acute MI.

Whilst the effects of rhPDGF-AB have been well established in models of acute MI, further work is required to investigate its affects in chronic heart failure. Attempting to address this we pursued a heart failure with preserved ejection fraction (HFpEF) model of chronic heart failure to investigate the effects of rhPDGF-AB and our novel mimetic peptides JC5 and JC5a. We carried out this work by validating the reported 'Two-Hit' approach to HFpEF, successfully replicating several key components of the HFpEF phenotype. Namely, maintained systolic function with reduced diastolic function in addition to significant weight gain, hypertension, and increased cardiomyocyte size. It also highlighted the significant role of metabolic processes in the development of HFpEF in this model. Despite these promising results we were unable to replicate significant changes to the cardiac ECM in this model. Of note the mouse strain we used for our validation of this model differed slightly to that used in the original reported data. This model was reported using the C57BL6/N whilst we chose to use the C57BL6/J due to difficulties locally sourcing the 6/N strain. Discrepancies between strains among C57BL6 mice have been reported across various murine models (227, 228) and is likely a factor in the differing results that we have seen from reported findings (50). Importantly, C57BL6/J have been

reported to have better mitochondrial respiration than C57BL6/N mice (227). The 'Two-Hit' approach to HFpEF relies on the onset of nitrosative stress to induce HFpEF (50). As a result, changes in mitochondrial respiration could have significant implications on the phenotype produced in this model across different C57BL6 strains.

The established mechanism of action for rhPDGF-AB post-MI is through modulation of the cardiac scar, angiogenesis, and the immune response (138). Given the similar function of our peptide mimetics JC5 and JC5a to rhPDGF-AB *in vitro* and *in vivo*, we hypothesise that their mechanism of action will closely align to that of rhPDGF-AB. The limited cardiac ECM changes identified in the 'Two-Hit' approach to HFpEF made this an inappropriate model for assessing the effects of our novel therapeutics. Despite not being appropriate for our applications, our validation of this approach in C57BL6/J mice successfully replicated several key aspects of the HFpEF phenotype. This work also added to our understanding of the significant metabolic processes in the development of HFpEF with several pathways affected in HFD+L-NAME treated mice.

5.2 FUTURE DIRECTIONS

The work in this thesis has shown that the JC5 and JC5a peptides mimic the therapeutic benefits of rhPDGF-AB whilst favourably improving ease of manufacture and potentially increasing biological half-life effectively addressing these particular shortcomings for rhPDGF-AB clinical translation. Although results of this thesis have highlighted the potential for our novel mimetic peptides JC5 and JC5a to replace rhPDGF-AB as a potential therapy for heart failure, further investigations are required to progress clinical translation.

5.2.1 Pharmacokinetic and pharmacodynamic studies

A key aim of developing an alternative to rhPDGF-AB for post-MI treatment was a need to improve its pharmacokinetic properties. The work in this thesis develops novel peptides that maintained cardiac therapeutic effects of rhPDGF-AB with an additional mechanism for improved pharmacokinetics. However, further work is required to investigate this in detail. Such experiments include *in vitro* via plasma stability assays (207) and *in vivo* assays in an appropriate murine model (229) to determine the half-life of JC5 and JC5a in addition to gaining an understanding of how these peptides are metabolised. These experiments are essential in confirming long term safety for therapeutic use as a part of the clinical translation of rhPDGF based therapies post-MI.

5.2.2 Mechanisms of action of novel peptides

Adding to our understanding of its safety for clinical use is greater understanding of the receptor signalling activity of JC5 and JC5a. In 'Research Chapter 2: Development of Novel Platelet Derived Growth Factor-AB Mimetics', we were able to confirm that JC5 and JC5a activate receptors by auto-phosphorylation of MAPK/Erk. Beyond this our understanding of receptor signalling of these peptides is limited. The aims of this work are to better understand the receptor signalling activity of JC5 and JC5a, to determine the mechanism of improved cardiac function post-MI, and to assess the dose response relationship of JC5 and JC5a. Further experiments in this will include surface plasmon resonance, to determine the binding affinity of our peptides to the PDGFR (220, 221) and phosphoproteomics to identify off target receptor signalling occurring post treatment (222, 223). At the conclusion of these studies, we would have a greater understanding of the *in vivo* functions of our novel mimetic peptides JC5 and JC5a that are required to carry these forward to a more clinically relevant large animal model.

5.2.3 Other disease models to test novel peptides

We have previously shown that rhPDGF-AB has favourable effects on the cardiac ECM and the work in this thesis shows that JC5 and JC5a have similar effects. Further *in vivo* experiments to assess the effects of JC5 and JC5a in other chronic heart failure could be pursued to expand its clinical applications. The HFpEF model explored throughout 'Chapter 1: Murine model of heart failure with preserved ejection fraction (HFpEF)' lacked significant effects in the ECM that we believed were necessary to test a PDGF based therapeutic. As a result, other models may be pursued. Murine models that could be considered in this context would be transverse aortic constriction (TAC) (230) derived models of HFpEF or ischaemic injury with TAC to develop HFrEF (231). Although HFpEF was explored as a model of chronic heart failure in this thesis, our understanding of JC5 and JC5a in addition to our greater understanding of HFpEF could indicate that pursuing murine models of HFrEF is more appropriate for these novel therapeutics.

Our greater understanding of HFpEF in the context of this work was the significance of metabolic pathways in the development of this HFpEF phenotype. In our proteomics experiments we identified significant changes in metabolic processes in HFD+L-NAME treated mice whilst identifying no changes in ECM processes. All previous work on rhPDGF-AB as a therapeutic post-MI shows effects on the ECM, angiogenesis, and immune response with no obvious effects on metabolic processes (57, 58, 219). Given our hypothesis that this mechanism of action will be reflected in JC5 and JC5a, we believe it would have minimal or no effect in a metabolically driven model of HFpEF. In the event that mechanistic studies on JC5 and JC5a highlighted potential metabolic effects leading to improved cardiac function then this murine model of HFpEF could be reconsidered. A metabolic mechanism of JC5 and JC5a would align more effectively with significant metabolic processes driving the development of HFpEF in this model. However, our understanding of JC5 and JC5a developed throughout this thesis and our established knowledge regarding the mechanism and function of

rhPDGF (57, 138) makes this unlikely with future efforts towards models of chronic heart failure likely focusing on ischemic based models.

Overall, the future directions of this project will aim to progress these lead candidates forward in clinical translation. The aim of these is develop and enhance our understanding of the safety and mechanisms of JC5 and JC5a in addition to efficacy studies in a clinically relevant pre-clinical model. These experiments are essential to the clinical translation and commercialisation of these peptides and would be a significant contribution towards eventual clinical trials and applications of these peptides.

5.3 CONCLUSION

Previous work has established the very promising effects of rhPDGF-AB as a novel therapeutic post-MI in improving cardiac function through modulation of the cardiac scar, angiogenesis, and immune response. Despite its impressive therapeutic effects, rhPDGF-AB is limited in clinical translation due to its inefficient and labour-intensive synthesis limiting scalability, and its poor pharmacokinetic properties limiting its clinical applications. In this thesis we have undergone lead optimisation utilising the loop III region of the PDGF B chain to develop an alternative therapeutic peptide that successfully mimics the biological effects of rhPDGF-AB *in vitro* and *in vivo* in a murine model of acute MI. Novel peptides JC5 and JC5a demonstrated comparable effects to rhPDGF-AB across *in vitro* assays of migration, collagen contraction, receptor activation, and angiogenesis. Furthermore, these peptides significantly improved cardiac function in a mouse model of myocardial infarction, aligning with the effects of rhPDGF-AB previously reported (57, 58, 138). The results presented here highlight the promising nature of synthetic novel mimetic peptides JC5 and JC5a as alternatives to rhPDGF-AB providing us with clinically viable and commercially attractive novel therapies for cardiac dysfunction after myocardial infarction.

REFERENCE LIST

1. Taylor CJ, Ordonez-Mena JM, Roalfe AK, Lay-Flurrie S, Jones NR, Marshall T, et al. Trends in survival after a diagnosis of heart failure in the United Kingdom 2000-2017: population based cohort study. BMJ. 2019;364:l223.
2. Mensah GA, Wei GS, Sorlie PD, Fine LJ, Rosenberg Y, Kaufmann PG, et al. Decline in Cardiovascular Mortality: Possible Causes and Implications. Circ Res. 2017;120(2):366-80.
3. Brown JC, Gerhardt TE, Kwon E. Risk Factors for Coronary Artery Disease. Treasure Island (FL): StatPearls Publishing; 2023 23rd January 2023.
4. Boateng S, Sanborn T. Acute myocardial infarction. Dis Mon. 2013;59(3):83-96.
5. Hutchins G, Bulkley B. Infarct Expansion Versus Extension: Two Different Complications of Acute Myocardial Infarction. Am J Cardiol. 1978;41(7):1127-32.
6. Reichardt IM, Robeson KZ, Regnier M, Davis J. Controlling cardiac fibrosis through fibroblast state space modulation. Cell Signal. 2021;79:109888.
7. Henderson NC, Rieder F, Wynn TA. Fibrosis: from mechanisms to medicines. Nature. 2020;587(7835):555-66.
8. Niino T, Shiono M, Yamamoto T, Inoue T, Hirose H, Saito A, et al. A Case of Left Ventricular Endomyocardial Fibrosis. Ann Thorac Cardiovasc Surg. 2002;8(3):173-6.
9. Canbay A, Feldstein A, Baskin-Bey E, Bronk SF, Gores GJ. The caspase inhibitor IDN-6556 attenuates hepatic injury and fibrosis in the bile duct ligated mouse. J Pharmacol Exp Ther. 2004;308(3):1191-6.
10. Glaser S, Obst A, Koch B, Henkel B, Grieger A, Felix SB, et al. Pulmonary hypertension in patients with idiopathic pulmonary fibrosis - the predictive value of exercise capacity and gas exchange efficiency. PLoS One. 2013;8(6):e65643.
11. Galati G, Leone O, Pasquale F, Olivotto I, Biagini E, Grigioni F, et al. Histological and Histometric Characterization of Myocardial Fibrosis in End-Stage Hypertrophic Cardiomyopathy: A Clinical-Pathological Study of 30 Explanted Hearts. Circ Heart Fail. 2016;9(9).
12. Sweeney M, Corden B, Cook SA. Targeting cardiac fibrosis in heart failure with preserved ejection fraction: mirage or miracle? EMBO Mol Med. 2020;12(10):e10865.
13. Bashey RI, Jimenez SA. Collagen in Heart Valves. Collagen 11988. p. 257-74.
14. Weber K, Janicki J, Shroff S, Pick R, Chen R, Bashey R. Collagen Remodeling of the PressureOverloaded, Hypertrophied Nonhuman Primate Myocardium. Circ Res. 1988;62:757-65.
15. Medugorac I, Jacob R. Characterisation of left ventricular collagen in the rat. Cardiovasc Res. 1983;17(1):15–21.
16. Szardien S, Nef HM, Voss S, Troidl C, Liebetrau C, Hoffmann J, et al. Regression of cardiac hypertrophy by granulocyte colony-stimulating factor-stimulated interleukin-1beta synthesis. Eur Heart J. 2012;33(5):595-605.
17. Walther T, Schubert A, Falk V, Binner C, Kanev A, Bleiziffer S, et al. Regression of Left Ventricular Hypertrophy After Surgical Therapy for Aortic Stenosis Is Associated With Changes in Extracellular Matrix Gene Expression. Circulation 2001;104.
18. Murphy SP, Ibrahim NE, Januzzi JL, Jr. Heart Failure With Reduced Ejection Fraction: A Review. JAMA. 2020;324(5):488-504.
19. Shah SJ, Kitzman DW, Borlaug BA, van Heerebeek L, Zile MR, Kass DA, et al. Phenotype-Specific Treatment of Heart Failure With Preserved Ejection Fraction: A Multiorgan Roadmap. Circulation. 2016;134(1):73-90.

20. Naing P, Forrester D, Kangaharan N, Muthumala A, Mon Myint S, Playford D. Heart failure with preserved ejection fraction: A growing global epidemic. Aus J Gen Prac. 2019;48(7).
21. Shah KS, Xu H, Matsouaka RA, Bhatt DL, Heidenreich PA, Hernandez AF, et al. Heart Failure With Preserved, Borderline, and Reduced Ejection Fraction: 5-Year Outcomes. J Am Coll Cardiol. 2017;70(20):2476-86.
22. Kasner M, Westermann D, Lopez B, Gaub R, Escher F, Kuhl U, et al. Diastolic tissue Doppler indexes correlate with the degree of collagen expression and cross-linking in heart failure and normal ejection fraction. J Am Coll Cardiol. 2011;57(8):977-85.
23. Streng KW, Nauta JF, Hillege HL, Anker SD, Cleland JG, Dickstein K, et al. Non-cardiac comorbidities in heart failure with reduced, mid-range and preserved ejection fraction. Int J Cardiol. 2018;271:132-9.
24. Zile MR, Gottdiener JS, Hetzel SJ, McMurray JJ, Komajda M, McKelvie R, et al. Prevalence and significance of alterations in cardiac structure and function in patients with heart failure and a preserved ejection fraction. Circulation. 2011;124(23):2491-501.
25. Morrissey C. Echo for diastology. Ann Card Anaesth. 2016;19(Supplement):S12-S8.
26. Fletcher P. Beta Blockers in Heart Failure. Aus Presc 2000;23(6):120-3.
27. SOLVD Investigators; Yusuf S PB, Davis CE, Hood WB, Cohn JN. Effect of enalapril on survival in patients with reduced left ventricular ejection fractions and congestive heart failure. N Engl J Med. 1991;325(5):293-302.
28. Dunlay SM, Roger VL, Redfield MM. Epidemiology of heart failure with preserved ejection fraction. Nat Rev Cardiol. 2017;14(10):591-602.
29. Anker SD, Butler J, Filippatos G, Ferreira JP, Bocchi E, Bohm M, et al. Empagliflozin in Heart Failure with a Preserved Ejection Fraction. N Engl J Med. 2021;385(16):1451-61.
30. Regan J, Mauro A, Carbone S, Marchetti C, Gill R, Mezzaroma E, et al. A mouse model of heart failure with preserved ejection fraction due to chronic infusion of a low subpressor dose of angiotensin II. . Am J Physiol Heart Circ Physiol. 2015;309(5).
31. Han YS, Arteaga GM, Sharain K, Sieck GC, Brozovich FV. Rat Model of Heart Failure With Preserved Ejection Fraction: Changes in Contractile Proteins Regulating Ca(2+) Cycling and Vascular Reactivity. Circulation. 2021;144(16):1355-8.
32. Briand F, Maupoint J, Brousseau E, Breyner N, Bouchet M, Costard C, et al. Elafibranor improves diet-induced nonalcoholic steatohepatitis associated with heart failure with preserved ejection fraction in Golden Syrian hamsters. Metabolism. 2021;117:154707.
33. Beznak M. Changes in heart weight and blood pressure following aortic constriction in rats. Can J Biochem. 1955;33:995-1002.
34. Murase T, Hattori T, Ohtake M, Abe M, Amakusa Y, Takatsu M, et al. Cardiac remodeling and diastolic dysfunction in DahlS.Z-Lepr(fa)/Lepr(fa) rats: a new animal model of metabolic syndrome. Hypertens Res. 2012;35(2):186-93.
35. Asrar ul Haq M, Wong C, Mutha V, Anavekar N, Lim K, Barlis P, et al. Therapeutic interventions for heart failure with preserved ejection fraction: A summary of current evidence. World J Cardiol. 2014;6(2):67-76.
36. Klotz S, Hay I, Zhang G, Maurer M, Wang J, Burkhoff D. Development of heart failure in chronic hypertensive Dahl rats: focus on heart failure with preserved ejection fraction. Hypertension. 2006;47(5):901-11.

37. Rame J, Ramilo M, Spencer N, Blewett C, Mehta S, Dries D, et al. Development of a Depressed Left Ventricular Ejection Fraction in Patients With Left Ventricular Hypertrophy and a Normal Ejection Fraction. Am J Cardiol 2004;93.
38. Kitzman DW, Brubaker P, Morgan T, Haykowsky M, Hundley G, Kraus WE, et al. Effect of Caloric Restriction or Aerobic Exercise Training on Peak Oxygen Consumption and Quality of Life in Obese Older Patients With Heart Failure With Preserved Ejection Fraction: A Randomized Clinical Trial. JAMA. 2016;315(1):36-46.
39. Haass M, Kitzman DW, Anand IS, Miller A, Zile MR, Massie BM, et al. Body mass index and adverse cardiovascular outcomes in heart failure patients with preserved ejection fraction: results from the Irbesartan in Heart Failure with Preserved Ejection Fraction (I-PRESERVE) trial. Circ Heart Fail. 2011;4(3):324-31.
40. van Bilsen M, Daniels A, Brouwers O, Janssen BJ, Derks WJ, Brouns AE, et al. Hypertension is a conditional factor for the development of cardiac hypertrophy in type 2 diabetic mice. PLoS One. 2014;9(1):e85078.
41. Grobe JL, Mecca AP, Mao H, Katovich MJ. Chronic angiotensin-(1-7) prevents cardiac fibrosis in DOCA-salt model of hypertension. Am J Physiol Heart Circ Physiol. 2006;290(6):H2417-23.
42. Young M, Fullerton M, Dilley R, Funder J. Mineralocorticoids, Hypertension, and Cardiac Fibrosis. J Clin Invest. 1994;93(6):2578–83.
43. Mohammed SF, Ohtani T, Korinek J, Lam CS, Larsen K, Simari RD, et al. Mineralocorticoid accelerates transition to heart failure with preserved ejection fraction via "nongenomic effects". Circulation. 2010;122(4):370-8.
44. Allan A, Fenning A, Levick S, Hoey A, Brown L. Reversal of cardiac dysfunction by selective ET-A receptor antagonism. Br J Pharmacol. 2005;146(6):846-53.
45. Goto K, Schauer A, Augstein A, Methawasin M, Granzier H, Halle M, et al. Muscular changes in animal models of heart failure with preserved ejection fraction: what comes closest to the patient? ESC Heart Fail. 2021;8(1):139-50.
46. Slater RE, Strom JG, Methawasin M, Liss M, Gotthardt M, Sweitzer N, et al. Metformin improves diastolic function in an HFpEF-like mouse model by increasing titin compliance. J Gen Physiol. 2019;151(1):42-52.
47. Weldon S, Winquist R, Madwed J. Differential Effects of L-NAME on Blood Pressure and Heart Rate Responses to Acetylc. J Pharm Exp Ther. 1995;272:126-33.
48. Pechánová O, Bernátová I, Pelouch V, Babál P. L-NAME-induced protein remodeling and fibrosis in the rat heart. Physiol Res 1999;48:353-62.
49. Coelho-Filho OR, Shah RV, Neilan TG, Mitchell R, Moreno H, Jr., Kwong R, et al. Cardiac magnetic resonance assessment of interstitial myocardial fibrosis and cardiomyocyte hypertrophy in hypertensive mice treated with spironolactone. J Am Heart Assoc. 2014;3(3):e000790.
50. Schiattarella GG, Altamirano F, Tong D, French KM, Villalobos E, Kim SY, et al. Nitrosative stress drives heart failure with preserved ejection fraction. Nature. 2019;568(7752):351-6.
51. Cao Y, Vergnes L, Wang YC, Pan C, Chella Krishnan K, Moore TM, et al. Sex differences in heart mitochondria regulate diastolic dysfunction. Nat Commun. 2022;13(1):3850.
52. Buddeke J, Valstar GB, van Dis I, Visseren FLJ, Rutten FH, den Ruijter HM, et al. Mortality after hospital admission for heart failure: improvement over time, equally strong in women as in men. BMC Public Health. 2020;20(1):36.

53. Steppich B, Groha P, Ibrahim T, Schunkert H, Laugwitz KL, Hadamitzky M, et al. Effect of Erythropoietin in patients with acute myocardial infarction: five-year results of the REVIVAL-3 trial. BMC Cardiovasc Disord. 2017;17(1):38.
54. Liu S, Li K, Florencio LW, Tang L, Heallen TR, Leach JP, et al. Gene therapy knockdown ofHippo signaling induces cardiomyocyte renewal in pigs after myocardial infarction. Sci Transl Med. 2021;13.
55. Chong JJ, Yang X, Don CW, Minami E, Liu YW, Weyers JJ, et al. Human embryonic-stem-cell-derived cardiomyocytes regenerate non-human primate hearts. Nature. 2014;510(7504):273-7.
56. Selvakumar D, Clayton ZE, Chong JJH. Robust Cardiac Regeneration: Fulfilling the Promise of Cardiac Cell Therapy. Clin Ther. 2020;42(10):1857-79.
57. Thavapalachandran S, Grieve S, Hume R, Le T, Raguram K, Hudson J, et al. Platelet-derived growth factor-AB improves scar mechanics and vascularity after myocardial infarction. Sci Transl Med. 2020;12.
58. Asli NS, Xaymardan M, Patrick R, Farbehi N, Cornwell J, Forte E, et al. PDGFRα signaling in cardiac fibroblasts modulates quiescence, metabolism and self-renewal, and promotes anatomical and functional repair. BioRxiv. 2019.
59. Pal US, Mohammad S, Singh RK, Das S, Singh N, Singh M. Platelet-rich growth factor in oral and maxillofacial surgery. Natl J Maxillofac Surg. 2012;3(2):118-23.
60. Solchaga LA, Hee CK, Roach S, Snel LB. Safety of recombinant human platelet-derived growth factor-BB in Augment((R)) Bone Graft. J Tissue Eng. 2012;3(1):2041731412442668.
61. Nevins M, Kao RT, McGuire MK, McClain PK, Hinrichs JE, McAllister BS, et al. Platelet-derived growth factor promotes periodontal regeneration in localized osseous defects: 36-month extension results from a randomized, controlled, double-masked clinical trial. J Periodontol. 2013;84(4):456-64.
62. Amado LC, Saliaris AP, Schuleri KH, St John M, Xie JS, Cattaneo S, et al. Cardiac repair with intramyocardial injection of allogeneic mesenchymal stem cells after myocardial infarction. Proc Natl Acad Sci U S A. 2005;102(32):11474-9.
63. Laflamme MA, Chen KY, Naumova AV, Muskheli V, Fugate JA, Dupras SK, et al. Cardiomyocytes derived from human embryonic stem cells in pro-survival factors enhance function of infarcted rat hearts. Nat Biotechnol. 2007;25(9):1015-24.
64. Menasche P, Vanneaux V, Hagege A, Bel A, Cholley B, Cacciapuoti I, et al. Human embryonic stem cell-derived cardiac progenitors for severe heart failure treatment: first clinical case report. Eur Heart J. 2015;36(30):2011-7.
65. Shiba Y, Gomibuchi T, Seto T, Wada Y, Ichimura H, Tanaka Y, et al. Allogeneic transplantation of iPS cell-derived cardiomyocytes regenerates primate hearts. Nature. 2016;538(7625):388-91.
66. Oyamada Y, Komatsu K, Kimura H, Mori M, Oyamada M. Differential Regulation of Gap Junction Protein (Connexin) Genes during Cardiomyocytic Differentiation of Mouse Embryonic Stem Cellsin Vitro. Exp Cell Res. 1996;229(2):318–26.
67. Skerjanc IS. Cardiac and Skeletal Muscle Development in P19 Embryonal Carcinoma Cells. Trends Cardiovasc Med. 1999;9(5).
68. Wobus AM, Wallukat G, Hescheler J. Pluripotent mouse embryonic stem cells are able to differentiate into cardiomyocytes expressing chronotropic responses to adrenergic and cholinergic agents and Ca2+ channel blockers. Differentiation. 1991;48(3):173-82.
69. van Laake LW, Passier R, Doevendans PA, Mummery CL. Human embryonic stem cell-derived cardiomyocytes and cardiac repair in rodents. Circ Res. 2008;102(9):1008-10.

70. Liu YW, Chen B, Yang X, Fugate JA, Kalucki FA, Futakuchi-Tsuchida A, et al. Human embryonic stem cell-derived cardiomyocytes restore function in infarcted hearts of non-human primates. Nat Biotechnol. 2018;36(7):597-605.
71. Zhang M, Methot D, Poppa V, Fujio Y, Walsh K, Murry C. Cardiomyocyte grafting for cardiac repair: graft cell death and anti-death strategies. J Mol Cell Cardiol. 2001;33(5):907-21.
72. Selvakumar D, Clayton ZE, Prowse A, Dingwall S, George J, Shah H, et al. Cellular Heterogeneity of Pluripotent Stem Cell Derived Cardiomyocyte Grafts is Mechanistically Linked to Treatable Arrhythmias. BioRxiv. 2022.
73. Marchiano S, Nakamura K, Reinecke H, Neidig L, Lai M, Kadota S, et al. Gene editing to prevent ventricular arrhythmias associated with cardiomyocyte cell therapy. Cell Stem Cell. 2023;30(4):396–414.
74. Carvalho T. Stem cell-derived heart cells injected into first patient. Nat Med. 2023;29(5):1030-1.
75. McDermott DF, Cheng SC, Signoretti S, Margolin KA, Clark JI, Sosman JA, et al. The high-dose aldesleukin "select" trial: a trial to prospectively validate predictive models of response to treatment in patients with metastatic renal cell carcinoma. Clin Cancer Res. 2015;21(3):561-8.
76. Powell JS, Pasi KJ, Ragni MV, Ozelo MC, Valentino LA, Mahlangu JN, et al. Phase 3 study of recombinant factor IX Fc fusion protein in hemophilia B. N Engl J Med. 2013;369(24):2313-23.
77. Maury S, Chevret S, Thomas X, Heim D, Leguay T, Huguet F, et al. Rituximab in B-Lineage Adult Acute Lymphoblastic Leukemia. N Engl J Med. 2016;375(11):1044-53.
78. Clark AJ, Wiles PG, Leiper JM, Knight G, Adeniyl-Jones RO, Watkins PJ, et al. A double-blind crossover trial comparing human insulin (recombinant DNA) with animal insulins in the treatment of previously insulin-treated diabetic patients. Diabetes Care 1982:129-34.
79. Ebrahimi SB, Samanta D. Engineering protein-based therapeutics through structural and chemical design. Nat Commun. 2023;14(1):2411.
80. Simons M, Annex BH, Laham RJ, Kleiman N, Henry T, Dauerman H, et al. Pharmacological treatment of coronary artery disease with recombinant fibroblast growth factor-2: double-blind, randomized, controlled clinical trial. Circulation. 2002;105(7):788-93.
81. Osterziel KJ, Strohm O, Schuler J, Friedrich M, Hanlein D, Willenbrock R, et al. Randomised, double-blind, placebo-controlled trial of human recombinant growth hormone in patients with chronic heart failure due to dilated cardiomyopathy. Lancet. 1998;351(9111):1233-7.
82. Isgaard J, Bergh C, Caidahl K, Lomsky M, Hjalmarson A, Bengtsson B. A placebo-controlled study of growth hormone in patients with congestive heart failure. Euro Heart J. 1998;19(11):1704-11.
83. Grines CL, Watkins MW, Mahmarian JJ, Iskandrian AE, Rade JJ, Marrott P, et al. A randomized, double-blind, placebo-controlled trial of Ad5FGF-4 gene therapy and its effect on myocardial perfusion in patients with stable angina. J Am Coll Cardiol. 2003;42(8):1339-47.
84. Stewart DJ, Hilton JD, Arnold JM, Gregoire J, Rivard A, Archer SL, et al. Angiogenic gene therapy in patients with nonrevascularizable ischemic heart disease: a phase 2 randomized, controlled trial of AdVEGF(121) (AdVEGF121) versus maximum medical treatment. Gene Ther. 2006;13(21):1503-11.
85. Baehr A, Umansky KB, Bassat E, Jurisch V, Klett K, Bozoglu T, et al. Agrin Promotes Coordinated Therapeutic Processes Leading to Improved Cardiac Repair in Pigs. Circulation. 2020;142(9):868-81.
86. Rutherford RB. Platelet Factors Stimulate Fibroblasts and Smooth Muscle Cells Quiescent in Plasma Serum to Proliferate J Cell Bio. 1976;69:196-203.

87. Ross R, Glomset J, Kariya B, Harker L. A Platelet-Dependent, Serum Factor That Stimulates the Proliferation of Arterial Smooth Muscle Cells In Vitro. Proc Natl Acad Sci U S A. 1974;71(4):1207-10.
88. Battegay EJ, Rupp J, Iruela-Arispe L, Sage EH, Pech M. PDGF-BB Modulates Endothelial Proliferation and Angiogenesis In Vitro via PDGF B-Receptors. J Cell Bio. 1994;125(4):917-28.
89. Seifert RA, Hart CE, Phillips PE, Forstrom JW, Ross R, Murray MJ, et al. Two Different Subunits Associate to Create Isoform-Specific Platelet-derived Growth Factor Receptors. J Bio Chem. 1989;264(15):8771-8.
90. Li X, Pontén A, Aase K, Karlsson L, Abramsson A, Uutela M, et al. PDGF-C is a new protease-activated ligand for the PDGF α-receptor. Nat Cell Bio. 2000;2:302-9.
91. LaRochelle W, Jeffers M, McDonald W, Chillakuru R, Giese N, Lokker N, et al. PDGF-D, a new protease-activated growth factor. Nat Cell Bio 2001;3:517-21.
92. He C, Medley SC, Hu T, Hinsdale ME, Lupu F, Virmani R, et al. PDGFRbeta signalling regulates local inflammation and synergizes with hypercholesterolaemia to promote atherosclerosis. Nat Commun. 2015;6:7770.
93. Chen YT, Chang FC, Wu CF, Chou YH, Hsu HL, Chiang WC, et al. Platelet-derived growth factor receptor signaling activates pericyte-myofibroblast transition in obstructive and post-ischemic kidney fibrosis. Kidney Int. 2011;80(11):1170-81.
94. Pierce G, Mustoe T, Senior R, Reed J, Griffin G, Thomason A, et al. In vivo incisional wound healing augmented by platelet-derived growth factor and recombinant c-sis gene homodimeric proteins. J Exp Med. 1988;167(3):974–87.
95. Pinto M, Dye W, Jacobsen B, Horwitz K. Malignant stroma increases luminal breast cancer cell proliferation and angiogenesis through platelet-derived growth factor signaling. BMC Cancer. 2014;14(735).
96. Forsberg K, Valyi-Nagy I, Heldin C, Herlyn M, Westermark B. Platelet-derived growth factor (PDGF) in oncogenesis: Development of a vascular connective tissue stroma in xenotransplanted human melanoma producing PDGF-BB. Proc Natl Acad Sci U S A. 1993;90:393-7.
97. Kimura I, Tsuneki H, Okabe M, Ogasawara M. Platelet-Derived Growth Factor Blocks the Cell-Cycle Transition from the Go to G1 Phase in Subcultured Angiogenic Endothelial Cells in Rat Thoracic Aorta. Jpn J Pharmacol. 1997;74:303-11.
98. Ferns GA, Raines EW, Sprugel KH, A.S. M, Reidy MA, Ross R. Inhibition of neointimal smooth muscle accumulation after angioplasty by an antibody to PDGF. Science 1991;253.
99. Deuel T, Senior R, Huang J, Griffin G. Chemotaxis of monocytes and neutrophils to platelet-derived growth factor. J Clin Invest. 1982;69(4):1046-9.
100. Senior R, Griffin G, Huang J, Walz D, Deuel T. Chemotactic activity of platelet alpha granule proteins for fibroblasts. J Cell Bio. 1983;96(2):382-5.
101. Seppä H, Grotendorst G, Seppä S, Schiffmann E, Martin G. Platelet-derived Growth Factor Is Chemotactic for Fibroblasts. J Cell Bio. 1982;92(2):584-8.
102. Grotendorst G, Seppä H, Kleinman H, Martin G. Attachment of smooth muscle cells to collagen and their migration toward platelet-derived growth factor. Proc Natl Acad Sci U S A. 1981;78(6):3669-72.
103. Diliberto PA, Gordon GW, Yu CL, Earp HS, Herman B. Platelet-derived growth factor (PDGF) alpha receptor activation modulates the calcium mobilizing activity of the PDGF beta receptor in Balb/c3T3 fibroblasts. J Bio Chem. 1992;267(17):11888-97.
104. Samson SC, Khan AM, Mendoza MC. ERK signaling for cell migration and invasion. Front Mol Biosci. 2022;9:998475.

105. Heidaran MA, Pierce JH, Yu JC, Lombardi D, Artrip JE, Fleming TP, et al. Role of alpha beta receptor heterodimer formation in beta platelet-derived growth factor (PDGF) receptor activation by PDGF-AB. J Bio Chem. 1991;266(30):20232-7.
106. Evrova O, Buschmann J. In vitro and in vivo effects of PDGF-BB delivery strategies on tendon healing: a review. Eur Cell Mater. 2017;34:15-39.
107. Chen PH, Chen X, He X. Platelet-derived growth factors and their receptors: structural and functional perspectives. Biochim Biophys Acta. 2013;1834(10):2176-86.
108. Werner SG, R. Regulation of wound healing by growth factors and cytokines. Physio Rev. 2003;83(3):835-70.
109. Centrella M, McCarthy TL, Kusmik WF, Canalis E. Relative binding and biochemical effects of heterodimeric and homodimeric isoforms of platelet-derived growth factor in osteoblast-enriched cultures from fetal rat bone. J Cell Physiol. 1991;147(3):420-6.
110. Donovan J, Shiwen X, Norman J, Abraham D. Platelet-derived growth factor alpha and beta receptors have overlapping functional activities towards fibroblasts. Fibrogenesis Tissue Repair. 2013;6(10).
111. Boström H, Willetts K, Pekny M, Levéen P, Lindahl P, Hedstrand H, et al. PDGF-A signaling is a critical event in lung alveolar myofibroblast development and alveogenesis. Cell 1996;85(6):863-73.
112. Brennan J, Tilmann C, Capel B. Pdgfr-alpha mediates testis cord organization and fetal Leydig cell development in the XY gonad. Genes Dev. 2003;17(6):800-10.
113. Soriano P. The PDGF alpha receptor is required for neural crest cell development and for normal patterning of the somites. Development. 1997;124(14):2691-700.
114. Tallquist M, Weismann K, Hellström M, Soriano P. Early myotome specification regulates PDGFA expression and axial skeleton development. Development. 2000;127(23):5059-70.
115. Kaminski W, Lindahl P, Lin N, Broudy V, Crosby J, Hellström M, et al. Basis of hematopoietic defects in platelet-derived growth factor (PDGF)-B and PDGF beta-receptor null mice. Blood. 2001;97(7):1990-8.
116. Wang P, Song L, Ge H, Jin P, Jiang Y, Hu W, et al. Crenolanib, a PDGFR inhibitor, suppresses lung cancer cell proliferation and inhibits tumor growth in vivo. Onco Targets Ther. 2014;7:1761-8.
117. Andrae J, Gallini R, Betsholtz C. Role of platelet-derived growth factors in physiology and medicine. Genes Dev. 2008;22(10):1276-312.
118. Oefner C, D'Arcy A, Winkler FK, Eggimann B, Hosang M. Crystal structure of human platelet-derived growth factor BB. EMBO J. 1992;11(11):3921-6.
119. Fredriksson L, Li H, Eriksson U. The PDGF family: four gene products form five dimeric isoforms. Cytokine Growth Factor Rev. 2004;15(4):197-204.
120. Shim AH, Liu H, Focia PJ, Chen X, Lin PC, He X. Structures of a platelet-derived growth factor/propeptide complex and a platelet-derived growth factor/receptor complex. Proc Natl Acad Sci U S A. 2010;107(25):11307-12.
121. Schilling D, Reid IJ, Hujer A, Morgan D, Demoll E, Bummer P, et al. Loop III region of platelet-derived growth factor (PDGF) B-chain mediates binding to PDGF receptors and heparin. J Biochem. 1998;333:637-44.
122. Kreysing J, Ostman A, van de Poll M, Bäckström G, Heldin C. Identification of three amino acid residues in the B-chain of platelet-derived growth factor with different importance for binding to PDGF and -receptors. FEBS Letters. 1996;385:181-4.
123. Fenstermaker RA, Poptic E, Bonfield TL, Knauss TC, Corsillo L, Piskurich JF, et al. A cationic region of the platelet-derived growth factor (PDGF) A-chain (Arg159-Lys160-Lys161) is required for

receptor binding and mitogenic activity of the PDGF-AA homodimer. J Bio Chem. 1993;268(14):10482-9.
124. Ostman A, Andersson M, Hellman U, Heldin CH. Identification of three amino acids in the platelet-derived growth factor (PDGF) B-chain that are important for binding to the PDGF beta-receptor. J Bio Chem. 1991;266(16):10073-7.
125. Clements JM, Bawden LJ, Bloxidge RE, Catlin G, Cook AL, Craig S, et al. Two PDGF-B chain residues, arginine 27 and isoleucine 30, mediate receptor binding and activation. EMBO 1991;10(13).
126. Jaumann M, Tatje D, Hoppe J. Identification of individual amino acids in platelet-derived growth factor that contribute to the specificity towards the B-type receptor FEBS Lett. 1992;302: 265-8.
127. Robson M, Phillips L, Thomason A, Robson L, Pierce G. Platelet-derived growth factor BB for the treatment of chronic pressure ulcers. Lancet 1992;339(8784):23-5.
128. Bohm AM, Dirckx N, Tower RJ, Peredo N, Vanuytven S, Theunis K, et al. Activation of Skeletal Stem and Progenitor Cells for Bone Regeneration Is Driven by PDGFRbeta Signaling. Dev Cell. 2019;51(2):236-54 e12.
129. Li F, Yu F, Xu X, Li C, Huang D, Zhou X, et al. Evaluation of Recombinant Human FGF-2 and PDGF-BB in Periodontal Regeneration: A Systematic Review and Meta-Analysis. Sci Rep. 2017;7(1):65.
130. Fang R, Galiano R. A review of becaplermin gel in the treatment of diabetic neuropathic foot ulcers. Biologics. 2008;2(1).
131. JAMA. Drugs and Cancer Risk. JAMA. 2008;300(4):386.
132. Ziyadeh N, Fife, Daniel Walker, Alexander M. Wilkinson, Gregg S. Seeger, John D. A Matched Cohort Study of the Risk of Cancer in Users of Becaplermin. Adv Skin Wound Care. 2011;24(1).
133. Lin X, Takahashi K, Liu Y, Derrien A, Zamora PO. A synthetic, bioactive PDGF mimetic with binding to both alpha-PDGF and beta-PDGF receptors. Growth Factors. 2007;25(2):87-93.
134. Zamora PO, Pena LA, Lin X, inventors; BioSurface Engineering Technologies, Inc., Rockville, MD (US) assignee. Dual chain synthetic heparin-binding growth factor analogs. United States2012 24 April 2012.
135. Jehanli A, Patel G, Olabiran Y, Brennand DM, Kakkar VV, inventors; Trigen Limited, London (GB) assignee. Platelet-derived growth factor analogues. United States2002 26 February 2002.
136. Pinto AR, Ilinykh A, Ivey MJ, Kuwabara JT, D'Antoni ML, Debuque R, et al. Revisiting Cardiac Cellular Composition. Circ Res. 2016;118(3):400-9.
137. Chong JJ, Chandrakanthan V, Xaymardan M, Asli NS, Li J, Ahmed I, et al. Adult cardiac-resident MSC-like stem cells with a proepicardial origin. Cell Stem Cell. 2011;9(6):527-40.
138. Hume RD, Deshmukh T, Doan T, Shim WJ, Kanagalingam S, Tallapragada V, et al. PDGF-AB Reduces Myofibroblast Differentiation Without Increasing Proliferation After Myocardial Infarction. JACC: Basic to Translational Science. 2023.
139. Bowen-Pope DF, Malpass TW, Foster DM, Ross R. Platelet-derived growth factor in vivo: levels, activity, and rate of clearance. Blood. 1984;64(2):458-69.
140. Gunaydin H, Altman MD, Ellis JM, Fuller P, Johnson SA, Lahue B, et al. Strategy for Extending Half-life in Drug Design and Its Significance. ACS Med Chem Lett. 2018;9(6):528-33.
141. Atterwill CK, Wing MG. In vitro preclinical lead optimisation technologies (PLOTs) in pharmaceutical development. Toxicol Lett. 2002;127:143-51.
142. Ballard P, Bradbury RH, Harris CS, Hennequin LF, Hickinson M, Kettle JG, et al. Inhibitors of epidermal growth factor receptor tyrosine kinase: optimisation of potency and in vivo pharmacokinetics. Bioorg Med Chem Lett. 2006;16(18):4908-12.

143. Currie GM. Pharmacology, Part 1: Introduction to Pharmacology and Pharmacodynamics. J Nucl Med Technol. 2018;46(2):81-6.
144. David E, Tramontin T, Zemmel R. Pharmaceutical R&D: the road to positive returns. Nat Rev Drug Discov. 2009;8(8):609-10.
145. Xu X, Vugmeyster Y. Challenges and opportunities in absorption, distribution, metabolism, and excretion studies of therapeutic biologics. AAPS J. 2012;14(4):781-91.
146. Bhawani S, Husaini A, Ahmad F, Asaruddin M. Polymer Based Protein Therapeutics. Curr Protein Pept Sci. 2018;19(10):972-82.
147. Chaudhury C, Brooks C, Carter D, Robinson J, Anderson C. Albumin Binding to FcRn: Distinct from the FcRn-IgG Interaction. Biochemistry. 2006;45:4983-90.
148. Zorzi A, Middendorp SJ, Wilbs J, Deyle K, Heinis C. Acylated heptapeptide binds albumin with high affinity and application as tag furnishes long-acting peptides. Nat Commun. 2017;8:16092.
149. Matthews JE, Stewart MW, De Boever EH, Dobbins RL, Hodge RJ, Walker SE, et al. Pharmacodynamics, pharmacokinetics, safety, and tolerability of albiglutide, a long-acting glucagon-like peptide-1 mimetic, in patients with type 2 diabetes. J Clin Endocrinol Metab. 2008;93(12):4810-7.
150. Strohl WR. Fusion Proteins for Half-Life Extension of Biologics as a Strategy to Make Biobetters. BioDrugs. 2015;29(4):215-39.
151. de Bruyn M, Bremer E, Helfrich W. Antibody-based fusion proteins to target death receptors in cancer. Cancer Lett. 2013;332(2):175-83.
152. Zollner S, Schuermann D, Raquet E, Mueller-Cohrs J, Weimer T, Pragst I, et al. Pharmacological characteristics of a novel, recombinant fusion protein linking coagulation factor VIIa with albumin (rVIIa-FP). J Thromb Haemost. 2014;12(2):220-8.
153. Shapiro AD, Ragni MV, Valentino LA, Key NS, Josephson NC, Powell JS, et al. Recombinant factor IX-Fc fusion protein (rFIXFc) demonstrates safety and prolonged activity in a phase 1/2a study in hemophilia B patients. Blood. 2012;119(3):666-72.
154. Santagostino E, Negrier C, Klamroth R, Tiede A, Pabinger-Fasching I, Voigt C, et al. Safety and pharmacokinetics of a novel recombinant fusion protein linking coagulation factor IX with albumin (rIX-FP) in hemophilia B patients. Blood. 2012;120(12):2405-11.
155. Halpern W, Riccobene T, Agostini H, Baker K, Stolow D, Gu M, et al. Albugranin, a recombinant human granulocyte colony stimulating factor (G-CSF) genetically fused to recombinant human albumin induces prolonged myelopoietic effects in mice and monkeys. Pharm Res. 2002;19(11):1720-9.
156. Tzaban S, Massol RH, Yen E, Hamman W, Frank SR, Lapierre LA, et al. The recycling and transcytotic pathways for IgG transport by FcRn are distinct and display an inherent polarity. J Cell Biol. 2009;185(4):673-84.
157. Rath T, Baker K, Dumont JA, Peters RT, Jiang H, Qiao SW, et al. Fc-fusion proteins and FcRn: structural insights for longer-lasting and more effective therapeutics. Crit Rev Biotechnol. 2015;35(2):235-54.
158. Teitel J, Sholzberg M, Iorio A. Extended half-life factor VIII concentrates in adults with hemophilia A: Comparative pharmacokinetics of two products. Res Pract Thromb Haemost. 2021;5(2):349-55.
159. Driessler F, Miguelino MG, Pierce GF, Peters RT, Sommer JM. Evaluation of recombinant factor VIII Fc (Eloctate) activity by thromboelastometry in a multicenter phase 3 clinical trial and correlation with bleeding phenotype. Blood Coagul Fibrinolysis. 2017;28(7):540-50.

160. Dumont JA, Liu T, Low SC, Zhang X, Kamphaus G, Sakorafas P, et al. Prolonged activity of a recombinant factor VIII-Fc fusion protein in hemophilia A mice and dogs. Blood. 2012;119(13):3024-30.
161. Bjorkman S, Folkesson A, Jonsson S. Pharmacokinetics and dose requirements of factor VIII over the age range 3-74 years: a population analysis based on 50 patients with long-term prophylactic treatment for haemophilia A. Eur J Clin Pharmacol. 2009;65(10):989-98.
162. Press Release: Strong 2021 sales and business EPS growth enabling increased investment in R&D [press release]. Sanofi, 4 February 2022 2022.
163. Dixon F, Maurer P, Deichmiller M. Half-lives of homologous serum albumins in several species. Proc Soc Exp Biol Med. 1953;83:287-8.
164. Curry S, Mandelkow H, Brick P, Franks N. Crystal structure of human serum albumin complexed with fatty acid reveals an symmetric distribution of binding sites. Nat Struct Bio. 1998;5(9).
165. Bush MA, Matthews JE, De Boever EH, Dobbins RL, Hodge RJ, Walker SE, et al. Safety, tolerability, pharmacodynamics and pharmacokinetics of albiglutide, a long-acting glucagon-like peptide-1 mimetic, in healthy subjects. Diabetes Obes Metab. 2009;11(5):498-505.
166. Reusch J, Stewart MW, Perkins CM, Cirkel DT, Ye J, Perry CR, et al. Efficacy and safety of once-weekly glucagon-like peptide 1 receptor agonist albiglutide (HARMONY 1 trial): 52-week primary endpoint results from a randomized, double-blind, placebo-controlled trial in patients with type 2 diabetes mellitus not controlled on pioglitazone, with or without metformin. Diabetes Obes Metab. 2014;16(12):1257-64.
167. Pratley RE, Nauck MA, Barnett AH, Feinglos MN, Ovalle F, Harman-Boehm I, et al. Once-weekly albiglutide versus once-daily liraglutide in patients with type 2 diabetes inadequately controlled on oral drugs (HARMONY 7): a randomised, open-label, multicentre, non-inferiority phase 3 study. Lancet Diabetes Endocrinol. 2014;2(4):289-97.
168. Tarantino MD, Bussel JB, Blanchette VS, Despotovic J, Bennett C, Raj A, et al. Romiplostim in children with immune thrombocytopenia: a phase 3, randomised, double-blind, placebo-controlled study. Lancet. 2016;388(10039):45-54.
169. Kuter D, Rummel M, Boccia R, Macik B, Pabinger I, Selleslag D, et al. Romiplostim or standard of care in patients with immune thrombocytopenia. N Engl J Med. 2010;363(20):1889-99.
170. Wu B, Sun YN. Pharmacokinetics of Peptide-Fc fusion proteins. J Pharm Sci. 2014;103(1):53-64.
171. Ather S, Chan W, Bozkurt B, Aguilar D, Ramasubbu K, Zachariah AA, et al. Impact of noncardiac comorbidities on morbidity and mortality in a predominantly male population with heart failure and preserved versus reduced ejection fraction. J Am Coll Cardiol. 2012;59(11):998-1005.
172. Hamdani N, Franssen C, Lourenco A, Falcao-Pires I, Fontoura D, Leite S, et al. Myocardial titin hypophosphorylation importantly contributes to heart failure with preserved ejection fraction in a rat metabolic risk model. Circ Heart Fail. 2013;6(6):1239-49.
173. Ward AO, Janbandhu V, Chapman G, Dunwoodie SL, Harvey RP. An image analysis protocol using CellProfiler for automated quantification of post-ischemic cardiac parameters. STAR Protoc. 2022;3(1):101097.
174. Lorenz J. A practical guide to evaluating cardiovascular, renal, and pulmonary function in mice. Am J Physiol Regul Integr Comp Physiol. 2002;282(6):1565-82.
175. McMullen J, Shioi T, Zhang L, Tarnavski O, Sherwood M, Kang P, et al. Phosphoinositide 3-kinase(p110α) plays a critical role for the induction of physiological, but not pathological, cardiac hypertrophy. Proc Natl Acad Sci U S A. 2003:12355-60.

176. Zhang L, Chi J, Chen J, Jiang S, Wu D. Effects of swimming on the development of atherosclerosis in mice. Am J Transl Res. 2021;12(13):13759-67.
177. Deichl A, Wachter R, Edelmann F. Comorbidities in heart failure with preserved ejection fraction. Herz. 2022;47(4):301-7.
178. Cornuault L, Mora P, Rouault P, Foussard N, Chapouly C, Alzieu P, et al. Increased endothelium activation and leakage do not promote diastolic dysfunction in mice fed with a high fat diet and treated with L-NAME BioRxiv. 2023.
179. Cornuault L, Rouault P, Duplàa C, Couffinhal T, Renault M. Diastolic dysfunction in high fat diet + L-NAME treated mice is associated with endothelial dysfunction. Archives of Cardiovascular Diseases Supplements. 2021;13(2).
180. Mattson D. Comparison of arterial blood pressure in different strains of mice. Am J Hypertens 2001;14(5):405-8.
181. Wilde E AA, Thakore P, Baldissera L Jr, Alawi KM, Keeble J, Nandi M, Brain SD. Tail-Cuff Technique and Its Influence on Central Blood Pressure in the Mouse. J Am Heart Assoc. 2017;6(6).
182. Zhao X HD, Gao S, Hong C, Vatner DE, Vatner SF. Arterial Pressure Monitoring in Mice. Curr Protoc Mouse Biol. 2011(1):105-22.
183. Zhang S, Hulver M, McMillan R, Cline M, Gilbert E. The pivotal role of pyruvate dehydrogenase kinases in metabolic flexibility. Nutr Metab. 2014;11(1).
184. Zhao G, Jeoung NH, Burgess SC, Rosaaen-Stowe KA, Inagaki T, Latif S, et al. Overexpression of pyruvate dehydrogenase kinase 4 in heart perturbs metabolism and exacerbates calcineurin-induced cardiomyopathy. Am J Physiol Heart Circ Physiol. 2008;294(2):H936-43.
185. Newhardt MF, Batushansky A, Matsuzaki S, Young ZT, West M, Chin NC, et al. Enhancing cardiac glycolysis causes an increase in PDK4 content in response to short-term high-fat diet. J Biol Chem. 2019;294(45):16831-45.
186. Fatmi MK, Ren D, Fedorova J, Zoungrana LI, Wang H, Davitt K, et al. Cardiomyocyte Pdk4 response is associated with metabolic maladaptation in aging. Aging Cell. 2023;22(4):e13800.
187. Wang H, Sreenivasan U, Hu H, Saladino A, Polster BM, Lund LM, et al. Perilipin 5, a lipid droplet-associated protein, provides physical and metabolic linkage to mitochondria. J Lipid Res. 2011;52(12):2159-68.
188. Mason R, Watt M. Unraveling the roles of PLIN5: linking cell biology to physiology. . Trends Endocrinol Metab. 2015;26(3):144-52.
189. Zheng P, Xie Z, Yuan Y, Sui W, Wang C, Gao X, et al. Plin5 alleviates myocardial ischaemia/reperfusion injury by reducing oxidative stress through inhibiting the lipolysis of lipid droplets. Sci Rep. 2017;7:42574.
190. Drevinge C, Dalen KT, Mannila MN, Tang MS, Stahlman M, Klevstig M, et al. Perilipin 5 is protective in the ischemic heart. Int J Cardiol. 2016;219:446-54.
191. Bekeova C, Anderson-Pullinger L, Boye K, Boos F, Sharpadskaya Y, Herrmann JM, et al. Multiple mitochondrial thioesterases have distinct tissue and substrate specificity and CoA regulation, suggesting unique functional roles. J Biol Chem. 2019;294(50):19034-47.
192. Fujita M, Momose A, Ohtomo T, Nishinosono A, Tanonaka K, Toyoda H, et al. Upregulation of fatty acyl-CoA thioesterases in the heart and skeletal muscle of rats fed a high-fat diet. Biol Pharm Bull. 2011;34(1):87-91.
193. Schiattarella GG, Altamirano F, Kim SY, Tong D, Ferdous A, Piristine H, et al. Xbp1s-FoxO1 axis governs lipid accumulation and contractile performance in heart failure with preserved ejection fraction. Nat Commun. 2021;12(1):1684.

194. Garcia-Puig A, Mosquera JL, Jimenez-Delgado S, Garcia-Pastor C, Jorba I, Navajas D, et al. Proteomics Analysis of Extracellular Matrix Remodeling During Zebrafish Heart Regeneration. Mol Cell Proteomics. 2019;18(9):1745-55.
195. Schiattarella GG, Rodolico D, Hill JA. Metabolic inflammation in heart failure with preserved ejection fraction. Cardiovasc Res. 2021;117(2):423-34.
196. Ock S, Ham W, Kang CW, Kang H, Lee WS, Kim J. IGF-1 protects against angiotensin II-induced cardiac fibrosis by targeting alphaSMA. Cell Death Dis. 2021;12(7):688.
197. Schenk S, Schoenhals GJ, de Souza G, Mann M. A high confidence, manually validated human blood plasma protein reference set. BMC Med Genomics. 2008;1:41.
198. Weisiger RA. Dissociation from albumin: A potentially rate-limiting step in the clearance of substances by the liver. Proc Natl Acad Sci U S A. 1985;82: 1563-7.
199. Wang LW, N. Zhang, W. Cheng, X. Yan, Z. Shao, G. Wang, X. Wang, R. Fu, C. Therapeutic peptides: current applications and future directions. Signal Transduct Target Ther. 2022;7(1):48.
200. Souren JEM, Ponec, M., & van Wijk, R. . Contraction of Collagen by Human Fibroblasts and Keratinocytes. In Vitro Cell Dev Biol. 1989;25(11):1039–45.
201. Reyhani VT, M. van Wieringen, T. Rask, L. Lennartsson, J. Rubin, K. PDGF-BB enhances collagen gel contraction through a PI3K-PLCgamma-PKC-cofilin pathway. Sci Rep. 2017;7(1):8924.
202. Lee JC, Kim YH, Lee TK, Kim IH, Cho JH, Cho GS, et al. Effects of ischemic preconditioning on PDGF-BB expression in the gerbil hippocampal CA1 region following transient cerebral ischemia. Mol Med Rep. 2017;16(2):1627-34.
203. Cucina A, Pagliei S, Borrelli V, Corvino V, Stipa F, Cavallaro A, et al. Oxidised LDL (OxLDL) induces production of platelet derived growth factor AA (PDGF AA) from aortic smooth muscle cells. . Eur J Vasc Endovasc Surg 1998;16(3):197-202.
204. Rashid FN CZ, Ogawa M, Perdomo J, Hume RD, Kizana E, Chong JJH. Platelet derived growth factor-A (Pdgf-a) gene transfer modulates scar composition and improves left ventricular function after myocardial infarction. Int J Cardiol. 2021;15(341):24-30.
205. French B, Kramer C. Mechanisms of Post-Infarct Left Ventricular Remodeling. . Drug Discov Today Dis Mech 2007;4(3):185-96.
206. Juhl P, Bondesen S, Hawkins CL, Karsdal MA, Bay-Jensen AC, Davies MJ, et al. Dermal fibroblasts have different extracellular matrix profiles induced by TGF-beta, PDGF and IL-6 in a model for skin fibrosis. Sci Rep. 2020;10(1):17300.
207. Konsoula R, Jung M. In vitro plasma stability, permeability and solubility of mercaptoacetamide histone deacetylase inhibitors. Int J Pharm. 2008;361(1-2):19-25.
208. Andes D, Marchillo K, Stamstad T, Conklin R. In vivo pharmacokinetics and pharmacodynamics of a new triazole, voriconazole, in a murine candidiasis model. Antimicrob Agents Chemother. 2003;47(10):3165-9.
209. Zhang Q, Zeng SX, Lu H. Determination of Maximum Tolerated Dose and Toxicity of Inauhzin in Mice. Toxicol Rep. 2015;2:546-54.
210. Gao Y, Shen JK, Choy E, Zhang Z, Mankin HJ, Hornicek FJ, et al. Pharmacokinetics and tolerability of NSC23925b, a novel P-glycoprotein inhibitor: preclinical study in mice and rats. Sci Rep. 2016;6:25659.
211. Aston WJ, Hope DE, Nowak AK, Robinson BW, Lake RA, Lesterhuis WJ. A systematic investigation of the maximum tolerated dose of cytotoxic chemotherapy with and without supportive care in mice. BMC Cancer. 2017;17(1):684.

212. Santos EW, Oliveira DCd, Hastreiter A, Silva GBd, Beltran JSdO, Tsujita M, et al. Hematological and biochemical reference values for C57BL/6, Swiss Webster and BALB/c mice. Braz J Vet Res Anim Sci. 2016;53(2).
213. Mazzaccara C, Labruna G, Cito G, Scarfo M, De Felice M, Pastore L, et al. Age-Related Reference Intervals of the Main Biochemical and Hematological Parameters in C57BL/6J, 129SV/EV and C3H/HeJ Mouse Strains. PLoS One. 2008;3(11):e3772.
214. Braber S, Verheijden KA, Henricks PA, Kraneveld AD, Folkerts G. A comparison of fixation methods on lung morphology in a murine model of emphysema. Am J Physiol Lung Cell Mol Physiol. 2010;299(6):L843-51.
215. Fix A, Garman R. Practical aspects of neuropathology: a technical guide for working with the nervous system. Toxicol Pathol 2000;28(1):122-31.
216. Jackson L. Splenic melanosis in black mice: The Jackson Laboratory; 1989 [Available from: https://www.jax.org/news-and-insights/1989/october/splenic-melanosis-in-black-mice.
217. Tretter JT, Chakravarti S, Bhatla P. Use of echocardiographic subxiphoid five-sixth area length (bullet) method in evaluation of adequacy of borderline left ventricle in hypoplastic left heart complex. Ann Pediatr Cardiol. 2015;8(3):243-5.
218. Grune J, Blumrich A, Brix S, Jeuthe S, Drescher C, Grune T, et al. Evaluation of a commercial multi-dimensional echocardiography technique for ventricular volumetry in small animals. Cardiovasc Ultrasound. 2018;16(1):10.
219. Hume RD, Kanagalingam S, Deshmukh T, Chen S, Mithieux SM, Rashid FN, et al. Tropoelastin Improves Post-Infarct Cardiac Function. Circ Res. 2023;132(1):72-86.
220. Russo K, Ragone R, Facchiano AM, Capogrossi MC, Facchiano A. Platelet-derived growth factor-BB and basic fibroblast growth factor directly interact in vitro with high affinity. J Biol Chem. 2002;277(2):1284-91.
221. Gohring W, Sasaki T, Heldin CH, Timpl R. Mapping of the binding of platelet-derived growth factor to distinct domains of the basement membrane proteins BM-40 and perlecan and distinction from the BM-40 collagen-binding epitope. Eur J Biochem. 1998;255(1):60-6.
222. Liu X, Zhang Y, Ward LD, Yan Q, Bohnuud T, Hernandez R, et al. A proteomic platform to identify off-target proteins associated with therapeutic modalities that induce protein degradation or gene silencing. Sci Rep. 2021;11(1):15856.
223. Mayya V, Han DK. Phosphoproteomics by mass spectrometry: insights, implications, applications and limitations. Expert Rev Proteomics. 2009;6(6):605-18.
224. Lasky JA, Brody AR. Interstitial fibrosis and growth factors. Environ Health Perspect. 2000;108:751–62.
225. Akhmetshina A, Dees C, Pileckyte M, Maurer B, Axmann R, Jungel A, et al. Dual inhibition of c-abl and PDGF receptor signaling by dasatinib and nilotinib for the treatment of dermal fibrosis. FASEB J. 2008;22(7):2214-22.
226. Xu Z, Alloush J, Beck E, Weisleder N. A murine model of myocardial ischemia-reperfusion injury through ligation of the left anterior descending artery. J Vis Exp. 2014(86).
227. Zhou Z, Liu Z, Gao X, Long Q. Mitochondrial respiration in C57BL/6 substrains varies in response to myocardial infarction. J Bioenerg Biomembr. 2021;53(2):119-27.
228. Simon M, Greenaway S, White J, Fuchs H, Gailus-Durner V, Wells S, et al. A comparative phenotypic and genomic analysis of C57BL/6J and C57BL/6N mouse strains. Genome Biol 2013;14.

229. Tuntland T, Ethell B, Kosaka T, Blasco F, Zang RX, Jain M, et al. Implementation of pharmacokinetic and pharmacodynamic strategies in early research phases of drug discovery and development at Novartis Institute of Biomedical Research. Front Pharmacol. 2014;5:174.
230. Ichinose F, Bloch K, Wu J, Hataishi R, Aretz H, Picard M, et al. Pressure overload-induced LV hypertrophy and dysfunction in mice are exacerbated by congenital NOS3 deficiency. Am J Physiol Heart Circ Physiol. 2004;286(3):1070-5.
231. Weinheimer CJ, Lai L, Kelly DP, Kovacs A. Novel mouse model of left ventricular pressure overload and infarction causing predictable ventricular remodelling and progression to heart failure. Clin Exp Pharmacol Physiol. 2015;42(1):33-40.

CHAPTER 6: SUPPLEMENTARY MATERIALS

Table 6.1: Maximum tolerated dose study – mouse weights.

Weight of phase B mice at day 0 prior to osmotic mini pump implantation and day 28 following treatment with either of the novel mimetic peptides, JC5 and JC5a or either of the negative control peptides.

Mouse ID	Treatment Group	Day 0 Weight (g)	Day 28 Weight (g)
271456	JC5	26.00	26.90
271454	JC5	27.40	28.20
272455	JC5	25.70	25.50
271617	JC5	24.20	25.00
271453	JC5	27.30	28.60
271618	JC5	24.60	25.9
271516	JC5a	25.60	27.25
271050	JC5a	26.88	28.60
271427	JC5a	26.00	27.16
271425	JC5a	26.00	27.90
271517	JC5a	25.00	27.7
271515	JC5a	26.35	27.50
273979	Neg Con 5	30.00	31.00
273981	Neg Con 5	31.00	30.30
274025	Neg Con 5	31.23	29.04
274026	Neg Con 5	31.65	30.15
273980	Neg Con 5	30.51	30.31
274753	Neg Con 5	30.01	32.10
271625	Neg Con 5a	25.20	27.80
271428	Neg Con 5a	26.00	27.00
271624	Neg Con 5a	27.00	28.90
271426	Neg Con 5a	26.30	28.20
271623	Neg Con 5a	26.45	27.80
271626	Neg Con 5a	27.30	28.50

Table 6.2: Maximum tolerated dose study – organ weights.

Weight of phase B mice organs at day 28 following treatment with either of the novel mimetic peptides, JC5 and JC5a or either of the negative control peptides.

Mouse ID	Treatment	Heart	Lungs	Kidneys	Liver	Spleen	Brain
271455	JC5	0.1449	0.1683	0.3232	1.3790	0.0636	0.4405
271456	JC5	0.1601	0.1860	0.3899	1.4794	0.0716	0.4069
271454	JC5	0.1492	0.1579	0.3466	1.5925	0.0916	0.4569
271617	JC5	0.1419	0.1687	0.3346	1.3600	0.0640	0.4317
271453	JC5	0.1557	0.1927	0.3625	1.6751	0.0662	0.4410
271618	JC5	0.1461	0.1035	0.3519	1.4906	0.0812	0.4329
271050	JC5a	0.1578	0.1669	0.3899	1.7389	0.0942	0.4441
271516	JC5a	0.1616	0.1476	0.3683	1.6224	0.0687	0.4556
271427	JC5a	0.1465	0.1442	0.3751	1.5172	0.0979	0.4715
271425	JC5a	0.1561	0.1622	0.3816	1.7115	0.0851	0.4573
271517	JC5a	0.1799	0.1553	0.4225	1.1559	0.1005	0.4567
271515	JC5a	0.1372	0.1624	0.3709	1.5754	0.1188	0.4322
273980	Neg Con 5	0.1533	0.1913	0.3918	1.7230	0.0891	0.4668
274026	Neg Con 5	0.1643	0.1901	0.4370	1.7759	0.0950	0.4432
274025	Neg Con 5	0.1525	0.1809	0.3593	1.6854	0.0719	0.4559
273981	Neg Con 5	0.1570	0.1778	0.4110	1.6700	0.0699	0.4489
273979	Neg Con 5	0.1682	0.1880	0.4635	1.750	0.1046	0.4635
274753	Neg Con 5	0.1871	0.1836	0.4110	1.9341	0.1023	0.4661
271624	Neg Con 5a	0.1505	0.1611	0.3918	1.5858	0.0838	0.4810
271428	Neg Con 5a	0.1642	0.1435	0.4029	1.3919	0.0957	0.4572
271625	Neg Con 5a	0.1420	0.1464	0.3796	1.5911	0.0857	0.4385
271426	Neg Con 5a	0.2146	0.1820	0.4732	1.1939	0.1430	0.4612
271623	Neg Con 5a	0.1501	0.1455	0.3728	1.4395	0.0779	0.4377
271626	Neg Con 5a	0.1641	0.1556	0.3871	1.5912	0.0800	0.4367